THESIS FOR THE DEGREE OF LICENTIATE OF ENGINEERING

Aerobic oxidative EDA complex mediated photoreactions

August Runemark

Department of Chemistry and Chemical Engineering

CHALMERS UNIVERSITY OF TECHNOLOGY

Gothenburg, Sweden 2021

Aerobic oxidative EDA complex mediated photoreactions

August Runemark

Technical report no 2021:16

Department of Chemistry and Biochemistry
Chalmers University of Technology
SE-412 96 Gothenburg
Sweden
Telephone + 46 (0)31-772 1000

Gothenburg, Sweden 2010

Abstract

Visible light is a convenient energy source for driving chemical reactions. Its lower energy, compared to ultraviolet irradiation, can be utilized to conduct organic reactions under mild conditions. During the last decades, the growing field of photoredox catalysis has proved this statement true, and a wide variety of radical reactions to form complex molecules has been developed. The photoredox catalysis cycle is typically based on photoactive transition metal complexes. Albeit being highly efficient in the conversion of light energy to chemical energy, these complexes suffer from drawbacks such as the scarcity of the metals. One solution to this problem is to use catalysts based on purely organic compounds. Another way of circumventing the use of catalysts altogether is to take advantage of electron donor acceptor (EDA) complexes. These molecular aggregates are formed when an electron rich molecule interact with an electron deficient partner. Given the right electronic properties of the two reactants, the EDA complex can be excited using visible light and thus induce a chemical reaction without the need of an external catalyst.

Oxidative reactions are essential in organic chemistry, and a range of oxidants are available. However, several oxidants rely on transition metals or are highly reactive and toxic. Air, with its high concentration of molecular oxygen, could be considered an ideal oxidant based on the availability, non-toxicity, and the formation of water as the byproduct. In this thesis, the combination of photoactive EDA complexes to induce chemical reactions, with aerobic oxygen as an oxidant, is investigated.

Two protocols for the visible light driven synthesis of substituted tetrahydroquinolines (THQ) have been developed. The reactions are driven by the excitation of photoactive EDA complexes formed between *N,N*-dialkylated anilines as donors and activated alkenes as acceptors. Aerobic oxygen drives the net-oxidative reactions to the final products. The mild reaction conditions, cheap and accessible reagents, and the excellent diastereoselectivity make the presented protocols attractive for the synthesis of the THQ scaffold.

List of publications

I. Visible-Light-Driven Stereoselective Annulation of Alkyl Anilines and Dibenzoylethylenes via Electron Donor–Acceptor Complexes, A. Runemark, S. C. Zacharias, and H. Sundén, J. Org. Chem. 2021, 86, 2, 1901–1910

II. Aerobic oxidative EDA catalysis. Synthesis of tetrahydroquinolines using a catalytic EDA active acceptor, A. Runemark and H. Sundén, *Manuscript*

Contribution report

Paper I: Outlined the study, performed the experimental work, interpreted the results.

Paper II: Outlined the study, performed the experimental work, interpreted the results.

Publications by the author not included in the thesis

III. Polycyclizations of Ketoesters: Synthesis of Complex Tricycles with up to Five Stereogenic Centers from Available Starting Materials, M. Kamlar, A. Runemark, I. Císařová, and H. Sundén, Org. Lett. 2020, 22, 21, 8387–8391

List of abbreviations

SET – Single Electron Transfer

BET – Back Electron Transfer

EnT – Energy Transfer

EDA – Electron Donor-Acceptor

CT – Charge Transfer

PT – Proton Transfer

NMR – Nuclear Magnetic Resonance

Eq – Equation

Equiv – Equivalents

A – Acceptor

D – Donor

HOMO – Highest Occupied Molecular Orbital

LUMO – Lowest Unoccupied Molecular Orbital

EA – Electron Affinity

IP – Ionization Potential

UV – Ultraviolet

EWG – Electron Withdrawing

EDG - Electron Donating Group

KIE – Kinetic isotope effect

SCE – Standard calomel electrode

THQ – Tetrahydroquinoline

DBE – Dibenzoyl ethylene

CFL -Compact fluorescent lamp

Contents

1. Introduction and Background

Since the dawn of civilization, mankind has taken advantage of chemicals and chemical technologies to improve her life.[1] Pigments, metals, soap and fabrics are some chemical products that have been produced using advanced processes for millennia. With new insights in the underlaying processes of the world of chemistry and physics, recent centuries have then shown an enormous increase of this utilization of the powers of molecules. The discovery of oil and other fossil products came with an immense number of unprecedented materials, medications, and complex chemical structures. As a result, our modern society has formed. Nevertheless, as a by effect, problems have arisen and today we face the effects of our extensive use of fossil fuels, the production of plastic materials and the pollution with manmade chemicals. To tackle these challenges, the chemical industry must change. The advent of *green chemistry* is one of the answers to this. Following a certain set of guidelines, the production and use of chemicals are supposed to become less hazardous, having less impact on the global and local environment, and constitute less health risks. The principles, as adopted from Anastas and Warner, can be summarized as follows:

1. Prevention
2. Atom Economy
3. Less Hazardous Chemical Syntheses
4. Designing Safer Chemicals
5. Safer Solvents and Auxiliaries
6. Design for Energy Efficient
7. Use of Renewable Feedstocks
8. Reduce Derivatives
9. Catalysis
10. Design for Degradation
11. Real-time analysis for Pollution Prevention
12. Inherently Safer Chemistry for Accident Prevention

All these principles can be associated with *methodology development*, i.e. the development and optimization of the production of chemicals. New ways to produce essential chemicals using fewer toxic reagents (principle 3 and 12), less amount of waste (principle 2, 8 and 9), and depend less on fossil fuels as raw materials (principle 7), are constantly needed.

Photochemical methods can be of importance to meet many of these needs. Foremost, the possibility to forage the energy from the sun to drive the production of chemicals would potentially lead to less dependence on fossil fuels and lower emissions. Light mediated reactions also have the potential of being highly selective, atom economic and produce little waste. Photosynthesis in plants and algae is an example of a brilliant way to harvest light energy to furnish highly complex molecular structures with molecular oxygen as the sole byproduct. The use of carbon dioxide and water, readily available in our atmosphere, as starting materials for the construction of carbohydrates also provides an inspiration for the design of new man-made chemical processes. Reactions using readily available reagents such as carbon dioxide, water or oxygen could tie to several of the twelve principles of green chemistry.

In this work, methodology development for using light as an efficient energy source, and aerobic oxygen as an abundant and safe reagent, is investigated.

2. Theory

2.1 Electron Transfer

Maybe the most fundamental reaction in a chemical context is the transfer of one electron from one species to another. This superficially simple process has been the subject of immense research during the last century due to its fundamental role. To understand redox reactions, both thermal and - of more importance for this work – photochemical, a very brief background to electron transfer processes is needed.

Consider a simple case of the single electron transfer (SET) from a donor (D) and an acceptor (A). Schematically it can be viewed according to equation 1.[2]

$$D + A \rightarrow D^+ + A^- \quad (1)$$

If D and A are free entities not connected by chemical bonds prior to the SET, this simple transfer can further be divided in three steps: the association of A and D for form an encounter complex (eq. 2), the electron transfer event (eq. 3), and finally the dissociation of the oxidized donor and the reduced acceptor (eq. 4).

$$D + A \rightleftharpoons D - A \quad (2)$$

$$D - A \rightleftharpoons D^+ - A^- \quad (3)$$

$$D^+ - A^- \rightleftharpoons D^+ + A^- \quad (4)$$

Step 3 is here the most important to describe further. Therein lies the key to much to the thermodynamics of the electron transfer process. Like any reaction, the step can be associated with a certain energy change. Fundamentally, the total energy change involves the energy required to remove one electron from D (eq. 5) and the energy associated with the gain of one electron to A (eq. 6). Considering a reaction in gas phase, these two energies are nothing but the ionization potential (IP) of D and the negative IP of A^- (also referred to as *electron affinity,* EA).

$$D \rightarrow D^+ + e^- \quad (5)$$

$$A + e^- \rightarrow A^- \quad (6)$$

Thus, the total energy change of the combined half-reactions 5 and 6 can be expressed as equation 7:

$$\Delta E = IP_D - EA_A \quad (7)$$

This expression gives a very simple picture of what fundamentally drives the electron transfer; however, it cannot directly be applied to solution chemistry due to the influence of solvent interactions. Experimentally determined potentials for the half-reactions 5 and 6 are needed. The *redox potential* E^0 is the answer to this problem. Superficially it is a "corrected" version of the IP and EA for the reactions 5 and 6 and considers the solvent effects. E^0 relates to Gibbs free energy change of the reaction according to equation 8:

$$\Delta G = -nFE_{reaction} = -nF[E^0(D^+/D) - E^0(A/A^-)] \quad (8)$$

Where *n* is the number of electrons involved in the transfer and F is the faraday constant. The unit of the Gibbs free energy will thus, using the equation 8, be in electron volts. Noteworthy, the redox potential is always expressed relative to a reference reaction of which there are several in the literature. Equation 8 can however

not at all fully describe the thermodynamics of the electron transfer. Consider the change in charge associated with equation 3. Surely, the coulombic interactions are different between D and A compared to D^+ and A^-. This would give rise to binding interactions affecting the overall energy change, depending on the strength of dielectric continuum that the solvent surrounding the species forms. To correct for this, another term can be introduced called electrostatic work term w, according to equation 9.

$$\Delta G = -nFE_{reaction} = nF\left[E^0\left(\frac{D^+}{D}\right) - E^0\left(\frac{A}{A^-}\right)\right] - w_P \qquad (9)$$

Where the indexation denotes the product (P) side. If the reactants are not neutral, another work term for the reactant side should be included. The work term w_p can be expressed in terms of the distance between the charged species, their charge, and the dielectric constant of the solvent according to equation 10:

$$w_p = \frac{(z_{D^+} + z_{A^-})e^2}{d\varepsilon_s} \qquad (10)$$

2.2 Photoinduced Electron transfer

The discussion so far has assumed the species D and A to be in their ground state. Either of them can however be promoted to their excited state prior to the electron transfer process. The thermodynamics in such a case changes as the energy of the excited states must be taken into consideration. Equation 11 describes the process where D or A absorbs a photon of appropriate energy to form the excited state, denoted with *.[2]

$$D + h\nu \rightarrow D^* \; or \; A + h\nu \rightarrow A^* \qquad (11)$$

$$D^* + A \rightarrow D^+ + A^- \qquad (12)$$

$$D + A^* \rightarrow D^+ + A^- \qquad (13)$$

The extra energy factor associated with the promotion to the excited state can be expressed in terms of the energy difference between the S_0 and S_1 state of either D or A, and is usually denoted $E_{0,0}$. The associated Gibbs free energy is thus $\Delta G_{0,0}$. Added to equation 9, an expression for the free energy change of photoinduced electron transfer can be written according to equation 14:

$$\Delta G = nF\left[E^0\left(\frac{D^+}{D}\right) - E^0\left(\frac{A}{A^-}\right)\right] - w_P - \Delta G_{0,0} \qquad (14)$$

Photoinduced electron transfer is of fundamental importance within the field of light mediated organic reactions. Returning to the example of plants, the core of the photosynthetic process is the generation of charged radical species through photoinduced electron transfer. Likewise, an immense number of man-made synthetic processes have been developed relying on the same concept. In this context, equation 9 becomes very important when designing suitable donor and acceptor pairs, solvents, and other reaction conditions.

The fate of the charged species D^+ and A^- is the next problem of concern; unless rapid forward chemical processes drive them to products, they will participate in back electron transfer (BET) reforming D and A, render the electron transfer ultimately useless from a synthetic perspective.

2.3 Photochemical Reactions *via* SET

2.3.1 Photoredox catalysis

During the last decades a new area of photochemistry has emerged, based not on the light absorbing properties of reactants themselves, but rather of a photocatalyst.[3] The concept of photoredox catalysis ultimately relies on the theory outlined in the previous chapter of this thesis, and is outlined in Figure 1.[3] A molecule, in this case a catalyst, in its excited state (cat*) can transfer an electron to or from a reaction partner D or A (compare equation 12 and 13). The reduced, or oxidized, reactant can then in turn take part in radical reactions while the oxidized or reduced catalyst can return to its original oxidation state by a second redox process.

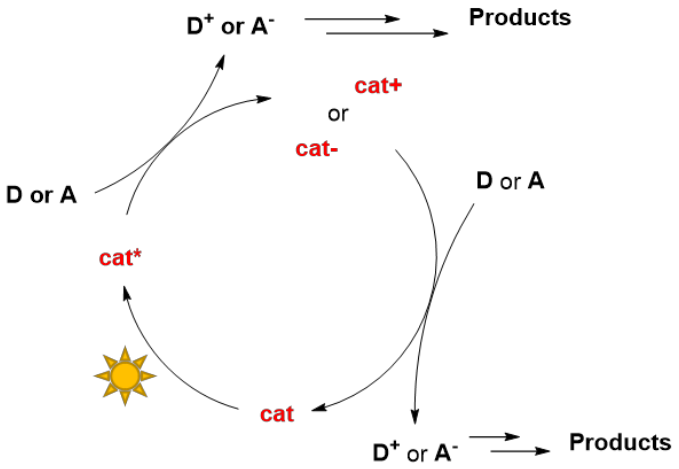

Figure 1. Simplified schematic representation of the main steps in the photoredox catalytic cycle.

Utilizing a photoredox catalyst that absorbs in the visible range of the spectrum, low energy light can be harvested to induce photochemical reactions without exciting the reactants themselves. This leads to suppression of unwanted side reactions and potentially high selectivity.

Depending on the structure of the catalyst, its electronic nature and redox potentials can be tuned to match certain substrates. Classically, transition metal-based complexes are used in homogeneous photoredox catalytic reactions. Iridium and ruthenium polypyridyl complexes (Scheme 1d) are among the most commonly used due to their excellent photophysical and redox properties.[4] However, several catalysts purely based on organic compounds have been developed.[5,6]

Initial findings in the 1970's by Kellog and co-workers (Scheme 1a) shows rate enhancement in the reduction of **1** by dihydropyridines with addition of a ruthenium polypyridyl complex under photochemical conditions[7] However, it took until early 2000's before the field of photoredox catalysis started to develop towards its current status. In 2010, Stephenson and co-workers reported an aza-Henry reaction between nitromethane and tetrahydroisoquinoline **2** (Scheme 1b).[8] The reaction is proposed to occur as the amine **2** as a donor that reduces an excited iridium complex to furnish an amine radical cation that further oxidizes to an iminium ion which reacts with nitromethane. The reduced catalyst is re-oxidized by the action of molecular oxygen to close the catalytic cycle.

Scheme 1. Examples of photoredox catalysis in organic synthesis

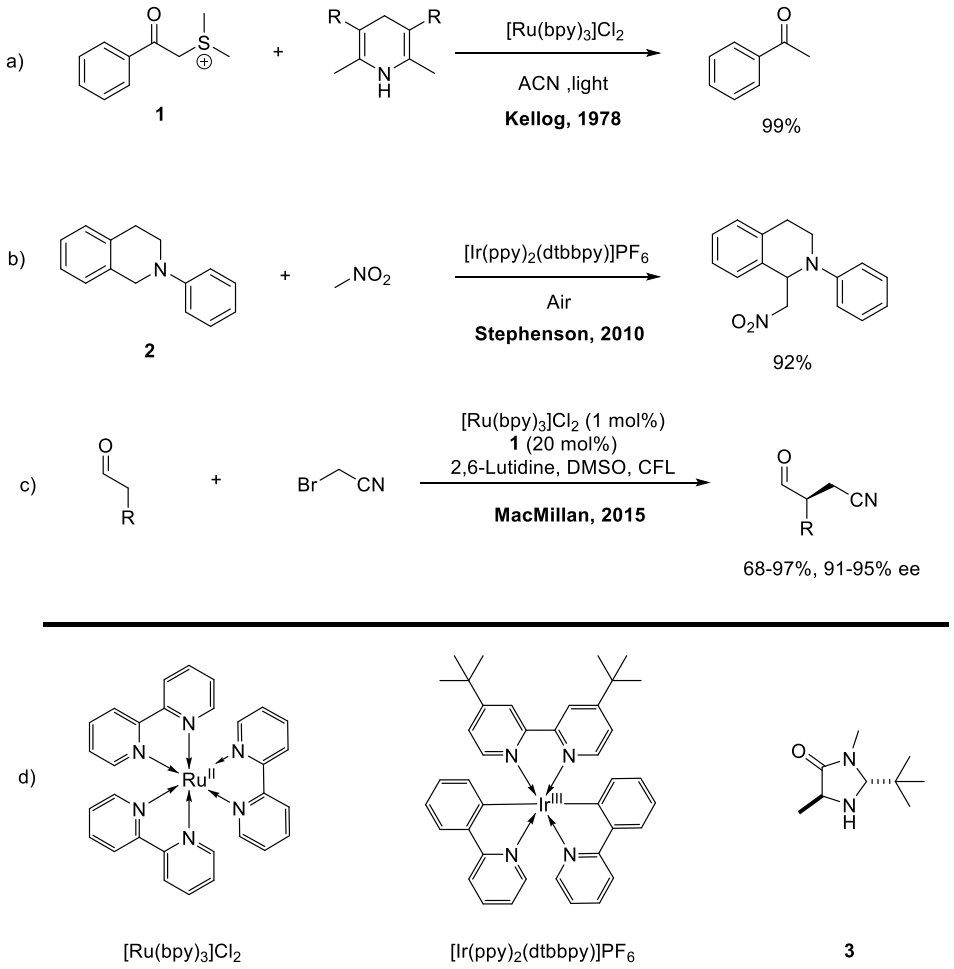

Asymmetric synthesis can efficiently be achieved with photoredox catalysis, such as in the work of MacMillan and co-workers in 2015 (Scheme 1c).[9] Here the authors present an enantioselective coupling reaction between aldehydes and cyanobromides using $[Ru(dby)_3]Cl_2$ as the photoactive catalyst and the homochiral amine **3** as an organocatalyst to induce the enantio-control.

Example b in Scheme 1 exemplifies an excellent feature of photoredox catalysis: the possibility to use molecular oxygen as the terminal oxidant in a controlled fashion. The reaction of **2** with nitromethane is essentially an oxidative coupling with the loss of two hydrogen atoms.

Amine α-C-H functionalization such as example b in Scheme 1 is a common reaction type for photoredox catalysis due to the oxidation potential of alkyl and aryl substituted amines, and the importance of such transformation for the construction of biologically active compounds.[3]

One of the main features of the photoredox catalyst lies in its possibility to harvest visible light with high efficiency and release it to chemical potential energy in a selective fashion. Using high energy UV light, photo induced electron transfer between excited reactants can result in similar reactivity, however with the drawback of the selectivity and energy efficiency.

A major drawback with the use of transition metal based photoredox catalysts is the high price and scarcity of the metals in the earth's core. Using the homogeneous conditions typically applied in photoredox catalysis, the recovery of the catalyst poses significant problems. Cheaper and more available catalysts based on simple organic compounds, or catalyst free conditions, therefore is advantageous.

2.4 Electron Donor Acceptor complexes

Another approach to enable photochemical activation of compounds not absorbing in a certain region of the spectrum is *via* electron donor acceptor (EDA) complexes. EDA complexes, or charge transfer (CT) complexes, are the result of a weak interaction between two species – an electron rich donor and an electron deficient acceptor. In terms of frontier molecular orbital theory, the nature of the interaction involves orbital mixing of the highest occupied molecular orbital (HOMO) of the donor and the lowest unoccupied molecular orbital (LUMO) of the acceptor, giving rise to two new orbitals, as depicted in Figure 2.

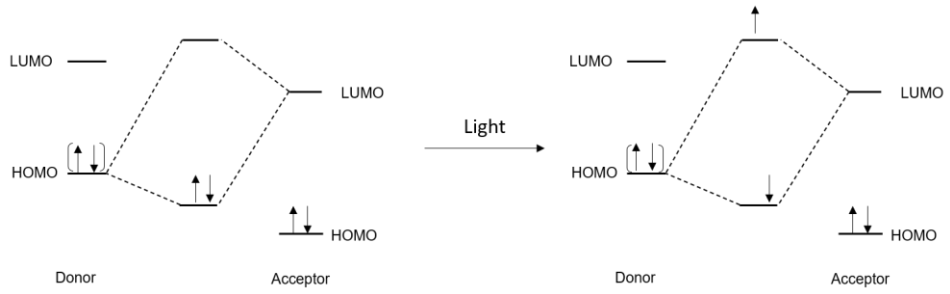

Figure 2. Schematic representation of the orbital mixing of a donor and acceptor forming an EDA complex.

The ground state complex can be excited by light of appropriate energy, promoting an electron from the HOMO to higher energy states of the complex. This spectroscopic feature is a typical characteristic of an EDA complex, resulting in an absorption band not observed in the individual donor and acceptor species. The bathochromic shift of the charge transfer (CT) band often makes the formation of an EDA complex possible to observe by the naked eye as a color change when mixing the donor and acceptor in solution. After excitation, the complex can either relax to its ground state or result in a net SET from the donor to the acceptor, forming a radical ion pair (RIP). The RIP can further undergo BET, reforming the original species, or dissociate in solution. In terms of synthetic usefulness, the latter process is favorable giving access to reactive radical species that can participate in useful chemical reactions. Overcoming the BET by making the dissociation and forward processes more favorable has been achieved using different approaches, and in recent decades the synthetic powers of EDA complexes have been developed and remains a subject of high interest.[10–12] Prototypical early examples of intermolecular interactions classified as EDA complexes include mixtures of halogens and aromatic hydrocarbons. The appearance of intense absorption bands in the ultraviolet region upon mixing iodine and diethyl ether was investigated and concluded to be a result of a 1:1 iodine-ether complex.[13]

2.4.1 EDA Complexes in Organic Synthesis

After the initial observations of EDA complexes in the first half of the 20th century, a long time passed before synthetic methods relying on their photochemistry were designed.[11] Pioneering work was done in the 1970's and 80' (Scheme 2).[14] In 1979, Kochi and co-workers reported the photochemical addition reaction of tetramethyl tin over the double bond of tetracyanoethylene (Scheme 2a). The reaction is proposed to proceed *via* the activation of an EDA complex (**EDA-1)** formed between the electron deficient alkene and the tetramethyl tin by 436 nm light.[15] In a following paper in 1987, Kochi and co-workers reported another EDA complex (**EDA-2**) formed between the electron rich 4'-methyl anisole and tetranitromethane (Scheme 2b).[14] Irradiation with visible light resulted in the aromatic nitration of the methyl anisole.

Another early example of an aromatic substitution reaction driven by EDA complexes is the formation of phenylacetone by the irradiation of a mixture of iodo- or bromobenzene and acetone enolate (Scheme 2c).[16] In this example, the EDA complex **EDA-3** is proposed to act as an initiator for a radical chain reaction leading to the final substitution product.

Scheme 2. Early examples of organic reaction driven by the photochemical activation of EDA complexes

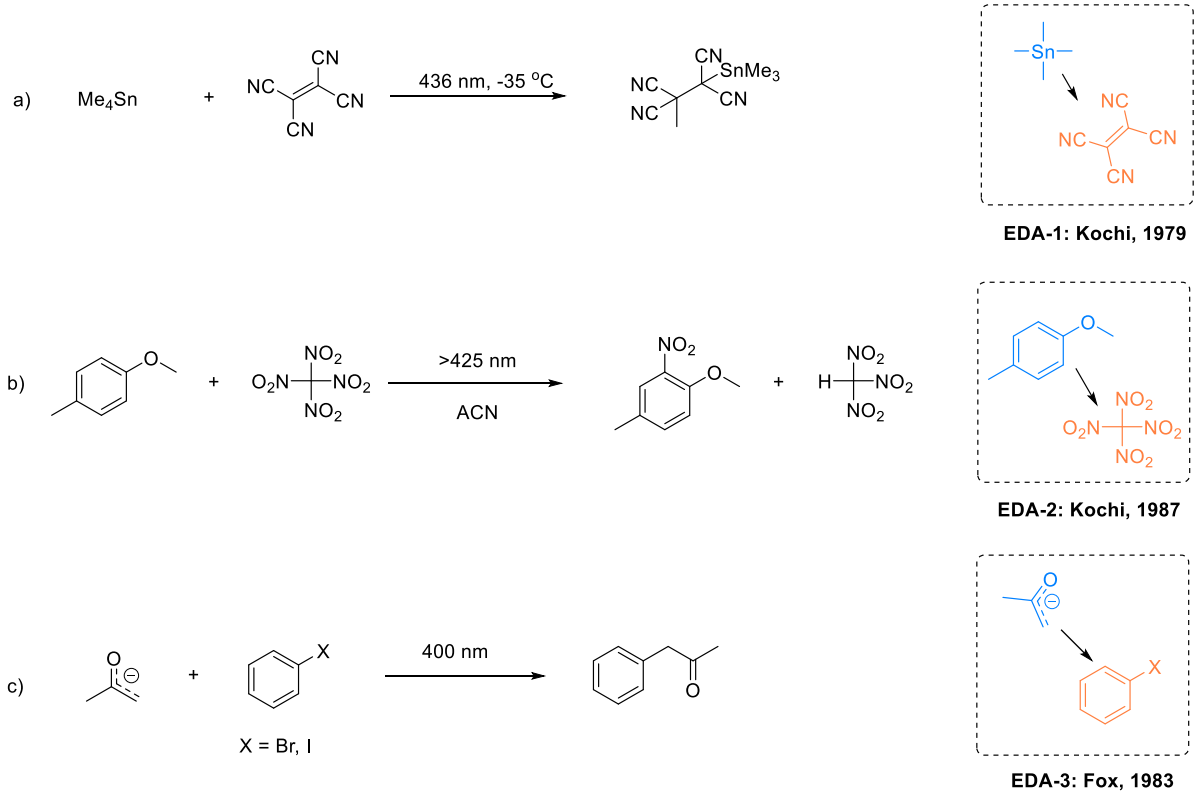

Over the last decade, a wide range of different approaches to utilize EDA complexes in synthetic organic chemistry have been developed.[10,11] Examples include arylations,[17] stereoselective alkylations,[18] oxidative annulations,[19] and acylations.[20]

One of the most challenging problems when attempting to use EDA complexes in organic synthesis is the possibility of BET. A common approach to overcome this problem is to design donors or acceptors that quickly undergoes irreversible fragmentation after SET.[10,21] This approach was used by Melchiorre and co-workers in 2014 to achieve enantioselective alkylation of cyclic ketones under photochemical conditions (Scheme 3a).[22]

Scheme 3. Light-mediated enantioselective alkylation of ketones *via* an EDA complex.

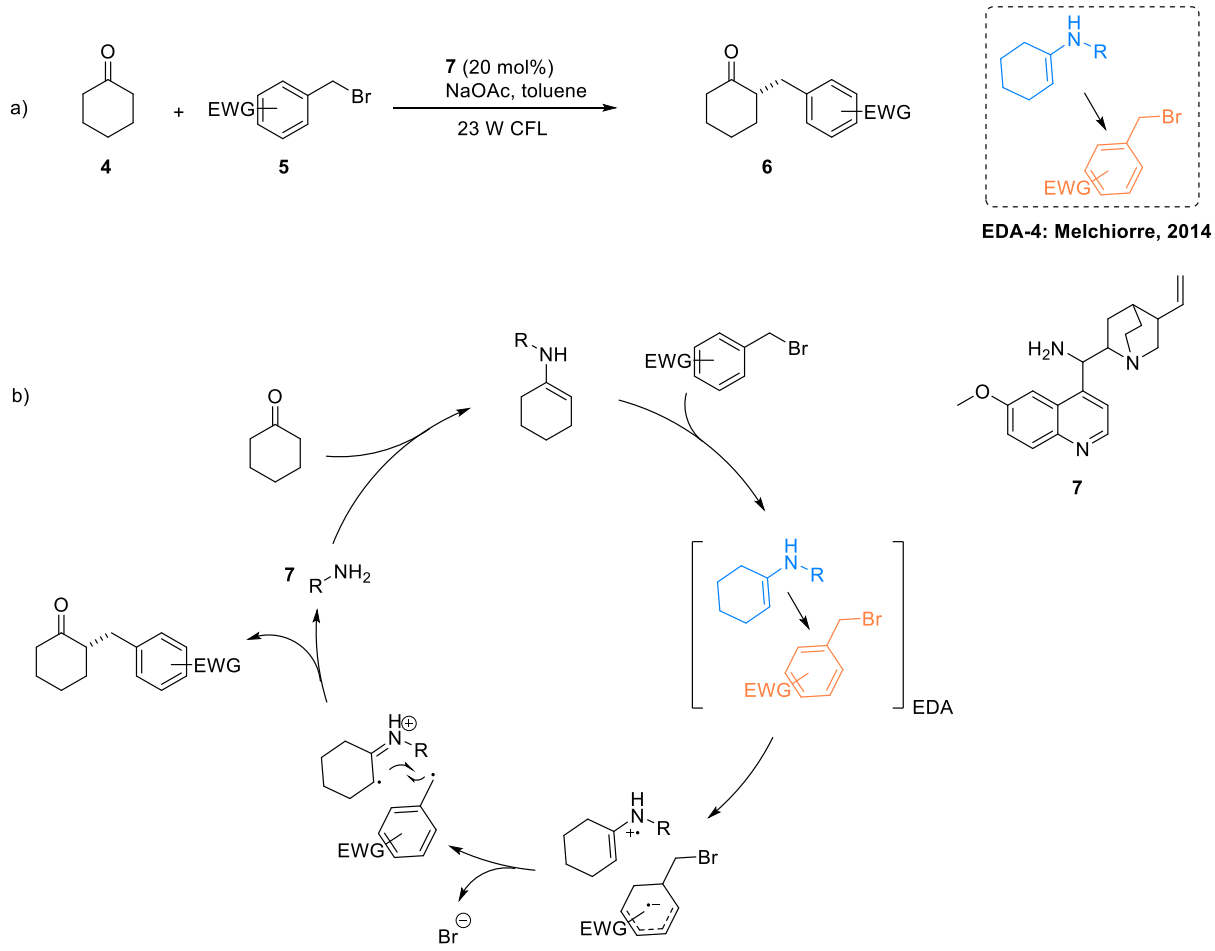

The proposed mechanism for the alkylation reaction is outlined in Scheme 3b. Key steps are the formation of a homochiral enamine intermediate by the reaction of **4** with the amine catalyst **7**, that acts as a donor in an EDA complex with an electron deficient benzyl bromide **5**. Upon excitation of the complex, a SET occurs to form a radical ion pair (RIP). The RIP can then undergo BET in an unproductive fashion, or irreversibly collapse with the loss of a bromide ion, forming a neutral benzyl radical that readily couples with the enamine radical cation. Hydrolysis then yields the final product and reforms the amine catalyst. The reaction exemplifies not only the efficient use of a leaving group (bromide anion) to drive the reaction to completion, but also the use of a catalytic EDA complexes.

In the catalytic regime, substrates that do not themselves exhibit the necessary electron properties to take part in the formation of EDA complexes can be activated using an external reagent. For example, in Scheme 3, the ketone **4** is covalently activated by its reaction with a primary amine **7** forming the electron rich enamine. The

enamine enables selectivity in the form of enantiocontrol of the reaction. Furthermore, the approach is potentially very general as the external activating reagent, the amine in this example, can be tailored to specific substrate.

Another catalytic approach is to use a catalyst that relies on non-covalent interactions and, in its native form, can form an EDA complex with a reactant, facilitating a SET with multiple turnovers. In Scheme 4 and Scheme 5, two recent examples of this method are outlined.[21,23]

Scheme 4. 3-Acetoxy quinuclidine as a catalytic donor in EDA complex photochemistry

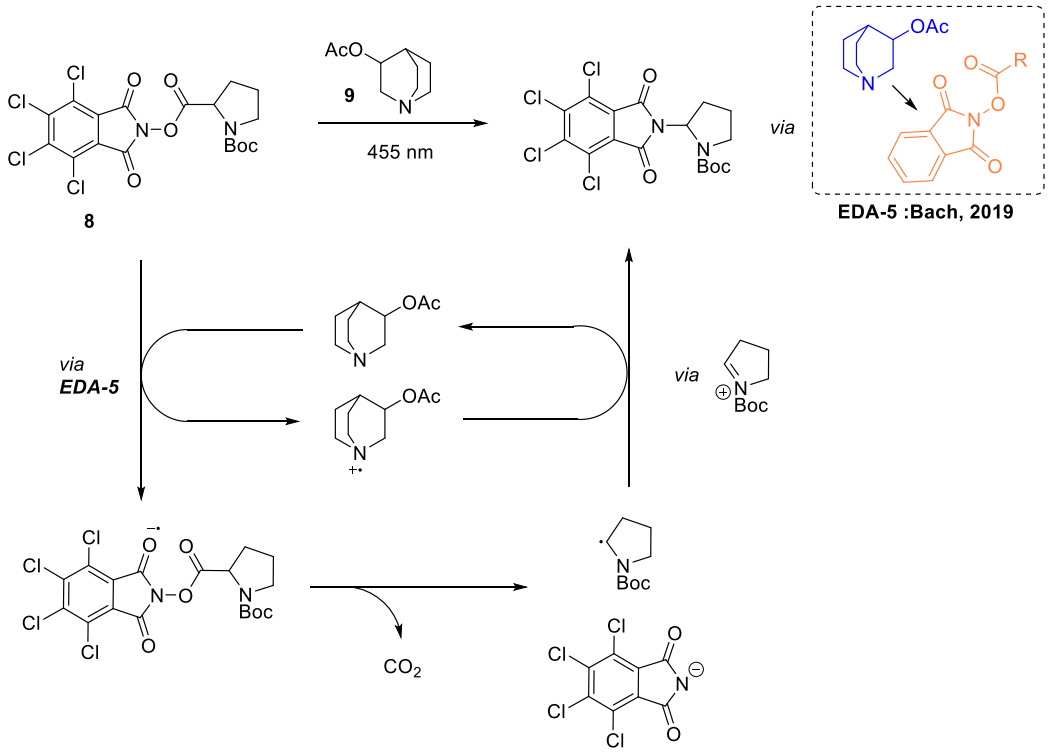

Bach and co-workers used quinuclidine derivate **9** as a catalytic donor in a decarboxylation reaction of activated esters **8** (Scheme 4).[23] The amine radical cation formed after SET within the EDA complex **EDA-5** is proposed to act as an oxidant in the turnover event, closing a net redox neutral catalytic cycle. Likewise, in an aromatic alkylation reaction developed by Stephenson and co-workers (Scheme 5) the methoxynaphthalene **11** is proposed to act as a donor in its neutral form. Together with the activated ester it forms **EDA-6** which after photoexcitation rapidly fragments to form carbon dioxide, a pyridine derivative, a carbon centered radical and the oxidized form of **11**. The carbon centered radical reacts with an arene and after SET to $\mathbf{11}^{\cdot+}$, the final product **12** is formed. Noteworthy in both these examples is the release of carbon dioxide as a strong driving force for the reaction, constituting yet another example of the approach of using leaving groups to minimize the BET.

Scheme 5. Methoxynapthalene as a catalytic donor in an aromatic alkylation reaction

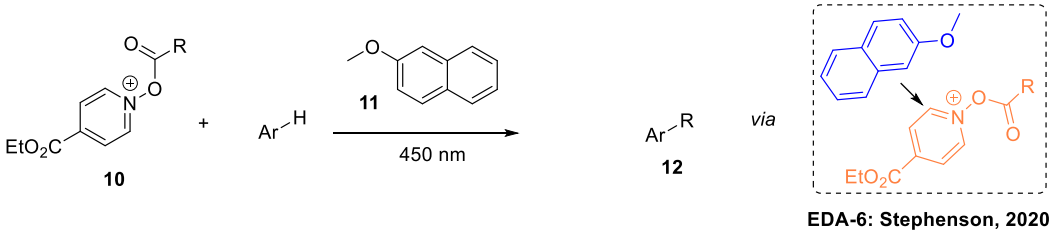

Proposed Mechanism

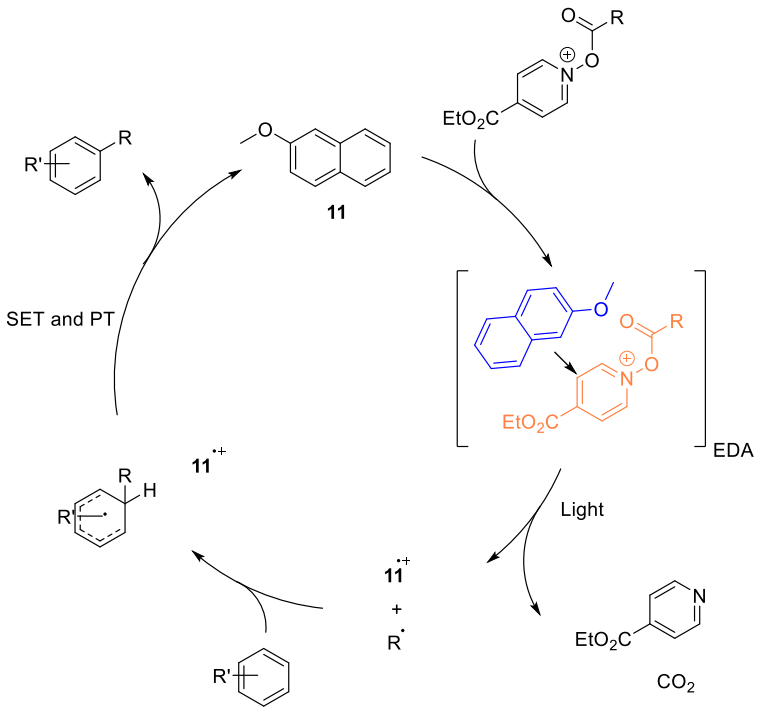

Additionally, several other examples of EDA complex within the catalytic regime can be found in the literature, based on electron rich aromatics and amines.[10,24–26]

2.4.2 Oxygen as Terminal Oxidant in EDA mediated Reactions

The examples of light promoted reactions outlined in the previous chapter are generally of net redox neutral character. However, dehydrogenative coupling reactions, such as the iridium catalyzed photomediated aza-Henry reaction in Scheme 1b, are of great interest in organic chemistry.[27] Being ultimately an oxidation, an external stoichiometric oxidant is needed to drive the reaction. Several different reagents are available, classically relying on stoichiometric amounts of metal-based oxidants, or otherwise highly reactive and thus inherently dangerous reagents. The use of such reagents is not only hazardous but also produces toxic waste in large amounts. An attractive alternative would be to use the constantly available atmospheric molecular oxygen as the terminal oxidant, producing hydrogen peroxide or water as sole byproducts.

Among oxidative reactions driven by the light activation of EDA complexes, molecular oxygen has been used as the terminal oxidant in several cases.[19,28–30] Examples include the oxidative annulation reaction between substituted dimethyl anilines and maleimides reported by Sundén and co-workers 2018 (Scheme 6).[19] The complex **EDA-7** is the proposed light active species and generates an α-amino alkyl radical and a maleimide radical upon excitation by UV-light. The aerobic oxygen is needed to drive the reaction to completion by oxidizing the enol maleimide radical.

Scheme 6. Aerobic oxidative annulation between anilines and maleimides

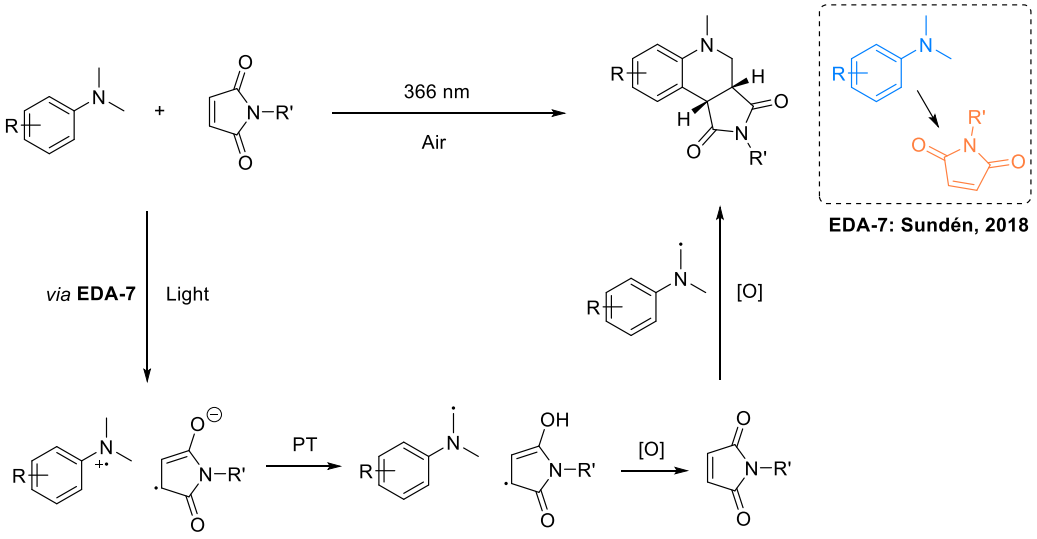

In 2019, Guo and co-workers reported another oxidative annulation reaction forming substituted indoles *via* complex **EDA-8** (Scheme 7).[28] In this case, aerobic oxygen and perfluoro butyl iodide acts as co-oxidants.

Scheme 7. Synthesis of indoles under aerobic conditions driven by a photoactive EDA complex

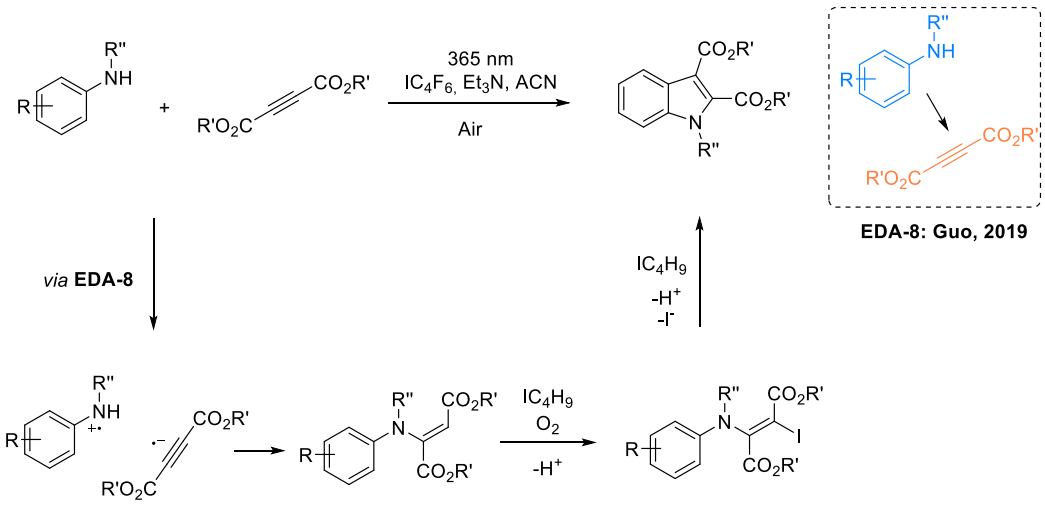

3. Aim

The aim of this thesis is to investigate novel photoactive EDA complexes and develop their use for the construction of C-C bonds under aerobic conditions.

4. Visible Light Driven Stereoselective Annulation of Alkyl Anilines and Dibenzoylethylenes via Electron Donor-Acceptor Complexes (Paper I)

4.1 Functionalization of Amines *via* SET

Being an electron rich class of compounds, amines are readily functionalized by means of oxidation (Scheme 8).[31] The single electron oxidation of a tertiary amine generates the amine radical cation which can deprotonated to the α-amino alkyl radical. This radical can act as a nucleophile in the presence of a suitable radical acceptor, or it can be further oxidized to the iminium ion reversing the polarity of the α-carbon. The latter is the case in e.g., the aza-Henry reaction presented in Scheme 1b, where nitromethane anion acts as a nucleophile.

Scheme 8. Schematic representation of the fate of a dimethyl amine tertiary amine in oxidative processes.

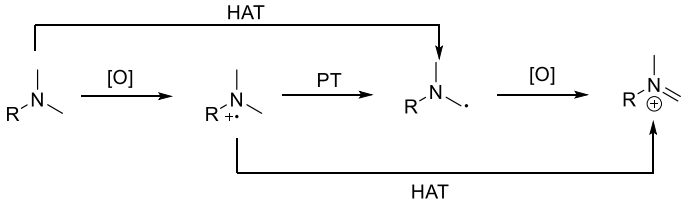

Both strategies are useful for the α-functionalization of amines, and a wide array of different conditions has been developed to selectively form the radical or iminium intermidiates.[31]

4.2 Visible Light Promoted Oxidative Annulation Reactions

The construction of N-heterocycles is ubiquitous in organic chemistry and their importance within the pharmaceutical industry cannot be overrated.[32] The constant development and improvement of methods to construct known, and new, structures of this class is therefore ever-growing. One subclass is the tetrahydroquinoline (THQ) scaffold (Scheme 9). The core motif can be found in a variety of biologically active compounds.[33,34] Examples include molecules with antiviral,[35–37] antibiotic,[38,39] and cytotoxic activity.[40,41] Due to its importance, a wide variety of conditions to furnish the THQ scaffold has been reported, including the aza-Diels-Alder, the Grieco, and the Povarov reactions.[35–37] Additional to thermal conditions, several methods relying on photoexcitation can be found in the literature.[42–47] Typically, a photoredox catalyst is needed to carry out the oxidative annulation reaction outlined in Scheme 9 under photochemical conditions.

Scheme 9. The construction of the THQ structure by an oxidative annulation reaction.

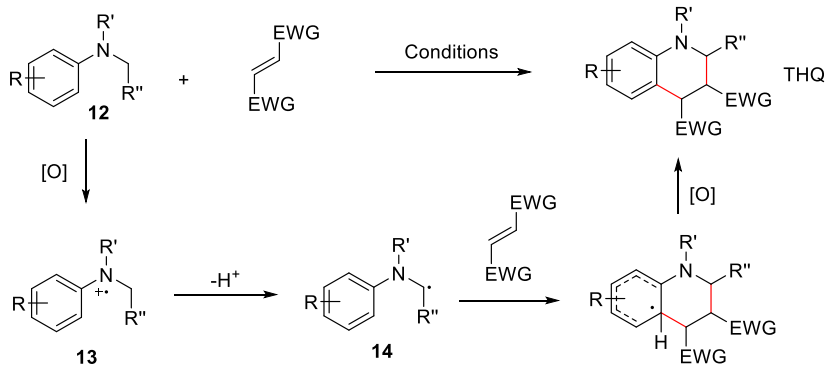

Using an appropriate single electron oxidant, the amine **12** can be transformed to its corresponding radical cation **13**. Due to the quite facile oxidation ($E^0(D^+/D$) around 0.7-1.3 V vs. SCE), [48] a wide array of oxidants can be used as acceptors in the SET. In the cation **13**, the α-protons are rendered acidic (pK_a ca 9 for the *N,N*-dimethylaniline radical cation),[49] and can be deprotonated to form the α-amino alkyl radical **14.**[31] Due to the nucleophilic nature of the radical, it can attack an electron deficient alkene, and *via* intramolecular cyclization and subsequent aromatization, the THQ structure can be formed.

The general mechanism outlined in Scheme 9 is the working principle of several developed methods in the literature (Scheme 10).

Scheme 10. Examples of oxidative annulation reactions to furnish the THQ scaffold.

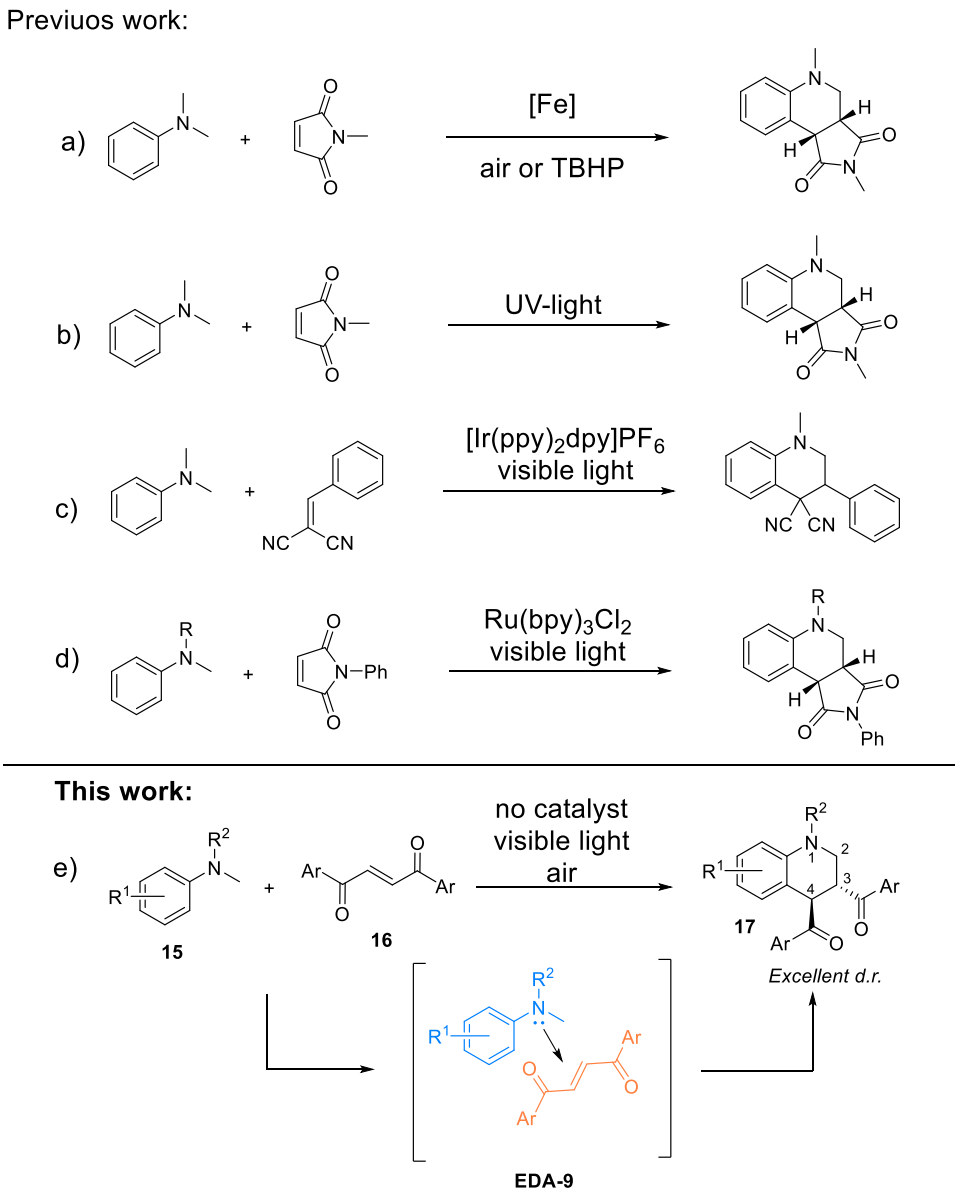

The previous methods typically require a transition metal complex as catalyst (Scheme 10 a, c and d), or high energy UV light as the energy source (Scheme 10b). Inspired by the work by Sundén and co-workers,[19] reporting a catalyst free version of the annulation reaction (Scheme 10b) relying on complex **EDA-7** (Scheme 6), it was hypothesized that the 1,2-dibenzoylethylene **16** could be used as an acceptor in the same manner together with the amine **15** to form **EDA-9**. Photoactivation of **EDA-9** followed by CT would render an a-amino radical that would undergo a Michael addition annulation sequence to render a novel class of 3,4-substituted THQs **17**.

4.3 Development of Reaction Conditions

As a model reaction, the 4',N,N-trimethylaniline **18**, and 1,2-dibenzoyl ethylene **16** (DBE) was chosen as reactants. Initial investigations confirmed the formation of an EDA complex between **16** and **18** (Figure 3). Upon mixing of the two components in acetonitrile as solvent, a color change from light yellow to orange could be observed. UV-vis measurements confirmed the formation a new absorption band in the visible region not present in the single components.

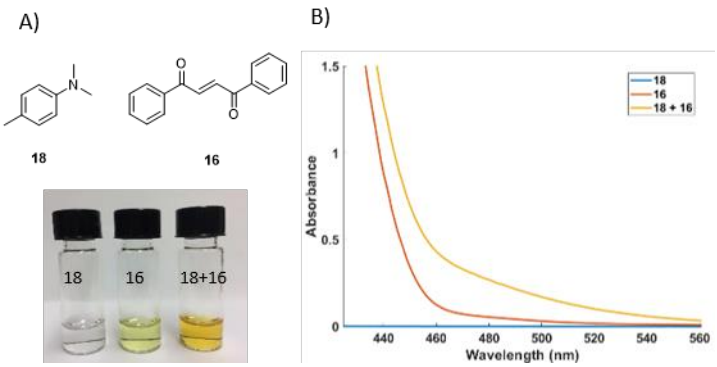

*Figure 3. A) Photos of **18**, **16**, and **18 + 16** in acetonitrile; B) UV-vis absorption spectra of **1a** (0.1 M), **2a** (0.1 M), **1a + 2a** in acetonitrile.*

This typical indication of an EDA complex prompted investigation of the photoproducts upon excitation with visible light. Due to the broad emission spectrum, high power and availability, a compact fluorescent light (CFL) was used as irradiation source.

After an irradiation time of 4 hours, the formation of THQ **19** could be observed in 25% yield. Albeit a low yield, this result promoted further investigations and optimizations. Notably, only the *trans* diastereomer of **19** was observed. In Table 1, results from the optimization of the reaction conditions are presented.

Table 1. Optimization of the reaction conditions

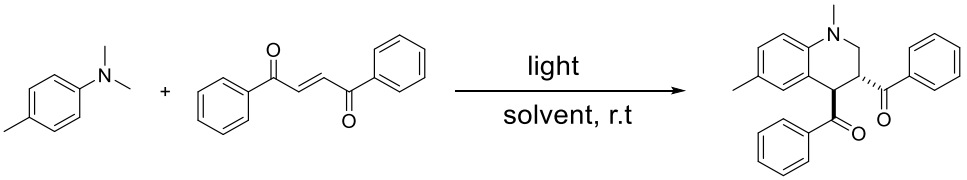

18 **16** **19**

Entry[a]	Solvent	Light	Yield **19** (%)	d.r.[b]
1	Acetonitrile	CFL	25	>25:1
2	Methanol	CFL	14	>25:1
3	THF	CFL	29	>25:1
4	Ethyl acetate	CFL	17	>25:1
5	Dichloromethane	CFL	40	>25:1
6	1,2-Dichloroethane	CFL	41	>25:1
7	1,2-Dimethoxyethane	CFL	32	>25:1
8	1,4-Dioxane	CFL	65	>25:1
9	1,4-Dioxane	CFL	30[c]	>25:1
10	1,4-Dioxane	CFL	0[d]	-
11	1,4-Dioxane	CFL	12[e]	>25:1
12	1,4-Dioxane	CFL	37[f]	>25:1
13	1,4-Dioxane/water	CFL	47[f]	>25:1
14	1,4-Dioxane	Blue LED	23	>25:1
15	1,4-Dioxane	CFL	68[g]	>25:1
16	1,4-Dioxane	CFL	73[h]	>25:1
17	1,4-Dioxane	UV-CFL	30	>25:1
18	1,4-Dioxane	-	0[i]	-
19	1,4-Dioxane	Blue LED	60[h, j]	>25:1

a) Reaction conditions: **18** (0.7 mmol) and **16** (0.1 mmol) in 3 mL solvent irradiated with 2x 15 W compact fluorescent lamps in room temperature for 4 hours; b) determined by NMR with 1,2,4,5-tetramethylbenzene as internal standard; c) 4 equiv. amine; d) under Ar; e) under O_2; f) $K_2S_2O_8$ (2 equiv.) used as an additive; g) acetic acid (30 equiv.) used as additive; h) acetic acid (80 equiv.) used as additive; i) reaction performed in absence of light; j) reaction time 12 hours.

Due to the nature of the EDA complex interaction, and the SET event, the choice of solvent is highly important (compare to equation 10). A survey of solvents was therefore investigated, and 1,4-dioxane was found to be the best choice, promoting a yield of 65% (Table 1, entry 8). More polar solvents, such as methanol, showed inferior results (Table 1, entry 2). The choice of solvent in this reaction influences both the formation and stability of the EDA complex and its photophysical properties, as well as the subsequent radical reactions.

To increase the yield further, the effect of different additives was investigated. It was hypothesized that a Lewis acid would coordinate the carbonyl compound **16** and hence lower the energy of the LUMO to facilitate the SET from the donor **18**. However, no improvements could be seen. The Bronsted base cesium carbonate resulted in lower yield; however acetic acid could increase the yield to 73%. The effect of acetic acid on similar reactions has been reported previously.[50]

4.4 Reaction scope and limitations

With our optimized conditions in hand, a survey of different 1,2-dibenzoyl ethylenes was tested in the reaction (Scheme 11). Simple alkyl substituted DBEs, gave the products **20-23** in moderate yields. A slight effect of the electronic nature of the acceptor DBE could be observed in the series, where the more electron rich 4,4'-bis-*tert*-butyl substituted DBE gave decreased yield of **22** compared to the 4,4'-bis-methyl substituted analogue **20**. This trend is expected since the electron affinity of the acceptor is highly important both in the formation of the EDA complex, and for the SET event. Accordingly, methoxy substituted DBE provided the compound **24** in 50% yield. Following the same trend, the compounds **26** and **27** could be isolated in good yields of 84% and 72% respectively, probably partly as a result of the electron withdrawing properties of the bromide and chloride substituents. The trifluoromethyl compound **25**, however, resulted in a sluggish reaction and only 28% could be isolated. In this case the low yield could be explained by low selectivity and side reactions.

To investigate if any selectivity in the radical Michael addition is present, an unsymmetric DBE with a methoxy substituent in the *para* position on one of the aryl rings, was subjected to the reaction conditions. However, no selectivity could be observed, and the two regio-isomers **28a** and **28b** were isolated as an inseparable mixture in equimolar amount. Interestingly, the combined yield of 64% was higher than for **24**, reflecting the importance of the electronic nature of the DBE reaction partner.

Notably, no instance of the formation of the *syn*-diastereomer of the products was observed when investigating the scope, disclosing the excellent diastereoselectivity of the delevoped reaction. The *anti*-configuration was confirmed by single crystal X-ray diffraction of the compound **35** (Figure 4).

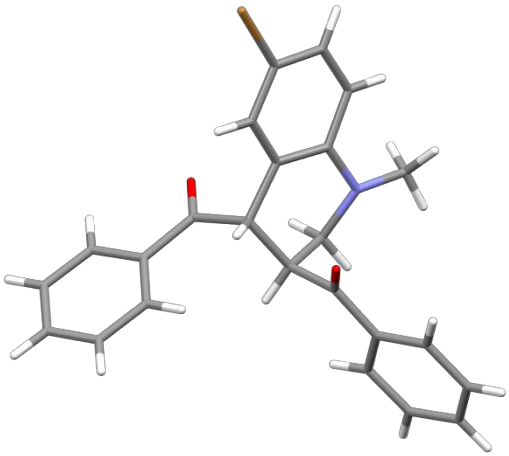

*Figure 4. Asymmetric unit of compound **35.***

Scheme 11. Investigation of the scope with respect to the dibenzoyl ethylene reaction partner.

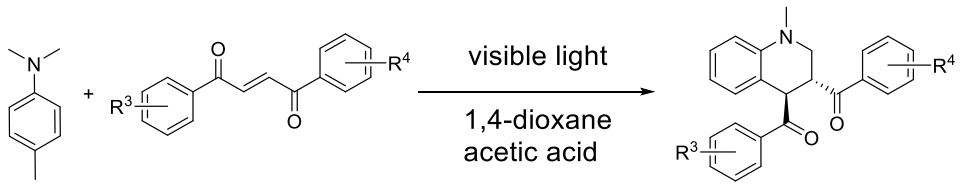

18 **19-28**

Substituted Dibenzoylethylene

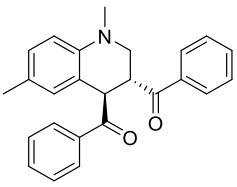

19 (73%, d.r. >25:1)

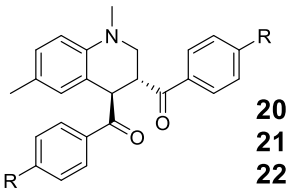

20, R = Me (63%, d.r. >25:1)
21, R = *i*-Bu (52%, d.r. >25:1)
22, R = *t*-Bu (45%,d.r. >25:1)

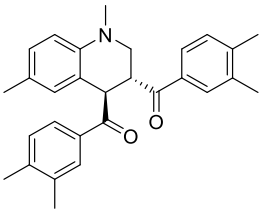

23 (46%,d.r. >25:1)

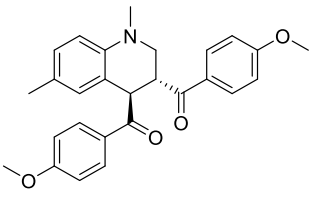

24 (50%, d.r. >25:1)

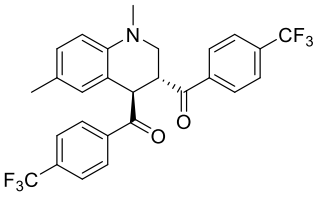

25 (28%, d.r. n.d.)

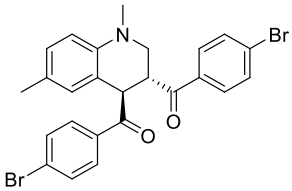

26 (84%, d.r. >25:1)

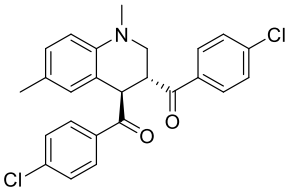

27 (72%, d.r. >25:1)

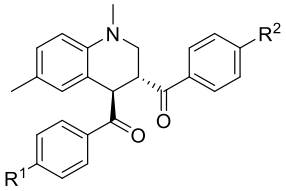

28a, R^1 = OMe, R^2 = H
28b R^1 = H, R^2 = OMe
(64%, d.r. >25:1) 1:1

Next, a set of dialkylated anilines were subjected to the reaction conditions in combination with the acceptor **19** (Scheme 12). As the rate determining step of the reaction likely involves a SET from the amine to the alkene, the oxidation potential of the amine is expected to have significant influence on the reaction outcome (see equation 9). More electron rich (lower oxidation potential) amines would be expected to take part more easily in the SET. Accordingly, the simple *N,N*-dimethylaniline afforded product **29** in decreased yield of 59 %, compared to the more electron rich 4',*N,N*-trimethylaniline. The formation of the EDA complex is further influenced by steric effects, and when the 2',*N,N*-trimethylaniline was combined with the acceptor **19**, a much weaker color change was observed. As a result, the reaction rate was significantly decreased for the photochemical reaction and compound **30** was only observed in trace amounts under the present conditions. Introduction of two methyl groups in the *meta* positions on the aniline also resulted in lower reaction rate, however not to the same degree.

A notable property of the reaction is the complete selectivity towards reaction at *N*-methyl groups of the dialkyl aniline. When the *N*-Me-*N*-Et-aniline was used as the substrate, only compound **37** was observed, and could be isolated in 46 % yield. The same selectivity was observed for *N*-Me-*N*-Bu-aniline and *N*-Me-*N*-Bn-aniline. The reason for this reactivity can be explained by the difference in pKa of the two different types of α-protons in the amine radical cation formed after SET, and the reactivity of the primary *versus* the secondary carbon centered radical formed after the deprotonation.[51] According to DFT calculations for a similar system, the energy barrier for the radical Michael addition of methyl radical to methyl vinyl ketone is lower by 6.9 kcal/mol compared to the same addition by the benzyl radical.[51] Likely, a similar scenario is true for the radical addition to the DBE, resulting in the observed selectivity. When *N*-Me-aniline was tested as the substrate however, no annulation product could be observed. The reason for this is probably due to the much faster BET compared to deprotonation, and the failure to furnish the α-aminoalkyl radical from secondary anilines is well known.[52] Finally, *N,N*-diethylaniline, albeit visibly forming an EDA complex with the acceptor **16**, results in no product formation upon irradiation. The reason for this could also likely be explained by the relative rates of deprotonation and BET.

Scheme 12. Investigation of the scope with respect to the aniline reaction partner.

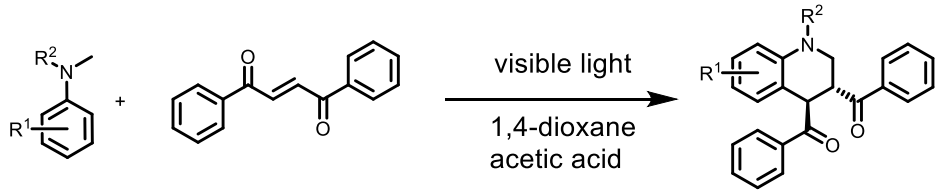

16 **29-41**

Substituted Aniline

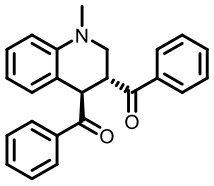

29 (59%, d.r. >25:1)

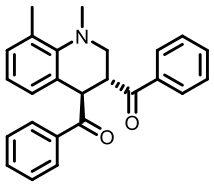

30 (traces)

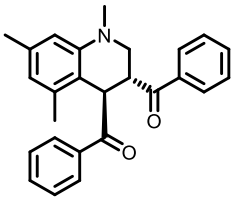

31 (42%, d.r. >25:1)

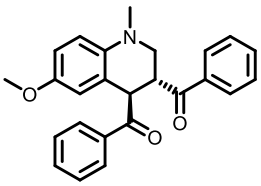

32 (61%, d.r. >25:1)

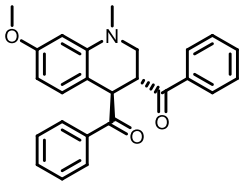

33 (28%, d.r. >25:1)

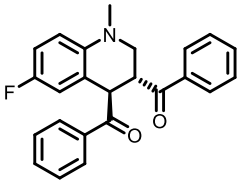

34 (51%, d.r. >25:1)

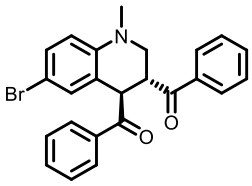

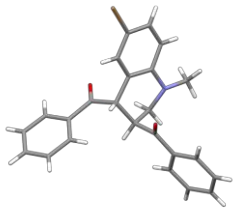

35 (24%, d.r. >25:1)

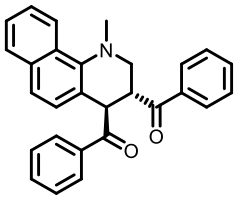

36 (18%, d.r. n.d.)

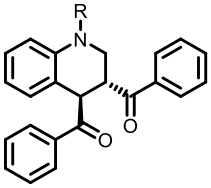

37, R = Et (46%, d.r. n.d.)
38, R = *n*-Bu (60%, d.r. n.d.)
39, R = Bn (25%,d.r. >25:1)
40, R = H (traces)

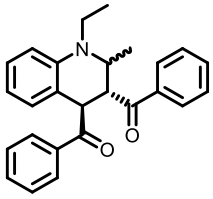

41 (traces)

Apart from the selectivity towards reactivity at the N-Me group of the aniline reaction partner, another significant feature of the developed protocol is the complete selectivity towards the formation of the *anti*-diastereomer. Since the E/Z photoisomerization of **16** and related structures is well known,[53] we wanted to investigate if the starting configuration of the double bond would influence the diastereoselectivity. Accordingly, the *Z*-isomer of **16** was subjected to the reaction conditions in combination with **18**. Notably, only the *anti*-isomer of **19** was observed, albeit in lower yield. The diastereoconvergent feature is signifying that that geometry of the alkene is of little impotence for the reaction outcome and that there is a bond rotation involved in the mechanism after radical addition to the double bond.

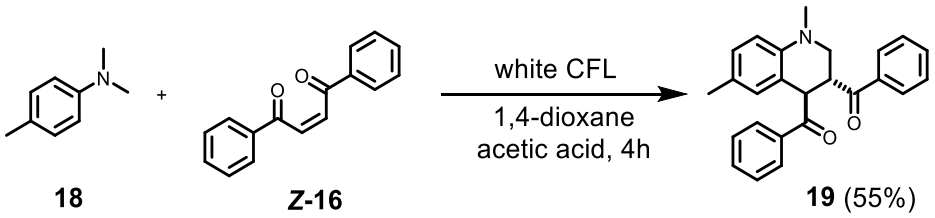

18 ***Z*-16** **19** (55%)

The lower reaction rate can be explained by the difference in redox potential between ***E*-16** and ***Z*-16**,[54] rendering the *Z*-isomer a slightly weaker acceptor.

4.5 Proposed mechanism

Based on the literature and control experiments, which concluded that light irradiation and oxygen are needed to promote the reaction (Table 1, entry 10 and 18), in combination with an observed quantum yield of 4.5, a proposed mechanism could be postulated (Scheme 13). Initially, an EDA complex forms between the donor and acceptor, as evident by the emergence of a new charge transfer band in the absorption spectrum (Figure X). Light excitation of this complex results in a SET and, after proton transfer, the α-amino alkyl radical **A** and the enol radical **B**. The radical **A** readily reacts with **16**, forming intermediate **C**.

Scheme 13. Proposed mechanism for the oxidative annulation reaction.

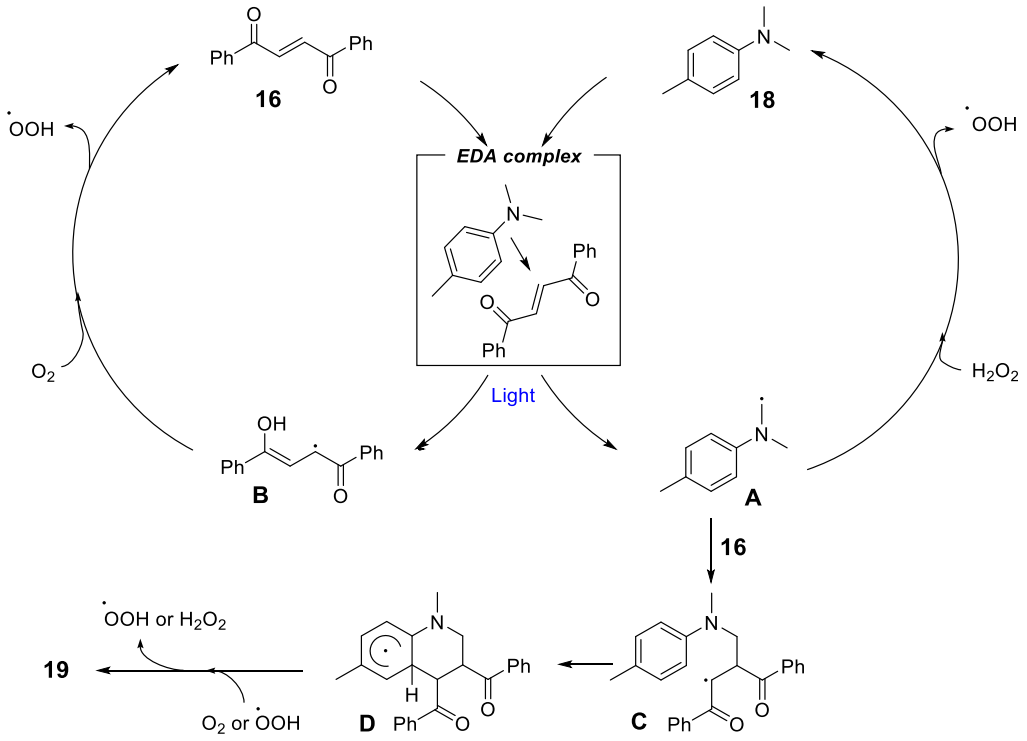

In this step it is hypothesized that the diasteroeoselectivity occurs as the result of a steric clash between the two phenyl groups. Intermediate **C** the undergoes intramolecular cyclization and after aromatization the final product **19** is formed. The radical **B** is proposed to be oxidized back to **16**, with the generation of a hydroxyperoxyl radical. The oxygen centered radical can then either generate **A** by hydrogen atom abstraction from **18**, or oxidize the intermediate **D**.[55] Due to a quantum yield above one, it is possible that **D** also can be oxidized by molecular oxygen, forming another hydroxyperoxyl radical that can propagate a radical chain mechanism.

4.6 Applicability and derivatization

To improve the step economy and investigate the modularity of the reaction, a multicomponent variant was developed (Scheme X). The acceptor **16** could efficiently be formed *in situ* from the corresponding penyl glyoxal and Wittig reagent. In combination with **18** under irradiation, the desired product could be isolated in 40 % yield, corresponding to an average of 80 % yield per bond. This method could prove useful when developing unsymmetric variants of **19** without the need of synthesizing the corresponding DBE.

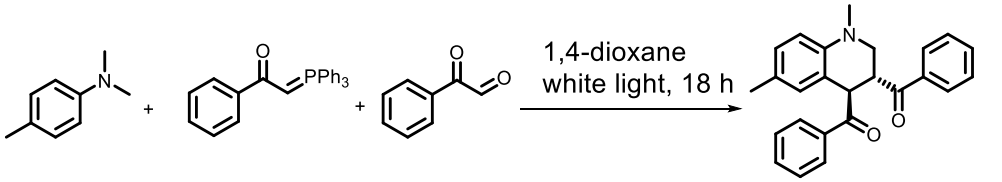

Derivatization of the formed product was also briefly investigated. The 1,4-dicarbonyl compound **19** is set up for a range of different condensation reactions with the potential of delivering fused heterocyclic compounds. To test this hypothesis, **19** was subjected to ammonium acetate in acetic acid (Scheme 14a) to yield the pyrrole derivative **44**. Interestingly, only the oxidized 3*H*-pyrrole compound could be isolated under these conditions.

*Scheme 14. Derivatisation of the THQ **19**.*

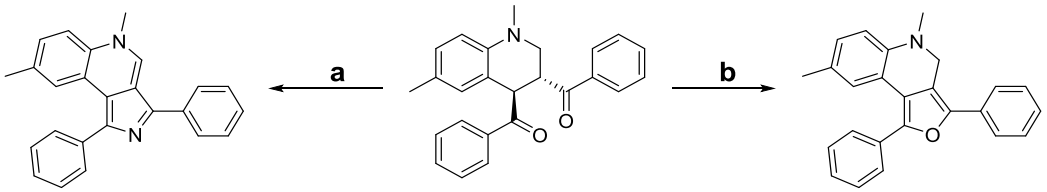

44 (43%) **19** **45** (56%)

Likewise, upon reaction of **19** in acidic conditions and acetic anhydride, the fused furan derivative **45** could be isolated in moderate yield. These derivatizations demonstrate the potential use of THQ structures of the type **19** as starting materials for novel fused heterocycles.

4.7 Conclusion

In summary, a protocol for the synthesis of novel THQ derivatives using mild conditions and visible light irradiation was developed. The reaction is proposed to proceed *via* the photoactivation of an EDA complex between *N,N*-dialkyl anilines as donors and 1,2-dibenzoyl ethylenes as acceptors. The excellent diastereoselectivity and the substrate scope presented shows that the method is a viable pathway to 3,4-disubstituted THQs. Furthermore, complete selectivity towards *N*-Me activation allows for the selective construction of *N*-substituted THQs. The mild conditions, and use of aerobic oxygen as the terminal oxidant, makes the developed protocol attractive from a sustainability perspective.

5. Aerobic oxidative EDA catalysis. Synthesis of tetrahydroquinolines using a catalytic EDA active acceptor (Paper II)

5.1 Catalytic EDA complexes

As outlined in section 2.4.1, the classical approach of stoichiometric EDA complexes limits the available substrates to specific combinations of donors and acceptors. If substrates with mismatched redox potentials could be activated by a catalyst and then take part in the complex formation, the generality of the EDA complex photochemistry could be broadened.[10] Different methods relying on enamine activation[22], iminium ion activation,[56,57] or enolate formation[58] have been developed within the catalytic regime. In these examples, a transient donor or acceptor is formed *in situ via* covalent activation and takes part in the EDA complex formation. Scheme 15a illustrates two examples of another approach where an external donor is present in catalytic amount.[21,23] This approach offers more flexibility in terms of radical formation if a general donor can be applied. Despite the many examples of external donors in EDA complex driven photoreactions, very little research towards using catalytic acceptors in the same manner can be found in the literature. In 2020, Ooi and coworkers reported the use of a triaryl borane as a catalytic acceptor for the net redox neutral coupling between tetrahydroisoquinolines and α,β-unsaturated ketones (Scheme 15b).[59] However, to the best of our knowledge, no system for the oxidative coupling between amines and activated alkenes based on a catalytic acceptor can be found in the literature.

Based on the results presented in the previous Chapter 4, it was hypothesized that the acceptor **16** could be a suitable candidate for a catalytic donor system under oxidative conditions.

Scheme 15. Examples of catalytic photoactive EDA complexes in organic synhtesis.

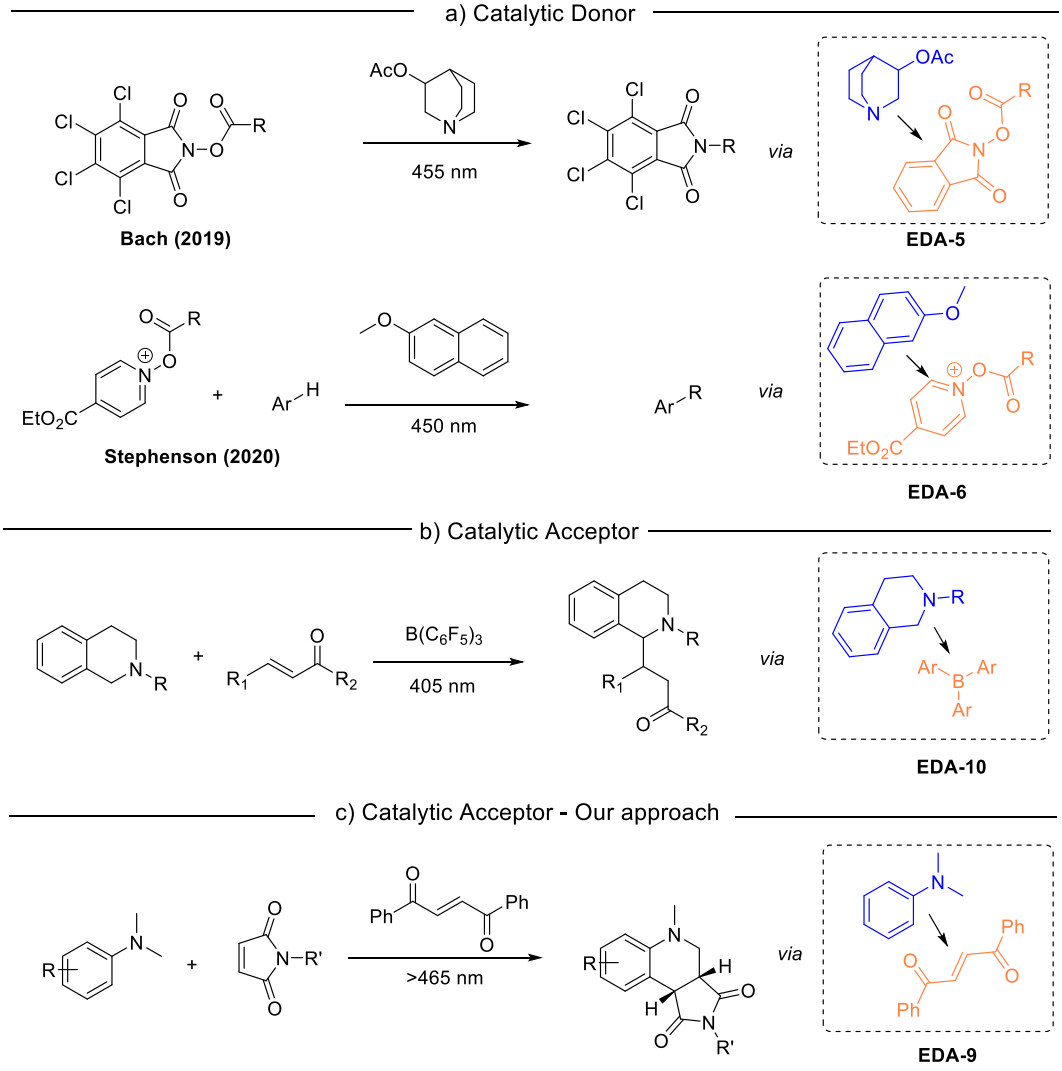

5.2 Optimization of conditions

As the model system for the evaluation of the hypothesis was chosen the oxidative annulation reaction between *N,N*-dialkylanilines and maleimides due to the known reactivity of α-aminoalkyl radicals with maleimides.[19,43–46,55,60–81] It is known that the reaction between maleimides and dialkylanilines proceeds smoothly under UV-irradiation,[19] however using visible light the reaction is slow. By contrast, the reaction of **16** with *N,N*-dimethylanilines can be promoted with visible light as outlined in Paper I. It was therefore postulated that a catalytic amount of the EDA complex between **16** and *N,N*-dimethylaniline would produce α-aminoalkyl radicals by excitation with visible light that could react with maleimides to furnish annulation products. Under oxidative conditions, **16** could be regenerated according to Figure 5.

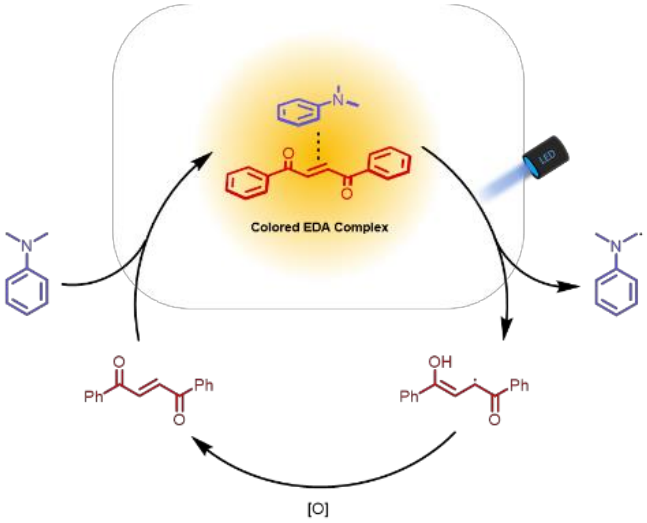

Figure 5. Schematic overview of the hypothesis.

To study the outlined hypothesis we choose to the reaction between *N,N*-dimethylaniline **46** and *N*-phenylmaleimide **47** to form the annulation product **48** as our model reaction. Based on the solvent screening outlined in Paper I, and in the literature for similar systems,[19] 1,4-dioxane was chosen as the solvent for optimization. Initially a compact fluorescent lamp (CFL) was chosen as the irradiation source. The background reaction between **46** and **47** proceeded to 7% yield (Table 2, entry 1) of **48** after 6 hours irradiation time. However, the addition of only 1 mol % **16** promoted a significant increase in the product formation to 53% (Table 2, entry 2). Increasing the loading of **16** to 5 mol %, a yield of 80 % was observed.

Table 2. Optimization of the reaction conditions.

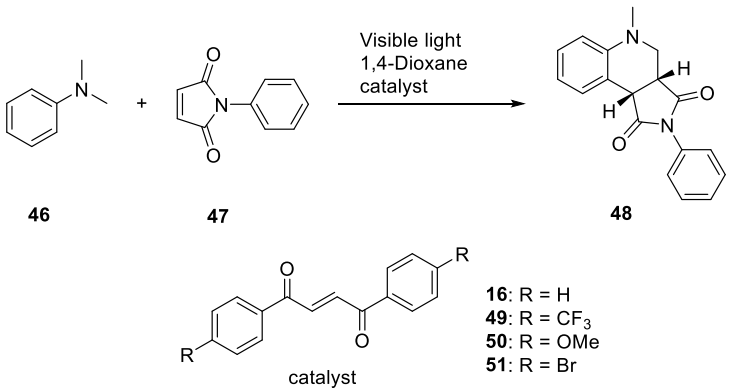

entry	cat. (mol%)	light source	**46** (eq.)	time (h)	yield **48** (%) [b]
1	-	CFL	7	6	7[c]
2	**16** (1)	CFL	7	6	53
3	**16** (5)	CFL	7	6	80
4	**49** (5)	CFL	7	6	26
5	**50** (5)	CFL	7	6	80
6	**51** (5)	CFL	7	6	26
7	**16** (5)	CFL	1	6	40
8	**16** (5)	CFL	2	6	42
9	**16** (5)	CFL	5	6	82
10	**16** (5)	-	7	7	12[d]
11	**16** (8)	Green LED	7	26	56
12	**16** (5)	Blue LED	7	7	85
13	**16** (5)	Blue LED	7	7	3[e]

The electronic properties of the DBE catalyst should play an important role if it acts as a single electron acceptor in the reaction. To evaluate this, a set of *para*-substituted DBEs was tested as catalysts in the reaction. It was observed that the electron withdrawing groups trifluoromethyl and bromide lowered the reaction rate significantly (Table 1, entries 4 and 6) while the electron donating group methoxy did not affect the yield (Table 1, entry 5). The stoichiometry of **46** was briefly investigated and it was found that with only 5 equivalents, the reaction proceeded smoothly. Changing the light source to a blue LED (emission maximum of 465 nm) increased the yield to 85 %, and this was chosen to be the optimized conditions in the study.

5.3 Scope and limitations

Different maleimides were tested as Michael acceptors in the reaction to evaluate the generality of the developed system (Scheme 16). *N*-Aryl substituted maleimides were generally well tolerated (compounds **48** and **53**-**56** in 63 – 80% yield), except for *p*-methoxyphenyl which provided compound **52** in only 36 % yield. The reason for this could be the strong electron donating properties of the methoxy group rendering the maleimide a worse acceptor for the α-aminoalkyl radical. *N*-Benzyl substituted maleimides provided compounds **57** and **63** in 63 % and 60 % yield, respectively.

Scheme 16. Investigation of the scope with respect to the alkene reaction partner.

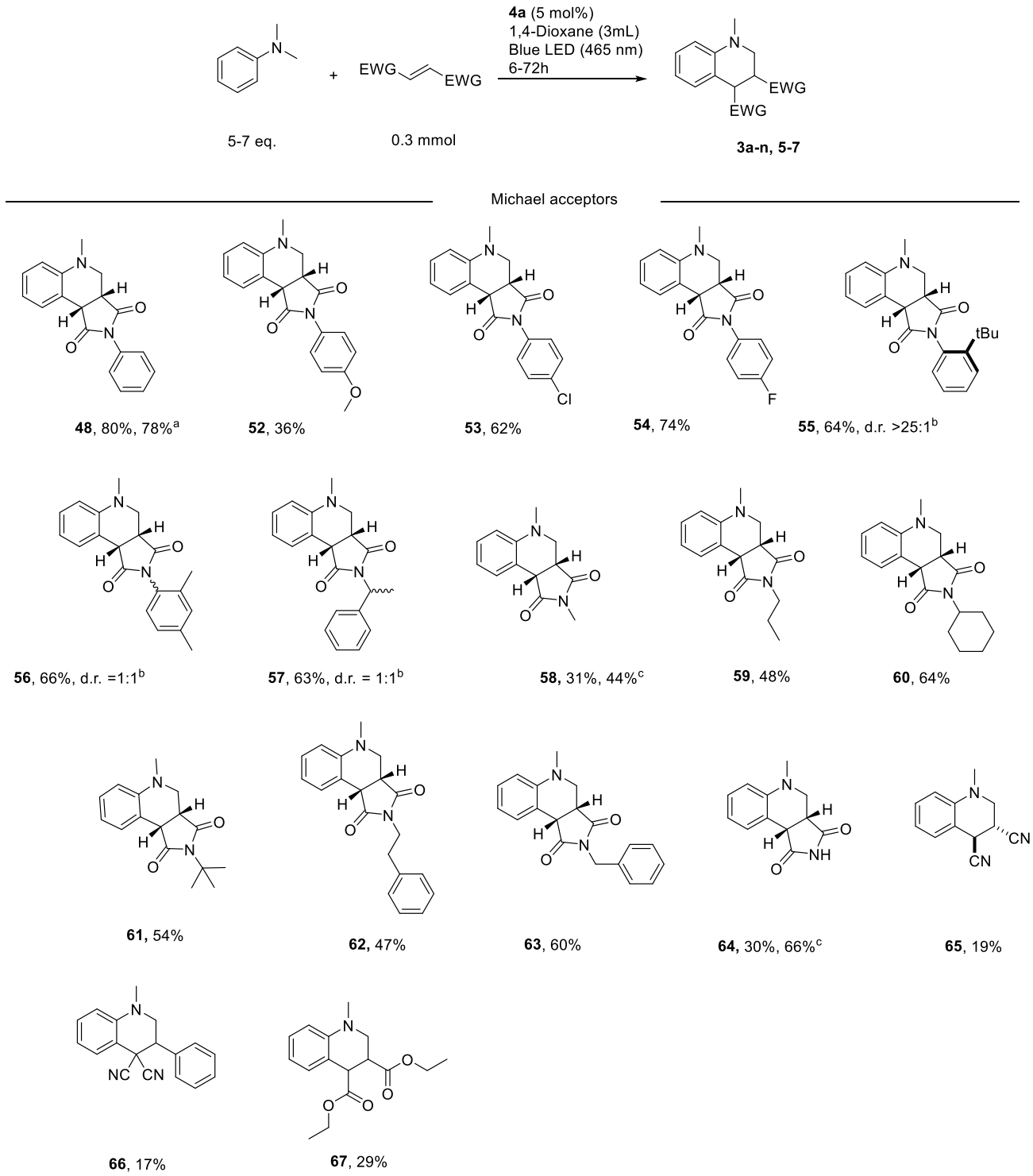

a) 4.4 mmol scale; b) determined by ^{1}H NMR; c) 18 hours reaction time

Compound **57** was obtained as a mixture of two diastereomers in equimolar amounts when starting from the enantiopure (S)-α-methyl benzylamine maleimide derivative. Separation of the diastereomers could not be achieved using standard flash chromatography, but if successful could provide a tool of preparing the two

enantiomers of the THQ scaffold after deprotection of the benzyl group. Complete diastereoselectivity was however observed for compound **55**. The energy barrier for rotation of the N-phenyl bond is significant due to the bulky *o*-*t*Bu group, but when heating **55** to 160 °C, the other diastereomer could be isolated.

Simple *N*-alkyl substituted maleimides performed worse, giving compounds **58**-**62** in 31 – 54 % yield. Likewise, unsubstituted maleimide and other Michael acceptors were poorly compatible with the reaction conditions, giving compounds **64** – **67** in 17-30 % yield.

Next, different anilines in combination with **47** were subjected to the reaction conditions giving the compounds **67** – **78** in 25 – 84 % yield. Generally, electron poor (compounds **71**-**73**) or sterically demanding (compounds **68** and **74**) anilines resulted in significant decrease in yield.

Consistent with the results presented in Paper I, *N*-alkyl-*N*-Me-anilines selectively reacted on the methyl group, giving the products **77** and **78** in 42 % and 58 % yield respectively. In line with the complete selectivity towards formation of methyl centered radicals, compound **79** was not observed when *N,N*-diethylaniline was used as the starting material.

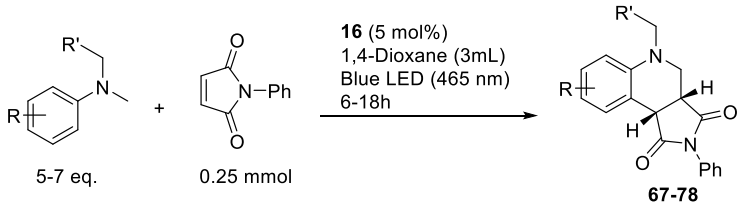

5-7 eq. 0.25 mmol **67-78**

Substituted Aniline

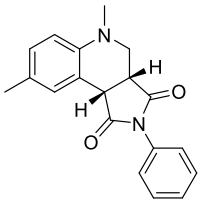

67, 84%

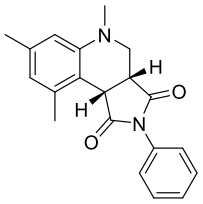

68, 53%

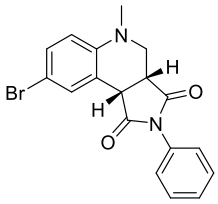

69, 70%[c]

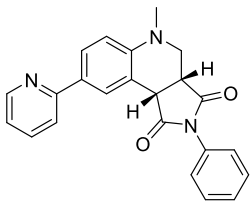

70, 68%[c]

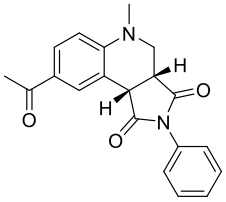

71, 47%

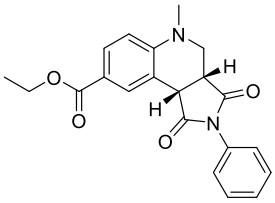

72, 30%

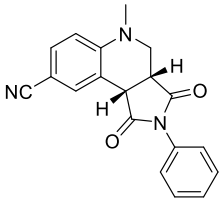

73, 25%[c]

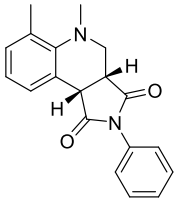

74, 43%

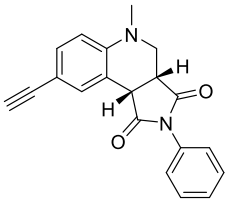

75, 25%

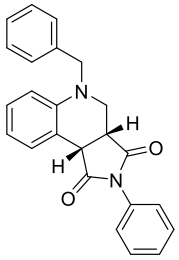

76, 42%

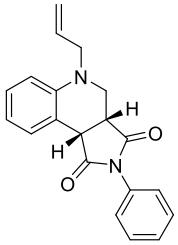

77, 58%

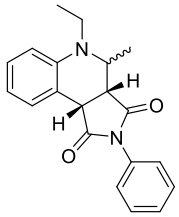

78, n.d[b]

5.4 Investigation of the mechanism

To get insight in the mechanism of the reaction, a series of control experiments were carried out. Firstly, it was evident that oxygen played a crucial role as the terminal oxidant since the reaction did not proceed under an atmosphere of nitrogen (Scheme 17a). Likewise, the reaction did not proceed to a significant degree when carried out in the dark at elevated temperatures. To confirm the radical character of the reaction, the known radical scavenger butylated hydroxy toluene (BHT) was used as additive under the optimized conditions. The addition of BHT lead to significant decrease in yield, supporting the notion of a radical pathway (Scheme 17b). The reaction was also carried out in the presence of histidine, to rule out any significant contribution from singlet oxygen (Scheme 17b).[55]

Scheme 17. Control experiments.

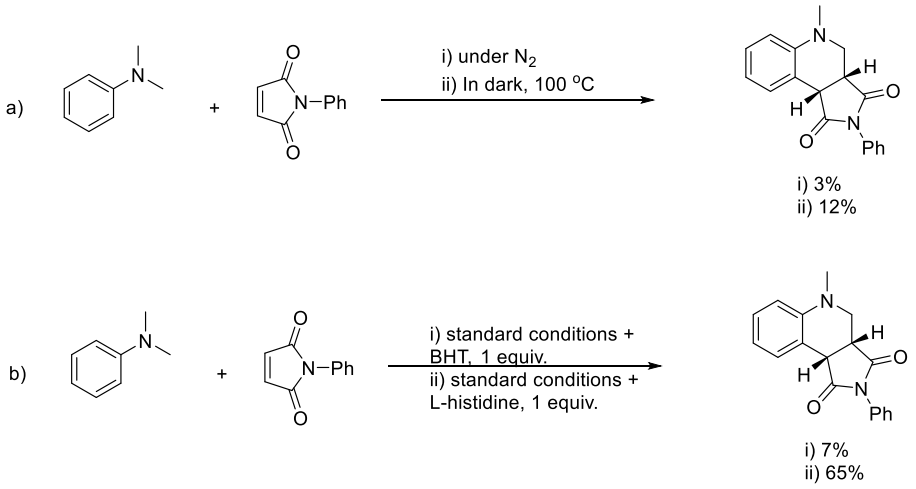

The effect of deuterium substitution on the aniline reaction partner was then investigated. Due to the higher mass of the deuterium atom compared to the hydrogen atom, the energy barrier for C-D cleavage is higher than C-H cleavage. This results in a decrease in reaction rate for reactions in which the rate determining step involves the break of a C-H bond if the hyrdogen is changed to a deuterium. A measure of this phenomena is the kinetic isotope effect (KIE), and in the context for this work it can be expressed according to equation 15:

$$KIE = \frac{k_H}{k_D} \qquad (15)$$

Where k_H is the rate constant for the reaction involving C-H cleavage, and k_D is the rate constant for the reaction involving the C-D cleavage. Depending on the nature of the reaction (e.g. hydrogen atom abstraction or deprotonation), different values of the KIE can be observed. Therefore, isotope experiments can provide important insights in the mechanism of a reaction.

Accordingly, two different isotope experiments were investigated (Scheme 18)

Scheme 18. Kinetic isotope effect experiments.

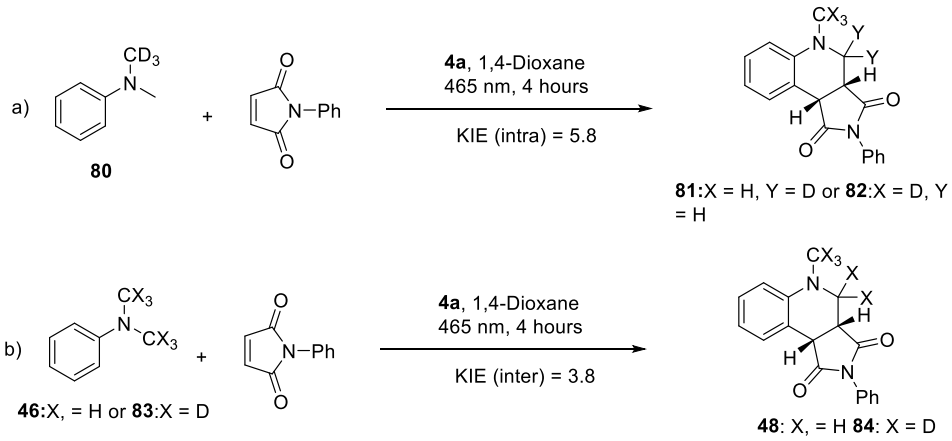

First, the *intramolecular* KIE was measured by using the deuterated aniline **80** as the starting material. The reaction was stopped after 4 hours irradiation time and then the ratio between the compounds **81** and **82** was calculated using ^{1}H NMR of the crude reaction mixture. It was observed that reaction at the CH_3 group was 5.8 times faster than the corresponding reaction at the CD_3 group. Next, an *intermolecular* KIE was established by carrying out a competition experiment where a 1:1 mixture of **46** and the deuterated aniline **83** was reacted with **47**. The ratio between the products **48** and **84** was then calculated using ^{1}H NMR on the crude reaction mixture. In this case a KIE of 3.8 was observed.

The fact that an overall KIE of 3.8 was observed suggests that the C-H cleavage could have a role in the rate determining step. More importantly, the difference between the intramolecular and intermolecular KIE gives some meaningful clues to the mechanism. If the reaction proceeds *via* a one-step hydrogen atom transfer (HAT) mechanism, the intra- and intermolecular KIE would be expected to be identical. However, if a two-step mechanism with similar energy barriers is operating, a difference in the two KIEs can be observed. The reaction basis for a kinetic model in the oxidative demethylation of *N,N*-dimethylanilines, as outlined by Watanabe and co-workers, is outlined in Scheme 19.[82] In the two-step reaction aniline **46** is reversibly oxidized to the radical cation **85** which is then irreversibly deprotonated to the radical **86** (Scheme 19a). The observed overall reaction is presented in Scheme 19b.

Scheme 19. The two-step formation of amino alkyl radical.

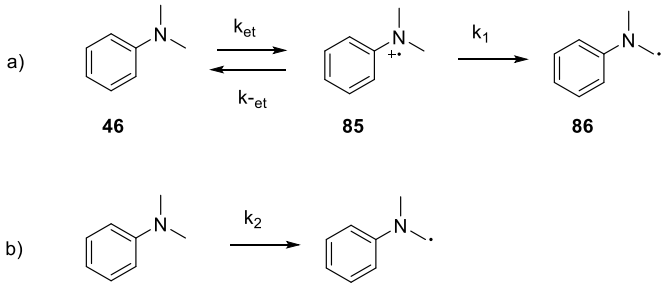

In these reactions, the intramolecular KIE depends only on the rate of the deprotonation and can be expressed as $k_{1,H}/k_{1,D}$. The intermolecular KIE will depend on the overall rate k_2, and can be expressed as $k_{2,H}/k_{2,D}$. With the

assumption that the concentration of **85** is constant, the ratio between k_1 and k_{-et} will determine k_2. Accordingly, $k_{1,H}/k_{1,D}$ and $k_{2,H}/k_{2,D}$ will be different. The relation between the two ratios can be expressed according to equation 16.[82]

$$\frac{k_{2,H}}{k_{2,D}} = \frac{k_{1,H}}{k_{1,D}}\left(\frac{k_{-et}+k_{1,D}}{k_{-et}+k_{1,H}}\right) \quad (16)$$

Two extremes can be distinguished: $k_{-et} << k_1$ and $k_{-et} >> k_1$. In the former case, the overall KIE will be 1. In other words, the very slow BET compared to the deprotonation renders the SET the completely rate determining step. In the latter case, equation 15 simplifies to $k_{2,H}/k_{2,D} = k_{1,H}/k_{1,D}$, and the deprotonation step becomes the rate determining. In cases where BET and deprotonation occurs at similar rate, a difference in the $k_{2,H}/k_{2,D}$ and $k_{1,H}/k_{1,D}$ is observed. Importantly, the relation $k_{2,H}/k_{2,D} \leq k_{1,H}/k_{1,D}$ is always true for the system outlined in Scheme 19. With this background, the KIE experiments in Scheme 18 (intramolecular KIE of 5.8 and intermolecular KIE of 3.8) suggests a two-step mechanism involving an intermediate amine radical cation as in Scheme 19.

To further test the hypothesis that a buildup of a positive charge occurs in the intermediate, a Hammett analysis was performed (Figure 6).

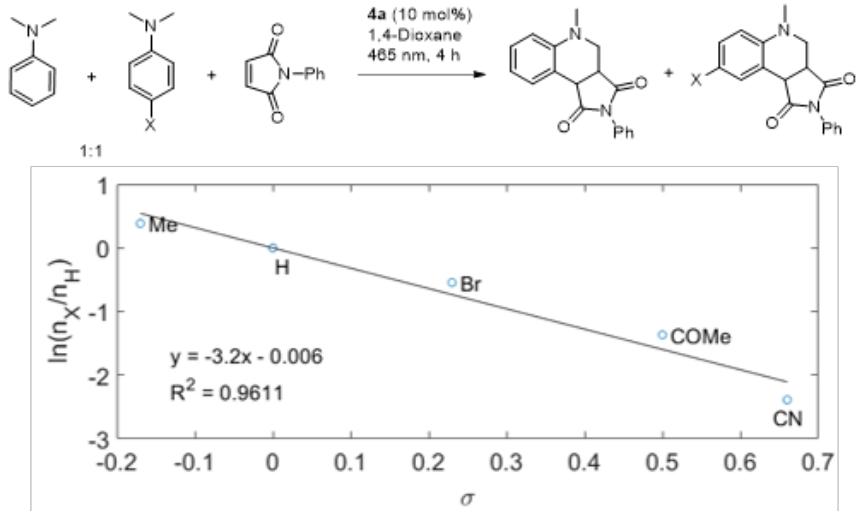

Figure 6. Investigation of the effect of aromatic substituents on the relative reaction rate.

For the analysis, a series of competition experiments were carried out where mixtures of **46** and *p*-substituted *N,N*-dimethylanilines in equimolar amounts were used as reactants in the photoreaction. The ratio of the corresponding products was then measured using ^{1}H NMR and were plotted against the Hammett sigma parameter. A significant influence on the electronic properties of the anilines was observed, in line with the formation of a radical cation intermediate.[83,84]

Based on the results from the control experiment and previous reports on similar systems, a mechanism for the developed photoreaction could be postulated (Scheme 20).[19,55,69,75,85] The formation of the α-aminoalkyl radical can be rationalized according to two different scenarios. In the first case (cycle A in Scheme 20), **16** absorbs a photon and is promoted to its excited state, **16***. This strong oxidant can then accept an electron from **46** to form the radical anion of **16** and an amine radical cation. Oxygen then intercepts the radical anion to reform **16**, whereas the radical cation is deprotonated to form an α-aminoalkyl radical. In the other scenario (cycle B inScheme 20), **16** acts as an acceptor in a ground-state EDA complex together with the amine **46**. Excitation of

this complex results in the formation of the radical anion of **16** and the radical cation of **46**. Deprotonation of the amine radical cation to yield the α-aminoalkyl radical can then occur in the solvent cage or after dissociation of the radical ion pair. Regardless of the mechanism, the α-aminoalkyl radical then takes part in a Giese radical addition with **47** to form a transient cyclohexadienyl radical that is readily oxidized to form the final product.

Scheme 20. Proposed mehcanism.

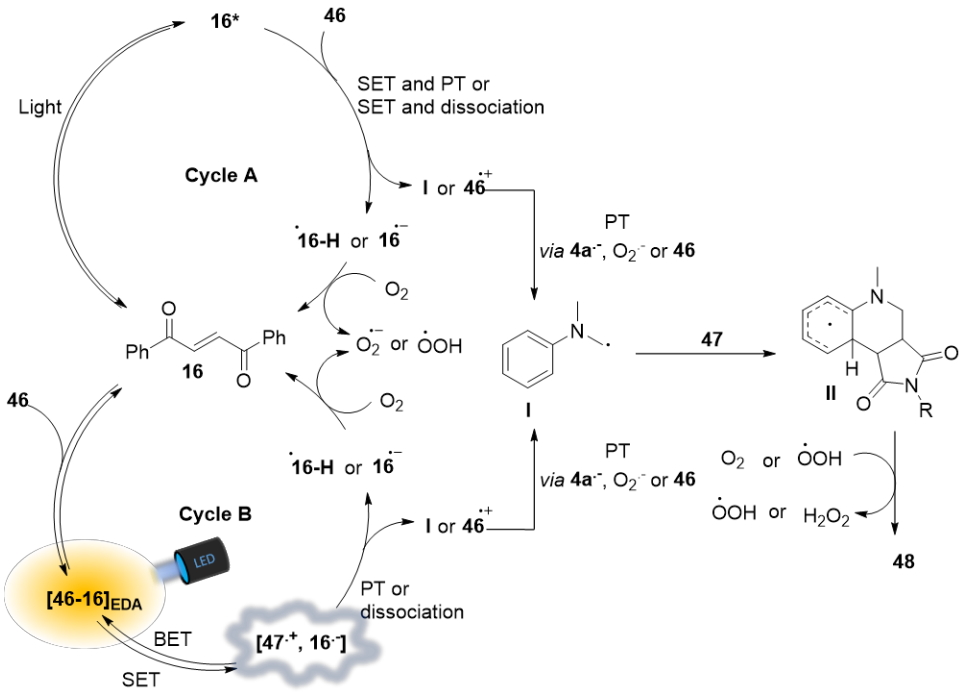

It is difficult to distinguish between whether cycle A or cycle B is operating. However, the observation that the reaction can be promoted, albeit with lower reaction rate, by 525 nm LED suggests that cycle B is contributing to a significant degree. At this wavelength, **16** has a very low absorption compared to the EDA complex between **16** and amines (Figure 3).

5.6 Conclusion

In the discussed paper, a new photocatalytic system for the oxidative annulation reaction between *N,N*-dialkyl anilines and activated alkenes has been developed. The catalyst, 1,2-dibenzoyl ethylene, is postulated to form a photoactive EDA complex with the amine reaction partner which drives the reaction. The products, tetrahydroquinolines, can be formed in high yields and under mild reaction conditions with low energy light. Being a simple and available compound, the 1,2-dibenzoyl ethylene is an attractive catalyst for the type of reaction developed. Its use as a catalytic acceptor in an EDA complex driven reaction should further stimulate the field of EDA complex photochemistry in the quest of finding new reactivities.

Conclusions and outlook

In this thesis, two visible light-driven aerobic oxidative annulations have been reported. We have demonstrated that EDA complexes between 1,2-dibenzoyl ethylenes and *N,N*-dialkylanilines can drive the formation of a range of substituted tetrahydroquinoline derivatives under mild conditions using low energy light.

In the first part, we demonstrate the formation of a novel EDA complex between 1,2-dibenzoyl ethylenes and *N,N*-dialkylanilines. The complex absorbs in the visible region and gives access to a range of different 3,4-disubstituted tetrahydroquinolines upon photoexcitation. Products are formed with excellent diastereoselectivity and in moderate yields. Reaction conditions are mild, using visible light at room temperature and under ambient atmosphere. Aerobic oxygen acts as the terminal oxidant and is crucial to the reaction outcome. Furthermore, an operationally convenient multicomponent version of the reaction was developed, forming the activated alkene *in situ*, demonstrating the usability of the conditions.

In the second part, the synthetic powers of the EDA complex between 1,2-dibenzoyl ethylenes and *N,N*-dialkylanilines were expanded to the development of a catalytic protocol. In this method, the 1,2-dibenzoyl ethylene was used in catalytic amounts to drive photochemical reactions between *N,N*-dialkylanilines and maleimides. The turnover of the catalyst was achieved using aerobic oxidation. A range of substituted tetrahydroquinoline derivatives were obtained as products. The cheap and available catalyst, the mild reaction conditions and the use of aerobic oxygen as reagent, could make the developed protocol an attractive alternative for the formation of the target tetrahydroquinoline structures. Furthermore, we envision that this example of the use of a catalytic external acceptor for the formation of photo active EDA complexes will pave the way for the development of novel EDA mediated photochemistry.

Future research within the project will be focusing on the further development of aerobic oxidations in combination with photoactive EDA complexes. Aiming at the construction of complex molecular structures with visible light as the energy source, without the need of expensive transition metal-based photoredox catalysts.

References

(1) Rasmussen, S. C. Introduction − The Role of Chemical Technology in Early Civilizations. In *Chemical Technology in Antiquity*; ACS Symposium Series; American Chemical Society, 2015; Vol. 1211, p 1. https://doi.org/doi:10.1021/bk-2015-1211.ch001.

(2) GEORGE J. KAVARNOS. *Fundamentals of Photoinduced Electron Transfer*; VCH, 1993.

(3) Shaw, M. H.; Twilton, J.; MacMillan, D. W. C. Photoredox Catalysis in Organic Chemistry. *J. Org. Chem.* **2016**, *81* (16), 6898–6926. https://doi.org/10.1021/acs.joc.6b01449.

(4) Bevernaegie, R.; Wehlin, S. A. M.; Elias, B.; Troian-Gautier, L. A Roadmap Towards Visible Light Mediated Electron Transfer Chemistry with Iridium(III) Complexes. *ChemPhotoChem* **2021**, *5* (3), 217–234. https://doi.org/https://doi.org/10.1002/cptc.202000255.

(5) Vega-Peñaloza, A.; Mateos, J.; Companyó, X.; Escudero-Casao, M.; Dell'Amico, L. A Rational Approach to Organo-Photocatalysis: Novel Designs and Structure-Property Relationships. *Angew. Chemie Int. Ed.* **2021**, *60* (3), 1082–1097. https://doi.org/https://doi.org/10.1002/anie.202006416.

(6) Romero, N. A.; Nicewicz, D. A. Organic Photoredox Catalysis. *Chem. Rev.* **2016**, *116* (17), 10075–10166. https://doi.org/10.1021/acs.chemrev.6b00057.

(7) Hedstrand, D. M.; Kruizinga, W. H.; Kellogg, R. M. Light Induced and Dye Accelerated Reductions of Phenacyl Onium Salts by 1,4-Dihydropyridines. *Tetrahedron Lett.* **1978**, *19* (14), 1255–1258. https://doi.org/https://doi.org/10.1016/S0040-4039(01)94515-0.

(8) Condie, A. G.; González-Gómez, J. C.; Stephenson, C. R. J. Visible-Light Photoredox Catalysis: Aza-Henry Reactions via C–H Functionalization. *J. Am. Chem. Soc.* **2010**, *132* (5), 1464–1465. https://doi.org/10.1021/ja909145y.

(9) Welin, E. R.; Warkentin, A. A.; Conrad, J. C.; MacMillan, D. W. C. Enantioselective α-Alkylation of Aldehydes by Photoredox Organocatalysis: Rapid Access to Pharmacophore Fragments from β-Cyanoaldehydes. *Angew. Chemie Int. Ed.* **2015**, *54* (33), 9668–9672. https://doi.org/https://doi.org/10.1002/anie.201503789.

(10) Crisenza, G. E. M.; Mazzarella, D.; Melchiorre, P. Synthetic Methods Driven by the Photoactivity of Electron Donor–Acceptor Complexes. *J. Am. Chem. Soc.* **2020**, *142* (12), 5461–5476. https://doi.org/10.1021/jacs.0c01416.

(11) Lima, C. G. S.; de M. Lima, T.; Duarte, M.; Jurberg, I. D.; Paixão, M. W. Organic Synthesis Enabled by Light-Irradiation of EDA Complexes: Theoretical Background and Synthetic Applications. *ACS Catal.* **2016**, *6* (3), 1389–1407. https://doi.org/10.1021/acscatal.5b02386.

(12) Yuan, Y.; Majumder, S.; Yang, M.; Guo, S. Recent Advances in Catalyst-Free Photochemical Reactions via Electron-Donor-Acceptor (EDA) Complex Process. *Tetrahedron Lett.* **2020**, *61* (8), 151506. https://doi.org/10.1016/j.tetlet.2019.151506.

(13) Mulliken, R. S. Molecular Compounds and Their Spectra. III. The Interaction of Electron Donors and Acceptors. *J. Phys. Chem.* **1952**, *56* (7), 801–822. https://doi.org/10.1021/j150499a001.

(14) Sankararaman, S.; Haney, W. A.; Kochi, J. K. Annihilation of Aromatic Cation Radicals by Ion-Pair and Radical Pair Collapse. Unusual Solvent and Salt Effects in the Competition for Aromatic Substitution. *J. Am. Chem. Soc.* **1987**, *109* (25), 7824–7838. https://doi.org/10.1021/ja00259a035.

(15) Fukuzumi, S.; Mochida, K.; Kochi, J. K. A Unified Mechanism for Thermal and Photochemical Activation of Charge-Transfer Processes with Organometals. Steric Effects in the Insertion of Tetracyanoethylene. *J. Am. Chem. Soc.* **1979**, *101* (20), 5961–5972. https://doi.org/10.1021/ja00514a016.

(16) Fox, M. A.; Younathan, J.; Fryxell, G. E. Photoinitiation of the SRN1 Reaction by Excitation of Charge-Transfer Complexes. *J. Org. Chem.* **1983**, *48* (18), 3109–3112. https://doi.org/10.1021/jo00166a038.

(17) Tobisu, M.; Furukawa, T.; Chatani, N. Visible Light-Mediated Direct Arylation of Arenes and Heteroarenes Using Diaryliodonium Salts in the Presence and Absence of a Photocatalyst. *Chem. Lett.* **2013**, *42* (10), 1203–1205. https://doi.org/10.1246/cl.130547.

(18) Arceo, E.; Jurberg, I. D.; Álvarez-Fernández, A.; Melchiorre, P. Photochemical Activity of a Key Donor–Acceptor Complex Can Drive Stereoselective Catalytic α-Alkylation of Aldehydes. *Nat. Chem.* **2013**, *5* (9), 750–756. https://doi.org/10.1038/nchem.1727.

(19) Hsu, C.-W.; Sundén, H. α-Aminoalkyl Radical Addition to Maleimides via Electron Donor–Acceptor Complexes. *Org. Lett.* **2018**, *20* (7), 2051–2054. https://doi.org/10.1021/acs.orglett.8b00597.

(20) Guillemard, L.; Colobert, F.; Wencel-Delord, J. Visible-Light-Triggered, Metal- and Photocatalyst-Free Acylation of N-Heterocycles. *Adv. Synth. Catal.* **2018**, *360* (21), 4184–4190. https://doi.org/10.1002/adsc.201800692.

(21) McClain, E. J.; Monos, T. M.; Mori, M.; Beatty, J. W.; Stephenson, C. R. J. Design and Implementation of a Catalytic Electron Donor–Acceptor Complex Platform for Radical Trifluoromethylation and Alkylation. *ACS Catal.* **2020**, *10* (21), 12636–12641. https://doi.org/10.1021/acscatal.0c03837.

(22) Arceo, E.; Bahamonde, A.; Bergonzini, G.; Melchiorre, P. Enantioselective Direct α-Alkylation of Cyclic Ketones by Means of Photo-Organocatalysis. *Chem. Sci.* **2014**, *5* (6), 2438–2442. https://doi.org/10.1039/C4SC00315B.

(23) Bosque, I.; Bach, T. 3-Acetoxyquinuclidine as Catalyst in Electron Donor–Acceptor Complex-Mediated Reactions Triggered by Visible Light. *ACS Catal.* **2019**, *9* (10), 9103–9109. https://doi.org/10.1021/acscatal.9b01039.

(24) Fu, M.-C.; Shang, R.; Zhao, B.; Wang, B.; Fu, Y. Photocatalytic Decarboxylative Alkylations Mediated by Triphenylphosphine and Sodium Iodide. *Science (80-.).* **2019**, *363* (6434), 1429 LP – 1434. https://doi.org/10.1126/science.aav3200.

(25) Quint, V.; Morlet-Savary, F.; Lohier, J.-F.; Lalevée, J.; Gaumont, A.-C.; Lakhdar, S. Metal-Free, Visible Light-Photocatalyzed Synthesis of Benzo[b]Phosphole Oxides: Synthetic and Mechanistic Investigations. *J. Am. Chem. Soc.* **2016**, *138* (23), 7436–7441. https://doi.org/10.1021/jacs.6b04069.

(26) Shirke, R. P.; Ramasastry, S. S. V. Organocatalytic β-Azidation of Enones Initiated by an Electron-Donor–Acceptor Complex. *Org. Lett.* **2017**, *19* (19), 5482–5485. https://doi.org/10.1021/acs.orglett.7b02861.

(27) Batra, A.; Singh, K. N. Recent Developments in Transition Metal-Free Cross-Dehydrogenative Coupling Reactions for C–C Bond Formation. *European J. Org. Chem.* **2020**, *2020* (43), 6676–6703. https://doi.org/https://doi.org/10.1002/ejoc.202000785.

(28) Guo, W.; Tao, K.; Xie, Z.; Cai, L.; Zhao, M.; Tan, W.; Liu, G.; Mei, W.; Deng, L.; Fan, X.; Zheng, L. Photodriven Photocatalyst/Metal-Free Direct C-C/C-N Bond Formation: Synthesis of Indoles via EDA Complexes. *J. Org. Chem.* **2019**, *84* (21), 14168–14178. https://doi.org/10.1021/acs.joc.9b01689.

(29) Yang, X.; Zhu, Y.; Xie, Z.; Li, Y.; Zhang, Y. Visible-Light-Induced Charge Transfer Enables Csp3-H Functionalization of Glycine Derivatives: Access to 1,3-Oxazolidines. *Org. Lett.* **2020**, *22* (4), 1638–1643. https://doi.org/10.1021/acs.orglett.0c00234.

(30) Xia, Q.; Li, Y.; Cheng, L.; Liang, X.; Cao, C.; Dai, P.; Deng, H.; Zhang, W.; Wang, Q. Electron Donor–Acceptor Complex-Initiated Photochemical Cyanation for the Preparation of α-Amino Nitriles. *Org. Lett.* **2020**, *22* (24), 9638–9643. https://doi.org/10.1021/acs.orglett.0c03703.

(31) Nakajima, K.; Miyake, Y.; Nishibayashi, Y. Synthetic Utilization of α-Aminoalkyl Radicals and Related Species in Visible Light Photoredox Catalysis. *Acc. Chem. Res.* **2016**, *49* (9), 1946–1956. https://doi.org/10.1021/acs.accounts.6b00251.

(32) Kerru, N.; Gummidi, L.; Maddila, S.; Gangu, K. K.; Jonnalagadda, S. B. A Review on Recent Advances in Nitrogen-Containing Molecules and Their Biological Applications. *Molecules* **2020**, *25* (8). https://doi.org/10.3390/molecules25081909.

(33) Sridharan, V.; Suryavanshi, P. A.; Menéndez, J. C. Advances in the Chemistry of Tetrahydroquinolines. *Chem. Rev.* **2011**, *111* (11), 7157–7259. https://doi.org/10.1021/cr100307m.

(34) Muthukrishnan, I.; Sridharan, V.; Menéndez, J. C. Progress in the Chemistry of Tetrahydroquinolines. *Chem. Rev.* **2019**, *119* (8), 5057–5191. https://doi.org/10.1021/acs.chemrev.8b00567.

(35) Su, D.-S.; Lim, J. J.; Tinney, E.; Wan, B.-L.; Young, M. B.; Anderson, K. D.; Rudd, D.; Munshi, V.; Bahnck, C.; Felock, P. J.; Lu, M.; Lai, M.-T.; Touch, S.; Moyer, G.; DiStefano, D. J.; Flynn, J. A.; Liang, Y.; Sanchez, R.; Prasad, S.; Yan, Y.; Perlow-Poehnelt, R.; Torrent, M.; Miller, M.; Vacca, J. P.; Williams, T. M.; Anthony, N. J. Substituted Tetrahydroquinolines as Potent Allosteric Inhibitors of Reverse Transcriptase and Its Key Mutants. *Bioorg. Med. Chem. Lett.* **2009**, *19* (17), 5119–5123. https://doi.org/10.1016/j.bmcl.2009.07.031.

(36) Zhang, J.; Zhan, P.; Wu, J.; Li, Z.; Jiang, Y.; Ge, W.; Pannecouque, C.; De Clercq, E.; Liu, X. Synthesis and Biological Evaluation of Novel 5-Alkyl-2-Arylthio-6-((3,4-Dihydroquinolin-1(2H)-Yl)Methyl)Pyrimidin-4(3H)-Ones as Potent Non-Nucleoside HIV-1 Reverse Transcriptase Inhibitors. *Bioorg. Med. Chem.* **2011**, *19* (14), 4366–4376. https://doi.org/https://doi.org/10.1016/j.bmc.2011.05.024.

(37) Chander, S.; Wang, P.; Ashok, P.; Yang, L.-M.; Zheng, Y.-T.; Murugesan, S. Rational Design, Synthesis, Anti-HIV-1 RT and Antimicrobial Activity of Novel 3-(6-Methoxy-3,4-Dihydroquinolin-1(2H)-Yl)-1-(Piperazin-1-Yl)Propan-1-One Derivatives. *Bioorg. Chem.* **2016**, *67*, 75–83. https://doi.org/https://doi.org/10.1016/j.bioorg.2016.05.009.

(38) Ramesh, E.; Manian, R. D. R. S.; Raghunathan, R.; Sainath, S.; Raghunathan, M. Synthesis and Antibacterial Property of Quinolines with Potent DNA Gyrase Activity. *Bioorg. Med. Chem.* **2009**, *17* (2), 660–666. https://doi.org/10.1016/j.bmc.2008.11.058.

(39) Jarvest, R. L.; Berge, J. M.; Berry, V.; Boyd, H. F.; Brown, M. J.; Elder, J. S.; Forrest, A. K.; Fosberry, A. P.; Gentry, D. R.; Hibbs, M. J.; Jaworski, D. D.; O'Hanlon, P. J.; Pope, A. J.; Rittenhouse, S.; Sheppard, R. J.; Slater-Radosti, C.; Worby, A. Nanomolar Inhibitors of Staphylococcus Aureus Methionyl TRNA Synthetase with Potent Antibacterial Activity against Gram-Positive Pathogens. *J. Med. Chem.* **2002**, *45* (10), 1959–1962. https://doi.org/10.1021/jm025502x.

(40) Muñoz, A.; Sojo, F.; Arenas, D. R. M.; Kouznetsov, V. V; Arvelo, F. Cytotoxic Effects of New Trans-2,4-Diaryl-r-3-Methyl-1,2,3,4-Tetrahydroquinolines and Their Interaction with Antitumoral Drugs Gemcitabine and Paclitaxel on Cellular Lines of Human Breast Cancer. *Chem. Biol. Interact.* **2011**, *189* (3), 215–221. https://doi.org/10.1016/j.cbi.2010.11.010.

(41) Kouznetsov, V. V; Merchan-Arenas, D. R.; Tangarife-Castaño, V.; Correa-Royero, J.; Betancur-Galvis, L. Synthesis and Cytotoxic Evaluation of Novel 2-Aryl-4-(4-Hydroxy-3-Methoxyphenyl)-3-Methyl-6,7-Methylendioxy-1,2,3,4-Tetrahydroquinolines, Podophyllotoxin-like Molecules. *Med. Chem. Res.* **2016**, *25* (3), 429–437. https://doi.org/10.1007/s00044-015-1486-6.

(42) Zhu, S.; Das, A.; Bui, L.; Zhou, H.; Curran, D. P.; Rueping, M. Oxygen Switch in Visible-Light Photoredox Catalysis: Radical Additions and Cyclizations and Unexpected C–C-Bond Cleavage Reactions. *J. Am. Chem. Soc.* **2013**, *135* (5), 1823–1829. https://doi.org/10.1021/ja309580a.

(43) Yadav, A. K.; Yadav, L. D. S. Visible Light Photoredox Catalysis with N-Hydroxyphthalimide for [4+2] Cyclization between N-Methylanilines and Maleimides. *Tetrahedron Lett.* **2017**, *58* (6), 552–555. https://doi.org/10.1016/j.tetlet.2016.12.077.

(44) Guo, J.-T.; Yang, D.-C.; Guan, Z.; He, Y.-H. Chlorophyll-Catalyzed Visible-Light-Mediated Synthesis of Tetrahydroquinolines from N,N-Dimethylanilines and Maleimides. *J. Org. Chem.* **2017**, *82* (4), 1888–1894. https://doi.org/10.1021/acs.joc.6b03034.

(45) Liang, Z.; Xu, S.; Tian, W.; Zhang, R. Eosin Y-Catalyzed Visible-Light-Mediated Aerobic Oxidative Cyclization of N,N-Dimethylanilines with Maleimides. *Beilstein J. Org. Chem.* **2015**, *11*, 425–430. https://doi.org/10.3762/bjoc.11.48.

(46) Nicholls, T. P.; Constable, G. E.; Robertson, J. C.; Gardiner, M. G.; Bissember, A. C. Brønsted Acid Cocatalysis in Copper(I)-Photocatalyzed α-Amino C–H Bond Functionalization. *ACS Catal.* **2016**, *6* (1), 451–457. https://doi.org/10.1021/acscatal.5b02014.

(47) Chen, L.; Chao, C. S.; Pan, Y.; Dong, S.; Teo, Y. C.; Wang, J.; Tan, C.-H. Amphiphilic Methyleneamino Synthon through Organic Dye Catalyzed-Decarboxylative Aminoalkylation. *Org. Biomol. Chem.* **2013**, *11* (35), 5922–5925. https://doi.org/10.1039/C3OB41091A.

(48) Macdonald, T. L.; Gutheim, W. G.; Martin, R. B.; Guengerich, F. P. Oxidation of Substituted N,N-Dimethylanilines by Cytochrome P-450: Estimation of the Effective Oxidation-Reduction Potential of Cytochrome P-450. *Biochemistry* **1989**, *28* (5), 2071–2077. https://doi.org/10.1021/bi00431a016.

(49) Karki, S. B.; Dinnocenzo, J. P.; Jones, J. P.; Korzekwa, K. R. Mechanism of Oxidative Amine Dealkylation of Substituted N,N-Dimethylanilines by Cytochrome P-450: Application of Isotope Effect Profiles. *J. Am. Chem. Soc.* **1995**, *117* (13), 3657–3664. https://doi.org/10.1021/ja00118a001.

(50) Wu, G.; Li, Y.; Yu, X.; Gao, Y.; Chen, H. Acetic Acid Accelerated Visible-Light Photoredox Catalyzed N-Demethylation of N,N-Dimethylaminophenyl Derivatives. *Adv. Synth. Catal.* **2017**, *359* (4), 687–692. https://doi.org/10.1002/adsc.201601108.

(51) Leng, L.; Fu, Y.; Liu, P.; Ready, J. M. Regioselective, Photocatalytic α-Functionalization of Amines. *J. Am. Chem. Soc.* **2020**, *142* (28), 11972–11977. https://doi.org/10.1021/jacs.0c03758.

(52) Zhao, H.; Leonori, D. Minimization of Back-Electron Transfer Enables the Elusive Sp3 C–H Functionalization of Secondary Anilines. *Angew. Chemie Int. Ed.* **2021**, *60* (14), 7669–7674. https://doi.org/https://doi.org/10.1002/anie.202100051.

(53) Xu, K.; Fang, Y.; Yan, Z.; Zha, Z.; Wang, Z. A Highly Tunable Stereoselective Dimerization of Methyl Ketone: Efficient Synthesis of E- and Z-1,4-Enediones. *Org. Lett.* **2013**, *15* (9), 2148–2151. https://doi.org/10.1021/ol4006344.

(54) Garkani-Nejad, Z.; Rashidi-Nodeh, H. Comparison of Conventional Artificial Neural Network and Wavelet Neural Network in Modeling the Half-Wave Potential of Aldehydes and Ketones. *Electrochim. Acta* **2010**, *55* (8), 2597–2605. https://doi.org/10.1016/J.ELECTACTA.2009.11.083.

(55) Li, J.; Bao, W.; Zhang, Y.; Rao, Y. Cercosporin-Photocatalyzed Sp3 (C–H) Activation for the Synthesis of Pyrrolo[3{,}4-c]Quinolones. *Org. Biomol. Chem.* **2019**, *17* (40), 8958–8962. https://doi.org/10.1039/C9OB01946D.

(56) Morack, T.; Mück-Lichtenfeld, C.; Gilmour, R. Bioinspired Radical Stetter Reaction: Radical Umpolung Enabled by Ion-Pair Photocatalysis. *Angew. Chemie Int. Ed.* **2019**, *58* (4), 1208–1212. https://doi.org/doi:10.1002/anie.201809601.

(57) Cao, Z.-Y.; Ghosh, T.; Melchiorre, P. Enantioselective Radical Conjugate Additions Driven by a Photoactive Intramolecular Iminium-Ion-Based EDA Complex. *Nat. Commun.* **2018**, *9* (1), 3274. https://doi.org/10.1038/s41467-018-05375-2.

(58) Woźniak, Ł.; Murphy, J. J.; Melchiorre, P. Photo-Organocatalytic Enantioselective Perfluoroalkylation of β-Ketoesters. *J. Am. Chem. Soc.* **2015**, *137* (17), 5678–5681. https://doi.org/10.1021/jacs.5b03243.

(59) Aramaki, Y.; Imaizumi, N.; Hotta, M.; Kumagai, J.; Ooi, T. Exploiting Single-Electron Transfer in Lewis Pairs for Catalytic Bond-Forming Reactions. *Chem. Sci.* **2020**, *11* (17), 4305–4311. https://doi.org/10.1039/D0SC01159B.

(60) Hloušková, Z.; Klikar, M.; Pytela, O.; Almonasy, N.; Růžička, A.; Jandová, V.; Bureš, F. Structural Elaboration of Dicyanopyrazine: Towards Push–Pull Molecules with Tailored Photoredox Activity. *RSC Adv.* **2019**, *9* (41), 23797–23809. https://doi.org/10.1039/C9RA04731J.

(61) Yang, X.; Liang, T.; Sun, J.; Zaworotko, M. J.; Chen, Y.; Cheng, P.; Zhang, Z. Template-Directed Synthesis of Photocatalyst-Encapsulating Metal–Organic Frameworks with Boosted Photocatalytic Activity. *ACS Catal.* **2019**, *9* (8), 7486–7493. https://doi.org/10.1021/acscatal.9b01783.

(62) Mandal, T.; Das, S.; De Sarkar, S. Nickel(II) Tetraphenylporphyrin as an Efficient Photocatalyst Featuring Visible Light Promoted Dual Redox Activities. *Adv. Synth. Catal.* **2019**, *361* (13), 3200–3209. https://doi.org/10.1002/adsc.201801737.

(63) Nicholls, T. P.; Burt, L. K.; Simpson, P. V; Massi, M.; Bissember, A. C. Tricarbonyl Rhenium(i) Tetrazolato and N-Heterocyclic Carbene Complexes: Versatile Visible-Light-Mediated Photoredox Catalysts. *Dalt. Trans.* **2019**, *48* (33), 12749–12754. https://doi.org/10.1039/C9DT02533B.

(64) Sharma, K.; Das, B.; Gogoi, P. Synthesis of Pyrrolo[3,4-c]Quinoline-1,3-Diones: A Sequential Oxidative Annulation Followed by Dehydrogenation and N-Demethylation Strategy. *New J. Chem.* **2018**, *42* (23), 18894–18905. https://doi.org/10.1039/c8nj04443k.

(65) Yang, X.-L.; Guo, J.-D.; Lei, T.; Chen, B.; Tung, C.-H.; Wu, L.-Z. Oxidative Cyclization Synthesis of Tetrahydroquinolines and Reductive Hydrogenation of Maleimides under Redox-Neutral Conditions. *Org. Lett.* **2018**, *20* (10), 2916–2920. https://doi.org/10.1021/acs.orglett.8b00977.

(66) Ranieri, A. M.; Burt, L. K.; Stagni, S.; Zacchini, S.; Skelton, B. W.; Ogden, M. I.; Bissember, A. C.; Massi, M. Anionic Cyclometallated Platinum(II) Tetrazolato Complexes as Viable Photoredox Catalysts. *ChemRxiv* **2018**, 1–22.

(67) Firoozi, S.; Hosseini-Sarvari, M.; Koohgard, M. Solvent-Free and Room Temperature Visible Light-Induced C–H Activation: CdS as a Highly Efficient Photo-Induced Reusable Nano-Catalyst for the C–H Functionalization Cyclization of t-Amines and C–C Double and Triple Bonds. *Green Chem.* **2018**, *20* (24), 5540–5549. https://doi.org/10.1039/C8GC03297A.

(68) Hosseini-Sarvari, M.; Koohgard, M.; Firoozi, S.; Mohajeri, A.; Tavakolian, H. Alizarin Red S–TiO2-Catalyzed Cascade C(Sp3)–H to C(Sp2)–H Bond Formation/Cyclization Reactions toward Tetrahydroquinoline Derivatives under Visible Light Irradiation. *New J. Chem.* **2018**, *42* (9), 6880–6888. https://doi.org/10.1039/C8NJ00476E.

(69) Song, Z.; Antonchick, A. P. Catching α-Aminoalkyl Radicals: Cyclization between Tertiary Alkylanilines and Alkenes. *Tetrahedron* **2016**, *72* (48), 7715–7721. https://doi.org/https://doi.org/10.1016/j.tet.2016.04.052.

(70) Yadav, A. K.; Yadav, L. D. S. Intermolecular Cyclization of N-Methylanilines and Maleimides to Tetrahydroquinolines via K2S2O8 Promoted C(Sp3)–H Activation. *Tetrahedron Lett.* **2016**, *57* (13), 1489–1491. https://doi.org/https://doi.org/10.1016/j.tetlet.2016.02.078.

(71) Huo, C.; Chen, F.; Quan, Z.; Dong, J.; Wang, Y. Cobalt-Catalyzed Aerobic Oxidative Povarov Reaction of Tertiary Anilines with Dihydrofuran for the Synthesis of Hexahydrofuroquinolines. *Tetrahedron Lett.* **2016**, *57* (46), 5127–5131. https://doi.org/10.1016/j.tetlet.2016.10.031.

(72) Wang, Z. J.; Ghasimi, S.; Landfester, K.; Zhang, K. A. I. Bandgap Engineering of Conjugated Nanoporous Poly-Benzobisthiadiazoles via Copolymerization for Enhanced Photocatalytic 1,2,3,4-Tetrahydroquinoline Synthesis under Visible Light. *Adv. Synth. Catal.* **2016**, *358* (16), 2576–2582. https://doi.org/10.1002/adsc.201600125.

(73) Sakai, N.; Matsumoto, S.; Ogiwara, Y. Cobalt-Catalyzed Oxidative Annulation of Aromatic Tertiary Amines with Electron-Deficient Maleimides Leading to Tetrahydroquinoline Derivatives. *Tetrahedron Lett.* **2016**, *57* (49), 5449–5452. https://doi.org/10.1016/j.tetlet.2016.10.071.

(74) Tang, J.; Grampp, G.; Liu, Y.; Wang, B.-X.; Tao, F.-F.; Wang, L.-J.; Liang, X.-Z.; Xiao, H.-Q.; Shen, Y.-M. Visible Light Mediated Cyclization of Tertiary Anilines with Maleimides Using Nickel(II) Oxide Surface-Modified Titanium Dioxide Catalyst. *J. Org. Chem.* **2015**, *80* (5), 2724–2732. https://doi.org/10.1021/jo502901h.

(75) Ju, X.; Li, D.; Li, W.; Yu, W.; Bian, F. The Reaction of Tertiary Anilines with Maleimides under Visible Light Redox Catalysis. *Adv. Synth. Catal.* **2012**, *354* (18), 3561–3567. https://doi.org/10.1002/adsc.201200608.

(76) Nishino, M.; Hirano, K.; Satoh, T.; Miura, M. Copper-Catalyzed Oxidative Direct Cyclization of N-Methylanilines with Electron-Deficient Alkenes Using Molecular Oxygen. *J. Org. Chem.* **2011**, *76* (15), 6447–6451. https://doi.org/10.1021/jo2011329.

(77) Roy, R. B.; Swan, G. A. A Novel Formation of Quinoline Derivatives. *Chem. Commun. (London)* **1968**, No. 22, 1446–1447. https://doi.org/10.1039/C19680001446.

(78) Perumal, G.; Kandasamy, M.; Ganesan, B.; Govindan, K.; Sathya, H.; Hung, M.-Y.; Chandru Senadi, G.; Wu, Y.-C.; Lin, W.-Y. Visible Light-Induced N-Methyl Activation of Unsymmetric Tertiary Amines. *Tetrahedron* **2021**, *80*, 131891. https://doi.org/https://doi.org/10.1016/j.tet.2020.131891.

(79) Nikitas, N. F.; Theodoropoulou, M. A.; Kokotos, C. G. Photochemical Reaction of N,N-Dimethylanilines with N-Substituted Maleimides Utilizing Benzaldehyde as the Photoinitiator. *European J. Org. Chem.* **2021**, *2021* (7), 1168–1173. https://doi.org/https://doi.org/10.1002/ejoc.202001593.

(80) Almansaf, Z.; Hu, J.; Zanca, F.; Shahsavari, H. R.; Kampmeyer, B.; Tsuji, M.; Maity, K.; Lomonte, V.; Ha, Y.; Mastrorilli, P.; Todisco, S.; Benamara, M.; Oktavian, R.; Mirjafari, A.; Moghadam, P. Z.; Khosropour, A. R.; Beyzavi, H. Pt(II)-Decorated Covalent Organic Framework for Photocatalytic Difluoroalkylation and Oxidative Cyclization Reactions. *ACS Appl. Mater. Interfaces* **2021**, *13* (5), 6349–6358. https://doi.org/10.1021/acsami.0c21370.

(81) Xie, Z.; Li, F.; Niu, L.; Li, H.; Zheng, J.; Han, R.; Ju, Z.; Li, S.; Li, D. CuBr/NHPI Co-Catalyzed Aerobic Oxidative [3 + 2] Cycloaddition-Aromatization to Access 5{,}6-Dihydro-Pyrrolo[2{,}1-a]Isoquinolines. *Org. Biomol. Chem.* **2020**, *18* (35), 6889–6898. https://doi.org/10.1039/D0OB01403F.

(82) Goto, Y.; Watanabe, Y.; Fukuzumi, S.; Jones, J. P.; Dinnocenzo, J. P. Mechanisms of N-Demethylations Catalyzed by High-Valent Species of Heme Enzymes: Novel Use of Isotope Effects and Direct Observation of Intermediates. *J. Am. Chem. Soc.* **1998**, *120* (41), 10762–10763. https://doi.org/10.1021/ja981357u.

(83) Ratnikov, M. O.; Doyle, M. P. Mechanistic Investigation of Oxidative Mannich Reaction with Tert-Butyl Hydroperoxide. The Role of Transition Metal Salt. *J. Am. Chem. Soc.* **2013**, *135* (4), 1549–1557. https://doi.org/10.1021/ja3113559.

(84) Baciocchi, E.; Bietti, M.; Gerini, M. F.; Lanzalunga, O. Electron-Transfer Mechanism in the N-Demethylation of N,N-Dimethylanilines by the Phthalimide-N-Oxyl Radical. *J. Org. Chem.* **2005**, *70* (13), 5144–5149. https://doi.org/10.1021/jo0503916.

(85) Runemark, A.; Zacharias, S. C.; Sundén, H. Visible-Light-Driven Stereoselective Annulation of Alkyl Anilines and Dibenzoylethylenes via Electron Donor–Acceptor Complexes. *J. Org. Chem.* **2021**, *86* (2), 1901–1910. https://doi.org/10.1021/acs.joc.0c02819.

Paper I

JOC The Journal of Organic Chemistry

pubs.acs.org/joc Article

Visible-Light-Driven Stereoselective Annulation of Alkyl Anilines and Dibenzoylethylenes via Electron Donor–Acceptor Complexes

August Runemark, Savannah C. Zacharias, and Henrik Sundén*

Cite This: J. Org. Chem. 2021, 86, 1901–1910 Read Online

ACCESS | Metrics & More | Article Recommendations | Supporting Information

ABSTRACT: A catalyst-free, stereoselective visible-light-driven annulation reaction between alkenes and *N*,*N*-substituted dialkyl anilines for the synthesis of substituted tetrahydroquinolines is presented. The reaction is driven by the photoexcitation of an electron donor–acceptor (EDA) complex, and the resulting products are obtained in good to high yields with complete diastereoselectivity. Mechanistic rationale and photochemical characterization of the EDA-complex are provided.

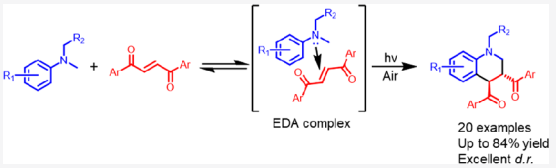

INTRODUCTION

Electron donor–acceptor (EDA) complexes have in recent years gained considerable attention in the field of organic chemistry due to their photochemical properties which can be used to mediate a number of advanced chemical transformations.[1−5] An EDA complex is the result of a weak association between an electron-rich donor and an electron-deficient acceptor and is characterized by a charge-transfer band in the absorption spectrum.[4] Due to the bathochromic shift of the charge-transfer band, with respect to the donor and acceptor, visible light can often be employed to induce a single electron transfer from the donor to the acceptor. The resulting radical pair can be used in synthetic chemistry,[1−4,6−12] including enantioselective alkylations,[13−17] aromatic alkylations,[16] and biaryl couplings.[18]

Recently, we reported an EDA-complex-driven protocol for the UV-light-induced generation of α-aminoalkyl radicals and their addition to maleimides to form fused tetrahydroquinolines (THQs) (Scheme 1a).[19]

The THQ is a highly desirable structural target in synthesis, as it can be found in a variety of biologically active compounds.[20,21] Examples include molecules with antiviral,[22−24] antibiotic,[25,26] and cytotoxic[27,28] activity. Thus, a diverse set of methodologies for the synthesis of the THQ-scaffold has been developed, and among the most versatile strategies are the aza-Diels–Alder, the Grieco, and the Povarov reactions.[22−24]

Additionally, several methods for the visible-light-driven construction of substituted THQ have been reported (Scheme 1b,c).[29−34] However, the use of photocatalysts is typically required, and substrates are generally limited to cyclic alkenes (Scheme 1a,c) or alkenes that cannot undergo photoisomerization (Scheme 1b).[35−37] To the best of our knowledge, no diastereoselective annulations between tertiary amines and alkenes that can undergo photoisomerization have been reported under photochemical conditions. Clearly, the possibility of alkene *E*/*Z*-isomerization under photochemical conditions poses a significant synthetic challenge for selectivity in the desired cyclization. But if successful, it could lead to the diastereoselective functionalization of THQ in the 3 and 4 positions (Scheme 1d). Inspired by these opportunities, we

Scheme 1. Light-Induced Construction of Tetrahydroquinolines

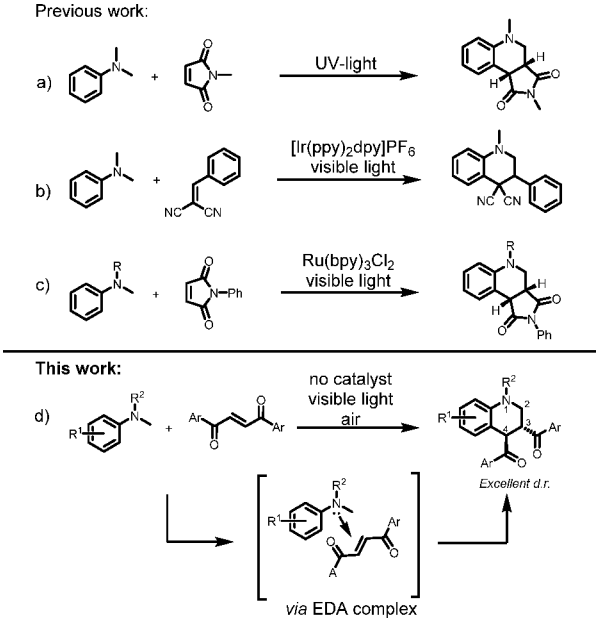

Received: November 25, 2020
Published: January 5, 2021

https://dx.doi.org/10.1021/acs.joc.0c02819
J. Org. Chem. 2021, 86, 1901–1910

envisioned that the more challenging acyclic internal alkenes could function as acceptors in novel EDA complexes with aromatic amines for the synthesis of substituted THQ (Scheme 1d) and that the cumbersome photoisomerization could be kept to a minimum with a light source operating in the visible region of the light spectrum.

Herein, we present a catalyst-free EDA-mediated diastereoselective synthesis of substituted THQ from tertiary amines and 1,2-dibenzoylethylene (DBE).

RESULTS AND DISCUSSION

To initiate our study, the interaction between 4′-*N*,*N*-trimethylaniline (**1a**) and 1,2-DBE (**2a**) was investigated (Figure 1). UV−vis measurements of **1a**, **2a**, and a mixture of

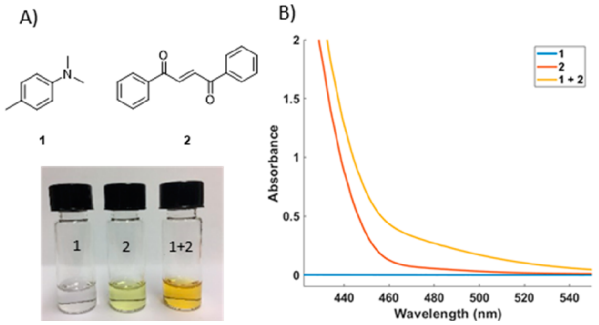

Figure 1. (A) Photos of **1a**, **2a**, and **1a** + **2a** in acetonitrile. (B) UV−vis absorption spectra of **1a** (0.1 M), **2a** (0.1 M), and **1a** + **2a** in acetonitrile.

the two compounds were performed. Upon mixing, a color change from light yellow to orange was observed (Figure 1A), and a new absorption band appeared in the visible region (Figure 1B), indicating an EDA interaction.

Next, the impact of visible light irradiation of a mixture of **1a** and **2a** was studied. Compact fluorescent light bulbs (CFLs) were used as the irradiation source (SI, Figure S2 for emission spectrum). The desired cyclized product **3a** was formed in 25% yield using acetonitrile as solvent (Table 1, entry 1). 1,4-Dioxane proved to be the best solvent for the reaction, providing the desired THQ in 65% yield (Table 1, entry 8). Other solvents, both polar and nonpolar, showed inferior results, correlating with previously published findings.[19,38] The impact of irradiation time on the formation of **3a** was investigated using gas chromatography, and a reaction time of 4 h was determined to be optimal (SI, Figure S5). Significant degradation of the desired product was observed after prolonged irradiation. A large stoichiometric excess of the amine was proven to be important, as using 4 molar equiv lowered the yield significantly (Table 1, entry 9). This can be rationalized as a result of increased concentration of the photoactive EDA complex with higher loadings of the donor (K_{EDA} = 0.42 M^{-1}, calculated using the Benesi−Hildebrand method, Figure S3). The role of the oxidant, oxygen, was then evaluated. When the reaction mixture was irradiated under inert atmosphere, the reaction was suppressed (Table 1, entry 10). Irradiating under an atmosphere of oxygen gas on the other hand resulted in a low yield and a sluggish reaction (Table 1, entry 11). Changing the oxidant to persulfate resulted in decreased yield (Table 1, entry 13). Addition of acetic acid increased the yield of **3a** to 73% (Table 1, entry 16), a result that correlates with the literature.[39] Alternative

Table 1. Screening of Reaction Conditions[a]

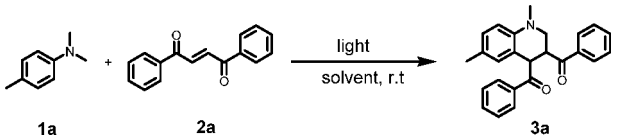

entry	solvent	light source	yield of **3a** (%)[b]	d.r.[b]
1	acetonitrile	CFL	25	>25:1
2	methanol	CFL	14	>25:1
3	tetrahydrofuran	CFL	29	>25:1
4	ethyl acetate	CFL	17	>25:1
5	dichloromethane	CFL	40	>25:1
6	1,2-dichloroethane	CFL	41	>25:1
7	1,2-dimethoxyethane	CFL	32	>25:1
8	1,4-dioxane	CFL	65	>25:1
9	1,4-dioxane	CFL	30[c]	>25:1
10	1,4-dioxane	CFL	0[d]	–
11	1,4-dioxane	CFL	12[e]	>25:1
12	1,4-dioxane	CFL	37[f]	>25:1
13	1,4-dioxane/water (2:1)	CFL	47[f]	>25:1
14	1,4-dioxane	blue LED	23	>25:1
15	1,4-dioxane	CFL	68[g]	>25:1
16	1,4-dioxane	CFL	73[h]	>25:1
17	1,4-dioxane	UV-CFL	30	>25:1
18	1,4-dioxane	–	0[i]	–
19	1,4-dioxane	blue LED	60[h,j]	>25:1

[a]Reaction conditions: **1a** (0.7 mmol) and **2a** (0.1 mmol) in 3 mL of solvent irradiated with two 15 W compact fluorescent lamps in room temperature for 4 h. [b]Determined by NMR with 1,2,4,5-tetramethylbenzene as internal standard. [c]4 equiv of amine. [d]Under Ar. [e]Under O_2. [f]$K_2S_2O_8$ (2 equiv) used as an additive. [g]Acetic acid (30 equiv) used as additive. [h]Acetic acid (80 equiv) used as additive. [i]Reaction performed in absence of light. [j]Reaction time of 12 h.

light sources, such as blue LED (450 nm) or UV-CFL (365 nm) performed worse than the regular CFL (Table 1, compare entries 14 and 17 with 8). However, the use of blue LED under the optimized reaction conditions (1,4-dioxane as solvent and acetic acid as additive) and longer reaction time provide the desired product in the yield of 60% (Table 1, entry 19). The exclusion of light resulted in complete suppression of the formation of the desired product, confirming the need for an excitation source (Table 1, entry 18).

With our optimized reaction conditions in hand, the generality of the reaction was examined (Scheme 2). Excellent diastereoselectivity toward the *anti*-diastereomer (confirmed by X-ray analysis, entry **3q**) was obtained for all substrates, and the *syn*-isomer of **3** was never observed. Symmetric DBEs with simple aliphatic substituents provided the corresponding THQs in moderate yields in combination with 4′-*N*,*N*-trimethylaniline (Scheme 2, **3b**−**e**). A clear effect of the electronic properties of substituents in the *p*-position on the 1,2-DBE can be observed as the yield decreases when more electron-donating substituents are introduced: *p*-H 73%, *p*-Me 63%, *i*-Bu 52%, and *tert*-Bu 45% (Scheme 2, **3a**−**3d**). The introduction of two methyl groups in *m*- and *p*-position likewise decreased the yield (Scheme 2, **3e**) as well as *p*-OMe (Scheme 2, **3f**). Mildly *σ*-withdrawing groups such as *p*-Br or *p*-Cl resulted in no change or a slight increase in the yield (Scheme 2, **3h**−**i**). When an unsymmetrical dibenzoyl ethylene was used as the substrate, the product was obtained as an inseparable mixture of the two regioisomers (Scheme 2, **3j**).

https://dx.doi.org/10.1021/acs.joc.0c02819
J. Org. Chem. 2021, 86, 1901−1910

Scheme 2. Substrate Scope of Anilines and Dibenzoylethylenes[a,b]

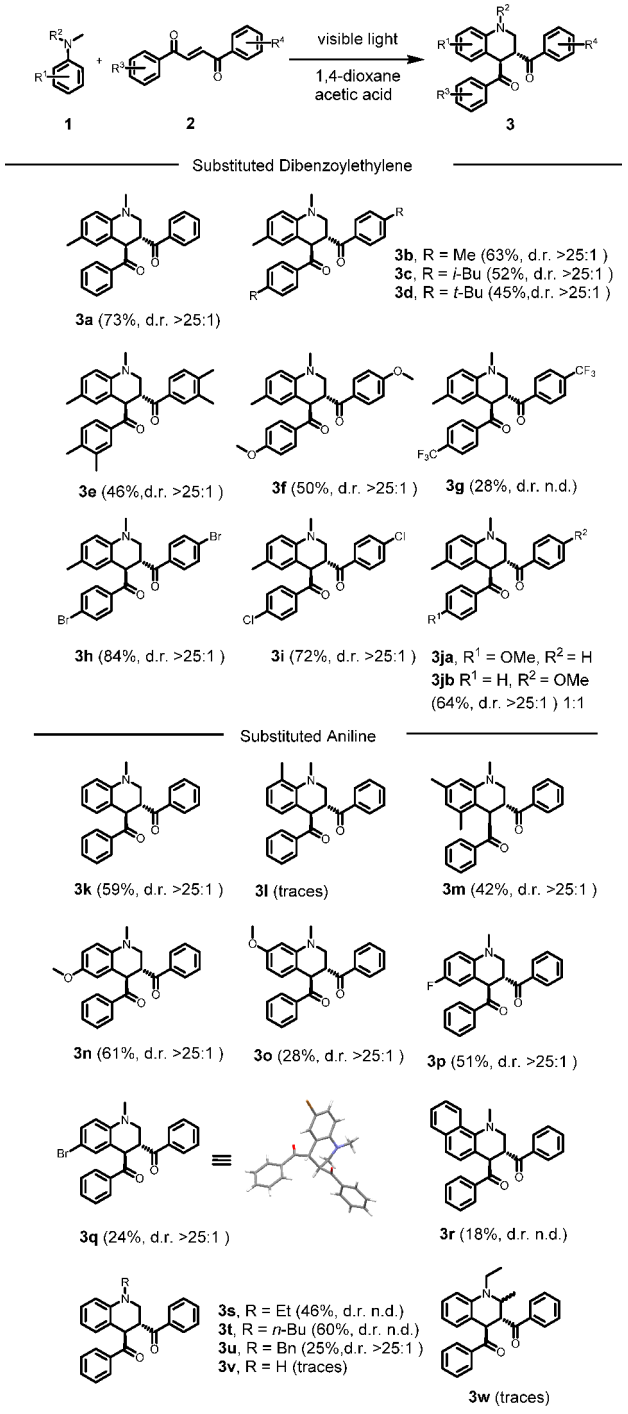

[a]Reaction conditions: Substituted 1,2-DBE (0.25 mmol) and aniline (1.75 mmol) in 1,4-dioxane (6 mL) and acetic acid (1 mL) was irradiated with CFL lamp for 4 h. [b]n.d. = not determined.

Next, the effect of substituents on the aniline reaction partner was evaluated. Electron-donating groups proved to be well tolerated (Scheme 2, **3n**) compared to σ-withdrawing groups such as *p*-F or *p*-Br (Scheme 2, **3p**−**q**). Introduction of a methoxy group in *m*-position resulted in a significantly decreased the yield (Scheme 2, **3o**). A significant steric effect was observed when a methyl group was introduced in the *o*-position on the aniline, as the reaction was completely suppressed (Scheme 2, **3i**). This result could be explained by a significantly weaker EDA complex formed between the reaction partners, something also indicated by the lack of color change upon mixing. The steric clash between the *o*-Me and the *N*-Me groups leads to a less planar and less conjugated aromatic amine weakening the interaction with the alkene. Introduction of two methyl groups in the less sterically demanding *m*-positions did not lead to a similar decrease in yield (Scheme 2, **3m**). We were also interested in investigating the regioselectivity of the reaction regarding the aniline reactant. Changing one of the *N*-methyl substituents to aliphatic in benzylic groups resulted in a complete selectivity toward reaction of the *N*-methyl group (Scheme 2, **3s**−**u**). When *N*,*N*-diethylaniline was used, no reaction took place (Scheme 2, **3w**). These results highlight the selectivity of the reaction toward *N*-methyl substituted anilines. However, subjecting monosubstituted *N*-methyl aniline to the reaction conditions resulted in complete suppression of reactivity (Scheme 2, **3v**). The impact of geometrical isomerism of the DBE substrate was then examined. It is reported that *E*-DBE undergoes isomerization to the *Z*-isomer under visible light irradiation.[40] In order to evaluate the impact of this background reaction, *Z*-DBE was subjected to the reaction conditions to furnish the desired product **3a**, albeit in a lower yield of 55% (Scheme 3). Complete diastereoselectivity toward

Scheme 3. Impact of Stereochemistry of the Substrate Dibenzoylethylene

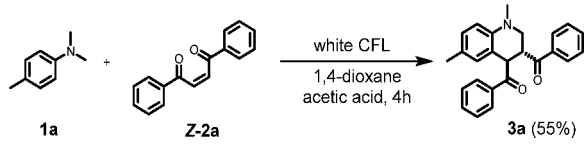

the *anti*-diastereomer was observed, suggesting that the cyclization reaction is not of concerted character. Notably, other acyclic activated olefins were not tolerated in the reaction such as benzylideneacetophenone, benzylidenemalonitrile, cinnamaldehyde, nitrostyrene, diethylfumarate, or diethylmaleate. These olefins did not provide the corresponding desired annulation products under the developed conditions.

To further probe the impact of light on the reaction, the illumination was cycled on/off, resulting in suppression of product formation in the absence of light (SI, Figure S6). This affirms the fact that the reaction requires constant illumination. In addition, the quantum yield of the reaction was determined to be 4.5 (SI, Section 8), which suggests that a radical chain process is involved in the mechanism. The role of oxygen was also investigated. The observation that the reaction is suppressed in the absence of oxygen (Scheme 1, entry 10) and the evidence for presence of hydrogen peroxide in the reaction mixture after irradiation (SI, Figure S4), demonstrates the role of ambient oxygen as an external oxidant. Based on these findings and support in the literature,[19,41−43] we propose the following mechanism (Scheme 4): The reaction commences with the formation of an EDA complex between reactants **1a** and **2a**. Upon irradiation with light, an electron transfer occurs, a key step which is supported by calculation of the Gibbs free energy change for the photoinduced electron transfer (SI Section 1.8). Subsequent proton-transfer results in the formation of the α-amino alkyl radical **A** and enol radical **B**. The enol radical **B** reacts with oxygen, regenerating **2a** and

https://dx.doi.org/10.1021/acs.joc.0c02819
J. Org. Chem. 2021, 86, 1901−1910

Scheme 4. Proposed Reaction Mechanism

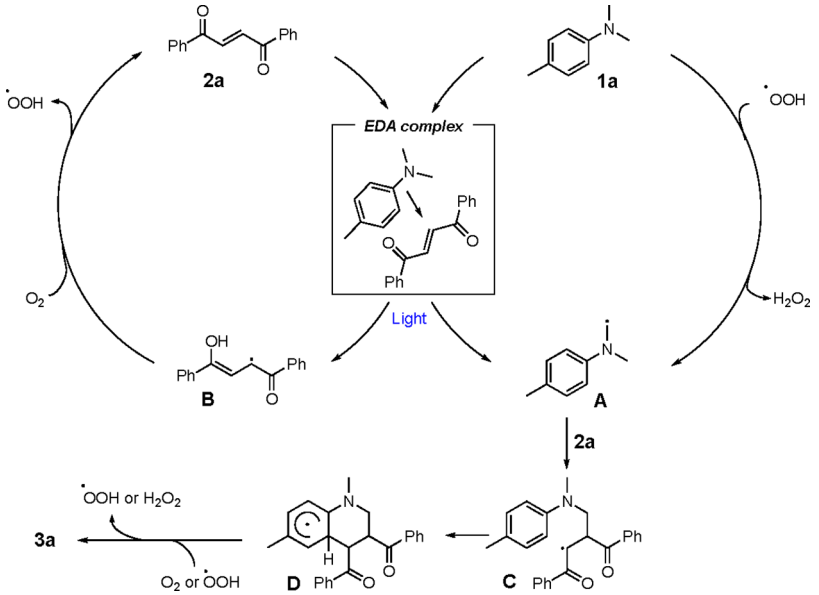

forming a hydroperoxyl radical and thus starting the self-propagating radical chain mechanism. In the next step, **2a** reacts with α-amino alkyl radical **A** to form **C**, and after cyclization, the radical intermediate **D** is formed. In the final step, **D** is oxidized to the desired product **3a** via two possible alternative pathways. The cyclohexadienyl radical intermediate **D** is oxidized by molecular oxygen[41,42] yielding **3a** and a second hydroperoxyl radical which in turn can propagate a radical chain reaction by oxidizing **1a** to **A**.[43,44] Alternatively, **D** can be intersected by a hydroperoxyl radical yielding **3a** and hydrogen peroxide as a byproduct.

In order to improve the step economy of the reaction, we were interested in the possibility of running the annulation as a multicomponent version with **2a** formed *in situ*. The one-pot version would circumvent a purification step and give potential access to a broader scope of the target compounds (**3**) while using simpler starting materials. As it turns out, the reaction between **1a**, phosphonium ylide **4**, and phenylglyoxal **5** works well, and **3a** could be obtained in 40% yield (Scheme 5), which corresponds to a yield per bond formed of 80%.

Scheme 5. Multicomponent Synthesis of 3a

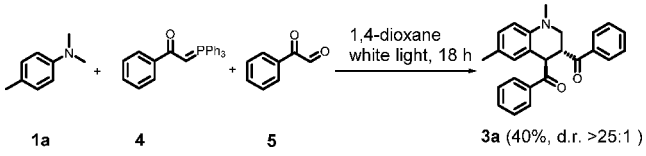

To investigate the synthetic usefulness of the 3,4-dibenzoyl-THQ structure, compound **3a** was treated with ammonium acetate in acetic acid[45] to yield fused 3*H*-pyrrole derivative **6** (Scheme 6). Subjecting **3a** to acid in acetic anhydride afforded fused furan derivative **7**.[46] These results highlight the possibility of efficient construction of fused heterocycles from the 3,4-dibenzoyl-THQ.

In summary, a protocol for the visible-light-mediated synthesis of substituted THQs has been developed. The reaction requires no photocatalyst and relies on photo-excitation of an EDA complex formed between *N*-alkyl-*N*-methylaniline and a 1,2-dibenzoyl ethylene, where atmospheric oxygen functions as the terminal oxidant. A broad substrate scope is presented, demonstrating the tolerance for common functional groups in the reaction. The resulting 3,4-dibenzoyl-THQ structure is further derivatized and proven to be a useful building block for the construction of fused heterocycles. Synthetic applications of other EDA complexes are currently being explored by our research group.

Scheme 6. Synthetic Applications

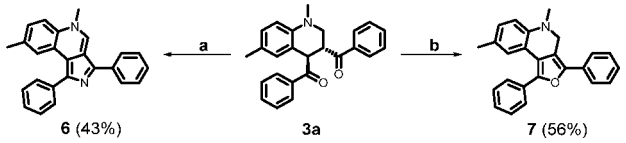

[a]NH_4OAc, AcOH, 120 °C, 5 h. [b]Ac_2O, HCl, 80 °C, 18 h.

EXPERIMENTAL SECTION

General Information. All reagents and solvents were purchased from Sigma-Aldrich and Alfa Aesar and used without any further purification unless specified. Purification of products was performed by an automated column chromatography Biotage Isolera Spektra One with Biotage SNAP-10 g KP-silica column together with a 1 g samplet cartridge using petroleum ether (40−60 °C)/ethyl acetate as the solvent mixture unless otherwise noted. ^{1}H (400 MHz) and ^{13}C (101 MHz) NMR spectra were acquired on an Agilent NMR machine at 25 °C. The chemical shifts for ^{1}H and ^{13}C NMR spectra are reported in parts per million (ppm) relative to the residual peak from solvent $CDCl_3$ as the internal standard: ^{1}H NMR at δ 7.26 ppm and ^{13}C NMR at δ 77.0 ppm for $CDCl_3$. All coupling constants (J) are reported in hertz (Hz) and multiplicities are indicated by s (singlet), d (doublet), dd (doublet of doublet), td (triplet of doublet), ddd (doublet of doublets of doublets), triplet (t), dt (doublet of triplet) and m (multiplet). Fourier-transform infrared (FT-IR) spectra were recorded on a PerkinElmer series FT-IR spectrometer and are reported in wavenumber (cm^{-1}). High-resolution mass spectrometry measurements (HRMS) were performed by CMSI service at Chalmers University of Technology, Gothenburg using an Agilent 6520 equipped with an electrospray interface operated in the positive ionization mode with quadrupole time-of-flight mass analyzer. UV−vis absorption spectra were recorded on a Cary 4000 UV−vis

https://dx.doi.org/10.1021/acs.joc.0c02819
J. Org. Chem. 2021, 86, 1901−1910

spectrophotometer, using 1 × 1 cm quartz cuvettes. All light promoted reactions were carried out in Biotage microwave vials (10−20 mL) under irradiation with two 20 W white CFL bulbs (Osram, 1200 lm) at a distance of 5 cm. Gas chromatographic studies were carried out using an Agilent 7820A gas chromatograph with an Agilent HP-5 19091J-413 column, and detection was accomplished using a flame ionization detector. Crystals of **3q** for single-crystal X-ray diffraction were grown using the layering technique from **3q** in dichloromethane and fresh hexane. The colorless yellow prism-shaped crystals appeared after 4 days. A Bruker D8 VENTURE Kappa Duo with a PHOTON III detector was used for the data collection. Collections were carried out at low temperature [120(2) K] using a Cryostream SAINT (version 7.60a; Bruker AXS, 2016) software to perform data reduction and unit cell refinement. The atomic coordinates were located using direct methods employed by SHELXS.[47] The successive refinements, once the atoms were placed in their postulated positions, were made using SHELXL.[48] X-Seed[49] was used for the data refinement. All non-hydrogen atoms were then refined anisotropically. The hydrogen atoms were placed in idealized positions in a riding model, after location on a Fourier difference map. An isotropic refinement was used for all hydrogen atoms, and temperature factors of 1.2 or 1.5 times that of the parent atoms were assigned.

Synthesis of Starting Materials. Amines **1i−k** were synthesized following a reported method.[50] To a solution of *N*-methylaniline (1.07 g, 10 mmol, 1 equiv) and potassium carbonate (4.8 g, 35 mmol, 3.5 equiv) in acetonitrile (9 mL) was added appropriate alkyl bromide (12 mmol, 1.2 equiv). The mixture was refluxed for 72 h and then cooled to room temperature. Solvent was removed under reduced pressure, and the residue was partitioned between water and dichloromethane. The aqueous phase was extracted three times with dichloromethane, and the combined organic phases were dried over anhydrous sulfate and concentrated under reduced pressure to yield an oily residue that was purified using column chromatography (SiO_2, petroleum spirits/ethyl acetate, 9:1).

*N-Ethyl-N-methylaniline (**1i**).* Purified using column chromatography (SiO_2, petroleum spirits/ethyl acetate, 9:1), yellow oil, 900 mg (67%). Spectroscopic data in accordance with the literature:[51] ^{1}H NMR (400 MHz, chloroform-*d*) δ 7.24 (m, 2H), 6.76−6.66 (m, 3H), 3.41 (qd, J = 7.1, 1.6 Hz, 2H), 2.91 (s, 3H), 1.16−1.10 (m, 3H) ppm; ^{13}C{^{1}H} NMR (101 MHz, chloroform-*d*) δ 149.1, 129.2, 116.0, 112.4, 46.8, 37.4, 11.2 ppm.

*N-Butyl-N-methylaniline (**1j**).* Purified using column chromatography (SiO_2, petroleum spirits/ethyl acetate, 9:1), yellow oil 1.45 g (89%). Spectroscopic data in accordance with the literature:[52] ^{1}H NMR (400 MHz, chloroform-*d*) δ 7.27−7.21 (m, 2H), 6.75−6.65 (m, 3H), 3.36−3.29 (m, 2H), 2.93 (s, 3H), 1.63−1.51 (m, 2H), 1.43−1.29 (m, 2H), 1.01−0.92 (t, 3H) ppm; ^{13}C{^{1}H} NMR (101 MHz, chloroform-*d*) δ 149.5, 129.3, 115.9, 112.2, 52.7, 38.4, 29.0, 20.5, 14.1 ppm.

*N-Benzyl-N-methylaniline (**1k**).* Purified using column chromatography (SiO_2, petroleum spirits/ethyl acetate, 9:1), yellow oil, 1.2 g (60%). Spectroscopic data in accordance with the literature:[52] ^{1}H NMR (400 MHz, chloroform-*d*) δ 7.35−7.22 (m, 6H), 7.19 (m, 2H), 6.63−6.56 (m, 2H), 4.51 (s, 2H), 3.01 (s, 3H) ppm; ^{13}C{^{1}H} NMR (101 MHz, chloroform-*d*) δ 148.7, 138.5, 131.9, 128.8, 127.2, 126.7, 114.0, 108.5, 56.7, 38.9 ppm.

1,2-Dibenzoyl ethylenes **2b−j** were synthesized according to a reported method.[40] The appropriate acetophenone (2 mmol, 1 equiv), iodine (4 mmol, 2 equiv), and copper(II)bromide (0.4 mmol, 0.2 equiv) were heated in DMF (2 mL) at 80 °C for 18−24 h. The reaction mixture was then cooled to room temperature, and excess iodine was quenched by addition of sodium thiosulfate solution. The aqueous mixture was extracted three times with ethyl acetate, and the combined organic phases were dried over sodium sulfate. After removal of the solvent, the solid residue was recrystallized from boiling heptane/ethyl acetate to yield the desired substituted *Z*-1,2-DBEs **2b−j**.

*(E)-1,4-Di-p-tolylbut-2-ene-1,4-dione (**2b**).* Yellow solid, 100 mg (38%), spectroscopic data in accordance with the literature:[40] ^{1}H NMR (400 MHz, chloroform-*d*) δ 8.01−7.94 (m, 6H), 7.35−7.30 (m, 4H), 2.44 (s, 6H) ppm; ^{13}C{^{1}H} NMR (101 MHz, chloroform-*d*) δ 189.5, 145.1, 135.1, 134.6, 129.7, 129.2, 21.9 ppm.

*(E)-1,4-Bis(4-isobutylphenyl)but-2-ene-1,4-dione (**2c**).* Yellow solid, 193 mg (55%), spectroscopic data in accordance with the literature:[40] ^{1}H NMR (400 MHz, chloroform-*d*) δ 8.04−7.96 (m, 6H), 7.30 (d, J = 8.2 Hz, 4H), 2.57 (d, J = 7.2 Hz, 4H), 1.93 (dt, J = 13.6, 6.8 Hz, 2H), 0.92 (d, J = 6.6 Hz, 12H) ppm; ^{13}C{^{1}H} NMR (101 MHz, chloroform-*d*) δ 189.6, 148.8, 135.1, 134.9, 129.8, 129.1, 45.6, 30.3, 22.5 ppm.

*(E)-1,4-Bis(4-(tert-butyl)phenyl)but-2-ene-1,4-dione (**2d**).* Yellow solid, 180 mg (52%), spectroscopic data in accordance with the literature:[40] ^{1}H NMR (400 MHz, chloroform-*d*) δ 8.05−7.99 (m, 6H), 7.58−7.52 (m, 4H), 1.36 (s, 18H) ppm; ^{13}C{^{1}H} NMR (101 MHz, chloroform-*d*) δ 189.6, 158.0, 135.1, 134.6, 129.1, 126.0, 35.4, 31.2 ppm.

*(E)-1,4-Bis(3,4-dimethylphenyl)but-2-ene-1,4-dione (**2e**).* Yellow solid, 200 mg (68%); mp 139−141 °C; ^{1}H NMR (400 MHz, chloroform-*d*) δ 8.00 (d, J = 2.4 Hz, 2H), 7.88−7.78 (m, 4H), 7.31−7.24 (m, 2H), 2.35 (s, 12H) ppm; ^{13}C{^{1}H} NMR (101 MHz, chloroform-*d*) δ 189.6, 143.7, 137.4, 134.9 (2C), 130.1, 123.0, 126.7, 20.2, 19.8 ppm; ATR-FTIR ν_{max} = 1645, 1601, 1409, 1299, 961, 752, 723 cm^{-1}; HRMS (ESI) m/z calcd $C_{20}H_{21}O_2$ [M + H]$^+$ 293.1536, found 293.1550.

*(E)-1,4-Bis(4-methoxyphenyl)but-2-ene-1,4-dione (**2f**).* Yellow solid, 148 mg (50%), spectroscopic data in accordance with the literature:[40] ^{1}H NMR (400 MHz, chloroform-*d*) δ 8.12−8.04 (m, 4H), 8.02 (s, 2H), 7.04−6.95 (m, 4H), 3.90 (s, 6H) ppm; ^{13}C{^{1}H} NMR (101 MHz, chloroform-*d*) δ 188.3, 164.3, 134.8, 131.5, 130.3, 114.3, 55.7 ppm.

*(E)-1,4-Bis(4-(trifluoromethyl)phenyl)but-2-ene-1,4-dione (**2g**).* Yellow solid, 86 mg (24%), spectroscopic data in accordance with the literature:[40] ^{1}H NMR (400 MHz, chloroform-*d*) δ 8.20−8.14 (m, 4H), 8.02 (s, 2H), 7.85−7.79 (m, 4H) ppm; ^{13}C{^{1}H} NMR (101 MHz, chloroform-*d*) δ 188.7, 139.4 (t, C−F, $^4J_{C-F}$ = 1.3 Hz), 135.35 (q, C−F, $^2J_{C-F}$ = 33 Hz), 135.27, 129.3, 126.2 (q, C−F, $^3J_{C-F}$ = 3.7 Hz), 123.6 (q, C−F, $^1J_{C-F}$ = 272.8 Hz) ppm.

*(E)-1,4-Bis(4-bromophenyl)but-2-ene-1,4-dione (**2h**).* Yellow solid, 275 mg (70%); mp 191−192 °C; ^{1}H NMR (400 MHz, chloroform-*d*) δ 7.97 (s, 2H), 7.91 (m, 4H), 7.72−7.65 (m, 4H) ppm; ^{13}C{^{1}H} NMR (101 MHz, chloroform-*d*) δ 188.7, 135.6, 135.0, 132.5, 130.5, 129.6 ppm; HRMS (ESI) m/z calcd $C_{16}H_{11}Br_2O_2$ [M + H]$^+$ 392.9120, found 392.9124.

*(E)-1,4-Bis(4-chlorophenyl)but-2-ene-1,4-dione (**2i**).* Yellow solid, 100 mg (33%), spectroscopic data in accordance with the literature:[40] ^{1}H NMR (400 MHz, chloroform-*d*) δ 8.02−7.98 (m, 4H), 7.97 (s, 2H), 7.56−7.44 (m, 4H) ppm; ^{13}C{^{1}H} NMR (101 MHz, chloroform-*d*) δ 188.4, 140.7, 135.2, 135.0, 130.4, 129.4 ppm.

*(E)-1-(4-Methoxyphenyl)-4-phenylbut-2-ene-1,4-dione (**2j**).* Isolated using column chromatography (SiO_2, 5% ethyl acetate in petroleum ether), yellow solid, 50 mg (19%), spectroscopic data in accordance with the literature:[40] ^{1}H NMR (400 MHz, chloroform-*d*) δ 8.12−8.03 (m, 4H), 8.00 (dd, J = 2.1, 0.5 Hz, 2H), 7.66−7.59 (m, 1H), 7.56−7.48 (m, 2H), 7.03−6.94 (m, 2H), 3.89 (s, 3H) ppm; ^{13}C{^{1}H} NMR (101 MHz, chloroform-*d*) δ 190.06, 188.05, 164.34, 137.08, 135.41, 134.52, 133.90, 131.46, 130.11, 128.98, 114.26, 55.70 ppm.

General Procedure for the Oxidative Annulation Reaction. To a 10 mL microwave vial were added substituted 1,2-DBE **2** (0.25 mmol), appropriate aniline derivative **1** (1.75 mmol), 1,4-dioxane (6 mL), and glacial acetic acid (1 mL). The mixture was irradiated using two 20 W white light CLF lamps, with a distance from the vial of 5 cm, for 4 h. To allow sufficient atmospheric oxygen into the reaction mixture, the vial was kept open during the course of the reaction. Solvent was then removed under reduced pressure, and the residue was purified using column chromatography (SiO_2, petroleum spirits/ethyl acetate) to yield the THQ **3**.

*(1,6-Dimethyl-1,2,3,4-tetrahydroquinoline-3,4-diyl)bis-(phenylmethanone) (**3a**).* Purified using column chromatography (SiO_2, 5% ethyl acetate in hexane), yellow solid, 67 mg, (73%); mp

https://dx.doi.org/10.1021/acs.joc.0c02819
J. Org. Chem. 2021, 86, 1901−1910

123−124 °C; ^{1}H NMR (400 MHz, chloroform-*d*) δ 8.11 (dd, *J* = 8.4, 1.4 Hz, 2H), 7.99−7.94 (m, 2H), 7.64−7.55 (m, 2H), 7.54−7.44 (m, 4H), 7.01−6.95 (m, 1H), 6.70−6.59 (m, 2H), 5.39 (dt, *J* = 9.2, 0.9 Hz, 1H), 4.49 (td, *J* = 9.6, 4.8 Hz, 1H), 3.49 (dd, *J* = 11.3, 4.9 Hz, 1H), 3.30 (dd, *J* = 11.3, 9.8 Hz, 1H), 2.90 (s, 3H), 2.11 (s, 3H) ppm; ^{13}C{^{1}H} NMR (101 MHz, chloroform-*d*) δ 202.5, 200.5, 144.0, 138.0, 136.1, 133.53, 133.48, 129.1 (2C), 129.0 (2C), 128.9 (2C), 128.65 (2C), 128.6, 128.2, 126.9, 122.5, 112.2, 53.2, 46.2, 45.5, 39.5, 20.5 ppm; ATR-FTIR ν_{max} = 1687, 1669, 1511, 1213, 967, 774, 690 cm^{-1}; HRMS (ESI) *m*/*z* calcd $C_{25}H_{24}NO_2$ [M + H]$^+$ 370.1807, found 370.1825.

*(1,6-Dimethyl-1,2,3,4-tetrahydroquinoline-3,4-diyl)bis(p-tolylmethanone) (**3b**).* Purified using column chromatography (SiO_2, 5% ethyl acetate in hexane), yellow solid, 63 mg (63%); mp 150−153 °C; ^{1}H NMR (400 MHz, chloroform-*d*) δ 8.03−7.96 (m, 2H), 7.88−7.81 (m, 2H), 7.32−7.21 (m, 4H), 6.95 (ddd, *J* = 8.3, 1.4, 0.8 Hz, 1H), 6.67−6.58 (m, 2H), 5.34 (d, *J* = 9.3 Hz, 1H), 4.44 (td, *J* = 9.7, 4.8 Hz, 1H), 3.45 (dd, *J* = 11.2, 4.8 Hz, 1H), 3.27 (dd, *J* = 11.3, 9.9 Hz, 1H), 2.89 (s, 3H), 2.43 (s, 3H), 2.40 (s, 3H), 2.09 (s, 3H) ppm; ^{13}C{^{1}H} NMR (101 MHz, chloroform-*d*) δ 202.1, 200.1, 144.44, 144.35, 144.1, 135.6, 133.6, 129.7 (2C), 129.6 (2C), 129.3 (2C), 128.9 (2C), 128.6, 128.5, 126.8, 122.9, 112.1, 53.4, 46.0, 45.36, 39.60, 21.9, 21.8, 20.5 ppm; ATR-FTIR ν_{max} = 1665, 1604, 1515, 1271, 1182, 828, 789 cm^{-1}; HRMS (ESI) *m*/*z* calcd $C_{27}H_{28}NO_2$ [M + H]$^+$ 398.2120, found 398.2132.

*(1,6-Dimethyl-1,2,3,4-tetrahydroquinoline-3,4-diyl)bis((4-isobutylphenyl)methanone) (**3c**).* Purified using column chromatography (SiO_2, 5% ethyl acetate in hexane), yellow solid, 61.9 mg (52%); mp 113−114 °C; ^{1}H NMR (400 MHz, chloroform-*d*) δ 8.00 (d, *J* = 8.3 Hz, 2H), 7.87 (d, *J* = 8.3 Hz, 2H), 7.29−7.19 (m, 4H), 6.95 (ddt, *J* = 8.3, 2.1, 0.8 Hz, 1H), 6.66−6.60 (m, 2H), 5.35 (d, *J* = 9.4 Hz, 1H), 4.46 (td, *J* = 9.7, 4.8 Hz, 1H), 3.47 (dd, *J* = 11.2, 4.8 Hz, 1H), 3.29 (dd, *J* = 11.2, 9.9 Hz, 1H), 2.90 (s, 3H), 2.54 (dd, *J* = 11.1, 7.2 Hz, 4H), 2.10 (s, 3H), 1.99−1.82 (m, 2H), 0.96−0.87 (m, 12H) ppm; ^{13}C{^{1}H} NMR (101 MHz, chloroform-*d*) δ 202.0, 200.1, 148.0, 147.9, 143.9, 135.8, 133.8, 129.5 (2C), 129.4 (2C), 128.9 (2C), 128.6 (2C), 128.50, 128.3, 126.6, 122.8, 112.0, 53.3, 46.1, 45.5, 45.4, 45.2, 39.5, 30.1, 22.4, 22.4, 22.3, 20.4 ppm; ATR-FTIR ν_{max} = 1668, 1603, 1514, 1270, 1181, 860, 799 cm^{-1}; HRMS (ESI) *m*/*z* calcd $C_{33}H_{40}NO_2$ [M + H]$^+$ 482.3059, found 482.3070.

*(1,6-Dimethyl-1,2,3,4-tetrahydroquinoline-3,4-diyl)bis((4-(tert-butyl)phenyl)methanone) (**3d**).* Purified using column chromatography (SiO_2, 5% ethyl acetate in hexane), yellow solid, 54.5 mg (45%); mp 179−181 °C; ^{1}H NMR (400 MHz, chloroform-*d*) δ 8.02 (d, *J* = 8.6 Hz, 2H), 7.89 (d, *J* = 8.6 Hz, 2H), 7.47 (dd, *J* = 15.8, 8.6 Hz, 3H), 6.99−6.92 (m, 1H), 6.67−6.59 (m, 2H), 5.35 (d, *J* = 9.4 Hz, 1H), 4.46 (td, *J* = 9.7, 4.8 Hz, 1H), 3.47 (dd, *J* = 11.3, 4.8 Hz, 1H), 3.28 (dd, *J* = 11.3, 9.9 Hz, 1H), 2.90 (s, 3H), 2.10 (s, 3H), 1.36 (s, 9H), 1.33 (s, 9H) ppm; ^{13}C{^{1}H} NMR (101 MHz, chloroform-*d*) δ 202.0, 199.9, 157.2, 157.0, 143.9, 135.4, 133.4, 128.9 (2C), 128.6 (2C), 128.5, 128.3, 126.7, 125.8 (2C), 125.7 (2C), 122.8, 111.9, 53.2, 45.9, 45.2, 39.5, 35.1, 35.1, 31.1, 31.0, 20.4 ppm; ATR-FTIR ν_{max} = 1668, 1604, 1514, 1270, 1188, 803 cm^{-1}; HRMS (ESI) *m*/*z* calcd $C_{33}H_{40}NO_2$ [M + H]$^+$ 482.3059, found 482.3069.

*(1,6-Dimethyl-1,2,3,4-tetrahydroquinoline-3,4-diyl)bis((3,4-dimethylphenyl)methanone) (**3e**).* Purified using column chromatography (SiO_2, 5% ethyl acetate in hexane), yellow solid, 43.4 mg (46%); mp 129−130 °C; ^{1}H NMR (400 MHz, chloroform-*d*) δ 7.85 (dd, *J* = 10.2, 2.4 Hz, 2H), 7.70 (dd, *J* = 10.2, 2.5 Hz, 2H), 7.25−7.18 (m, 2H), 6.95 (dd, *J* = 8.3, 2.2 Hz, 1H), 6.67−6.59 (m, 2H), 5.34 (d, *J* = 9.4 Hz, 1H), 4.45 (td, *J* = 9.7, 4.7 Hz, 1H), 3.49−3.41 (m, 1H), 3.28 (dd, *J* = 11.2, 10.0 Hz, 1H), 2.90 (d, *J* = 1.1 Hz, 3H), 2.34 (s, 3H), 2.32 (s, 3H), 2.31 (s, 3H), 2.29 (s, 3H), 2.09 (s, 3H) ppm; ^{13}C{^{1}H} NMR (101 MHz, chloroform-*d*) δ 202.4, 200.4, 144.0, 143.2, 143.1, 137.23, 137.20, 136.1, 134.1, 130.2, 130.14, 130.08, 129.9, 128.6, 128.5, 127.0, 126.8, 126.5, 123.1, 112.0, 53.5, 46.0, 45.3, 39.6, 20.5, 20.22, 20.18, 20.0, 19.9 ppm; ATR-FTIR ν_{max} = 1662, 1603, 1518, 1267, 1208, 794 cm^{-1}; HRMS (ESI) *m*/*z* calcd $C_{29}H_{32}NO_2$ [M + H]$^+$ 426.2433, found 426.2436.

*(1,6-Dimethyl-1,2,3,4-tetrahydroquinoline-3,4-diyl)bis((4-methoxyphenyl)methanone) (**3f**).* Purified using column chromatography (SiO_2, 5% ethyl acetate in hexane), off-white solid, 53.3 mg (50%); mp 139−140 °C; ^{1}H NMR (400 MHz, chloroform-*d*) δ 8.08 (d, *J* = 9.0 Hz, 2H), 7.95 (d, *J* = 8.9 Hz, 2H), 7.08−6.86 (m, 5H), 6.70−6.56 (m, 2H), 5.32 (dt, *J* = 9.7, 1.0 Hz, 1H), 4.44 (td, *J* = 10.0, 4.8 Hz, 1H), 3.88 (s, 3H), 3.86 (s, 3H), 3.44 (dd, *J* = 11.2, 4.8 Hz, 1H), 3.28 (dd, *J* = 11.2, 10.2 Hz, 1H), 2.90 (s, 3H), 2.09 (s, 3H) ppm; ^{13}C{^{1}H} NMR (101 MHz, chloroform-*d*) δ 200.9, 199.0, 163.9, 163.8, 144.0, 131.5 (2C), 131.2, 131.0 (2C), 129.1, 128.5, 128.4, 126.8, 123.1, 114.1 (2C), 114.0 (2C), 112.2, 55.59, 55.58, 53.6, 46.0, 45.0, 39.6, 20.5 ppm; ATR-FTIR ν_{max} = 1661, 1598, 1572, 1509, 1316, 1255, 1170, 845 cm^{-1}; HRMS (ESI) *m*/*z* calcd $C_{27}H_{28}NO_4$ [M + H]$^+$ 430.2018, found 430.2024.

*(1,6-Dimethyl-1,2,3,4-tetrahydroquinoline-3,4-diyl)bis((4-(trifluoromethyl)phenyl)methanone) (**3g**).* Purified using column chromatography (SiO_2, 5% ethyl acetate in hexane), thick yellow-orange oil, 35 mg (28%); ^{1}H NMR (400 MHz, chloroform-*d*) δ 8.25−8.13 (m, 2H), 8.08−8.01 (m, 2H), 7.83−7.71 (m, 4H), 6.99 (dq, *J* = 8.2, 0.9 Hz, 1H), 6.66 (d, *J* = 8.4 Hz, 1H), 6.54−6.48 (m, 1H), 5.32 (d, *J* = 9.5 Hz, 1H), 4.46 (td, *J* = 9.7, 5.1 Hz, 1H), 3.55−3.44 (m, 1H), 3.29 (dd, *J* = 11.2, 10.1 Hz, 1H), 2.90 (d, *J* = 0.7 Hz, 3H), 2.10 (s, 3H) ppm; ^{13}C{^{1}H} NMR (101 MHz, chloroform-*d*) δ 201.6, 199.8, 143.8, 140.5, 138.7, 134.8 (q, C−F, $^2J_{C-F}$ = 33 Hz), 134.7 (q, C−F, $^2J_{C-F}$ = 33 Hz), 129.4 (2C), 129.0 (2C), 128.2, 127.3, 126.4−125.8 (m, C−F, 4C), 123.7 (q, C−F, $^1J_{C-F}$ = 272.6 Hz), 123.6 (q, C−F, $^1J_{C-F}$ = 272.6 Hz), 121.9, 121.2, 112.4, 52.9, 46.6, 46.2, 39.5, 20.46 ppm; ^{19}F NMR (470 MHz, chloroform-*d*) δ −63.16(s, 3F), −63.23(s, 3F) ppm; ATR-FTIR ν_{max} = 1683, 1512, 1322, 1170, 1128, 1067 cm^{-1}; HRMS (ESI) *m*/*z* calcd $C_{27}H_{22}F_6NO_2$ [M + H]$^+$ 506.1555, found 506.1548.

*(1,6-Dimethyl-1,2,3,4-tetrahydroquinoline-3,4-diyl)bis((4-bromophenyl)methanone) (**3h**).* Purified using column chromatography (SiO_2, 5% ethyl acetate in hexane), yellow solid, 113.4 mg (84%); mp 128−130 °C; ^{1}H NMR (400 MHz, chloroform-*d*) δ 8.00−7.88 (m, 2H), 7.85−7.77 (m, 2H), 7.71−7.56 (m, 4H), 6.97 (ddt, *J* = 8.3, 2.2, 0.8 Hz, 1H), 6.65 (d, *J* = 8.3 Hz, 1H), 6.52 (dt, *J* = 2.0, 0.9 Hz, 1H), 5.30−5.16 (m, 1H), 4.39 (td, *J* = 9.9, 5.0 Hz, 1H), 3.44 (dd, *J* = 11.3, 5.0 Hz, 1H), 3.26 (dd, *J* = 11.3, 10.1 Hz, 1H), 2.90 (s, 3H), 2.09 (s, 3H) ppm; ^{13}C{^{1}H} NMR (101 MHz, chloroform-*d*) δ 201.4, 199.6, 143.8, 136.67, 134.7, 132.34 (2C), 132.28 (2C), 130.6 (2C), 130.2 (2C), 128.99, 128.98, 128.8, 128.3, 127.1, 122.3, 112.3, 53.2, 46.3, 45.6, 39.5, 20.5 ppm; ATR-FTIR ν_{max} = 2856, 1670, 1654, 1582, 1507, 1067, 1005, 816 cm^{-1}; HRMS (ESI) *m*/*z* calcd $C_{25}H_{22}Br_2NO_2$ [M + H]$^+$ 526.0017, found 526.0025.

*(1,6-Dimethyl-1,2,3,4-tetrahydroquinoline-3,4-diyl)bis((4-chlorophenyl)methanone) (**3i**).* Purified using column chromatography (SiO_2, 5% ethyl acetate in hexane), yellow solid, 83.1 mg (72%); mp 149−150 °C; ^{1}H NMR (400 MHz, chloroform-*d*) δ 8.03 (d, *J* = 8.6 Hz, 2H), 7.89 (d, *J* = 8.7 Hz, 2H), 7.46 (dd, *J* = 16.1, 8.6 Hz, 4H), 6.97 (ddt, *J* = 8.3, 2.1, 0.8 Hz, 1H), 6.65 (d, *J* = 8.4 Hz, 1H), 6.54 (dt, *J* = 2.0, 0.9 Hz, 1H), 5.28 (dd, *J* = 9.6, 1.1 Hz, 1H), 4.41 (td, *J* = 9.9, 5.0 Hz, 1H), 3.45 (dd, *J* = 11.3, 5.0 Hz, 1H), 3.27 (dd, *J* = 11.2, 10.1 Hz, 1H), 2.90 (s, 3H), 2.10 (s, 3H) ppm; ^{13}C{^{1}H} NMR (101 MHz, chloroform-*d*) δ 201.2, 199.4, 143.8, 140.2, 140.2, 136.3, 134.3, 130.5 (2C), 130.1 (2C), 129.34 (2C), 129.28 (2C), 128.8, 128.3, 127.0, 122.3, 112.2, 53.2, 46.3, 45.6, 39.5, 20.5 ppm; ATR-FTIR ν_{max} = 2859, 1673, 1587, 1512, 1399, 1204, 1090, 818 cm^{-1}; HRMS (ESI) *m*/*z* calcd $C_{25}H_{22}Cl_2NO_2$ [M + H]$^+$ 438.1028, found 438.1028.

*(3-Benzoyl-1,6-dimethyl-1,2,3,4-tetrahydroquinolin-4-yl)(4-methoxyphenyl)methanone (**3ja**) and (4-benzoyl-1,6-Dimethyl-1,2,3,4-tetrahydroquinolin-3-yl)(4-methoxyphenyl)methanone (**3jb**).* Purified using column chromatography (SiO_2, 1% ethyl acetate in hexane), thick yellow oil, 66 mg (64%); ^{1}H NMR (400 MHz, chloroform-*d*) δ 8.11−8.06 (m, overlapping **3ja** and **3jb**, 4H), 7.98−7.92 (m, overlapping **3ja** and **3jb**, 4H), 7.62−7.53 (m, overlapping **3ja** and **3jb**, 2H), 7.52−7.42 (m, overlapping **3ja** and **3jb**, 4H), 7.00−6.90 (m, overlapping **3ja** and **3jb**, 6H), 6.67−6.57 (m, overlapping **3ja** and **3jb**, 4H), 5.38−5.31 (m, overlapping **3ja** and **3jb**, 2H), 4.52−4.40 (m,

https://dx.doi.org/10.1021/acs.joc.0c02819
J. Org. Chem. 2021, 86, 1901−1910

overlapping **3ja** and **3ja**, 2H), 3.89 (s, OMe **3ja**, 3H), 3.86 (s, OMe **3jb**, 3H), 3.50−3.42 (m, overlapping **3ja** and **3jb**, 2H), 3.34−3.25 (m, overlapping **3ja** and **3jb**, 2H), 2.90 (s, NMe, 3H), 2.89 (s, NMe, 3H), 2.10 (s, ArMe **3ja**, 3H), 2.09 (s, ArMe **3jb**, 3H) ppm; $^{13}C\{^1H\}$ NMR (101 MHz, chloroform-*d*) δ 202.7, 200.8, 200.7, 198.8, 163.93, 163.89, 144.0, 138.1, 136.1, 133.5, 133.4, 131.5 (2C), 131.12, 131.05 (2C), 130.5, 129.1 (2C), 128.92 (2C), 128.85 (2C), 128.7 (2C), 128.6, 128.52, 128.49 (2C), 128.2, 126.81, 126.76, 122.8, 114.1, 114.0, 112.11, 112.09, 55.6 (2C), 53.5, 53.3, 46.3, 45.8, 45.4, 45.1, 39.57, 39.55, 20.49, 20.47 ppm; ATR-FTIR ν_{max} = 1660, 1598, 1572, 1509, 1317, 1257, 1170 cm^{-1}; HRMS (ESI) *m*/*z* calcd $C_{26}H_{26}NO_3$ $[M + H]^+$ 400.1911, found 400.1913.

*(1-Methyl-1,2,3,4-tetrahydroquinoline-3,4-diyl)bis-(phenylmethanone) (**3k**).* Purified using column chromatography (SiO_2, 5% ethyl acetate in hexane), yellow oil, 44.3 mg (59%); mp 104−105 °C; ^1H NMR (400 MHz, chloroform-*d*) δ 8.09 (d, *J* = 8.4 Hz, 2H), 8.00−7.94 (m, 2H), 7.59 (dtd, *J* = 8.5, 7.3, 1.3 Hz, 2H), 7.53−7.43 (m, 4H), 7.14 (tt, *J* = 7.2, 0.9 Hz, 1H), 6.78 (dd, *J* = 7.6, 1.3 Hz, 1H), 6.71 (dt, *J* = 8.4, 1.2 Hz, 1H), 6.60−6.54 (m, 1H), 5.38 (dd, *J* = 9.4, 1.2 Hz, 1H), 4.55−4.46 (m, 1H), 3.56−3.46 (m, 1H), 3.35 (ddd, *J* = 11.2, 10.1, 1.1 Hz, 1H), 2.93 (d, *J* = 1.1 Hz, 3H) ppm; $^{13}C\{^1H\}$ NMR (101 MHz, chloroform-*d*) δ 202.1, 200.5, 145.8, 137.9, 136.0, 133.5, 133.4, 129.0 (2C), 128.84 (2C), 128.77 (2C), 128.6 (2C), 127.9, 127.8, 122.1, 117.3, 111.7, 52.9, 46.1, 45.0, 39.2 ppm; ATR-FTIR ν_{max} = 1669, 1598, 1578,1506, 1448, 1228, 1202, 753, 703 cm^{-1}; HRMS (ESI) *m*/*z* calcd $C_{24}H_{22}NO_2$ $[M + H]^+$ 356.1651, found 356.1661.

*(1,5,7-Trimethyl-1,2,3,4-tetrahydroquinoline-3,4-diyl)bis-(phenylmethanone) (**3m**).* Purified using column chromatography (SiO_2, 5% ethyl acetate in hexane), white solid, 39.9 mg (42%); mp 198−199 °C; ^1H NMR (400 MHz, chloroform-*d*) δ 8.10−8.02 (m, 2H), 7.78 (dd, *J* = 7.4, 1.2 Hz, 2H), 7.63−7.52 (m, 2H), 7.52−7.40 (m, 4H), 6.52−6.38 (m, 2H), 5.46−5.33 (m, 1H), 3.83 (q, *J* = 1.5 Hz, 1H), 3.46 (dd, *J* = 11.9, 3.4 Hz, 1H), 3.41−3.31 (m, 1H), 2.71 (s, 3H), 2.26 (s, 3H), 2.06 (s, 3H) ppm; $^{13}C\{^1H\}$ NMR (101 MHz, chloroform-*d*) δ 201.8, 198.9, 146.9, 137.0, 136.3, 136.1, 135.6, 133.5, 133.0, 129.1 (2C), 128.8 (2C), 128.6 (2C), 128.3 (2C), 121.6, 116.0, 111.0, 50.4, 44.3, 43.2, 40.1, 21.8, 20.6 ppm; ATR-FTIR ν_{max} = 1680, 1577, 1447, 1331, 1268, 1214, 970, 702 cm^{-1}; HRMS (ESI) *m*/*z* calcd $C_{26}H_{26}NO_2$ $[M + H]^+$ 384.1964, found 384.1991.

*(6-Methoxy-1-methyl-1,2,3,4-tetrahydroquinoline-3,4-diyl)bis-(phenylmethanone) (**3n**).* Purified using column chromatography (SiO_2, 5% ethyl acetate in hexane), yellow solid, 58.6 mg (61%); 129−130 °C; ^1H NMR (400 MHz, chloroform-*d*) δ 8.14−8.04 (m, 2H), 7.96 (dt, *J* = 7.0, 1.5 Hz, 2H), 7.58 (dddd, *J* = 9.0, 7.0, 5.2, 1.4 Hz, 2H), 7.53−7.39 (m, 4H), 6.81−6.61 (m, 2H), 6.43 (dd, *J* = 2.9, 1.3 Hz, 1H), 5.41 (d, *J* = 9.2 Hz, 1H), 4.51 (tdd, *J* = 9.5, 4.9, 1.3 Hz, 1H), 3.57 (s, 3H), 3.46 (ddd, *J* = 11.2, 5.0, 1.3 Hz, 1H), 3.29−3.19 (m, 1H), 2.87 (s, 3H) ppm; $^{13}C\{^1H\}$ NMR (101 MHz, chloroform-*d*) δ 201.9, 200.4, 152.0, 140.9, 138.0, 136.1, 133.57, 133.56, 129.1 (2C), 129.0 (2C), 128.9 (2C), 128.7 (2C), 123.9, 114.6, 113.3, 113.2, 55.7, 53.5, 46.2, 45.4, 40.0 ppm; ATR-FTIR ν_{max} = 1663, 1594, 1579, 1510, 1447, 1209, 803, 689 cm^{-1}; HRMS (ESI) *m*/*z* calcd $C_{25}H_{24}NO_3$ $[M + H]^+$ 386.1756, found 386.1753.

*(7-Methoxy-1-methyl-1,2,3,4-tetrahydroquinoline-3,4-diyl)bis-(phenylmethanone) (**3o**).* Purified using column chromatography (SiO_2, 5% ethyl acetate in hexane), yellow solid, 26.9 mg (28%); mp 152−153 °C; ^1H NMR (400 MHz, chloroform-*d*) δ 8.07−8.00 (m, 2H), 7.85−7.77 (m, 2H), 7.57−7.49 (m, 2H), 7.46−7.38 (m, 4H), 7.13 (td, *J* = 8.3, 0.6 Hz, 1H), 6.42 (dd, *J* = 8.4, 0.8 Hz, 1H), 6.30 (dd, *J* = 8.2, 0.9 Hz, 1H), 5.46 (d, *J* = 5.5 Hz, 1H), 4.00 (ddd, *J* = 6.5, 5.5, 3.4 Hz, 1H), 3.50 (s, 3H), 3.44 (ddd, *J* = 11.7, 3.4, 0.6 Hz, 1H), 3.36−3.28 (m, 1H), 2.83 (s, 3H) ppm; $^{13}C\{^1H\}$ NMR (101 MHz, chloroform-*d*) δ 203.3, 199.6, 157.0, 148.0, 137.0, 136.1, 133.2, 132.7, 128.8 (2C), 128.57 (2C), 128.55 (2C), 128.4 (2C), 128.2, 110.5, 105.8, 100.6, 55.1, 51.6, 44.6, 41.5, 40.0 ppm; ATR-FTIR ν_{max} = 1677, 1579, 1447, 1211, 967, 700 cm^{-1}; HRMS (ESI) *m*/*z* calcd $C_{25}H_{24}NO_3$ $[M + H]^+$ 386.1756, found 386.1751.

*(6-Fluoro-1-methyl-1,2,3,4-tetrahydroquinoline-3,4-diyl)bis-(phenylmethanone) (**3p**).* Purified using column chromatography (SiO_2, 5% ethyl acetate in hexane), yellow solid, 49.9 mg (51%); mp 132−133 °C; ^1H NMR (400 MHz, chloroform-*d*) δ 8.13−8.07 (m, 2H), 8.00−7.90 (m, 2H), 7.65−7.55 (m, 2H), 7.54−7.43 (m, 4H), 6.85 (dddd, *J* = 9.0, 8.1, 2.9, 0.8 Hz, 1H), 6.63 (dd, *J* = 9.0, 4.8 Hz, 1H), 6.54 (ddd, *J* = 9.4, 2.9, 1.1 Hz, 1H), 5.38 (dd, *J* = 8.9, 1.0 Hz, 1H), 4.46 (td, *J* = 9.2, 4.9 Hz, 1H), 3.50 (dd, *J* = 11.4, 4.9 Hz, 1H), 3.29 (dd, *J* = 11.3, 9.5 Hz, 1H), 2.88 (s, 3H) ppm; $^{13}C\{^1H\}$ NMR (101 MHz, chloroform-*d*) δ 201.5, 200.1, 155.5(d, C−F, $^1J_{C-F}$ = 236.2 Hz), 142.8(d, C−F, $^4J_{C-F}$ = 1.9 Hz), 137.5, 135.9, 133.8, 133.7, 129.10 (2C), 129.06 (2C), 128.9 (2C), 128.6 (2C), 123.4 (d, C−F, $^3J_{C-F}$ = 6.9 Hz), 114.82 (d, C−F, $^2J_{C-F}$ = 23.3 Hz), 114.31 (d, C−F, $^2J_{C-F}$ = 21.8 Hz), 112.8 (d, C−F, $^3J_{C-F}$ = 7.7 Hz), 53.00, 45.86, 45.07, 39.77 ppm; ^{19}F NMR (470 MHz, chloroform-*d*) δ −127.15 to −127.23(m) ppm; ATR-FTIR ν_{max} = 1670, 1591, 1577, 1505, 1448, 1211, 906, 729, 685 cm^{-1}; HRMS (ESI) *m*/*z* calcd $C_{24}H_{21}FNO_2$ $[M + H]^+$ 374.1556, found 374.1572.

*(6-Bromo-1-methyl-1,2,3,4-tetrahydroquinoline-3,4-diyl)bis-(phenylmethanone) (**3q**).* Purified using column chromatography (SiO_2, 5% ethyl acetate in hexane), off-white solid, 26 mg (24%); mp 192−194 °C; ^1H NMR (400 MHz, chloroform-*d*) δ 8.10−8.03 (m, 2H), 7.97−7.88 (m, 2H), 7.67−7.55 (m, 2H), 7.54−7.42 (m, 4H), 7.22 (ddt, *J* = 8.7, 1.6, 0.7 Hz, 1H), 6.88−6.84 (m, 1H), 6.55 (dd, *J* = 8.9, 1.2 Hz, 1H), 5.36−5.30 (m, 1H), 4.44−4.33 (m, 1H), 3.53 (ddd, *J* = 11.5, 4.7, 1.3 Hz, 1H), 3.34 (ddd, *J* = 11.8, 9.3, 1.2 Hz, 1H), 2.88 (d, *J* = 1.3 Hz, 3H) ppm; $^{13}C\{^1H\}$ NMR (101 MHz, chloroform-*d*) δ 201.6, 200.0, 145.1, 137.5, 135.9, 133.9, 133.7, 130.8, 130.6, 129.2 (2C), 129.1 (2C), 129.0 (2C), 128.7 (2C), 123.8, 113.3, 109.3, 52.5, 45.8, 44.8, 39.4 ppm; ATR-FTIR ν_{max} = 1686, 1668, 1591, 1499, 1447, 1209, 699, 691 cm^{-1}; HRMS (ESI) *m*/*z* calcd $C_{24}H_{21}BrNO_2$ $[M + H]^+$ 434.0756, found 434.0752.

*(1-Methyl-1,2,3,4-tetrahydrobenzo[h]quinoline-3,4-diyl)bis-(phenylmethanone) (**3r**).* Purified using column chromatography (SiO_2, 5% ethyl acetate in hexane), white solid, 19.2 mg (18%); mp 197−200 °C; ^1H NMR (400 MHz, chloroform-*d*) δ 8.26−8.15 (m, 2H), 8.04−7.99 (m, 2H), 7.77−7.72 (m, 1H), 7.67−7.42 (m, 9H), 7.38 (d, *J* = 8.6 Hz, 1H), 6.99 (d, *J* = 8.5 Hz, 1H), 5.85 (d, *J* = 9.8 Hz, 1H), 4.82 (ddd, *J* = 11.3, 9.8, 3.3 Hz, 1H), 3.66 (dd, *J* = 13.5, 3.3 Hz, 1H), 3.39−3.28 (m, 1H), 3.28 (s, 3H) ppm; $^{13}C\{^1H\}$ NMR (101 MHz, chloroform-*d*) δ 203.0, 200.4, 138.3, 136.1, 133.7, 133.7, 133.6, 129.4 (2C), 129.09 (2C), 129.05 (2C), 128.99, 128.68, 128.6 (2C), 128.5, 126.0, 125.9, 124.0 (2C), 123.96, 123.89, 54.7, 46.0, 44.7, 40.3 ppm; ATR-FTIR ν_{max} = 1667, 1596, 1446, 1266, 1216, 1001, 986, 797, 783 cm^{-1}; HRMS (ESI) *m*/*z* calcd $C_{28}H_{24}NO_2$ $[M + H]^+$ 406.1807, found 406.1826.

*(1-Ethyl-1,2,3,4-tetrahydroquinoline-3,4-diyl)bis-(phenylmethanone) (**3s**).* Purified using column chromatography (SiO_2, 1% ethyl acetate in hexane), yellow oil, 42.4 mg (46%); ^1H NMR (400 MHz, chloroform-*d*) δ 8.13−8.06 (m, 2H), 8.03−7.91 (m, 2H), 7.64−7.55 (m, 2H), 7.54−7.42 (m, 4H), 7.11 (t, *J* = 7.8 Hz, 1H), 6.82−6.69 (m, 2H), 6.53 (dd, *J* = 8.3, 6.7 Hz, 1H), 5.38 (d, *J* = 9.4 Hz, 1H), 4.59−4.40 (m, 1H), 3.64−3.18 (m, 4H), 1.16 (t, *J* = 6.88 Hz, 3H) ppm; $^{13}C\{^1H\}$ NMR (101 MHz, chloroform-*d*) δ 202.3, 200.9, 144.3, 138.2, 136.2, 133.6, 133.5, 129.1 (2C), 129.0 (2C), 128.9 (2C), 128.7 (2C), 128.4, 128.1, 121.6, 116.7, 111.6, 50.3, 46.6, 45.7, 44.6, 11.1 ppm; ATR-FTIR ν_{max} = 1675, 1597, 1495, 1449, 1346, 743, 691 cm^{-1}; HRMS (ESI) *m*/*z* calcd $C_{25}H_{24}NO_2$ $[M + H]^+$ 370.1807, found 370.1817.

*(1-Butyl-1,2,3,4-tetrahydroquinoline-3,4-diyl)bis-(phenylmethanone) (**3t**).* Purified using column chromatography (SiO_2, 1% ethyl acetate in hexane), yellow oil, 57.4 mg (60%); ^1H NMR (400 MHz, chloroform-*d*) δ8.12−8.07 (m, 2H), 8.00−7.93 (m, 2H), 7.64−7.53 (m, 2H), 7.54−7.42 (m, 4H), 7.10 (dddd, *J* = 8.2, 7.3, 1.6, 0.8 Hz, 1H), 6.76 (dt, *J* = 7.6, 1.4 Hz, 1H), 6.69 (dd, *J* = 8.4, 1.1 Hz, 1H), 6.51 (td, *J* = 7.4, 1.2 Hz, 1H), 5.37 (d, *J* = 9.5 Hz, 1H), 4.47 (ddd, *J* = 10.1, 9.4, 4.2 Hz, 1H), 3.57 (dd, *J* = 11.6, 4.3 Hz, 1H), 3.47−3.31 (m, 2H), 3.28−3.15 (m, 1H), 1.64−1.52 (m, 2H), 1.42−1.30 (m, 2H), 0.94 (t, *J* = 7.3 Hz, 3H) ppm; $^{13}C\{^1H\}$ NMR (101 MHz, chloroform-*d*) δ 202.3, 200.8, 144.5, 138.2, 136.1, 133.63, 133.56, 129.1 (2C), 129.0 (2C), 128.9 (2C), 128.7 (2C), 128.4, 128.1, 121.5, 116.8, 111.8, 51.7, 51.3, 46.6, 44.5, 28.5, 20.5, 14.1 ppm;

https://dx.doi.org/10.1021/acs.joc.0c02819
J. Org. Chem. 2021, 86, 1901−1910

ATR-FTIR ν_{max} = 1678, 1599, 1502, 1457, 1449, 1218, 744 cm^{-1}; HRMS (ESI) *m/z* calcd $C_{27}H_{28}NO_2$ $[M + H]^+$ 398.2120, found 398.2110.

*(1-Benzyl-1,2,3,4-tetrahydroquinoline-3,4-diyl)bis-(phenylmethanone) (**3u**).* Purified using column chromatography (SiO_2, 1% ethyl acetate in hexane), yellow oil, 26.1 mg (25%); ^1H NMR (400 MHz, chloroform-*d*) δ 8.16−8.10 (m, 2H), 7.89−7.82 (m, 2H), 7.65−7.59 (m, 1H), 7.57−7.50 (m, 3H), 7.43−7.37 (m, 2H), 7.37−7.26 (m, 5H), 7.11−7.01 (m, 1H), 6.83 (d, *J* = 7.4 Hz, 1H), 6.74 (d, *J* = 8.3 Hz, 1H), 6.59 (t, *J* = 7.5 Hz, 1H), 5.48 (d, *J* = 9.2 Hz, 1H), 4.64−4.47 (m, 3H), 3.67 (dd, *J* = 11.8, 4.3 Hz, 1H), 3.52−3.41 (m, 1H) ppm; $^{13}C\{^1H\}$ NMR (101 MHz, chloroform-*d*) δ 202.3, 200.5, 145.0, 138.2, 138.0, 135.9, 133.6, 129.1 (2C), 129.0 (2C), 128.89 (2C), 128.87 (2C), 128.6 (2C), 128.4, 128.2, 127.9, 127.0 (2C), 125.9, 121.4, 117.4, 112.3, 55.4, 51.2, 46.4, 44.7 ppm; ATR-FTIR ν_{max} = 1677, 1599, 1497, 1449, 1220, 749, 696 cm^{-1}; HRMS (ESI) *m/z* calcd $C_{30}H_{26}NO_2$ $[M + H]^+$ 432.1958, found 432.1971.

Multicomponent Synthesis of 3a. For the multicomponent reaction, Wittig reagent **4** (74.4 mg, 0.2 mmol, 1 equiv), phenylglyoxal (35.5 mg, 0.26 mmol, 1.4 equiv), and amine **1a** (164 mg, 1.2 mmol, 6.2 equiv) were mixed in 1,4-dioxane (6 mL), and the reaction mixture was irradiated according to the general procedure for 18 h. Solvent was then removed under reduced pressure, and the product was isolated using flash chromatography (silica gel, 5% ethyl acetate in petroleum ethers) to yield the desired product **3a** (29 mg, 40%).

Synthesis of 3a on 1 mmol Scale. To a round-bottom flask were added 1,2-DBE **2a** (245.4 mg, 1 mmol), 4′,*N*,*N*-trimethylaniline **1a** (947 mg, 7 mmol), 1,4-dioxane (25 mL), and glacial acetic acid (4 mL). The mixture was irradiated using two 20 W white light CLF lamps, with a distance from the flask of 5 cm, for 18 h. To allow sufficient atmospheric oxygen into the reaction mixture, the flask was kept open during the course of the reaction. Solvent was then removed under reduced pressure, and the residue was purified using column chromatography (SiO_2, 5% ethyl acetate in petroleum spirits) to yield the THQ **3a** (204.1 mg, 53%).

Condensation Reaction of 3a with Ammonium Acetate to Pyrrole Derivative 6. Following a modified published procedure,[45] diketo compound **3a** (106.3 mg, 0.29 mmol, 1 equiv) was dissolved in glacial acetic acid (1.8 mL). Ammonium acetate (189 mg, 2.4 mmol, 8.2 equiv) was then added, and the mixture was heated to 120 °C using a heating block in a sealed vial for 4 h. The resulting deep red solution was concentrated in vacuo, and the product was isolated using column chromatography (SiO_2, 5% methanol in dichloromethane) as dark red crystals, 43 mg (43%); mp 223−225 °C; ^1H NMR (400 MHz, chloroform-*d*) δ 8.50 (s, 1H), 8.09 (dd, *J* = 2.1, 1.0 Hz, 1H), 7.81 (ddd, *J* = 8.2, 7.2, 1.3 Hz, 4H), 7.47 (t, *J* = 7.5 Hz, 2H), 7.43−7.29 (m, 4H), 7.22−7.14 (m, 2H), 3.99 (s, 3H), 2.30 (s, 3H) ppm; $^{13}C\{^1H\}$ NMR (101 MHz, chloroform-*d*) δ 145.1, 142.6, 137.5, 137.0, 136.6, 134.9, 130.7, 129.7 (2C), 128.8 (2C), 128.4 (2C), 128.0 (2C), 127.6, 127.4, 127.3, 124.2, 124.0, 117.4, 116.3, 115.4, 43.4, 21.5 ppm; ATR-FTIR ν_{max} = 1591, 1454, 1356, 1225, 807, 765, 694 cm^{-1}; HRMS (ESI) *m/z* calcd $C_{25}H_{21}N_2$ $[M + H]^+$ 349.1704, found 349.1717.

Synthesis of Furan Derivative 7. Following a modified published procedure,[46] diketo compound **3a** (40.7 mg, 0.11 mmol) was dissolved in acetic anhydride (1.0 mL). Concentrated hydrochloric acid (0.3 mL) was then added at 0 °C. The mixture was heated to 80 °C using a heating block in a sealed vial for 18 h. The resulting orange solution was concentrated in vacuo, and the product was isolated using column chromatography (SiO_2, 2% ethyl acetate in hexane) as an air sensitive yellow-orange oil, 21.8 mg (56%); ^1H NMR (400 MHz, chloroform-*d*) δ 7.88−7.81 (m, 2H), 7.61−7.55 (m, 2H), 7.51 (d, *J* = 2.1 Hz, 1H), 7.49−7.40 (m, 4H), 7.40−7.33 (m, 1H), 7.30 (ddt, *J* = 7.5, 5.8, 1.0 Hz, 1H), 7.05−6.98 (m, 1H), 6.74 (d, *J* = 8.3 Hz, 1H), 4.30 (s, 2H), 2.97 (s, 3H), 2.19 (s, 3H) ppm; $^{13}C\{^1H\}$ NMR (101 MHz, chloroform-*d*) δ 146.4, 145.1, 144.0, 131.9, 130.9, 129.0 (2C), 128.9 (2C), 128.7, 128.3, 127.9, 127.4 (2C), 127.3, 125.19 (2C), 125.15, 119.24, 119.16, 117.5, 113.2, 49.4, 39.5, 20.6 ppm; ATR-FTIR ν_{max} = 2924, 1598, 1493, 1448, 1242, 1126 cm^{-1}; HRMS (ESI) *m/z* calcd $C_{25}H_{22}NO$ $[M + H]^+$ 352.1701, found 352.1697.

■ ASSOCIATED CONTENT

Supporting Information

The Supporting Information is available free of charge at https://pubs.acs.org/doi/10.1021/acs.joc.0c02819.

Photophysical measurements, synthesis procedures, NMR characterization data, and X-ray crystallographic data for **3q** (CCDC 2008622) (PDF)

Accession Codes

CCDC 2008622 contains the supplementary crystallographic data for this paper. These data can be obtained free of charge via www.ccdc.cam.ac.uk/data_request/cif, or by emailing data_request@ccdc.cam.ac.uk, or by contacting The Cambridge Crystallographic Data Centre, 12 Union Road, Cambridge CB2 1EZ, UK; fax: +44 1223 336033.

■ AUTHOR INFORMATION

Corresponding Author

Henrik Sundén − *Department of Chemistry and Chemical Engineering, Chalmers University of Technology, 41296 Gothenburg, Sweden; Chemistry and Molecular Biology, University of Gothenburg, 41296 Gothenburg, Sweden;* orcid.org/0000-0001-6202-7557; Email: henrik.sunden@chem.gu.se

Authors

August Runemark − *Department of Chemistry and Chemical Engineering, Chalmers University of Technology, 41296 Gothenburg, Sweden;* orcid.org/0000-0002-3650-1881

Savannah C. Zacharias − *Chemistry and Molecular Biology, University of Gothenburg, 41296 Gothenburg, Sweden;* orcid.org/0000-0003-0895-9120

Complete contact information is available at: https://pubs.acs.org/10.1021/acs.joc.0c02819

Notes

The authors declare no competing financial interest.

■ ACKNOWLEDGMENTS

This work was supported by grants from the Swedish research council FORMAS (2019-00699) and from Olle Engkvists Stiftelse. The X-ray crystallographic data used in this work was collected by Ivana Císařová, Department of Inorganic Chemistry, Faculty of Science, Charles University, Hlavova 2030/8, 128 43 Prague 2, Czech Republic.

■ REFERENCES

(1) Yuan, Y.; Majumder, S.; Yang, M.; Guo, S. Recent Advances in Catalyst-Free Photochemical Reactions via Electron-Donor-Acceptor (EDA) Complex Process. *Tetrahedron Lett.* **2020**, *61* (8), 151506.

(2) Wei, Y.; Zhou, Q.-Q.; Tan, F.; Lu, L.-Q.; Xiao, W.-J. Visible-Light-Driven Organic Photochemical Reactions in the Absence of External Photocatalysts. *Synthesis* **2019**, *51* (16), 3021−3054.

(3) Crisenza, G. E. M.; Mazzarella, D.; Melchiorre, P. Synthetic Methods Driven by the Photoactivity of Electron Donor-Acceptor Complexes. *J. Am. Chem. Soc.* **2020**, *142* (12), 5461−5476.

(4) Lima, C. G. S.; de M. Lima, T.; Duarte, M.; Jurberg, I. D.; Paixão, M. W. Organic Synthesis Enabled by Light-Irradiation of EDA Complexes: Theoretical Background and Synthetic Applications. *ACS Catal.* **2016**, *6* (3), 1389−1407.

(5) Postigo, A. Electron Donor-Acceptor Complexes in Perfluoroalkylation Reactions. *Eur. J. Org. Chem.* **2018**, *2018* (46), 6391−6404.
(6) Guo, W.; Tao, K.; Xie, Z.; Cai, L.; Zhao, M.; Tan, W.; Liu, G.; Mei, W.; Deng, L.; Fan, X.; Zheng, L. Photodriven Photocatalyst/Metal-Free Direct C-C/C-N Bond Formation: Synthesis of Indoles via EDA Complexes. *J. Org. Chem.* **2019**, *84* (21), 14168−14178.
(7) Li, Z.; Ma, P.; Tan, Y.; Liu, Y.; Gao, M.; Zhang, Y.; Yang, B.; Huang, X.; Gao, Y.; Zhang, J. Photocatalyst- And Transition-Metal-Free α-Allylation of: N -Aryl Tetrahydroisoquinolines Mediated by Visible Light. *Green Chem.* **2020**, *22* (3), 646−650.
(8) Yang, X.; Zhu, Y.; Xie, Z.; Li, Y.; Zhang, Y. Visible-Light-Induced Charge Transfer Enables Csp3-H Functionalization of Glycine Derivatives: Access to 1,3-Oxazolidines. *Org. Lett.* **2020**, *22* (4), 1638−1643.
(9) Saritha, R.; Annes, S. B.; Saravanan, S.; Ramesh, S. Carbazole Based Electron Donor Acceptor (EDA) Catalysis for the Synthesis of Biaryl and Aryl-Heteroaryl Compounds. *Org. Biomol. Chem.* **2020**, *18* (13), 2510−2515.
(10) Chen, L.; Liang, J.; Chen, Z.; Chen, J.; Yan, M.; Zhang, X. A Convenient Synthesis of Sulfones via Light Promoted Coupling of Sodium Sulfinates and Aryl Halides. *Adv. Synth. Catal.* **2018**, *361* (5), 956−960.
(11) Morack, T.; Mück-Lichtenfeld, C.; Gilmour, R. Bioinspired Radical Stetter Reaction: Radical Umpolung Enabled by Ion-Pair Photocatalysis. *Angew. Chem., Int. Ed.* **2019**, *58* (4), 1208−1212.
(12) Bartolomeu, A. de A.; Silva, R. C.; Brocksom, T. J.; Noël, T.; de Oliveira, K. T. Photoarylation of Pyridines Using Aryldiazonium Salts and Visible Light: An EDA Approach. *J. Org. Chem.* **2019**, *84* (16), 10459−10471.
(13) Arceo, E.; Bahamonde, A.; Bergonzini, G.; Melchiorre, P. Enantioselective Direct α-Alkylation of Cyclic Ketones by Means of Photo-Organocatalysis. *Chem. Sci.* **2014**, *5* (6), 2438−2442.
(14) Cao, Z.-Y.; Ghosh, T.; Melchiorre, P. Enantioselective Radical Conjugate Additions Driven by a Photoactive Intramolecular Iminium-Ion-Based EDA Complex. *Nat. Commun.* **2018**, *9* (1), 3274.
(15) Woźniak, Ł.; Murphy, J. J.; Melchiorre, P. Photo-Organocatalytic Enantioselective Perfluoroalkylation of β-Ketoesters. *J. Am. Chem. Soc.* **2015**, *137* (17), 5678−5681.
(16) Kandukuri, S. R.; Bahamonde, A.; Chatterjee, I.; Jurberg, I. D.; Escudero-Adán, E. C.; Melchiorre, P. X-Ray Characterization of an Electron Donor-Acceptor Complex That Drives the Photochemical Alkylation of Indoles. *Angew. Chem., Int. Ed.* **2015**, *54* (5), 1485−1489.
(17) Arceo, E.; Jurberg, I. D.; Álvarez-Fernández, A.; Melchiorre, P. Photochemical Activity of a Key Donor-Acceptor Complex Can Drive Stereoselective Catalytic α-Alkylation of Aldehydes. *Nat. Chem.* **2013**, *5* (9), 750−756.
(18) Tobisu, M.; Furukawa, T.; Chatani, N. Visible Light-Mediated Direct Arylation of Arenes and Heteroarenes Using Diaryliodonium Salts in the Presence and Absence of a Photocatalyst. *Chem. Lett.* **2013**, *42* (10), 1203−1205.
(19) Hsu, C.-W.; Sundén, H. α-Aminoalkyl Radical Addition to Maleimides via Electron Donor-Acceptor Complexes. *Org. Lett.* **2018**, *20* (7), 2051−2054.
(20) Sridharan, V.; Suryavanshi, P. A.; Menéndez, J. C. Advances in the Chemistry of Tetrahydroquinolines. *Chem. Rev.* **2011**, *111* (11), 7157−7259.
(21) Muthukrishnan, I.; Sridharan, V.; Menéndez, J. C. Progress in the Chemistry of Tetrahydroquinolines. *Chem. Rev.* **2019**, *119* (8), 5057−5191.
(22) Su, D.-S.; Lim, J. J.; Tinney, E.; Wan, B.-L.; Young, M. B.; Anderson, K. D.; Rudd, D.; Munshi, V.; Bahnck, C.; Felock, P. J.; Lu, M.; Lai, M.-T.; Touch, S.; Moyer, G.; DiStefano, D. J.; Flynn, J. A.; Liang, Y.; Sanchez, R.; Prasad, S.; Yan, Y.; Perlow-Poehnelt, R.; Torrent, M.; Miller, M.; Vacca, J. P.; Williams, T. M.; Anthony, N. J. Substituted Tetrahydroquinolines as Potent Allosteric Inhibitors of Reverse Transcriptase and Its Key Mutants. *Bioorg. Med. Chem. Lett.* **2009**, *19* (17), 5119−5123.
(23) Zhang, J.; Zhan, P.; Wu, J.; Li, Z.; Jiang, Y.; Ge, W.; Pannecouque, C.; De Clercq, E.; Liu, X. Synthesis and Biological Evaluation of Novel 5-Alkyl-2-Arylthio-6-((3,4-Dihydroquinolin-1(2H)-Yl)Methyl)Pyrimidin-4(3H)-Ones as Potent Non-Nucleoside HIV-1 Reverse Transcriptase Inhibitors. *Bioorg. Med. Chem.* **2011**, *19* (14), 4366−4376.
(24) Chander, S.; Wang, P.; Ashok, P.; Yang, L.-M.; Zheng, Y.-T.; Murugesan, S. Rational Design, Synthesis, Anti-HIV-1 RT and Antimicrobial Activity of Novel 3-(6-Methoxy-3,4-Dihydroquinolin-1(2H)-Yl)-1-(Piperazin-1-Yl)Propan-1-One Derivatives. *Bioorg. Chem.* **2016**, *67*, 75−83.
(25) Ramesh, E.; Manian, R. D. R. S.; Raghunathan, R.; Sainath, S.; Raghunathan, M. Synthesis and Antibacterial Property of Quinolines with Potent DNA Gyrase Activity. *Bioorg. Med. Chem.* **2009**, *17* (2), 660−666.
(26) Jarvest, R. L.; Berge, J. M.; Berry, V.; Boyd, H. F.; Brown, M. J.; Elder, J. S.; Forrest, A. K.; Fosberry, A. P.; Gentry, D. R.; Hibbs, M. J.; Jaworski, D. D.; O'Hanlon, P. J.; Pope, A. J.; Rittenhouse, S.; Sheppard, R. J.; Slater-Radosti, C.; Worby, A. Nanomolar Inhibitors of Staphylococcus Aureus Methionyl TRNA Synthetase with Potent Antibacterial Activity against Gram-Positive Pathogens. *J. Med. Chem.* **2002**, *45* (10), 1959−1962.
(27) Muñoz, A.; Sojo, F.; Arenas, D. R. M.; Kouznetsov, V. V.; Arvelo, F. Cytotoxic Effects of New Trans-2,4-Diaryl-r-3-Methyl-1,2,3,4-Tetrahydroquinolines and Their Interaction with Antitumoral Drugs Gemcitabine and Paclitaxel on Cellular Lines of Human Breast Cancer. *Chem.-Biol. Interact.* **2011**, *189* (3), 215−221.
(28) Kouznetsov, V. V.; Merchan-Arenas, D. R.; Tangarife-Castaño, V.; Correa-Royero, J.; Betancur-Galvis, L. Synthesis and Cytotoxic Evaluation of Novel 2-Aryl-4-(4-Hydroxy-3-Methoxyphenyl)-3-Methyl-6,7-Methylendioxy-1,2,3,4-Tetrahydroquinolines, Podophyllotoxin-like Molecules. *Med. Chem. Res.* **2016**, *25* (3), 429−437.
(29) Zhu, S.; Das, A.; Bui, L.; Zhou, H.; Curran, D. P.; Rueping, M. Oxygen Switch in Visible-Light Photoredox Catalysis: Radical Additions and Cyclizations and Unexpected C-C-Bond Cleavage Reactions. *J. Am. Chem. Soc.* **2013**, *135* (5), 1823−1829.
(30) Yadav, A. K.; Yadav, L. D. S. Visible Light Photoredox Catalysis with N-Hydroxyphthalimide for [4 + 2] Cyclization between N-Methylanilines and Maleimides. *Tetrahedron Lett.* **2017**, *58* (6), 552−555.
(31) Guo, J.-T.; Yang, D.-C.; Guan, Z.; He, Y.-H. Chlorophyll-Catalyzed Visible-Light-Mediated Synthesis of Tetrahydroquinolines from N,N-Dimethylanilines and Maleimides. *J. Org. Chem.* **2017**, *82* (4), 1888−1894.
(32) Liang, Z.; Xu, S.; Tian, W.; Zhang, R. Eosin Y-Catalyzed Visible-Light-Mediated Aerobic Oxidative Cyclization of N,N-Dimethylanilines with Maleimides. *Beilstein J. Org. Chem.* **2015**, *11*, 425−430.
(33) Nicholls, T. P.; Constable, G. E.; Robertson, J. C.; Gardiner, M. G.; Bissember, A. C. Brønsted Acid Cocatalysis in Copper(I)-Photocatalyzed α-Amino C-H Bond Functionalization. *ACS Catal.* **2016**, *6* (1), 451−457.
(34) Chen, L.; Chao, C. S.; Pan, Y.; Dong, S.; Teo, Y. C.; Wang, J.; Tan, C.-H. Amphiphilic Methyleneamino Synthon through Organic Dye Catalyzed-Decarboxylative Aminoalkylation. *Org. Biomol. Chem.* **2013**, *11* (35), 5922−5925.
(35) Xin, J.-R.; Guo, J.-T.; Vigliaturo, D.; He, Y.-H.; Guan, Z. Metal-Free Visible Light Driven Synthesis of Tetrahydroquinoline Derivatives Utilizing Rose Bengal. *Tetrahedron* **2017**, *73* (31), 4627−4633.
(36) Nicholls, T. P.; Constable, G. E.; Robertson, J. C.; Gardiner, M. G.; Bissember, A. C. Bronsted Acid Cocatalysis in Copper(I)-Photocatalyzed α-Amino C-H Bond Functionalization. *ACS Catal.* **2016**, *6* (1), 451−457.
(37) Xu, G.-Q.; Li, C.-G.; Liu, M.-Q.; Cao, J.; Luo, Y.-C.; Xu, P.-F. Dual C-H Functionalization of N-Aryl Tetrahydroisoquinolines: A Highly Diastereoselective Synthesis of Dibenzo[a, f]Quinolizines via Visible-Light Induced Oxidation and Inverse Electron-Demand Aza-Diels-Alder Reaction. *Chem. Commun.* **2016**, *52* (6), 1190−1193.

https://dx.doi.org/10.1021/acs.joc.0c02819
J. Org. Chem. 2021, 86, 1901−1910

(38) Sun, D.; Hubig, S. M.; Kochi, J. K. Oxetanes from [2 + 2] Cycloaddition of Stilbenes to Quinone via Photoinduced Electron Transfer. *J. Org. Chem.* **1999**, *64* (7), 2250−2258.
(39) Wu, G.; Li, Y.; Yu, X.; Gao, Y.; Chen, H. Acetic Acid Accelerated Visible-Light Photoredox Catalyzed N-Demethylation of N,N-Dimethylaminophenyl Derivatives. *Adv. Synth. Catal.* **2017**, *359* (4), 687−692.
(40) Xu, K.; Fang, Y.; Yan, Z.; Zha, Z.; Wang, Z. A Highly Tunable Stereoselective Dimerization of Methyl Ketone: Efficient Synthesis of E- and Z-1,4-Enediones. *Org. Lett.* **2013**, *15* (9), 2148−2151.
(41) Curran, D. P.; Keller, A. I. Radical Additions of Aryl Iodides to Arenes Are Facilitated by Oxidative Rearomatization with Dioxygen. *J. Am. Chem. Soc.* **2006**, *128* (42), 13706−13707.
(42) Li, J.; Bao, W.; Zhang, Y.; Rao, Y. Cercosporin-Photocatalyzed Sp3 (C-H) Activation for the Synthesis of Pyrrolo[3{,}4-c]-Quinolones. *Org. Biomol. Chem.* **2019**, *17* (40), 8958−8962.
(43) Ju, X.; Li, D.; Li, W.; Yu, W.; Bian, F. The Reaction of Tertiary Anilines with Maleimides under Visible Light Redox Catalysis. *Adv. Synth. Catal.* **2012**, *354* (18), 3561−3567.
(44) Liu, Q.; Li, Y.-N.; Zhang, H.-H.; Chen, B.; Tung, C.-H.; Wu, L.-Z. Reactivity and Mechanistic Insight into Visible-Light-Induced Aerobic Cross-Dehydrogenative Coupling Reaction by Organo-photocatalysts. *Chem. - Eur. J.* **2012**, *18* (2), 620−627.
(45) Yamaguchi, M.; Fujiwara, S.; Manabe, K. Synthesis of 2,2,5-Trisubstituted 2H-Pyrroles and 2,3,5-Trisubstituted 1H-Pyrroles by Ligand-Controlled Site-Selective Dearomative C2-Arylation and Direct C3-Arylation. *Org. Lett.* **2019**, *21* (17), 6972−6977.
(46) Xuan, J.; Feng, Z.-J.; Chen, J.-R.; Lu, L.-Q.; Xiao, W.-J. Visible-Light-Induced C-S Bond Activation: Facile Access to 1,4-Diketones from *β*-Ketosulfones. *Chem. - Eur. J.* **2014**, *20* (11), 3045−3049.
(47) Sheldrick, G. M. A Short History of SHELX. *Acta Crystallogr., Sect. A: Found. Crystallogr.* **2008**, *64* (1), 112−122.
(48) Sheldrick, G. M. Crystal Structure Refinement with SHELXL. *Acta Crystallogr., Sect. C: Struct. Chem.* **2015**, *71* (1), 3−8.
(49) Barbour, L. J. X-Seed — A Software Tool for Supramolecular Crystallography. *J. Supramol. Chem.* **2001**, *1* (4), 189−191.
(50) Mandal, A. K.; Sreejith, S.; He, T.; Maji, S. K.; Wang, X.-J.; Ong, S. L.; Joseph, J.; Sun, H.; Zhao, Y. Three-Photon-Excited Luminescence from Unsymmetrical Cyanostilbene Aggregates: Morphology Tuning and Targeted Bioimaging. *ACS Nano* **2015**, *9* (5), 4796−4805.
(51) Katritzky, A. R.; Yao, G.; Lan, X.; Zhao, X. The Conversion of Secondary into Tertiary Amides Using Benzotriazole Methodology. *J. Org. Chem.* **1993**, *58* (8), 2086−2093.
(52) Barker, T. J.; Jarvo, E. R. Umpolung Amination: Nickel-Catalyzed Coupling Reactions of *N,N*-Dialkyl-*N*-Chloroamines with Diorganozinc Reagents. *J. Am. Chem. Soc.* **2009**, *131* (43), 15598−15599.

https://dx.doi.org/10.1021/acs.joc.0c02819
J. Org. Chem. 2021, 86, 1901−1910

Paper II

Aerobic oxidative EDA catalysis: Synthesis of tetrahydroquinolines using a catalytic EDA active acceptor

August Runemark, [b] and Henrik Sundén*[a]

[a] H. Sundén
Chemistry and Molecular Biology, University of Gothenburg, Kemivägen 10, 412 96, Gothenburg, Sweden
E-mail: henrik.sunden@chem.gu.se
[b] A. Runemark
Department of Chemistry and Chemical Engineering, Chalmers University of Technology, Kemivägen 10, 41296 Gothenburg, Sweden

Supporting information for this article is given via a link at the end of the document.

Abstract: A catalytic electron donor-acceptor (EDA) complex for the visible light driven annulation reaction between activated alkenes and *N,N*-substituted dialkyl anilines is reported. The key photoactive complex is formed *in situ* between dialkylated anilines as donors and 1,2-dibenzoylethylene as a catalytic acceptor. Aerobic oxidation drives the regeneration of the catalyst. Investigations into the mechanism are provided, revealing a rare example of a catalytic acceptor in photoactive EDA complexes that can give access to selective functionalization of aromatic amines under mild photochemical conditions.

Introduction

An EDA complex is a weak molecular aggregation between an electron-rich donor and an electron-poor acceptor.[1] A characteristic of EDA complexes is their associated charge transfer (CT) band in the electromagnetic spectrum. Excitation by light within this CT band results in a single electron transfer (SET) from the donor to the acceptor. The resulting radical species can subsequently undergo a range of different processes and take part in radical reactions. Due to the red-shifted absorption of the CT band, compared to the individual components of the EDA complex, visible light can often be used to induce reactivity in compounds otherwise not absorbing in this spectral region.[2]

Over the last decade, a wide range of different approaches to utilize EDA complexes in synthetic organic chemistry have been developed.[1–4] Examples include arylations,[5] stereoselective alkylations,[6] oxidative annulations,[7] and acylations.[8] The prototypical examples are coupling reactions between a donor and acceptor, driven by the formation of a stoichiometric EDA complex (Figure 1a),[7,9] although strategies to harvest the synthetic potential of EDA complexes have rapidly been expanded to include catalytic complexes (Figure 1b).[2,10–12]

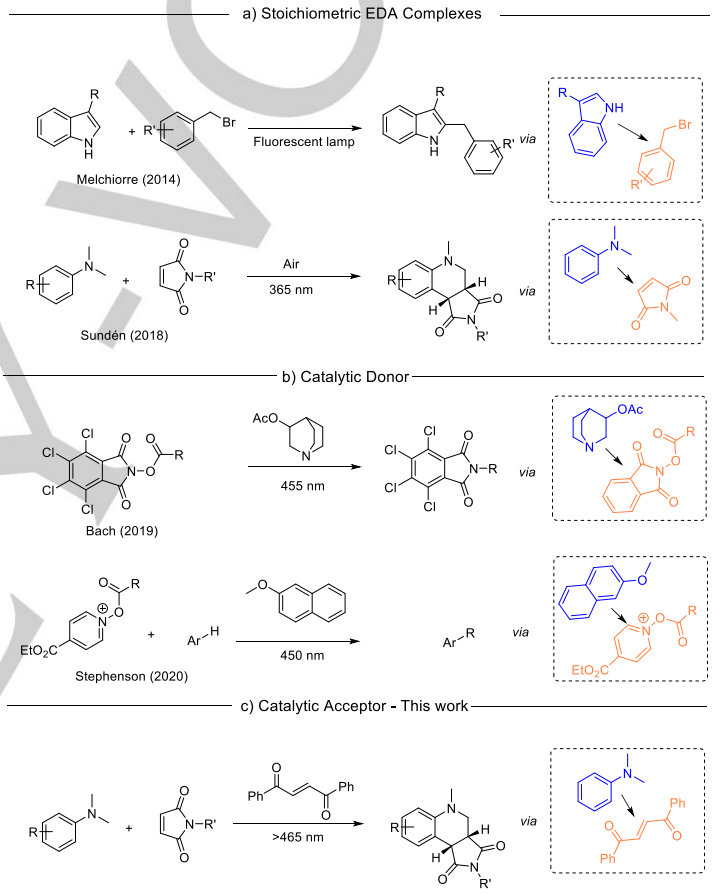

Scheme 1. a) Examples of stoichiometric EDA complexes in organic synthesis. b) Examples of external catalytic donors in organic synthesis. c) The work presented herein.

Within the catalytic regime, different approaches can be exploited depending on how the EDA complex is formed. The donor or acceptor can be formed *in situ* from a pre-catalyst, generating highly polarized species from non-reactive substrates. Examples include *in situ*-formed enamines and enolates as donors, or iminium ions as acceptors, that take part in the formation of photoactive EDA complexes.[6,13,14] Alternatively, an external donor can be present in catalytic amount that associates with an electron deficient reactant to form an EDA complex. After PET to the reactant, the donor can reform to close the catalytic cycle. Examples of these systems include the use of electron rich aromatics and amines.[10,11,15,16] Examples of systems using catalytic acceptors in the same

manner however still remain rare in the literature.[17] Using electron deficient species as additives in catalytic amounts would give access to novel reactivity of electron rich substrates, such as amines, through the formation of catalytic EDA complexes. Identification of such suitable acceptors, that could act as catalysts for photo-mediated synthesis, would constitute a significant contribution to the field of EDA driven transformations. Inspired by this opportunity, we set out to investigate this methodology in the generation of α-amino alkyl radicals. Herein we present a protocol using visible light to furnish a wide range of annulation products from aromatic amines and activated alkenes, driven by the formation of a photoactive catalytic EDA complex (Scheme 1c)

As a model system for this study, 1,2-dibenzoyl ethylene **4a** as a catalyst in combination with *N,N*-dimethylaniline **1a** was chosen due to the formation of an EDA-complex between the two species which absorbs strongly in the visible region (Figure 2).[18] It was thought that upon photoexcitation of this complex a SET from the amine to the **4a** would occur which results in the formation of an α-amino alkyl radical. This radical could rapidly react with a suitable reaction partner. With a suitable oxidant present, the enol radical formed could be regenerated to **4a**, closing the catalytic cycle (Scheme 1). Due to the nucleophilic nature of α-amino alkyl radicals, the proposed methodology could be utilized for a broad scope of electrophiles as reaction partners.

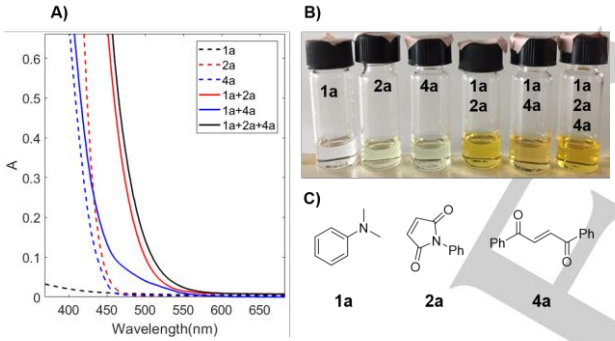

Figure 1. A) UV-vis spectrum of **1a** (0.4 M), **2a** (73 mM), **4a** (6 mM), and their EDA complexes in 1,4-dioxane; B) pictures of **1a**, **2a**, **4a**, their EDA complexes; C) Structure of **1a**, **2a,** and **4a**.

Results and Discussion

As a starting point for the study, *N*-substituted maleimides were chosen as reaction partners due to their well-known reactivity with aromatic α-amino alkyl radicals forming tetrahydroquinolines under a range of conditions.[7,19–45] The photochemically driven annulation reaction between DMA (**1a**) and *N*-phenyl maleimide (**2a**) to furnish the tetrahydroquinoline (**3a**) proceeds smoothly without external photocatalyst under UV-irradiation.[7] However, initial screening of reaction conditions, presented in Table 1, shows that visible light irradiation (white compact fluorescent lamp) in the absence of a catalyst results in a low yield. This slow background reactivity prompted us to use this reaction as a model for our system. Notably, the addition of only 1 mol% dibenzoyl ethylene (**4a**) resulted in significantly increased yield (Table 1, entry 2), supporting the feasibility of the outlined approach.

Higher loading of 5 mol% increased the yield further (Table 1, entry 3). The impact of aryl substitutions on the dibenzoyl ethylene catalyst, as a way to tune the catalytic properties, was briefly investigated (Table 1, entries 4-6). Electron withdrawing groups in *p*-position resulted in lower yields, while the introduction of an electron donating group did not affect the catalytic action significantly. Initially, using the amine in great excess (7 equiv.) we investigated the influence of decreasing amounts and found that with five equivalents of amine the reaction proceeded smoothly to yield the desired product at 82% yield (Table 1, entry 9). In order to investigate the effect of excitation wavelength on the reaction outcome, green and blue LEDs were used as light sources (Table 1, entries 11 and 12). Green light (525 nm) could promote the transformation to 50% yield using longer irradiation times. Blue LED (465 nm) on the other hand proved to be a suitable light source, driving the reaction to 85% yield. This result reflects the stronger absorption of the EDA complex in the blue region of the spectrum.

Table 1. Optimization of the reaction conditions

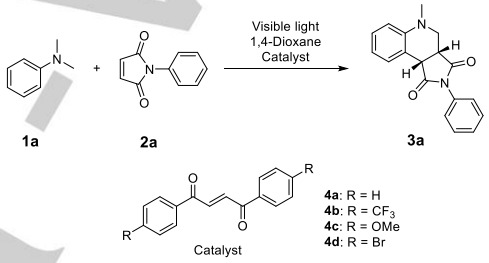

Entry[a]	Catalyst (mol%)	Light source	1a	Yield 3a[b]
1	-	CFL	7	7[c]
2	**4a** (1)	CFL	7	53
3	**4a** (5)	CFL	7	80
4	**4b** (5)	CFL	7	26
5	**4c** (5)	CFL	7	80
6	**4d** (5)	CFL	7	26
7	**4a** (5)	CFL	1	40
8	**4a** (5)	CFL	2	42
9	**4a** (5)	CFL	5	82
10	**4a** (5)	-	7	12[d]
11	**4a** (5)	Green LED	7	50[e]
12	**4a** (5)	Blue LED	7	85[f] (80)[f, g]
13	**4a** (5)	Blue LED	7	3[f, h]

[a] Conditions: **2a** (0.2 mmol), **1a** (1-7 equiv.) and catalyst in 3 mL 1,4-dioxane was irradiated for 1-26 hours under ambient atmosphere. [b] Determined by GC-FID using n-dodecane as internal standard. [c] Reaction performed in absence of catalyst. [d] reaction performed protected from light at 100 C. [e] Reaction time 30 hours. [f] Reaction time 7 hours. [g] Isolated yield. [f] Reaction carried out under an atmosphere of nitrogen.

With our optimized reaction conditions found, the substrate scope of the reaction was investigated (Table 2 and Table 3).

Due to the known EDA complexes between anilines and maleimides that potentially could drive the reactions to the desired product in the absence of any catalyst, a control experiment without the catalyst **4a** was performed for each entry (SI, Scheme S1).

Table 2. Scope of activated alkenes

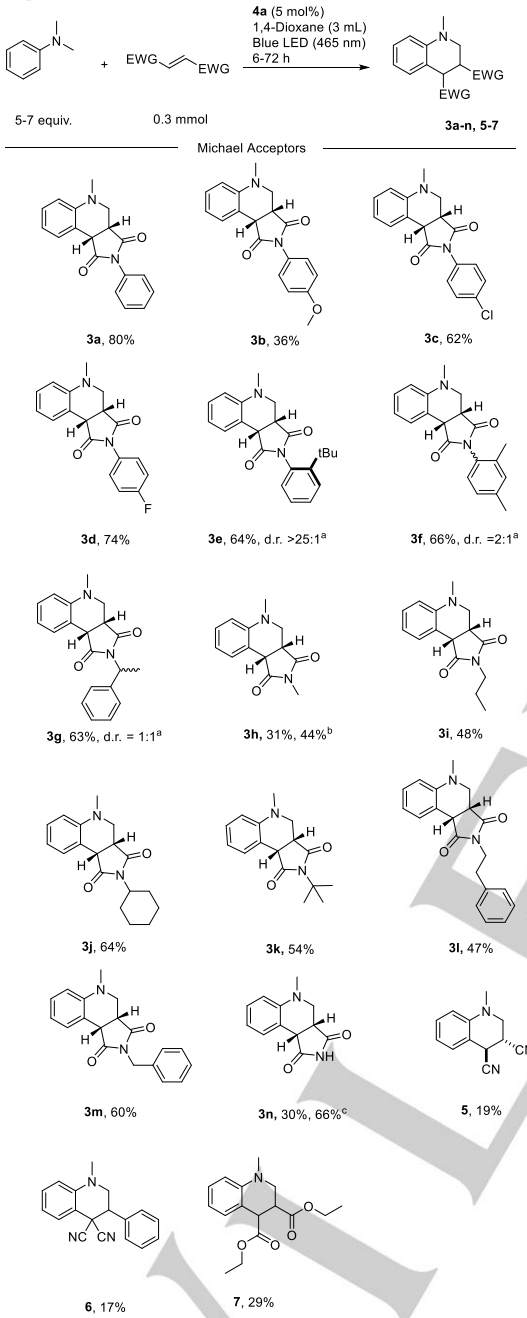

Conditions: alkene (0.3 mmol), amine (7 equiv.) and **4a** (5 mol%) in 3 mL 1,4-dioxane was irradiated for 6-72 hours under ambient atmosphere. Yields reported are isolated. [a] Diastereomeric ratio was determined by ^{1}H NMR. [c] Reaction time 18 hours. [c] Reaction time 72 hours.

First, the combination of DMA and different *N*-aryl substituted maleimides were subjected to the reaction conditions to give products **3b**-**3g** (Table 2). Electron rich *p*-OMe substituted maleimide gave product **3b** in low yield whereas the slightly electron withdrawing groups chloro and fluoro provided the desired products **3c** and **3d** in higher yields of 62% and 74% respectively. The sterically demanding *o*-substituted *tert*-butyl group was tolerated in the reaction giving the product **3e** in 64 % yield as a single diastereomer. On the other hand, compound **3f** bearing the smaller methyl group was obtained as an equimolar mixture of diastereomers in 65% yield. Next, a set of *N*-alkyl substituted maleimides were tested as Michael acceptors in the radical addition reaction. *N*-methyl maleimide provided a significantly slower reaction rate with a yield of 31% after 7 hours and 44% yield after 18 hours. More bulky substituents, such as propyl and *tert*-butyl, gave slightly increased yields of **3i** and **3k**, 48% and 54% respectively. Non-substituted maleimide provided the desired product **3n** in 30% yield, however longer reaction times promoted the reaction to proceed to 66% yield. Michael acceptors other than maleimides resulted in sluggish reactions under the current protocol giving products **5**-**7** in 17-29% yield.

Table 3. Scope of amines

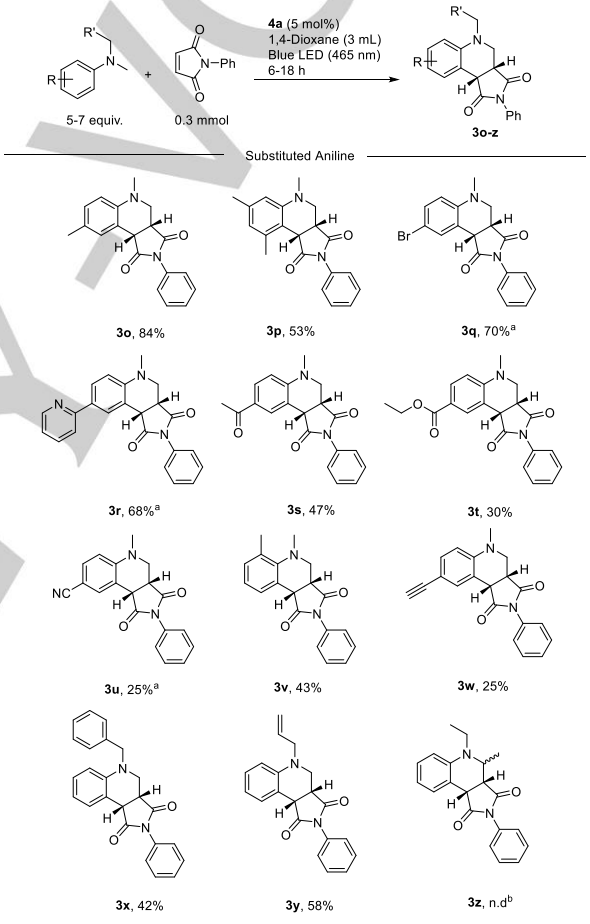

Conditions: alkene (0.3 mmol), amine (7 equiv.) and **4a** (5 mol%) in 3 mL 1,4-dioxane was irradiated for 6-18 hours under ambient atmosphere. Yields reported are isolated. [a] Reaction time 18 hours. [b] No product was observed in the crude reaction mixture by ^{1}H NMR analysis.

The effect of substitution on the aniline reaction partner was then explored giving products **3o**-**y** in 25-70% yield (Table 3). The reaction was found to be highly sensitive to the electronic nature of the acceptor amine. Electron deficient amines, such as *p*-aceto, *p*-carboxylate and *p*-CN, resulted in lower reaction rate, giving products **3s**-**u** in 47%, 30% and 25% yield respectively after 7-hour reaction time. This is presumably due to the higher oxidation potential of these amines.[46] Complete selectivity towards addition of methyl radical to the Michael acceptors was observed when different *N*-Me-*N*-alkyl anilines were subjected to the reaction conditions, providing compounds **3x** and **3y**,

consistent with the literature.[19,47] The sterically hindered *o*-methyl-DMA also resulted in lower reactivity (Table 3, entry **3v**). When *N,N*-diethyl aniline was subjected to the reaction conditions, no annulation product could be observed (Scheme 3, entry **3z**).

To showcase the scalability of the developed protocol, a gram scale reaction was carried out (Scheme 2). The desired product **3a** could efficiently be isolated in 78% yield after simple extraction and washing steps.

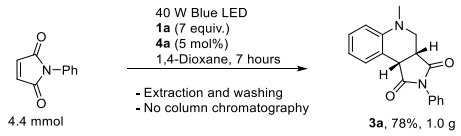

Scheme 2. Gram scale synthesis of **3a**.

To gain insight into the reaction mechanism, several control experiments were carried out. Firstly, when the reaction was carried out in the absence of light at 100 °C for 7 h (Table 1, Entry 10) a yield of 12% was determined. This result shows that, although a thermal background reaction can be active at elevated temperatures, light irradiation is needed to successfully drive the reaction. From the background reaction without **4a** as additive being investigated for all entries, it is evident that the catalyst is crucial for promoting the reaction using blue light. Although amines and maleimides form EDA complexes with absorption that tails into the visible region (Figure 1), the excitation of these complexes with visible light alone does not seem to result in the efficient formation of reactive radical species. Even with increased power (40 W) LED with an emission maximum of 440 nm, where the complex between **1a** and **2a** absorbs significantly, the background reaction proceeds slowly (SI, Figure S3).

When the reaction was carried out in the presence of the radical scavenger butylated hydroxytoluene (BHT), a significant decrease in yield was observed suggesting that the reaction proceeds *via* a radical pathway (Scheme 3a). The impact of a singlet oxygen scavenger, histidine, was also investigated and found to have little impact on the reaction outcome (Scheme 3a).[42]

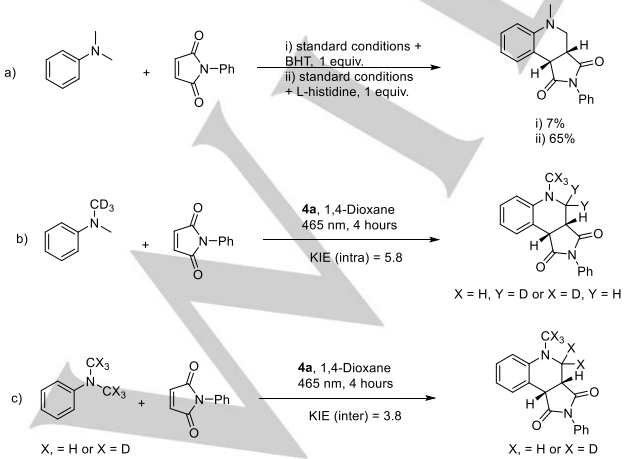

Scheme 3. Control experiments.

Next, kinetic isotope effect (KIE) experiments were then carried out (Scheme 3b-c). The intramolecular KIE was found to be 5.8 (Scheme 3b), whereas an intermolecular KIE of 3.8 was observed when running two parallel reactions with DMA-*d*6 and DMA or as a competition experiment (Scheme 3c). The observed difference suggests that the mechanism does not involve a single step C-H cleavage, such as hydrogen atom transfer (HAT), to a significant degree.[48,49] Instead, the formation of an α-amino alkyl radical from **3a** likely involves two consecutive steps: oxidation and C-H bond cleavage through proton transfer. The oxidation step is an equilibrium between electron transfer and back electron transfer (BET). In such a system, the intramolecular KIE will be higher than the intermolecular KIE with a difference determined by the ratio between the rate of C-H cleavage and the rate of BET.[48,50] To investigate the electronic effects of the amine donor, a series of competition experiment were carried out (Figure 2). A significant dependence of the natural logarithms of the relative rates on the Hammett σ_p parameter was observed with a slope of -3.2, suggesting that a SET is involved to a significant degree in the mechanism.[49,51]

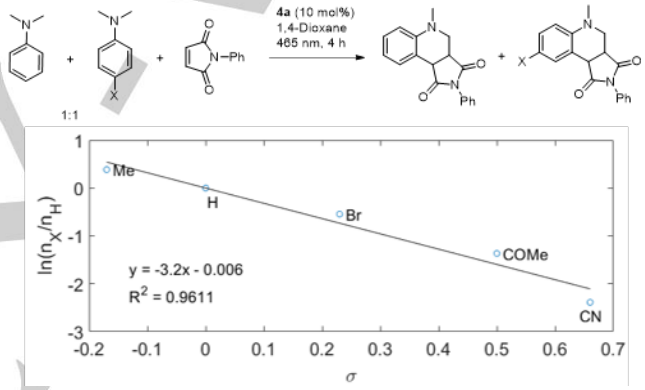

Figure 2. Competition experiment between para substituted DMA and plot of the natural logarithms of the relative product ratios, as determined by ^{1}H NMR analysis, versus the Hammet σ_p parameters.

To investigate the role of air in the reaction, a control experiment under nitrogen atmosphere was performed and resulted in a product yield of 3% (Table 1, Entry 13). The consumption of oxygen was then measured as a function of product formation, and it was observed that a slight excess of oxygen was needed to drive the reaction to completion (SI, Figure S6).

The quantum yield of the reaction at 450 nm was investigated using standard potassium ferrioxalate actinometry (SI) and was found to be 0.07. The low quantum yield can be attributed to the large concentration and absorption by other species such as the maleimide, and the EDA complex formed between DMA and the maleimide, leading to non-productive absorption of photons. Furthermore, given the difference in intra- and intermolecular KIE for the present system, a significant rate of back electron transfer can be expected leading to unproductive absorption of photons.

Based on the control experiments, a possible reaction mechanism can be postulated. The crucial role of **4a** on the reaction outcome can be rationalized according to two likely scenarios. In the first scenario (Scheme 3, cycle A) **4a** is locally

excited and promoted to its excited state which can oxidize the amine *via* SET, in line with a typical photo-redox catalytic cycle. In the second scenario, however, the key photoactive species is the ground state EDA complex between **4a** and the amine (Scheme 3, cycle B). Excitation of this complex results in the formation of the radical anion of **4a** and radical cation of the amine *via* a SET within the complex. Subsequently, the radical anion of **4a** can be oxidized by molecular oxygen to yield a superoxide anion, which readily can be protonated to form hydroperoxyl radical.[52] The deprotonation of the amine radical cation with pK_a of 9[53] can be achieved by proton transfer to either **1**, the radical anion of **4a**, or a superoxide radical, and yields an α-amino alkyl radical (**I**) that readily reacts with a Michael acceptor to form **II** which after aromatization forms the final product **3**. The regenerated **4a** can associate with an amine forming another EDA complex to close the catalytic cycle.

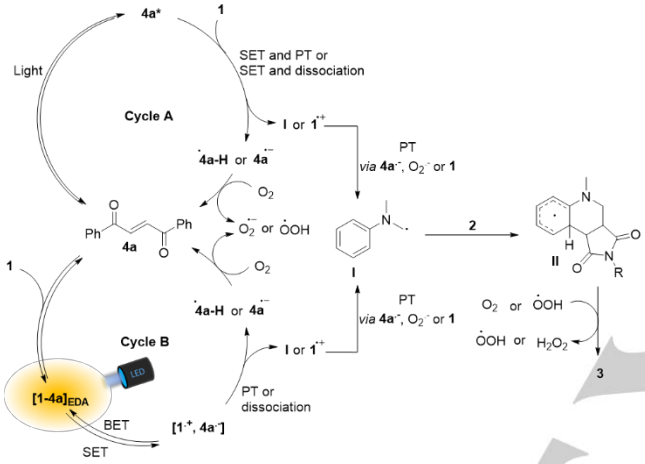

Scheme 4. Proposed mechanism.

To completely distinguish between the two scenarios under the developed conditions is however challenging. Due to the overlap in absorption of **4a** and its EDA complex with amines (Figure 1), it cannot be ruled out that **4a** is locally excited and acts as a sensitizer. However, the observation that the reaction proceeds with excitation by green light (525 nm) suggests that the EDA complex between **4a** and amines is a key intermediate in the reaction (Table 1, Entry 15). At this wavelength, **4a** has a very low absorption, however once the EDA complex between **1a** and **4a** has formed the absorbance is significantly increased. The observation that the maleimide reacts with the formed α-amino alkyl radical much faster than the available Michael acceptor **4a** can be rationalized in terms of electrophilicity and the stoichiometry of the reaction conditions.

Conclusion

In conclusion, a protocol for the visible light induced aerobic oxidative annulation reaction between dialkylanilines and activated alkenes has been disclosed. The reaction is postulated to proceed *via* the excitation of an EDA complex formed between the catalyst 1,2-dibenzoyl ethylene and the amine reaction partner. The simple structure and availability of the 1,2-dibenzoyl ethylene structure makes the developed protocol attractive as an alternative to complex photoredox catalysts. Furthermore, this example of a catalytic external acceptor could stimulate the field of EDA complex chemistry to pursue novel photoreactions.

Acknowledgements

This work was supported by grants from the Swedish research council FORMAS (2019-00699) and from Olle Engkvists Stiftelse.

Keywords: keyword 1 • keyword 2 • keyword 3 • keyword 4 • keyword 5

[1] C. G. S. Lima, T. de M. Lima, M. Duarte, I. D. Jurberg, M. W. Paixão, *ACS Catal.* **2016**, *6*, 1389–1407.

[2] G. E. M. Crisenza, D. Mazzarella, P. Melchiorre, *J. Am. Chem. Soc.* **2020**, *142*, 5461–5476.

[3] Y. Yuan, S. Majumder, M. Yang, S. Guo, *Tetrahedron Lett.* **2020**, *61*, 151506.

[4] A. Postigo, *European J. Org. Chem.* **2018**, *2018*, 6391–6404.

[5] M. Tobisu, T. Furukawa, N. Chatani, *Chem. Lett.* **2013**, *42*, 1203–1205.

[6] E. Arceo, I. D. Jurberg, A. Álvarez-Fernández, P. Melchiorre, *Nat. Chem.* **2013**, *5*, 750–756.

[7] C.-W. Hsu, H. Sundén, *Org. Lett.* **2018**, *20*, 2051–2054.

[8] L. Guillemard, F. Colobert, J. Wencel-Delord, *Adv. Synth. Catal.* **2018**, *360*, 4184–4190.

[9] S. R. Kandukuri, A. Bahamonde, I. Chatterjee, I. D. Jurberg, E. C. Escudero-Adán, P. Melchiorre, *Angew. Chemie Int. Ed.* **2015**, *54*, 1485–1489.

[10] E. J. McClain, T. M. Monos, M. Mori, J. W. Beatty, C. R. J. Stephenson, *ACS Catal.* **2020**, *10*, 12636–12641.

[11] I. Bosque, T. Bach, *ACS Catal.* **2019**, *9*, 9103–9109.

[12] E. de Pedro Beato, D. Spinnato, W. Zhou, P. Melchiorre, *J. Am. Chem. Soc.* **2021**, DOI 10.1021/jacs.1c05607.

[13] Ł. Woźniak, J. J. Murphy, P. Melchiorre, *J. Am. Chem. Soc.* **2015**, *137*, 5678–5681.

[14] T. Morack, C. Mück-Lichtenfeld, R. Gilmour, *Angew. Chemie Int. Ed.* **2019**, *58*, 1208–1212.

[15] M.-C. Fu, R. Shang, B. Zhao, B. Wang, Y. Fu, *Science (80-.).* **2019**, *363*, 1429 LP – 1434.

[16] V. Quint, F. Morlet-Savary, J.-F. Lohier, J. Lalevée, A.-C. Gaumont, S. Lakhdar, *J. Am. Chem. Soc.* **2016**, *138*, 7436–7441.

[17] Y. Aramaki, N. Imaizumi, M. Hotta, J. Kumagai, T. Ooi, *Chem. Sci.* **2020**, *11*, 4305–4311.

[18] A. Runemark, S. C. Zacharias, H. Sundén, *J. Org. Chem.* **2021**, *86*, 1901–1910.

[19] G. Perumal, M. Kandasamy, B. Ganesan, K. Govindan, H. Sathya, M.-Y. Hung, G. Chandru Senadi, Y.-C. Wu, W.-Y. Lin, *Tetrahedron* **2021**, *80*, 131891.

[20] K. Sharma, B. Das, P. Gogoi, *New J. Chem.* **2018**, *42*, 18894–18905.

[21] X.-L. Yang, J.-D. Guo, T. Lei, B. Chen, C.-H. Tung, L.-Z. Wu, *Org. Lett.* **2018**, *20*, 2916–2920.

[22] A. M. Ranieri, L. K. Burt, S. Stagni, S. Zacchini, B. W. Skelton, M. I. Ogden, A. C. Bissember, M. Massi, *ChemRxiv* **2018**, 1–22.

[23] S. Firoozi, M. Hosseini-Sarvari, M. Koohgard, *Green Chem.* **2018**,

20, 5540–5549.

[24] M. Hosseini-Sarvari, M. Koohgard, S. Firoozi, A. Mohajeri, H. Tavakolian, *New J. Chem.* **2018**, *42*, 6880–6888.

[25] A. K. Yadav, L. D. S. Yadav, *Tetrahedron Lett.* **2017**, *58*, 552–555.

[26] J.-T. Guo, D.-C. Yang, Z. Guan, Y.-H. He, *J. Org. Chem.* **2017**, *82*, 1888–1894.

[27] Z. Song, A. P. Antonchick, *Tetrahedron* **2016**, *72*, 7715–7721.

[28] T. P. Nicholls, G. E. Constable, J. C. Robertson, M. G. Gardiner, A. C. Bissember, *ACS Catal.* **2016**, *6*, 451–457.

[29] A. K. Yadav, L. D. S. Yadav, *Tetrahedron Lett.* **2016**, *57*, 1489–1491.

[30] N. F. Nikitas, M. A. Theodoropoulou, C. G. Kokotos, *European J. Org. Chem.* **2021**, *2021*, 1168–1173.

[31] C. Huo, F. Chen, Z. Quan, J. Dong, Y. Wang, *Tetrahedron Lett.* **2016**, *57*, 5127–5131.

[32] Z. J. Wang, S. Ghasimi, K. Landfester, K. A. I. Zhang, *Adv. Synth. Catal.* **2016**, *358*, 2576–2582.

[33] N. Sakai, S. Matsumoto, Y. Ogiwara, *Tetrahedron Lett.* **2016**, *57*, 5449–5452.

[34] J. Tang, G. Grampp, Y. Liu, B.-X. Wang, F.-F. Tao, L.-J. Wang, X.-Z. Liang, H.-Q. Xiao, Y.-M. Shen, *J. Org. Chem.* **2015**, *80*, 2724–2732.

[35] Z. Liang, S. Xu, W. Tian, R. Zhang, *Beilstein J. Org. Chem.* **2015**, *11*, 425–430.

[36] X. Ju, D. Li, W. Li, W. Yu, F. Bian, *Adv. Synth. Catal.* **2012**, *354*, 3561–3567.

[37] M. Nishino, K. Hirano, T. Satoh, M. Miura, *J. Org. Chem.* **2011**, *76*, 6447–6451.

[38] R. B. Roy, G. A. Swan, *Chem. Commun. (London)* **1968**, 1446–1447.

[39] Z. Almansaf, J. Hu, F. Zanca, H. R. Shahsavari, B. Kampmeyer, M. Tsuji, K. Maity, V. Lomonte, Y. Ha, P. Mastrorilli, S. Todisco, M. Benamara, R. Oktavian, A. Mirjafari, P. Z. Moghadam, A. R. Khosropour, H. Beyzavi, *ACS Appl. Mater. Interfaces* **2021**, *13*, 6349–6358.

[40] Z. Xie, F. Li, L. Niu, H. Li, J. Zheng, R. Han, Z. Ju, S. Li, D. Li, *Org. Biomol. Chem.* **2020**, *18*, 6889–6898.

[41] Z. Hloušková, M. Klikar, O. Pytela, N. Almonasy, A. Růžička, V. Jandová, F. Bureš, *RSC Adv.* **2019**, *9*, 23797–23809.

[42] J. Li, W. Bao, Y. Zhang, Y. Rao, *Org. Biomol. Chem.* **2019**, *17*, 8958–8962.

[43] X. Yang, T. Liang, J. Sun, M. J. Zaworotko, Y. Chen, P. Cheng, Z. Zhang, *ACS Catal.* **2019**, *9*, 7486–7493.

[44] T. Mandal, S. Das, S. De Sarkar, *Adv. Synth. Catal.* **2019**, *361*, 3200–3209.

[45] T. P. Nicholls, L. K. Burt, P. V Simpson, M. Massi, A. C. Bissember, *Dalt. Trans.* **2019**, *48*, 12749–12754.

[46] T. L. Macdonald, W. G. Gutheim, R. B. Martin, F. P. Guengerich, *Biochemistry* **1989**, *28*, 2071–2077.

[47] L. Leng, Y. Fu, P. Liu, J. M. Ready, *J. Am. Chem. Soc.* **2020**, *142*, 11972–11977.

[48] E. Baciocchi, O. Lanzalunga, A. Lapi, L. Manduchi, *J. Am. Chem. Soc.* **1998**, *120*, 5783–5787.

[49] E. Baciocchi, M. Bietti, M. F. Gerini, O. Lanzalunga, *J. Org. Chem.* **2005**, *70*, 5144–5149.

[50] Y. Goto, Y. Watanabe, S. Fukuzumi, J. P. Jones, J. P. Dinnocenzo, *J. Am. Chem. Soc.* **1998**, *120*, 10762–10763.

[51] M. O. Ratnikov, M. P. Doyle, *J. Am. Chem. Soc.* **2013**, *135*, 1549–1557.

[52] M. Hayyan, M. A. Hashim, I. M. AlNashef, *Chem. Rev.* **2016**, *116*, 3029–3085.

[53] S. B. Karki, J. P. Dinnocenzo, J. P. Jones, K. R. Korzekwa, *J. Am. Chem. Soc.* **1995**, *117*, 3657–3664.

Supporting Information for Aerobic oxidative EDA catalysis: Synthesis of tetrahydroquinolines using a catalytic EDA active acceptor

August Runemark[a], and Henrik Sundén[b*]

[a]Department of Chemistry and Chemical Engineering, Chalmers University of Technology, Kemivägen 10, 41296 Göteborg, Sweden; [b]Chemistry and Molecular Biology, University of Gothenburg, Kemivägen 10, 412 96, Gothenburg.

Contents

1.1 General information

All reagents and solvents were purchased from Sigma-Aldrich and Alfa Aesar and used without any further purification unless specified notice. Purification was performed by an automated column chromatography Biotage Isolera™ Spektra One with Biotage SNAP®-10 g KP-silica column together with a 1 g samplet® cartridge using n-heptane or petroleum ether (40–60 °C)/ethyl acetate as solvent mixture unless otherwise noted. ^{1}H (400 MHz) and ^{13}C (101 MHz) NMR spectra were acquired on an Agilent NMR machine at 25 °C. The chemical shifts for ^{1}H and ^{13}C NMR spectra are reported in parts per million (ppm) relative to the residual peak from solvent $CDCl_3$ as the internal standard; ^{1}H NMR at δ 7.26 ppm and ^{13}C NMR at δ 77.0 ppm for $CDCl_3$. All coupling constants (*J*) are reported in Hertz (Hz) and multiplicities are indicated by s (singlet), d (doublet), dd (doublet of doublet), td (triplet of doublet), ddd (doublet of doublets of doublets), triplet (t), dt (doublet of triplet) and m (multiplet). Infrared (IR) spectra were recorded on a Perkin Elmer series FT-IR Spectrometer and are reported in wavenumber (cm^{-1}). High resolution mass spectrometry measurements were performed by CMSI service at Chalmers University of Technology. An Agilent 6520 equipped with an electrospray interface operated in positive ionization mode. UV-Vis absorption spectra were recorded on a Cary 4000 UV/Vis spectrometer, using 1x1 cm quartz cuvettes. All light promoted reactions were carried out in Biotage microwave vials (2-5 mL) under irradiation with a commercial LED strip, a commercial compact fluorescent lamp, Kessil PR160L-440 LED lamp, or Kessil PR160L-525 LED lamp. Gas chromatographic studies was performed using an Agilent 7820A equipped with a flame ionization detector and an Agilent HP-5 19091J-413 column. Emission spectrum of light sources were measured using an AvaSpec-2048.

1.2 UV-vis spectrum of 1a, 2a, 4a, and their mixtures

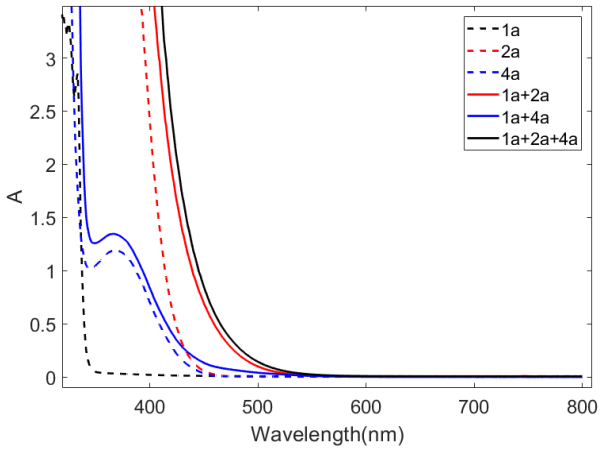

*Figure S1. UV-vis spectrum of **1a** (0.4 M), **2a** (73 mM), **4a** (6 mM), and their EDA complexes in 1,4-dioxane.*

1.3 Emission spectrum of irradiation source

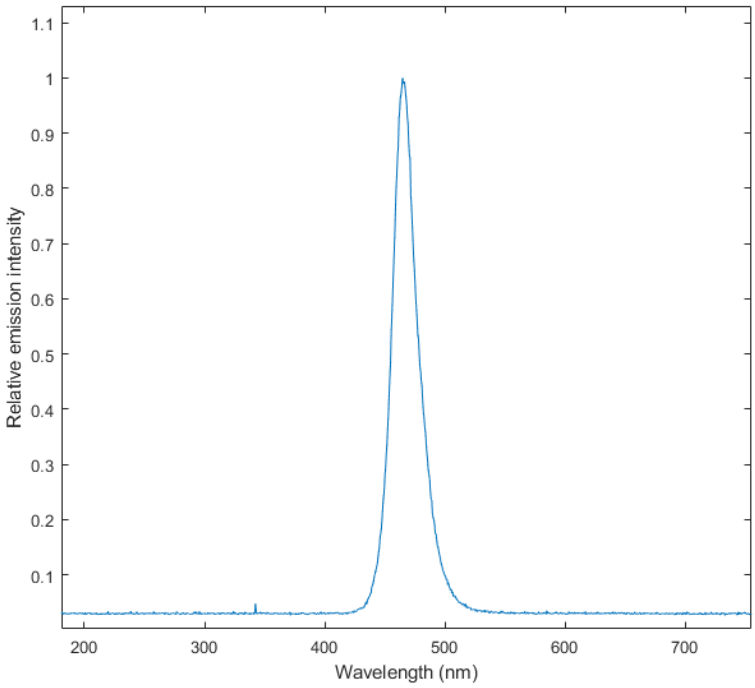

Figure 2. The normalized emission spectrum of the blue LED lamp used for the photoreaction, with λ_{max} of 465 nm

1.4 Investigation of the background reaction without catalyst

For each entry where the possibility of maleimide-amine EDA complex formation, a control experiment was carried out without the catalyst **4a**, under otherwise identical conditions (Scheme S1).

Scheme S1. Background reaction between maleimides and N,N-dialkylanilines under irradiation with blue LED.

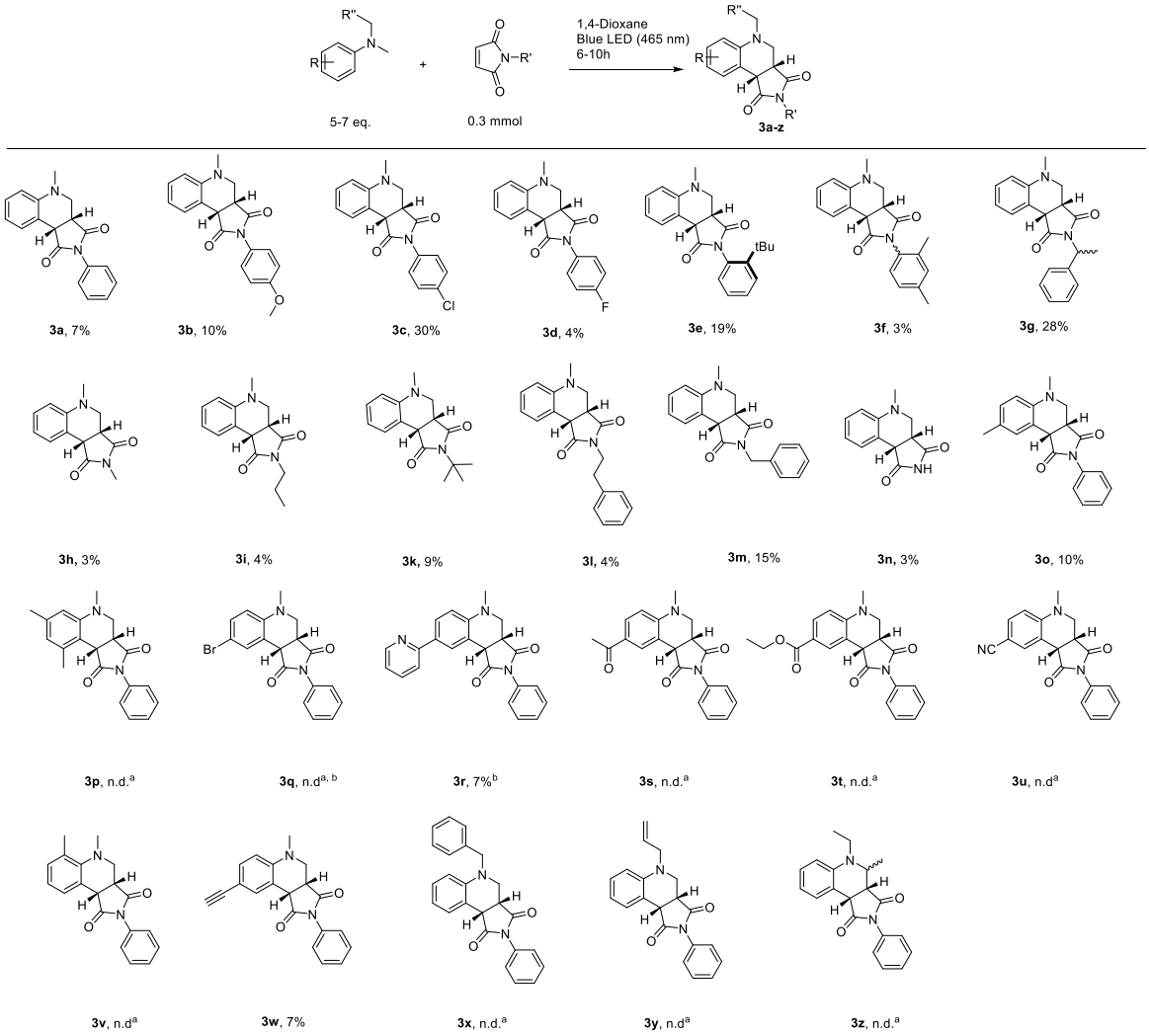

Conditions: maleimide (0.3 mmol) and amine (7 equiv.) in 3 mL 1,4-dioxane was irradiated for 6-18 hours under ambient atmosphere. Yields reported are isolated. a) No, or trace amounts, of product was observed in the crude reaction mixture by ^{1}H NMR analysis. b) Reaction time 18 hours.

1.5 Reaction profile with and without 4a

The formation of **3a** when using a 40W blue (440 nm) LED was followed over time in the presence and absence of **4a** as catalyst (Figure S3). It was observed that the formation of product was significantly faster in the presence of the catalyst.

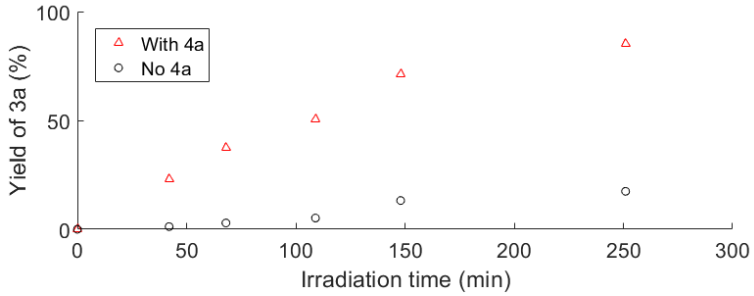

*Figure S3. Yield of product **3a** over time in presence (red triangles) and absence (black circles) of the catalyst **4a**. Measured as duplicates.*

1.6 Kinetic Isotope Effect investigations

Intramolecular KIE

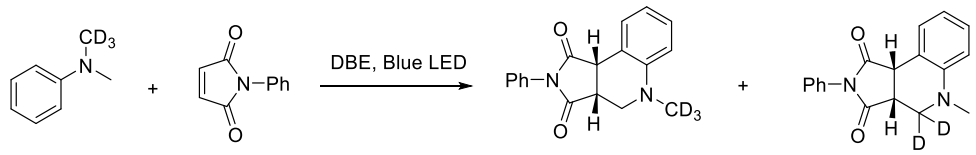

Following a modified published procedure,[3] *N*-phenylmaleimide (7.6 mg, 0.044 mmol, 1 equiv.), *N*-(CD_3)-*N*-(CH_3)-aniline (20.5 mg, 0.17 mmol, 3.8 equiv.) and 1,2-dibenzoyl ethylene (0.8 mg, 0.0034 mmol, 0.08 equiv.) were added to a 2-5 mL Biotage microwave vial. 1,4-Dioxane (1 mL) was then added and the reaction mixture was irradiated using 465 nm LED strip for 4 hours. Solvent was then removed under reduced pressure and the residue dried in vacuo. The resulting crude product mixture was then dissolved in deuterated chloroform and was analyzed by ^{1}H NMR. Based on comparison of the integrals of the N(CH_3) group and the CH_2 group, the intramolecular KIE was estimated to be **5.8**.

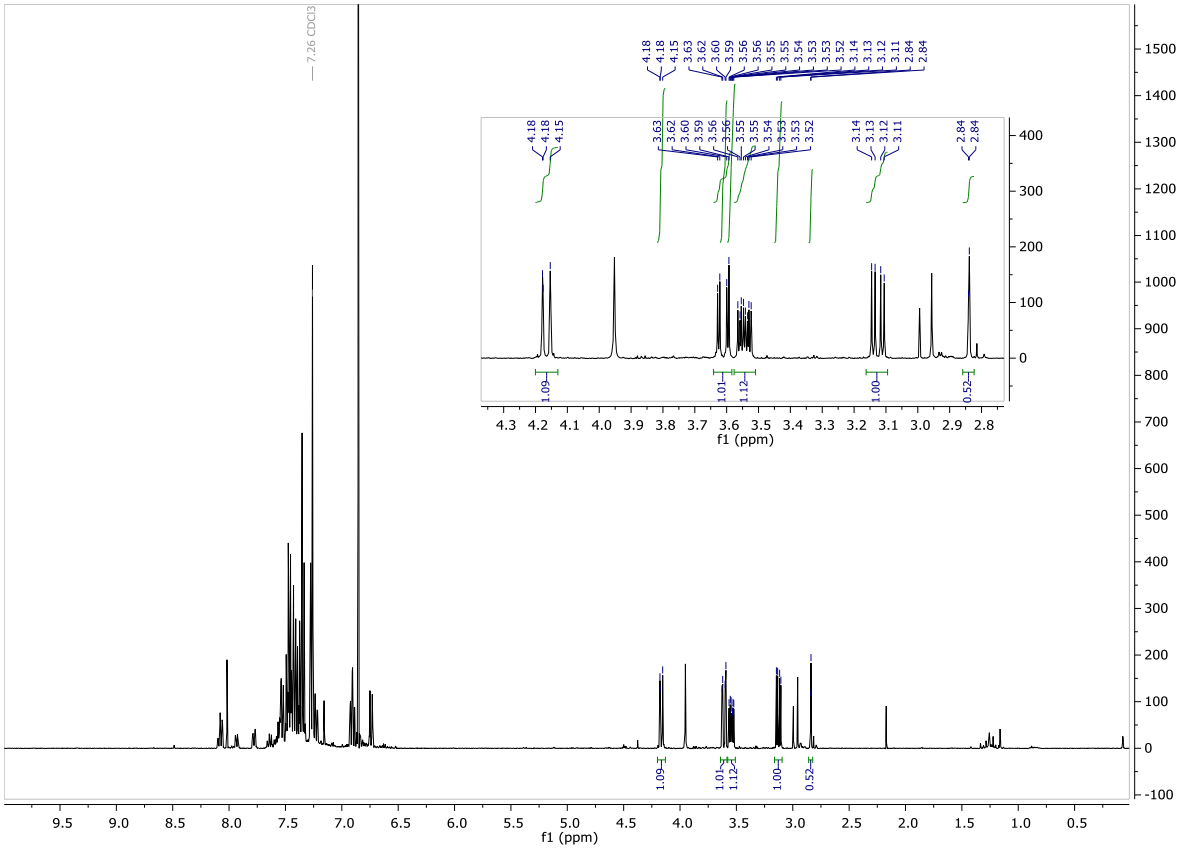

Intermolecular KIE

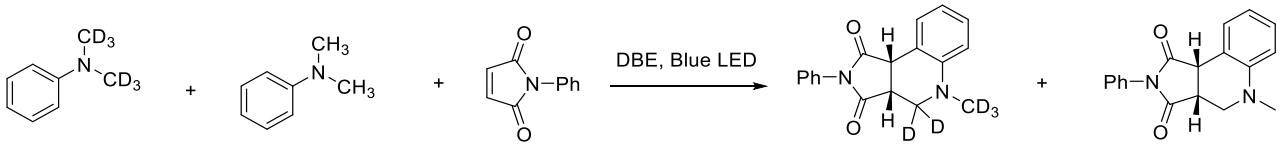

Following a modified published procedure,[3] *N*-phenylmaleimide (8.0 mg, 0.046 mmol, 1 equiv.), *N,N*-$(CD_3)_2$-aniline (14.6 mg, 0.12 mmol, 2.5 equiv.), *N,N*-dimethylaniline (13.9 mg, 0.12 mmol, 2.5 equiv.), and 1,2-dibenzoyl ethylene (0.8 mg, 0.0034 mmol, 0.08 equiv.) were added to a 2-5 mL Biotage microwave vial. 1,4-Dioxane (1 mL) was then added, and the reaction mixture was irradiated using 465 nm LED strip for 5 hours. Solvent was then removed under reduced pressure and the residue dried in vacuo. The resulting crude product mixture was then dissolved in deuterated chloroform and was analyzed by ^{1}H NMR. Based on comparison of the integrals of the N(CH_3) group and the benzylic CH group, the intramolecular KIE was estimated to be **3.8**.

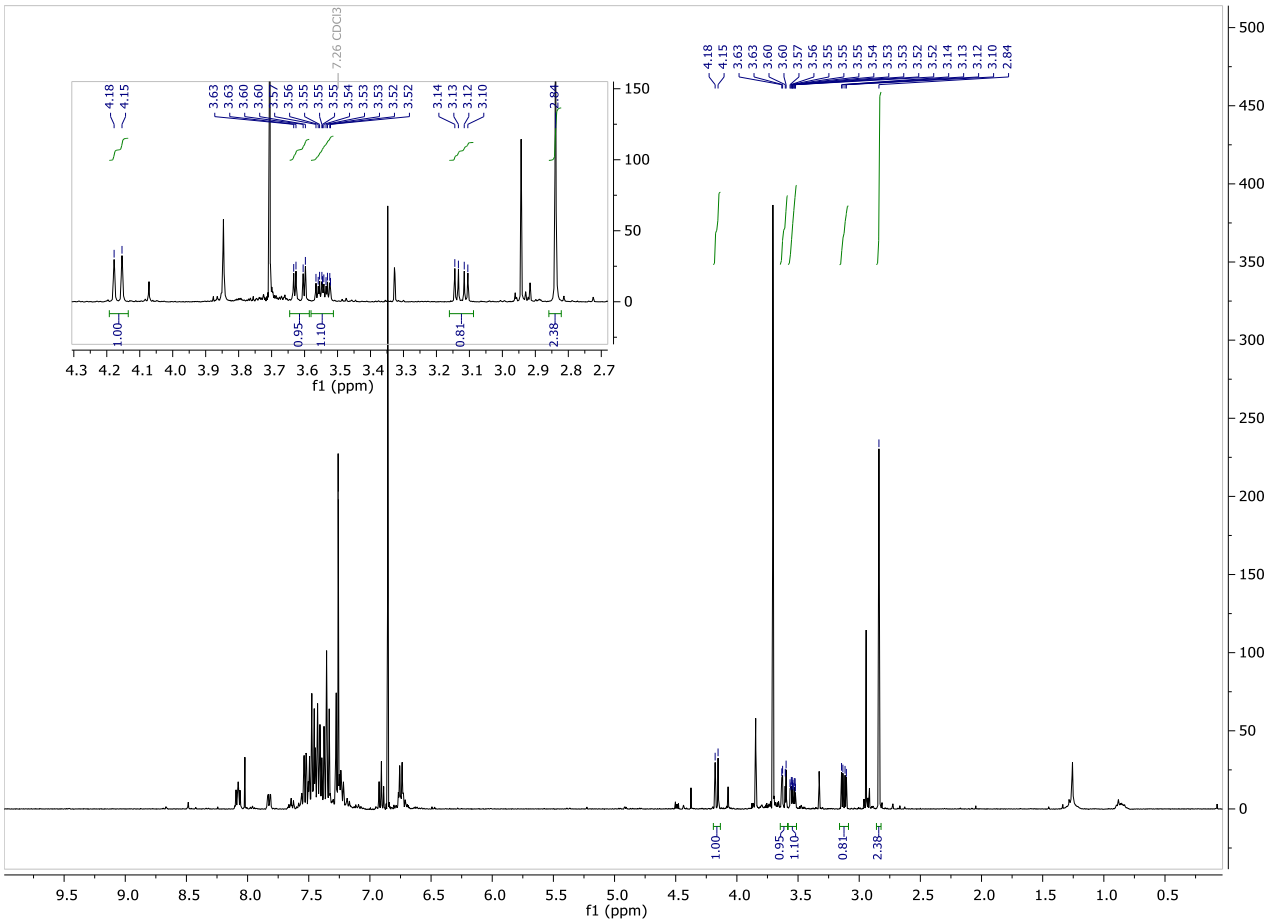

1.7 Competition experiments

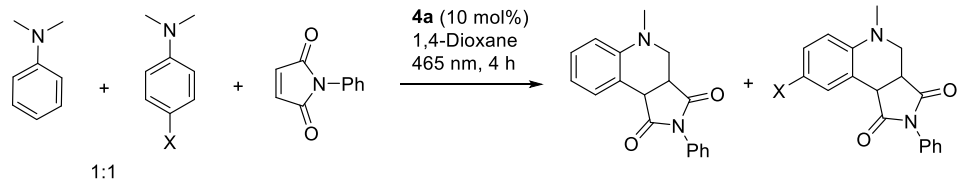

To investigate the impact of substituents on the amine reaction partner, four reactions were set up:

A: To a 2-5 mL Biotage microwave vial was added **2a** (18.4 mg, 0.11 mmol), **1a** (35 mg, 0.29 mmol), 4'-*N,N*-trimethyl aniline (39 mg, 0.29 mmol), **4a** (2.2 mg, 0.009 mmol) and 3 mL 1,4-Dioxane.

B: To a 2-5 mL Biotage microwave vial was added **2a** (17.7 mg, 0.10 mmol), **1a** (24 mg, 0.20 mmol), *p*-CN-*N,N*-dimethyl aniline (29 mg, 0.20 mmol), **4a** (2.2 mg, 0.009 mmol) and 3 mL 1,4-Dioxane.

C: To a 2-5 mL Biotage microwave vial was added **2a** (17.1 mg, 0.10 mmol), **1a** (25 mg, 0.21 mmol), *p*-Br-*N,N*-dimethyl aniline (42.8 mg, 0.21 mmol), **4a** (2.2 mg, 0.009 mmol) and 3 mL 1,4-Dioxane.

D: To a 2-5 mL Biotage microwave vial was added **2a** (16.8 mg, 0.97 mmol), **1a** (27 mg, 0.22 mmol), *p*-COMe-*N,N*-dimethyl aniline (36.0 mg, 0.22 mmol), **4a** (2.2 mg, 0.009 mmol) and 3 mL 1,4-Dioxane.

The four reactions where then irradiated using 465 nm LED strip for 4 hours. The ratio of the products was then calculated by ^{1}H NMR analysis of the crude reaction mixture. To establish the electronic effect, the natural logarithm of the ratio was plotted against the Hammett σ_p parameter (Figure S4).[2]

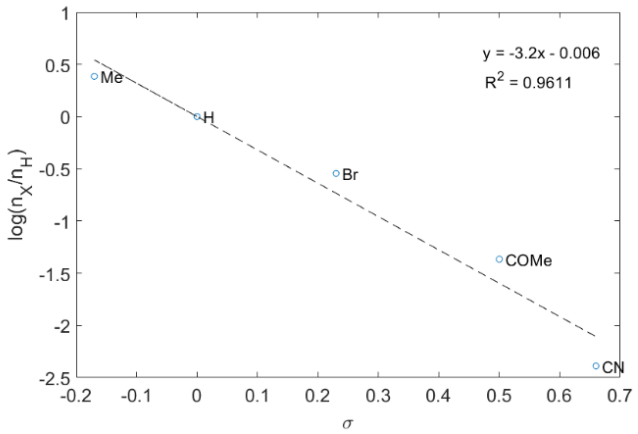

Figure S4. Plot of the ratio of products n(X)/n(H) plotted against the Hammett parameter σ_p.

1.8 Measurement of oxygen consumption

To estimate the amount of oxygen consumed in the photoreaction, an in-house made set up was prepared consisting of two vertically placed 20 mL burettes filled to half heigh with water and connected at the bottom with a rubber tube. One of the burettes was connected to a Schlenk tube containing the reaction mixture with a rubber tube. All fittings were carefully sealed with Teflon tape to ensure a closed system. The other burette was left open to the atmosphere at the top. The reaction mixture was then irradiated. The gas volume displaced by water as the oxygen in the closed system was consumed, was monitored over time. Aliquots of the reaction mixture was taken using a Hamilton 20 µL syringe for GC-FID analysis at regular time intervals. Based on the atmospheric pressure measured in the house (103 hPa) and the volume of displaced gas, the molar amount of oxygen was estimated using the ideal gas law. It was assumed that all gas displaced was due to consumption of oxygen. The amount of product **3a** formed was then plotted against the molar amount of oxygen consumed (Figure S6). A slope of 1.3 was observed, suggesting that 1.3 molecules of dioxygen is consumed per product formed.

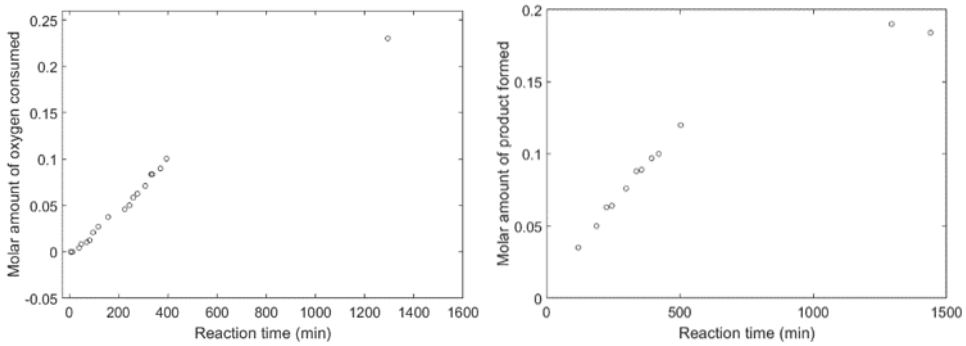

*Figure S5. Consumption of oxygen (left) and formation of **3a** (right) over time. Amount of product was determined using GC-FID using n-dodecane as the internal standard.*

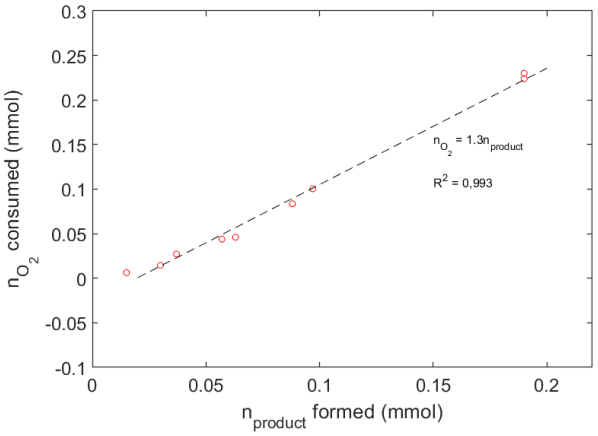

Figure S6. Molar amount of oxygen consumed as a function of product formation.

1.9 Quantum yield determination

Following a published procedure,[1] actinometer solution was prepared by dissolving potassium ferrioxalate (mg) and 280 µL concentrated sulfuric acid in 100 mL deionized water in a volumetric flask. A buffer solution was separately prepared from sodium acetate (mg) and concentrated sulfuric aicd (1 mL) in 100 mL deionized water in a volumetric flask. Finally, 1,10-phenanthroline (200 mg) was dissolved in 100 mL water in a separate volumetric flask.

To measure the light intensity of the light source, 2 mL of the actinometer solution was transferred to a 1x1 cm quartz cuvette and was irradiated for a set time. Care was taken to exclude light exposure of the solution prior and after irradiation. Five different 2 mL portions of the solution were thus irradiated at different times (5, 10, 20, 29 and 60 minutes). After irradiation, each sample was added to a 10 mL volumetric flask containing 2 mL buffer solution and 1 mL 1,10-phenathroline solution. Water was then added to the mark. After resting in room temperature protected from light for 30 minutes, 3 mL of each resulting solution was transferred to 1x1 cm quartz cuvettes and the absorbance at 510 nm was noted and compared to a blank stored protected from light. With the reported molar absorptivity of the iron(II)phenanthroline complex (11 100 L mol^{-1} cm^{-1}) and the difference in absorption between the developed blank and each sample, the molar amount of iron(II) formed during the irradiation was determined according to equation (1).

$$moles\ Fe(II) = \frac{V1*V3*\Delta A_{510\ nm}}{10^3*V2*l*\varepsilon_{510\ nm}} \qquad (1)$$

Where V1 is the volume of the irradiated sample, V2 is the volume of the irradiated sample taken for the determination of amount of Fe(II), V3 is the final volume of the sample measured, l is the path length of light (1 cm), $\Delta A_{510\ nm}$ is the difference in absorption between the irradiated samples and the reference sample kept in dark, and $\varepsilon_{510\ nm}$ is the molar extinction coefficient of the iron(II) phenanthroline complex (11 100 L mol^{-1} cm^{-1}).

The amount of iron(II) was then plotted as a function of irradiation time and from the slope of the fitted data, the photon flux can be calculated according to eq. 2,

$$photon\ flux = \frac{\frac{dx}{dt}}{\phi(450\ nm)*(1-10^{-A(450\ nm)})} \qquad (2)$$

where dx/dt is the rate of formation of iron(II), $\phi(450\ nm)$ is the quantum yield for the ferrioxalate actinometer at 450 nm excitation (0.9) and A(450 nm) is the absorbance of the ferrioxalate actinometer at the irradiation wavelength (0.228). Consequently, the photon flux was determined to be $1*10^{-9}$ moles of photons s^{-1}.

Reactions prepared protected from light. DBE, Maleimide and dodecane mixed in a vial and separately the amine and dioxane in another vial. When in dark room, the amine solution was added to the solids and when solids were dissolved 3 mL was transferred to a 1x1 cm quartz vial and irradiated with 450 nm (5 nm slit) for different times. The molar amount of product formed was determined using GC-FID with n-dodecane as internal standard and was plotted as a function of time. The quantum yield (moles of product formed per moles of absorbed photons) was then calculated according to equation 3:

$$\phi = \frac{moles\ product\ formed/time}{photon\ flux*(1-10^{-A(reaction\ mixture\ at\ 450\ nm)})} \qquad (3)$$

Accordingly, a quantum yield of 0.07 could be estimated.

1.10 Synthesis of starting materials

General procedure for the synthesis of *N*-substituted maleimides

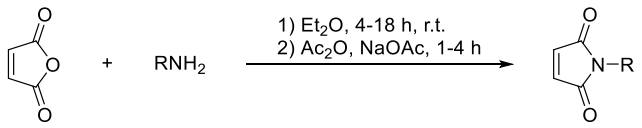

Maleimides **2b**, **2d**, **2e**, **2f**, and **2l** were synthesized following a modified reported method.[4] The appropriate amine (10 mmol) dissolved in diethyl ether (5 mL) was added to a stirred solution of maleic anhydride (10 mmol, 1 g) in diethyl ether (10 mL). The solution was stirred at room temperature for 4-18 hours and the resulting suspension was filtered. The collected solids were washed with diethyl ether and then dried in vacuo and directly added to acetic anhydride (6 mL) followed by sodium acetate (1 equiv.). The suspension was heated to 120 °C until full conversion as followed by TLC (1-4 hours reaction time). The solvent was then removed under reduced pressure and the residue was taken up ethyl acetate and washed with saturated sodium bicarbonate solution and brine. The organic phase was then dried over anhydrous sodium sulphate and was concentrated under reduced pressure. The solid residue was recrystallized from ethanol or ethyl acetate to afford the desired maleimide as a crystalline solid or purified by column chromatography for oils.

1-(4-methoxyphenyl)-1H-pyrrole-2,5-dione (2b)[6]

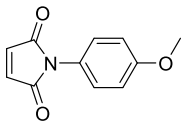

Yellow solid afforded after recrystallization from ethanol, 1.2 g (58%); Spectroscopic data in accordance with literature;[6] **^{1}H NMR (400 MHz, Chloroform-*d*)** δ = 7.25 – 7.19 (m, 2H), 7.02 – 6.94 (m, 2H), 6.84 (s, 2H), 3.83 (s, 3H) ppm; **^{13}C NMR (101 MHz, Chloroform-*d*)** δ = 169.9, 159.3, 134.2, 127.7, 123.8, 114.6, 55.6 ppm.

1-(4-fluorophenyl)-1H-pyrrole-2,5-dione (2d)[7]

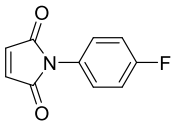

Yellow crystalline solid obtained after recrystallization from ethyl acetate/heptane, 937 mg (50%); spectroscopic data in accordance with literature;[7] **^{1}H NMR (400 MHz, Chloroform-*d*)** δ = 7.38 – 7.28 (m, 2H), 7.21 – 7.12 (m, 2H), 6.86 (d, *J* = 0.8 Hz, 2H); ^{13}C NMR (101 MHz, Chloroform-*d*) δ 169.5, 163.2, 134.4, 128.0 (d, *J* = 8.7 Hz), 116.3 (d, *J* = 22.9 Hz) ppm; **^{13}C NMR (101 MHz, Chloroform-*d*)** δ = 169.5, 163.2, 160.7, 134.4, 128.0 (d, *J* = 8.7 Hz), 116.3 (d, *J* = 22.9 Hz) ppm.

1-(2-(tert-butyl)phenyl)-1H-pyrrole-2,5-dione (2e)[9]

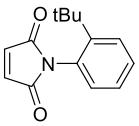

Off-white solid obtained after recrystallization twice from ethanol (500 mg, 36%). Spectroscopic data in accordance with literature;[9] **^{1}H NMR (400 MHz, Chloroform-*d*)** δ = 7.59 (dd, *J* = 8.2, 1.5 Hz, 1H), 7.41 (tdd, *J* = 7.4, 1.6, 0.8 Hz, 1H), 7.31 – 7.27 (m, 1H), 6.93 – 6.87 (m, 3H), 1.30 (s, 9H) ppm; **^{13}C NMR (101 MHz, Chloroform-*d*)** δ = 171.0, 149.7, 135.1, 131.5, 130.0, 129.3, 128.8, 127.5, 35.6, 31.7 ppm.

1-(2,4-dimethylphenyl)-1H-pyrrole-2,5-dione (2f)[8]

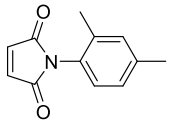

Yellow oil obtained after column chromatography (silica, 10% ethyl acetate in petroleum spirits) 1.47 g (34%); spectroscopic data in accordance with literature;[8] **^{1}H NMR (400 MHz, Chloroform-*d*)** δ = 7.14 (dq, *J* = 2.0, 0.7 Hz, 1H), 7.13 – 7.08 (m, 1H), 6.99 (d, *J* = 8.0 Hz, 1H), 6.86 (s, 2H), 2.35 (s, 3H), 2.11 (s, 3H) ppm; **^{13}C NMR (101 MHz, Chloroform-*d*)** δ = 167.0, 139.7, 136.3, 134.5, 132.0, 128.6, 127.8, 127.3, 21.3, 17.9 ppm.

1-phenethyl-1H-pyrrole-2,5-dione (2l)[5]

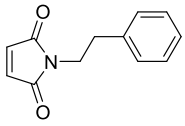

Pink flakes isolated after recrystallization from ethanol twice, 894 mg (44%); Spectroscopic data in accordance with the literature;[5] **^{1}H NMR (400 MHz, Chloroform-*d*)** δ = 7.33 – 7.26 (m, 2H), 7.25 – 7.17 (m, 3H), 6.65 (s, 2H), 3.82 – 3.72 (m, 2H), 2.95 – 2.83 (m, 2H) ppm; **^{13}C NMR (101 MHz, Chloroform-*d*)** δ = 170.7, 138.0, 134.2, 129.0, 128.7, 126.8, 39.3, 34.7 ppm.

1.11 Synthesis of tetrahydroquinolone compounds

General procedure for the visible light driven aerobic oxidative annulation reaction

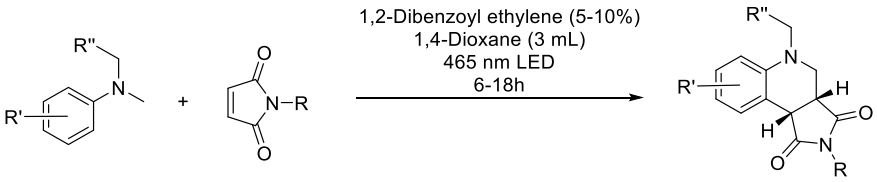

To a 2-5 mL Biotage microwave vial was added *N*-substituted maleimide (0.25 mmol, 1 equiv.), the appropriate amine (1.75 mmol, 7 equiv.) and 1,2-dibenzoyl ethylene (0.013 mmol, 0.05 equiv.). 1,4-Dioxane (3 mL) was then added and the solution was irradiated using a 465 nm LED stripe for 6-18 hours. The solvent was then removed under reduced pressure and the crude residue was loaded on a silica column and eluted with a mixture of 5% ethyl acetate in petroleum ethers to afford the desired tetrahydroquinoline products **3a-y**.

5-methyl-2-phenyl-3a,4,5,9b-tetrahydro-1H-pyrrolo[3,4-c]quinoline-1,3(2H)-dione (3a)[10]

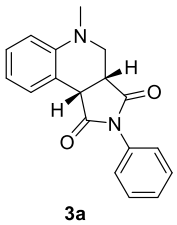

3a

Starting with 43 mg *N*-phenyl maleimide following the general procedure, **3a** was afforded as a yellow solid (58.3 mg, 80%). For the gram scale synthesis version, to a 100 mL round bottom flask was added *N*-phenylmaleimide (762 mg, 4.4 mmol, 1 equiv.), 1,2-dibenzoyl ethylene (52 mg, 0.22 mmol, 0.05 equiv.), *N,N*-dimethylaniline (3.7 g, 30.5 mmol, 6.9 equiv.), and 1,4-dioxane (50 mL). The reaction mixture was then placed 5 cm from a 40 W blue LED lamp and was irradiated for 7 hours under strong stirring. The round bottom flask was kept open during the reaction to facilitate easy diffusion of oxygen to drive the reaction. After full conversion, as judged by TLC (20% ethyl acetate in n-heptane), the solvent was removed under reduced pressure and the residue was taken up in ethyl acetate. Excess aniline was removed by washing with 10 mL 1 M HCl thrice. The organic layer was then washed with brine and was dried over sodium sulphate. Solvent was then removed under reduced pressure to yield a brown solid that was suspended in ethyl acetate/ heptane and was collected by filtration. The solids were washed with a small amount of ethanol and then excessive amounts of n-heptane. After drying in vacuo, **3a** was obtained as an off-white powder (1.0 g, 3.4 mmol, 78%). Spectroscopic data was in accordance with the literature;[10] **^{1}H NMR (400 MHz, Chloroform-*d*)** δ = 7.54 (dd, *J* = 7.6, 1.4 Hz, 1H), 7.47 – 7.40 (m, 2H), 7.39 – 7.32 (m, 1H), 7.29 – 7.21 (m, 3H), 6.92 (tt, *J* = 7.5, 1.2 Hz, 1H), 6.76 (d, *J* = 8.2 Hz, 1H), 4.17 (d, *J* = 9.6 Hz, 1H), 3.66 – 3.59 (m, 1H), 3.59 – 3.51 (m, 1H), 3.14 (ddd, *J* = 11.4, 4.4, 1.0 Hz, 1H), 2.85 (s, 3H) ppm; **^{13}C NMR (101 MHz, Chloroform-*d*)** δ = 177.8, 175.9, 148.5, 132.1, 130.5, 129.1, 128.8, 128.6, 126.5, 119.9, 118.7, 112.8, 50.8, 43.7, 42.3, 39.6 ppm.

2-(4-methoxyphenyl)-5-methyl-3a,4,5,9b-tetrahydro-1H-pyrrolo[3,4-c]quinoline-1,3(2H)-dione (3b)[11]

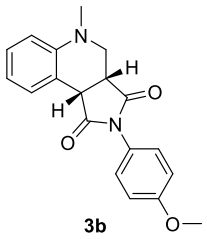

3b

Starting with 49.9 mg *N*-(4-methoxyphenyl)maleimide following the general procedure provided **3b** as a yellow solid (27.4 mg, 36%). Spectroscopic data was in accordance with the literature;[11] **^{1}H NMR (400 MHz, Chloroform-*d*)** δ = 7.53 (ddd, *J* = 7.5, 1.6, 0.8 Hz, 1H), 7.27 – 7.21 (m, 1H), 7.21 – 7.14 (m, 2H), 6.98 – 6.90 (m, 3H), 6.75 (dd, *J* = 8.2, 1.1 Hz, 1H), 4.14 (d, *J* = 9.5 Hz, 1H), 3.80 (s, 3H), 3.60 (dd, *J* = 11.4, 2.8 Hz, 1H), 3.52 (ddd, *J* = 9.6, 4.4, 2.7 Hz, 1H), 3.12 (dd, *J* = 11.5, 4.4 Hz, 1H), 2.84 (s, 3H) ppm; **^{13}C NMR (101 MHz, Chloroform-*d*)** δ = 178.1, 176.1, 159.5, 148.6, 130.5, 128.8, 127.7, 124.7, 119.8, 118.8, 114.4, 112.7, 55.6, 50.8, 43.6, 42.2, 39.6 ppm.

2-(4-chlorophenyl)-5-methyl-3a,4,5,9b-tetrahydro-1H-pyrrolo[3,4-c]quinoline-1,3(2H)-dione (3c)[10]

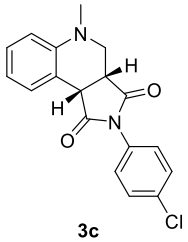

3c

Starting with 52.6 mg *N*-(4-chlorophenyl)maleimide following the general procedure provided a white solid (51 mg, 62%). Spectroscopic data was in accordance with the literature;[10] **^{1}H NMR (400 MHz, Chloroform-*d*)** δ = 7.51 (ddd, *J* = 7.5, 1.7, 0.8 Hz, 1H), 7.45 – 7.34 (m, 2H), 7.29 – 7.20 (m, 4H), 6.92 (td, *J* = 7.5, 1.1 Hz, 1H), 6.75 (dd, *J* = 8.3, 1.1 Hz, 1H), 4.15 (d, *J* = 9.6 Hz, 1H), 3.60 (dd, *J* = 11.5, 2.7 Hz, 1H), 3.52 (ddd, *J* = 9.6, 4.4, 2.7 Hz, 1H), 3.11 (dd, *J* = 11.5, 4.4 Hz, 1H), 2.84 (s, 3H) ppm; **^{13}C NMR (101 MHz, Chloroform-*d*)** δ = 177.5, 175.6, 148.6, 134.3, 130.5, 130.4, 129.3, 128.9, 127.7, 119.9, 118.5, 112.7, 50.7, 43.7, 42.2, 39.6 ppm.

2-(4-fluorophenyl)-5-methyl-3a,4,5,9b-tetrahydro-1H-pyrrolo[3,4-c]quinoline-1,3(2H)-dione (3d)[12]

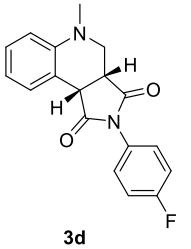

3d

Starting with 48.3 mg of *N*-(4-fluorophenyl)maleimide following the general procedure provided a white solid (57.5 mg, 74%). Spectroscopic data was in accordance with the literature;[12] **^{1}H NMR (400 MHz, Chloroform-*d*)** δ = 7.52 (ddd, *J* = 7.6, 1.6, 0.8 Hz, 1H), 7.29 – 7.20 (m, 3H), 7.15 – 7.07 (m, 2H), 6.92 (td, *J* = 7.5, 1.2 Hz, 1H), 6.75 (dd, *J* = 8.3, 1.1 Hz, 1H), 4.15 (d, *J* = 9.6 Hz, 1H), 3.60 (dd, *J* = 11.5, 2.7 Hz, 1H), 3.52 (ddd, *J* = 9.6, 4.4, 2.6 Hz, 1H), 3.11 (dd, *J* = 11.5, 4.4 Hz, 1H), 2.84 (s, 3H); **^{13}C NMR (101 MHz, Chloroform-*d*)** δ = 177.8, 175.8, 162.2 (d, $^1J_{C\text{-}F}$ = 248.4 Hz), 148.6, 130.4, 128.8, 128.3 (d, $^3J_{C\text{-}F}$ = 8.7 Hz), 128.0 (d, $^4J_{C\text{-}F}$ = 3.3 Hz), 119.8, 118.5, 116.1 (d, $^2J_{C\text{-}F}$ = 22.9 Hz) , 112.7, 50.7, 43.7, 42.2, 39.5 ppm.

2-(2-(tert-butyl)phenyl)-5-methyl-3a,4,5,9b-tetrahydro-1H-pyrrolo[3,4-c]quinoline-1,3(2H)-dione (3e)

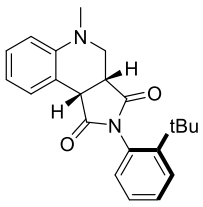

3e

Starting with 58.9 mg of *N*-(2-*tert*butylphenyl)maleimide following the general procedure with irradiation time of 18 hours **3e** as an orange oil (56.9 mg, 64%). **^{1}H NMR (400 MHz, Chloroform-*d*)** δ = 7.54 (dddd, *J* = 22.0, 7.5, 1.5, 0.7 Hz, 2H), 7.39 – 7.32 (m, 1H), 7.29 – 7.23 (m, 1H), 7.22 – 7.16 (m, 1H), 6.92 (tt, *J* = 7.5, 0.9 Hz, 1H), 6.78 (dd, *J* = 8.2, 1.1 Hz, 1H), 6.68 (dd, *J* = 7.8, 1.5 Hz, 1H), 4.16 (d, *J* = 9.6 Hz, 1H), 3.61 (ddd, *J* = 11.4, 2.8, 0.7 Hz, 1H), 3.58 – 3.48 (m, 1H), 3.11 (ddd, *J* = 11.4, 4.6, 0.8 Hz, 1H), 2.86 (d, *J* = 0.7 Hz, 3H), 1.36 (t, *J* = 0.6 Hz, 9H) ppm; **^{13}C NMR (101 MHz, Chloroform-*d*)** δ = 179z.1, 176.9, 162.5, 148.9, 147.8, 131.0, 130.6, 129.8, 128.8, 128.7, 127.4, 119.9, 119.1, 112.6, 51.1, 44.0, 42.6, 39.6, 35.8, 31.8 ppm; **FTIR** ν = 2958, 1709, 1495, 1375, 1316, 1195, 1181 cm^{-1}; **HRMS (ESI)** m/z calcd $C_{22}H_{24}N_2O_2$ $[M+H]^+$ 349.1916, found 349.1917.

2-(2-(tert-butyl)phenyl)-5-methyl-3a,4,5,9b-tetrahydro-1H-pyrrolo[3,4-c]quinoline-1,3(2H)-dione (3e')

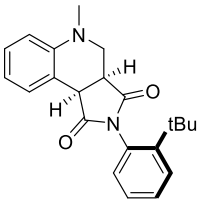

3e'

The diastereomer **3e'** was furnished from **3e** accordingly: to a 2-5 mL Biotage microwave vial was added **3e** (20 mg, 0.057 mmol). The vial was then capped and heated to 160 °C using a metal heating block. After 1 hour heating the vial was cooled to room temperature and the crude mixture was purified using silica flash chromatography (10% ethyl acetate in petroleum ethers) to afford **3e** (8.4 mg, 42%) and **3e'** (6.9 mg, 35%) as white solids. **m.p.** 195.4 – 196.7 °C; **^{1}H NMR (400 MHz, Chloroform-*d*)** δ = 7.54 – 7.46 (m, 2H), 7.36 (ddd, *J* = 8.1, 7.3, 1.6 Hz, 1H), 7.29 (dd, *J* = 7.5, 1.5 Hz, 1H), 7.25 – 7.19 (m, 1H), 6.92 – 6.85 (m, 2H), 6.73 (dd, *J* = 8.3, 1.1 Hz, 1H), 4.18 (d, *J* = 9.5 Hz, 1H), 3.70 (dd, *J* = 11.5, 2.2 Hz, 1H), 3.54 (ddd, *J* = 9.6, 4.0, 2.2 Hz, 1H), 3.16 (dd, *J* = 11.5, 4.0 Hz, 1H), 2.84 (s, 3H), 1.00 (s, 9H) ppm; **^{13}C NMR (101 MHz, Chloroform-*d*)** δ = 179.1, 177.0, 148.8, 148.6, 131.4, 130.9, 130.3, 129.8, 128.8, 128.4, 127.5, 119.8, 118.1, 112.4, 50.4, 45.0, 43.1, 39.1, 35.1, 30.7 ppm; **FTIR** ν = 2966, 1710, 1497, 1371, 1265, 1180 cm^{-1}; **HRMS (ESI)** m/z calcd $C_{22}H_{24}N_2O_2$ $[M+H]^+$ 349.1916, found 349.1921.

2-(2,4-dimethylphenyl)-5-methyl-3a,4,5,9b-tetrahydro-1H-pyrrolo[3,4-c]quinoline-1,3(2H)-dione (3f)

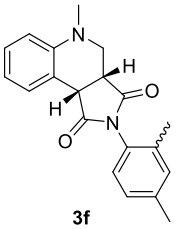

3f

Starting with 53.0 mg of *N*-(2,4-dimethylphenyl)maleimide following the general procedure provided **3f** as a 2:1 mixture of diastereomers as an orange oil (55.3 mg, 66%). **^{1}H NMR (400 MHz, Chloroform-*d*)** δ = 7.56 – 7.48 (m, 3H), 7.26 – 7.22 (m, 3H), 7.15 – 6.98 (m, 8H), 6.95 – 6.88 (m, 3H), 6.86 – 6.72 (m, 4H), 4.23 – 4.12 (m, 3H), 3.66 – 3.50 (m, 6H), 3.15 – 3.06 (m, 3H), 2.86 (s, 3H), 2.85 (s, 6H), 2.35 – 2.28 (m, 9H), 2.16 (s, 3H), 1.80 (s, 6H) ppm; **^{13}C NMR (101 MHz, Chloroform-*d*)** δ = 178.1, 177.9, 176.1, 175.9, 148.7 (2C), 139.6, 139.4, 135.6, 135.0, 131.9 (2C), 130.5, 130.4, 128.7, 128.6, 128.0, 127.6 (3C) 119.8 (2C), 119.2, 118.8, 112.6, 112.4, 51.2, 50.9, 44.4, 43.7, 42.9, 42.4, 39.6, 39.3, 21.3(2C), 17.8, 17.0 ppm; **FTIR** ν = 2924, 1706, 1498, 1386, 1197, 1180 cm^{-1}; **HRMS (ESI)** m/z calcd $C_{20}H_{20}N_2O_2$ $[M+H]^+$ 321.1603, found 321.1612.

5-methyl-2-(1-phenylethyl)-3a,4,5,9b-tetrahydro-1H-pyrrolo[3,4-c]quinoline-1,3(2H)-dione (3g)[13]

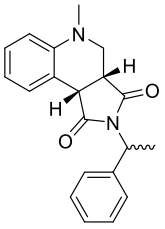

3g

Starting with 54.4 mg of 1-(1-phenylethyl)-1H-pyrrole-2,5-dione following the general procedure provided **3g** as a 1:1 mixture of diastereomers as a brown oil (54.6 mg, 63%). Spectroscopic data was in accordance with the literature.[13] **^{1}H NMR (400 MHz, Chloroform-*d*)** δ = 7.48 – 7.43 (m, 2H), 7.35 (ddtd, *J* = 6.1, 4.6, 1.6, 0.7 Hz, 4H), 7.32 – 7.18 (m, 8H), 6.89 (dtd, *J* = 8.7, 7.5, 1.2 Hz, 2H), 6.72 (ddd, *J* = 8.2, 2.2, 1.1 Hz, 2H), 5.47 – 5.31 (m, 2H), 3.98 – 3.87 (m, 2H), 3.44 (ddd, *J* = 11.4, 9.2, 3.0 Hz, 2H), 3.37 – 3.24 (m, 2H), 3.04 (ddd, *J* = 11.3, 6.4, 4.6 Hz, 2H), 2.82 (s, 3H), 2.78 (s, 3H), 1.79 (d, *J* = 7.3 Hz, 3H), 1.75 (d, *J* = 7.3 Hz, 3H) ppm; **^{13}C NMR (101 MHz, Chloroform-*d*)** δ = 178.6, 178.5, 176.7, 176.5, 148.6 (2C), 139.5 (2C), 130.3 (2C), 128.6 (2C), 128.5, 128.4, 127.7 (2C), 127.2 (2C), 119.8, 119.7, 119.3, 119.0, 112.5 (2C), 51.2, 51.0, 50.7, 50.6, 43.5, 43.4, 42.1, 42.0, 39.5, 39.4, 16.9, 16.8 ppm.

2,5-dimethyl-3a,4,5,9b-tetrahydro-1H-pyrrolo[3,4-c]quinoline-1,3(2H)-dione (3h)[11]

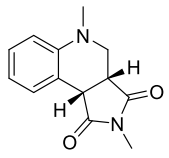

3h

Starting from 27.8 mg *N*-methylmaleimide following the general procedure, **3h** as a white solid (18.0 mg, 31%) was isolated; spectroscopic data was in accordance with the literature;[11] **^{1}H NMR (400 MHz, Chloroform-*d*)** δ = 7.47 (ddd, *J* = 7.4, 1.7, 0.8 Hz, 1H), 7.24 – 7.14 (m, 1H), 6.89 (td, *J* = 7.5, 1.1 Hz, 1H), 6.69 (dd, *J* = 8.3, 1.1 Hz, 1H), 3.99 (d, *J* = 9.4 Hz, 1H), 3.53 (dd, *J* = 11.5, 2.5 Hz, 1H), 3.36 (ddd, *J* = 9.4, 4.4, 2.4 Hz, 1H), 3.03 (dd, *J* = 11.5, 4.4 Hz, 1H), 2.98 (s, 3H), 2.79 (s, 3H); **^{13}C NMR (101 MHz, Chloroform-*d*)** δ = 178.9, 176.9, 148.5, 130.3, 128.7, 119.8, 118.9, 112.7, 50.6, 43.7, 42.1, 39.6, 25.5 ppm.

5-methyl-2-propyl-3a,4,5,9b-tetrahydro-1H-pyrrolo[3,4-c]quinoline-1,3(2H)-dione (3i)[10]

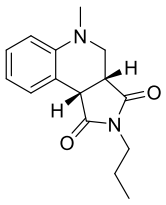

3i

Starting from 34,1 mg *N*-propylmaleimide following the general procedure, **3i** as a white solid (30.2 mg, 48%) was isolated. Spectroscopic data was in accordance with the literature;[10] **^{1}H NMR (400 MHz, Chloroform-*d*)** δ = 7.48 – 7.42 (m, 1H), 7.22 – 7.14 (m, 1H), 6.87 (td, *J* = 7.4, 1.2 Hz, 1H), 6.69 (dd, *J* = 8.2, 1.3 Hz, 1H), 3.95 (d, *J* = 9.3 Hz, 1H), 3.53 – 3.40 (m, 3H), 3.33 (ddd, *J* = 9.0, 4.3, 2.4 Hz, 1H), 3.01 (dd, *J* = 11.5, 4.5 Hz, 1H), 2.78 (s, 3H), 1.66 – 1.47 (m, 2H), 0.81 (td, *J* = 7.4, 1.7 Hz, 3H) ppm; **^{13}C NMR (101 MHz, Chloroform-*d*)** δ = 178.9, 176.9, 148.4, 130.3, 128.6, 119.8, 119.2, 112.6, 50.6, 43.6, 42.1, 41.0, 39.5, 21.0, 11.1 ppm.

2-cyclohexyl-5-methyl-3a,4,5,9b-tetrahydro-1H-pyrrolo[3,4-c]quinoline-1,3(2H)-dione (3j)[10]

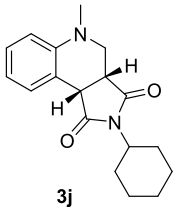

3j

Starting from 47.4 mg *N*-cyclohexylmaleimide following the general procedure, **3j** as a yellow oil (49.9 mg, 64%) was isolated. Spectroscopic data was in accordance with the literature;[10] **^{1}H NMR (400 MHz, Chloroform-*d*)** δ = 7.46 (ddd, *J* = 7.5, 1.7, 0.7 Hz, 1H), 7.23 – 7.14 (m, 1H), 6.88 (td, *J* = 7.5, 1.1 Hz, 1H), 6.69 (dd, *J* = 8.2, 1.1 Hz, 1H), 4.00 – 3.85 (m, 2H), 3.45 (dd, *J* = 11.4, 3.0 Hz, 1H), 3.28 (ddd, *J* = 9.5, 4.6, 3.0 Hz, 1H), 3.02 (dd, *J* = 11.4, 4.6 Hz, 1H), 2.79 (s, 3H), 2.21 – 1.96 (m, 2H), 1.84 – 1.72 (m, 2H), 1.66 – 1.58 (m, 1H), 1.58 – 1.49 (m, 2H), 1.37 – 1.09 (m, 3H) ppm; **^{13}C NMR (101 MHz, Chloroform-*d*)** δ = 178.8, 176.9, 148.5, 130.3, 128.5, 119.5, 119.1, 112.4, 52.2, 50.9, 43.1, 41.8, 39.5, 28.9, 28.8, 25.9, 25.8, 25.1 ppm.

2-(tert-butyl)-5-methyl-3a,4,5,9b-tetrahydro-1H-pyrrolo[3,4-c]quinoline-1,3(2H)-dione (3k)[10]

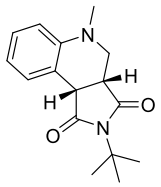

3k

37.8 mg *N-tBu*-maleimide provided an orange oil, 37.3 mg (54%). Spectroscopic data was in accordance with the literature;[10] **^{1}H NMR (400 MHz, Chloroform-*d*)** δ = 7.45 (dddd, *J* = 7.5, 1.7, 0.9, 0.4 Hz, 1H), 7.25 – 7.18 (m, 1H), 6.88 (td, *J* = 7.5, 1.2 Hz, 1H), 6.72 (dd, *J* = 8.2, 1.1 Hz, 1H), 3.83 (d, *J* = 9.7 Hz, 1H), 3.44 (dd, *J* = 11.4, 3.1 Hz, 1H), 3.21 (ddd, *J* = 9.7, 4.6, 3.1 Hz, 1H), 3.01 (dd, *J* = 11.4, 4.6 Hz, 1H), 2.81 (s, 3H), 1.54 (s, 9H) ppm; **^{13}C NMR (101 MHz, Chloroform-*d*)** δ = 179.6, 177.9, 148.2, 130.4, 128.6, 119.7, 119.4, 112.7, 58.9, 51.0, 43.1, 42.2, 39.7, 28.5 ppm.

5-methyl-2-phenethyl-3a,4,5,9b-tetrahydro-1H-pyrrolo[3,4-c]quinoline-1,3(2H)-dione (3l)

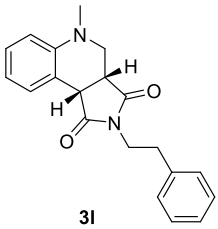

3l

Starting with 52.9 mg *N*-phenetylmaleimide following the general procedure provided **3l** as an orange oil (39.4 mg, 47%). **^{1}H NMR (400 MHz, Chloroform-*d*)** δ = 7.45 (ddd, *J* = 7.6, 1.6, 0.8 Hz, 1H), 7.25 – 7.13 (m, 4H), 7.10 (dd, *J* = 7.7, 1.9 Hz, 2H), 6.89 (td, *J* = 7.4, 1.1 Hz, 1H), 6.71 (dd, *J* = 8.3, 1.1 Hz, 1H), 3.93 (d, *J* = 9.4 Hz, 1H), 3.74 (t, *J* = 7.4 Hz, 2H), 3.47 (dd, *J* = 11.5, 2.6 Hz, 1H), 3.28 (ddd, *J* = 9.4, 4.4, 2.6 Hz, 1H), 3.01 (dd, *J* = 11.5, 4.4 Hz, 1H), 2.85 (td, *J* = 7.2, 1.4 Hz, 2H), 2.78 (s, 3H) ppm; **^{13}C NMR (101 MHz, Chloroform-*d*)** δ = 178.5, 176.6, 148.4, 137.8, 130.2, 128.9, 128.6, 128.5, 126.6, 119.6, 118.8, 112.5, 50.4, 43.5, 42.0, 40.5, 39.5, 33.5 ppm; **ATR-FTIR** ν = 2949, 1698, 1499, 1401, 1354, 1159 cm^{-1}; **HRMS (ESI)** m/z calcd $C_{20}H_{20}N_2O_2$ $[M+H]^+$ 321.1603, found 321.1610.

2-benzyl-5-methyl-3a,4,5,9b-tetrahydro-1H-pyrrolo[3,4-c]quinoline-1,3(2H)-dione (3m)[10]

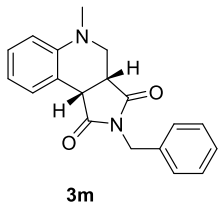

3m

Starting with 46.5 mg *N*-benzylmaleimide following the general procedure provided a white solid (45.3 mg, 60%). Spectroscopic data was in accordance with the literature;[10] **^{1}H NMR (400 MHz, Chloroform-*d*)** δ = 7.51 – 7.41 (m, 1H), 7.38 – 7.13 (m, 6H), 6.90 (td, *J* = 7.5, 1.2 Hz, 1H), 6.71 (dd, *J* = 8.2, 1.1 Hz, 1H), 4.76 – 4.51 (m, 2H), 3.99 (d, *J* = 9.4 Hz, 1H), 3.50 (dd, *J* = 11.5, 2.7 Hz, 1H), 3.36 (ddd, *J* = 9.4, 4.6, 2.8 Hz, 1H), 3.05 (dd, *J* = 11.5, 4.6 Hz, 1H), 2.80 (s, 3H) ppm; **^{13}C NMR (101 MHz, Chloroform-*d*)** δ = 178.4, 176.5, 148.5, 135.7, 130.3, 128.7, 128.7, 128.4, 127.9, 119.8, 119.0, 112.6, 50.8, 43.7, 42.9, 42.2, 39.5 ppm.

5-methyl-3a,4,5,9b-tetrahydro-1H-pyrrolo[3,4-c]quinoline-1,3(2H)-dione (3n)[14]

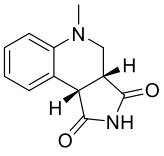
3n

Starting with 25.9 mg maleimide following the general procedure provided **3n** as an off-white solid after column chromatography using 0-4 % methanol in dichloromethane (17.2 mg, 30%). Spectroscopic data was in accordance with the literature;[14] **^{1}H NMR (400 MHz, Chloroform-*d*)** δ = 8.56 (s, 1H), 7.50 – 7.36 (m, 1H), 7.25 – 7.17 (m, 1H), 6.89 (td, *J* = 7.4, 1.1 Hz, 1H), 6.72 (dd, *J* = 8.3, 1.1 Hz, 1H), 4.02 (d, *J* = 9.5 Hz, 1H), 3.50 (dd, *J* = 11.5, 2.6 Hz, 1H), 3.41 (ddd, *J* = 9.5, 4.5, 2.6 Hz, 1H), 3.02 (ddd, *J* = 11.5, 4.4, 0.8 Hz, 1H), 2.81 (s, 3H) ppm; **^{13}C NMR (101 MHz, Chloroform-*d*)** δ = 179.0, 177.0, 148.5, 130.2, 128.8, 119.9, 118.5, 112.7, 50.5, 44.9, 43.4, 39.6 ppm.

5,8-dimethyl-2-phenyl-3a,4,5,9b-tetrahydro-1H-pyrrolo[3,4-c]quinoline-1,3(2H)-dione (3o)[10]

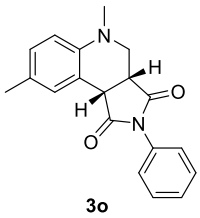
3o

Starting with 43.0 mg *N*-phenylmaleimide following the general procedure provided a white solid (48.6 mg, 64%). Spectroscopic data was in accordance with the literature;[10] **^{1}H NMR (400 MHz, Chloroform-*d*)** δ = 7.46 – 7.38 (m, 2H), 7.37 – 7.30 (m, 2H), 7.29 – 7.23 (m, 2H), 7.07 – 6.98 (m, 1H), 6.65 (d, *J* = 8.3 Hz, 1H), 4.11 (d, *J* = 9.5 Hz, 1H), 3.58 (dd, *J* = 11.4, 2.7 Hz, 1H), 3.50 (ddd, *J* = 9.6, 4.4, 2.7 Hz, 1H), 3.05 (dd, *J* = 11.4, 4.4 Hz, 1H), 2.79 (s, 3H), 2.29 (s, 3H) ppm; **^{13}C NMR (101 MHz, Chloroform-*d*)** δ = 177.9, 176.0, 146.4, 132.1, 131.0, 129.4, 129.2, 129.1, 128.6, 126.5, 118.7, 112.7, 51.1, 43.7, 42.3, 39.8, 20.6 ppm.

5,7,9-trimethyl-2-phenyl-3a,4,5,9b-tetrahydro-1H-pyrrolo[3,4-c]quinoline-1,3(2H)-dione (3p)[12]

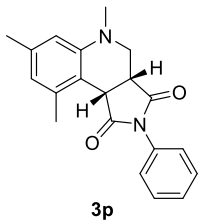
3p

Starting with 42.4 mg *N*-phenylmaleimide following the general procedure provided **3p** as a yellow solid (41.8 mg, 53%). Spectroscopic data was in accordance with the literature;[12] **^{1}H NMR (400 MHz, Chloroform-*d*)** δ = 7.44 – 7.37 (m, 2H), 7.36 – 7.29 (m, 1H), 7.28 – 7.22 (m, 2H), 6.71 – 6.36 (m, 2H), 4.45 (d, *J* = 9.8 Hz, 1H), 3.54 (dd, *J* = 11.3, 1.6 Hz, 1H), 3.48 (ddd, *J* = 9.8, 4.8, 1.7 Hz, 1H), 2.91 (dd, *J* = 11.3, 4.8 Hz, 1H), 2.76 (s, 3H), 2.53 (s, 3H), 2.27 (s, 3H) ppm; **^{13}C NMR (101 MHz, Chloroform-*d*)** δ = 178.7, 176.0, 150.1, 138.4, 137.9, 132.2, 129.1, 128.6, 126.6, 123.7, 116.6, 111.6, 52.7, 44.8, 40.0, 39.4, 21.7, 20.4 ppm.

8-bromo-5-methyl-2-phenyl-3a,4,5,9b-tetrahydro-1H-pyrrolo[3,4-c]quinoline-1,3(2H)-dione (3q)[3]

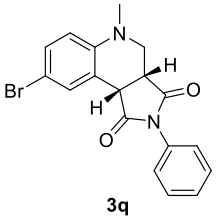
3q

Starting with 46.3 mg *N*-phenylmaleimide following the general provided **3q** as a yellow solid (69.3 mg, 70%). Spectroscopic data was in accordance with the literature;[3] **^{1}H NMR (400 MHz, Chloroform-*d*)** δ = 7.64 (m, 1H), 7.48 – 7.39 (m, 2H), 7.40 – 7.33 (m, 1H), 7.31 (m, 1H), 7.29 – 7.21 (m, 2H), 6.60 (dd, *J* = 8.8, 1.9 Hz, 1H), 4.10 (dd, *J* = 9.6, 1.8 Hz, 1H), 3.60 (m, 1H), 3.56 – 3.45 (m, 1H), 3.11 (m, 1H), 2.82 (d, *J* = 1.9 Hz, 3H) ppm; **^{13}C NMR (101 MHz, Chloroform-*d*)** δ = 177.4, 175.2, 147.6, 132.8, 131.9, 131.6, 129.2, 128.8, 126.4, 120.5, 114.4, 111.8, 50.5, 43.4, 41.9, 39.6 ppm.

5-methyl-2-phenyl-8-(pyridin-2-yl)-3a,4,5,9b-tetrahydro-1H-pyrrolo[3,4-c]quinoline-1,3(2H)-dione (3r)

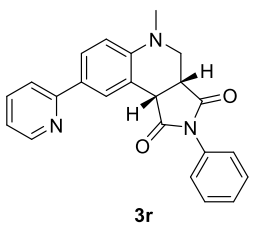
3r

Starting with 18.1 mg *N*-phenylmaleimide following the general procedure using irradiation time of 18 hours, provided **3r** as a yellow foam (26.4 mg, 68%). **m.p.** 183.5 – 184.6 °C; **^{1}H NMR (400 MHz, Chloroform-*d*)** δ = 8.16 (p, *J* = 1.0 Hz, 1H), 7.90 (dt, *J* = 8.7, 1.7 Hz, 1H), 7.69 (dt, *J* = 4.9, 1.4 Hz, 2H), 7.40 (ddd, *J* = 7.6, 6.6, 1.4 Hz, 2H), 7.37 – 7.29 (m, 1H), 7.26 (dt, *J* = 8.3, 1.4 Hz, 3H), 7.14 (qd, *J* = 4.6, 1.3 Hz, 1H), 6.82 (dd, *J* = 8.6, 1.3 Hz, 1H), 4.28 – 4.18 (m, 1H), 3.64 (ddd, *J* = 11.5, 2.9, 1.3 Hz, 1H), 3.56 (dddd, *J* = 8.7, 4.3, 2.8, 1.3 Hz, 1H), 3.18 (ddd, *J* = 11.5, 4.4, 1.3 Hz, 1H), 2.89 (s, 3H) ppm; **^{13}C NMR (101 MHz, Chloroform-*d*)** δ = 177.6, 175.8, 157.0, 149.4, 149.2, 137.0, 132.1, 130.6, 129.1, 129.0, 128.7, 127.5, 126.5, 121.5, 120.0, 118.5, 113.0, 50.4, 43.5, 42.2, 39.6 ppm; **FTIR ν̃** = 1704, 1568, 1469, 1370, 1152, 776, 761, 691, 576 cm^{-1}; **HRMS (ESI)** m/z calcd $C_{23}H_{19}N_3O_2$ $[M+H]^+$ 370.1556, found 370.1556.

8-acetyl-5-methyl-2-phenyl-3a,4,5,9b-tetrahydro-1H-pyrrolo[3,4-c]quinoline-1,3(2H)-dione (3s)[15]

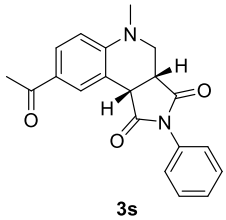

3s

Starting with 43.5 mg *N*-phenylmaleimide following the general procedure, **3s** was obtained as an off-white solid (39.5 mg, 47%). Spectroscopic data was in accordance with the literature;[15] **^{1}H NMR (400 MHz, Chloroform-*d*)** δ = 8.13 (dd, *J* = 2.2, 0.9 Hz, 1H), 7.85 (dd, *J* = 8.7, 2.1 Hz, 1H), 7.47 – 7.39 (m, 2H), 7.39 – 7.32 (m, 1H), 7.28 – 7.20 (m, 2H), 6.74 (d, *J* = 8.7 Hz, 1H), 4.19 (dd, *J* = 9.5, 0.9 Hz, 1H), 3.67 (dd, *J* = 11.7, 3.0 Hz, 1H), 3.58 (ddd, *J* = 9.6, 4.5, 2.9 Hz, 1H), 3.25 (dd, *J* = 11.7, 4.5 Hz, 1H), 2.93 (s, 3H), 2.54 (s, 3H) ppm; **^{13}C NMR (101 MHz, Chloroform-*d*)** δ = 196.5, 177.0, 175.4, 151.8, 131.9, 131.3, 129.6, 129.1, 128.7, 128.6, 126.3, 117.2, 112.1, 49.6, 43.0, 41.7, 39.5, 26.3 ppm.

Ethyl-5-methyl-1,3-dioxo-2-phenyl-2,3,3a,4,5,9b-hexahydro-1H-pyrrolo[3,4-c]quinoline-8-carboxylate (3t)

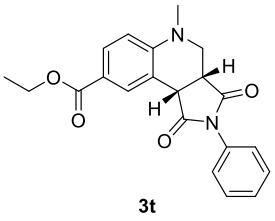

3t

Starting with 43.3 mg *N*-phenylmaleimide following the general procedure, the product was obtained as an off-white solid after silica column chromatography using 0-10% EtOAc in petroleum ether. Subsequent recrystallization from hot ethyl acetate afforded compound **3s** as a yellow crystalline solid (26.9 mg, 29%). **m.p.** 156.5 – 157.8 °C; **^{1}H NMR (400 MHz, Chloroform-*d*)** δ = 8.21 (d, *J* = 2.0 Hz, 1H), 7.91 (dd, *J* = 8.7, 2.0 Hz, 1H), 7.42 (dd, *J* = 8.3, 6.6 Hz, 2H), 7.38 – 7.32 (m, 1H), 7.25 (dd, *J* = 7.4, 1.6 Hz, 2H), 6.73 (d, *J* = 8.7 Hz, 1H), 4.42 – 4.27 (m, 2H), 4.19 (d, *J* = 9.4 Hz, 1H), 3.67 (dd, *J* = 11.6, 2.5 Hz, 1H), 3.62 – 3.51 (m, 1H), 3.22 (dd, *J* = 11.7, 4.2 Hz, 1H), 2.92 (s, 3H), 1.37 (t, *J* = 7.1 Hz, 3H) ppm; **^{13}C NMR (101 MHz, Chloroform-*d*)** δ = 177.2, 175.4, 166.5, 151.7, 131.9, 131.9, 130.7, 129.1, 128.7, 126.4, 121.3, 117.4, 112.1, 60.7, 49.9, 43.2, 41.8, 39.5, 14.6 ppm; **ATR-FTIR** ν = 1709, 1700, 1606, 1517, 1500, 1373, 1272, 1178, 1152, 759 cm^{-1}; **HRMS (ESI+)** m/z calcd $C_{21}H_{20}N_2O_4$ $[M+H]^+$ 365.1501, found 365.1501.

5-methyl-1,3-dioxo-2-phenyl-2,3,3a,4,5,9b-hexahydro-1H-pyrrolo[3,4-c]quinoline-8-carbonitrile (3u)

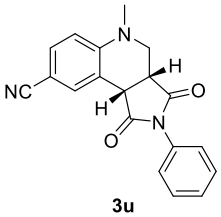

3u

Starting with 39.7 mg *N*-phenylmaleimide following the general provided **3u** as a yellow solid (18 mg, 25. **m.p.** 194.0 – 194.9 °C; **^{1}H NMR (400 MHz, Chloroform-*d*)** δ = 7.82 (dd, *J* = 2.1, 0.8 Hz, 1H), 7.51 – 7.41 (m, 3H), 7.41 – 7.35 (m, 1H), 7.29 – 7.20 (m, 2H), 6.74 (d, *J* = 8.6 Hz, 1H), 4.16 (dd, *J* = 9.6, 0.8 Hz, 1H), 3.69 (dd, *J* = 11.8, 3.1 Hz, 1H), 3.59 (ddd, *J* = 9.6, 4.5, 3.1 Hz, 1H), 3.29 (dd, *J* = 11.8, 4.5 Hz, 1H), 2.94 (s, 3H) ppm; **^{13}C NMR (101 MHz, Chloroform-*d*)** δ = 176.7, 174.8, 151.2, 134.2, 133.1, 131.7, 129.3, 128.9, 126.3, 119.6, 118.3, 112.8, 101.8, 49.4, 42.8, 41.4, 39.5 ppm; **FTIR ν** = 3066, 2931, 2217, 1710, 1604, 1514, 1497, 1374 cm^{-1}; **HRMS (ESI)** m/z calcd $C_{19}H_{15}N_3O_2$ $[M+H]^+$ 318.1243, found 318.1253.

5,6-dimethyl-2-phenyl-3a,4,5,9b-tetrahydro-1H-pyrrolo[3,4-c]quinoline-1,3(2H)-dione (3v)[11]

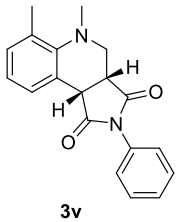

3v

Yellow oil (32.9 mg, 43%); Spectroscopic data was in accordance with the literature;[11] **^{1}H NMR (400 MHz, Chloroform-*d*)** δ = 7.57 (ddt, *J* = 7.6, 1.6, 0.7 Hz, 1H), 7.49 – 7.41 (m, 2H), 7.41 – 7.34 (m, 1H), 7.29 – 7.23 (m, 2H), 7.14 (ddt, *J* = 7.4, 1.6, 0.7 Hz, 1H), 7.06 (t, *J* = 7.5 Hz, 1H), 4.16 (d, *J* = 8.9 Hz, 1H), 3.60 – 3.45 (m, 2H), 3.45 – 3.32 (m, 1H), 2.74 (s, 3H), 2.30 (s, 3H) ppm; **^{13}C NMR (101 MHz, Chloroform-*d*)** δ = 177.9, 175.9, 146.8, 132.9, 132.1, 130.6, 129.3, 129.1, 128.8, 128.6, 126.4, 124.0, 123.1, 51.5, 42.2, 41.7, 39.0, 17.8 ppm.

8-ethynyl-5-methyl-2-phenyl-3a,4,5,9b-tetrahydro-1H-pyrrolo[3,4-c]quinoline-1,3(2H)-dione (3w)[15]

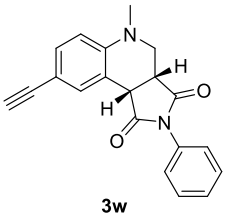

3w

Starting with 41.3 mg *N*-phenylmaleimide following the general procedure provided **3w** as a yellow solid (19 mg, 25%). Spectroscopic data was in accordance with the literature;[15] **^{1}H NMR (400 MHz, Chloroform-*d*)** δ = 7.68 (dd, *J* = 2.0, 0.9 Hz, 1H), 7.49 – 7.40 (m, 2H), 7.40 – 7.31 (m, 2H), 7.30 – 7.21 (m, 3H), 6.67 (d, *J* = 8.5 Hz, 1H), 4.12 (dt, *J* = 9.6, 0.6 Hz, 1H), 3.63 (dd, *J* = 11.6, 2.8 Hz, 1H), 3.54 (ddd, *J* = 9.6, 4.4, 2.8 Hz, 1H), 3.17 (dd, *J* = 11.6, 4.4 Hz, 1H), 3.00 (s, 1H), 2.86 (s, 3H) ppm**; ^{13}C NMR (101 MHz, Chloroform-*d*)** δ = 177.4, 175.4, 148.7, 134.2, 132.8, 132.0, 129.2, 128.7, 126.4, 118.2, 112.8, 112.6, 83.9, 76.1, 50.2, 43.3, 41.8, 39.5 ppm.

5-benzyl-2-phenyl-3a,4,5,9b-tetrahydro-1H-pyrrolo[3,4-c]quinoline-1,3(2H)-dione (3x)[16]

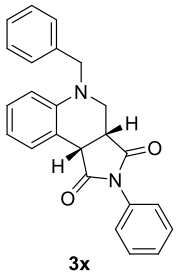

3x

Starting with 40.5 mg *N*-phenylmaleimide following the general procedure provided **3u** as a yellow oil (36.6 mg, 42%). Spectroscopic data was in accordance with the literature;[16] **^{1}H NMR (400 MHz, Chloroform-*d*)** δ = 7.60 – 7.52 (m, 1H), 7.47 (dd, *J* = 8.3, 6.8 Hz, 2H), 7.43 – 7.36 (m, 1H), 7.34 – 7.22 (m, 7H), 7.19 – 7.11 (m, 1H), 6.90 (td, *J* = 7.5, 1.1 Hz, 1H), 6.76 (d, *J* = 1.0 Hz, 1H), 4.55 – 4.25 (m, 2H), 4.19 (d, *J* = 9.5 Hz, 1H), 3.70 (dd, *J* = 11.7, 2.9 Hz, 1H), 3.55 (ddd, *J* = 9.5, 4.4, 2.8 Hz, 1H), 3.28 (dd, *J* = 11.7, 4.4 Hz, 1H) ppm**; ^{13}C NMR (101 MHz, Chloroform-*d*)** δ = 177.6, 175.9, 147.6, 137.8, 132.2, 130.7, 130.3, 129.2, 128.7, 128.7, 128.6, 127.5, 127.4, 126.5, 119.9, 119.0, 113.6, 55.5, 49.2, 44.3, 42.6 ppm.

5-allyl-2-phenyl-3a,4,5,9b-tetrahydro-1H-pyrrolo[3,4-c]quinoline-1,3(2H)-dione (3y)[16]

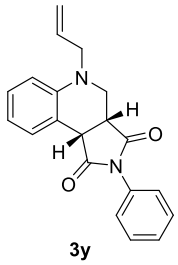

3y

Starting with 41.6 mg *N*-phenylmaleimide following the general procedure provided **3v** as a yellow oil (44.1 mg, 58%). Spectroscopic data was in accordance with the literature;[16] **^{1}H NMR (400 MHz, Chloroform-*d*)** δ = 7.54 (ddd, *J* = 7.6, 1.7, 0.8 Hz, 1H), 7.47 – 7.40 (m, 2H), 7.40 – 7.33 (m, 1H), 7.30 – 7.23 (m, 2H), 7.24 – 7.16 (m, 1H), 6.89 (td, *J* = 7.5, 1.1 Hz, 1H), 6.78 (dd, *J* = 8.3, 1.1 Hz, 1H), 5.87 (ddt, *J* = 17.3, 10.3, 5.8 Hz, 1H), 5.34 – 5.21 (m, 2H), 4.15 (d, *J* = 9.5 Hz, 1H), 3.96 – 3.74 (m, 2H), 3.68 (dd, *J* = 11.8, 2.9 Hz, 1H), 3.54 (ddd, *J* = 9.5, 4.3, 2.8 Hz, 1H), 3.15 (dd, *J* = 11.8, 4.3 Hz, 1H) ppm; **^{13}C NMR (101 MHz, Chloroform-*d*)** δ = 177.7, 175.9, 147.4, 133.3, 132.1, 130.7, 129.1, 128.6, 128.6, 126.4, 119.6, 118.9, 118.3, 113.3, 53.6, 47.8, 44.1, 42.5 ppm.

1-methyl-1,2,3,4-tetrahydroquinoline-3,4-dicarbonitrile (5)

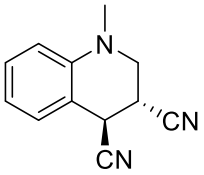

5

Starting with fumaronitrile (18.7 mg) following the general procedure, **5** was afforded as a white solid (8.9 mg, 19%). **^{1}H NMR (400 MHz, Chloroform-*d*)** δ 7.33 – 7.14 (m, 3H), 6.81 (td, *J* = 7.5, 1.1 Hz, 1H), 6.72 (dd, *J* = 8.3, 1.0 Hz, 1H), 4.25 (d, *J* = 5.7 Hz, 1H), 3.69 (dd, *J* = 12.0, 3.1 Hz, 1H), 3.59 – 3.41 (m, 2H), 3.01 (s, 3H); **^{13}C NMR (101 MHz, Chloroform-*d*)** δ 144.4, 130.7, 129.5, 118.5, 118.2, 117.4, 112.8, 111.6, 50.1, 39.2, 32.9, 28.8.

1-methyl-3-phenyl-2,3-dihydroquinoline-4,4(1H)-dicarbonitrile (6)[13]

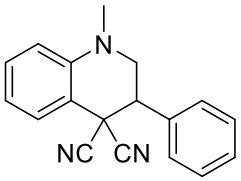

6

Starting with benzylidenemalonitrile (34 mg), **6** was afforded as a white solid (9.9 mg, 17%). Spectroscopic data was in accordance with the literature;[13] **^{1}H NMR (400 MHz, Chloroform-*d*)** δ 7.91 (ddd, *J* = 8.5, 1.3, 0.6 Hz, 1H), 7.51 – 7.42 (m, 5H), 7.39 – 7.32 (m, 1H), 6.82 (ddd, *J* = 7.8, 7.3, 1.1 Hz, 1H), 6.75 (dd, *J* = 8.4, 1.1 Hz, 1H), 3.97 (dd, *J* = 12.4, 11.4 Hz, 1H), 3.61 (dd, *J* = 11.4, 3.9 Hz, 1H), 3.52 (dd, *J* = 12.4, 3.9 Hz, 1H), 3.03 (s, 3H); **^{13}C NMR (101 MHz, Chloroform-*d*)** δ 144.1, 134.9, 131.9, 129.6, 129.3, 129.0, 128.6, 117.8, 115.3, 114.2, 112.9, 112.7, 51.5, 45.7, 42.6, 38.9.

diethyl (3R,4R)-1-methyl-1,2,3,4-tetrahydroquinoline-3,4-dicarboxylate (7)[17]

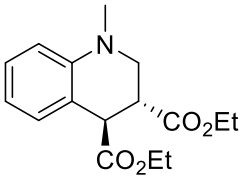

5

Starting with diethyl fumarate (25.8 mg), following the general procedure, **7** was obtained as a colorless oil (13 mg, 29%). spectroscopic data was in accordance with the literature;[17] **^{1}H NMR (400 MHz, Chloroform-*d*)** δ = 7.22 (dt, *J* = 7.7, 1.4 Hz, 1H), 7.14 (dddd, *J* = 8.1, 7.3, 1.7, 0.7 Hz, 1H), 6.81 – 6.58 (m, 2H), 4.30 – 4.07 (m, 5H), 3.59 – 3.49 (m, 1H), 3.46 – 3.34 (m, 2H), 2.92 (s, 3H), 1.29 (t, *J* = 7.1 Hz, 3H), 1.23 (t, *J* = 7.1 Hz, 3H) ppm; **^{13}C NMR (101 MHz, Chloroform-*d*)** δ = 173.3, 172.2, 145.8, 129.2, 128.5, 117.9, 117.3, 112.0, 61.4, 61.2, 50.4, 44.8, 41.3, 39.5, 14.3 (2C) ppm.

2.1 References

(1) Kandukuri, S. R.; Bahamonde, A.; Chatterjee, I.; Jurberg, I. D.; Escudero-Adán, E. C.; Melchiorre, P. X-Ray Characterization of an Electron Donor–Acceptor Complex That Drives the Photochemical Alkylation of Indoles. *Angew. Chemie Int. Ed.* **2015**, *54* (5), 1485–1489. https://doi.org/10.1002/anie.201409529.

(2) Hansch, C.; Leo, A.; Taft, R. W. A Survey of Hammett Substituent Constants and Resonance and Field Parameters. *Chem. Rev.* **1991**, *91* (2), 165–195. https://doi.org/10.1021/cr00002a004.

(3) Li, J.; Bao, W.; Zhang, Y.; Rao, Y. Cercosporin-Photocatalyzed Sp3 (C–H) Activation for the Synthesis of Pyrrolo[3{,}4-c]Quinolones. *Org. Biomol. Chem.* **2019**, *17* (40), 8958–8962. https://doi.org/10.1039/C9OB01946D.

(4) Xu, W.-L.; Tang, L.; Ge, C.-Y.; Chen, J.; Zhou, L. Synthesis of Tetrahydroisoindolinones via a Metal-Free Dehydrogenative Diels-Alder Reaction. *Adv. Synth. \& Catal.* **2019**, *361* (10), 2268–2273. https://doi.org/https://doi.org/10.1002/adsc.201801436.

(5) Jiang, S.; Tala, S. R.; Lu, H.; Zou, P.; Avan, I.; Ibrahim, T. S.; Abo-Dya, N. E.; Abdelmajeid, A.; Debnath, A. K.; Katritzky, A. R. Design, Synthesis, and Biological Activity of a Novel Series of 2,5-Disubstituted Furans/Pyrroles as HIV-1 Fusion Inhibitors Targeting Gp41. *Bioorg. Med. Chem. Lett.* **2011**, *21* (22), 6895–6898. https://doi.org/https://doi.org/10.1016/j.bmcl.2011.08.081.

(6) Lu, C.-D.; Chen, Z.-Y.; Liu, H.; Hu, W.-H.; Mi, A.-Q.; Doyle, M. P. A Facile Three-Component One-Pot Synthesis of Structurally Constrained Tetrahydrofurans That Are t-RNA Synthetase Inhibitor Analogues. *J. Org. Chem.* **2004**, *69* (14), 4856–4859. https://doi.org/10.1021/jo0497508.

(7) Matuszak, N.; Muccioli, G. G.; Labar, G.; Lambert, D. M. Synthesis and in Vitro Evaluation of N-Substituted Maleimide Derivatives as Selective Monoglyceride Lipase Inhibitors. *J. Med. Chem.* **2009**, *52* (23), 7410–7420. https://doi.org/10.1021/jm900461w.

(8) Samgina, T. Y.; Gorshkov, V. A.; Vorontsov, E. A.; Bagrov, V. V; Nifant'ev, I. E.; Lebedev, A. T. New Cysteine-Modifying Reagents: Efficiency of Derivatization and Influence on the Signals of the Protonated Molecules of Disulfide-Containing Peptides in Matrix-Assisted Laser Desorption/Ionization Mass Spectrometry. *J. Anal. Chem.* **2010**, *65* (13), 1320–1327. https://doi.org/10.1134/S1061934810130034.

(9) Salewska, N.; Boros-Majewska, J.; Łącka, I.; Chylińska, K.; Sabisz, M.; Milewski, S.; Milewska, M. J. Chemical Reactivity and Antimicrobial Activity of N-Substituted Maleimides. *J. Enzyme Inhib. Med. Chem.* **2012**, *27* (1), 117–124. https://doi.org/10.3109/14756366.2011.580455.

(10) Hsu, C.-W.; Sundén, H. α-Aminoalkyl Radical Addition to Maleimides via Electron Donor–Acceptor Complexes. *Org. Lett.* **2018**, *20* (7), 2051–2054. https://doi.org/10.1021/acs.orglett.8b00597.

(11) Tang, J.; Grampp, G.; Liu, Y.; Wang, B.-X.; Tao, F.-F.; Wang, L.-J.; Liang, X.-Z.; Xiao, H.-Q.; Shen, Y.-M. Visible Light Mediated Cyclization of Tertiary Anilines with Maleimides Using Nickel(II) Oxide Surface-Modified Titanium Dioxide Catalyst. *J. Org. Chem.* **2015**, *80* (5), 2724–2732. https://doi.org/10.1021/jo502901h.

(12) Yang, X.-L.; Guo, J.-D.; Lei, T.; Chen, B.; Tung, C.-H.; Wu, L.-Z. Oxidative Cyclization Synthesis of Tetrahydroquinolines and Reductive Hydrogenation of Maleimides under Redox-Neutral Conditions. *Org. Lett.* **2018**, *20* (10), 2916–2920. https://doi.org/10.1021/acs.orglett.8b00977.

(13) Nicholls, T. P.; Constable, G. E.; Robertson, J. C.; Gardiner, M. G.; Bissember, A. C. Bronsted Acid Cocatalysis in Copper(I)-Photocatalyzed α-Amino C-H Bond Functionalization. *ACS Catal.* **2016**, *6* (1), 451–457. https://doi.org/10.1021/acscatal.5b02014.

(14) Huang, P.; Wang, P.; Wang, S.; Tang, S.; Lei, A. Electrochemical Oxidative [4 + 2] Annulation of Tertiary Anilines and Alkenes for the Synthesis of Tetrahydroquinolines. *Green Chem.* **2018**, *20* (21), 4870–4874. https://doi.org/10.1039/c8gc02463d.

(15) Sharma, K.; Das, B.; Gogoi, P. Synthesis of Pyrrolo[3,4-c]Quinoline-1,3-Diones: A Sequential Oxidative Annulation Followed by Dehydrogenation and N-Demethylation Strategy. *New J. Chem.* **2018**, *42* (23), 18894–18905. https://doi.org/10.1039/c8nj04443k.

(16) Perumal, G.; Kandasamy, M.; Ganesan, B.; Govindan, K.; Sathya, H.; Hung, M.-Y.; Chandru Senadi, G.; Wu, Y.-C.; Lin, W.-Y. Visible Light-Induced N-Methyl Activation of Unsymmetric Tertiary Amines. *Tetrahedron* **2021**, *80*, 131891. https://doi.org/https://doi.org/10.1016/j.tet.2020.131891.

(17) Song, Z.; Antonchick, A. P. Catching α-Aminoalkyl Radicals: Cyclization between Tertiary Alkylanilines and Alkenes. *Tetrahedron* **2016**, *72* (48), 7715–7721. https://doi.org/https://doi.org/10.1016/j.tet.2016.04.052.

3.1 NMR spectra

Starting material

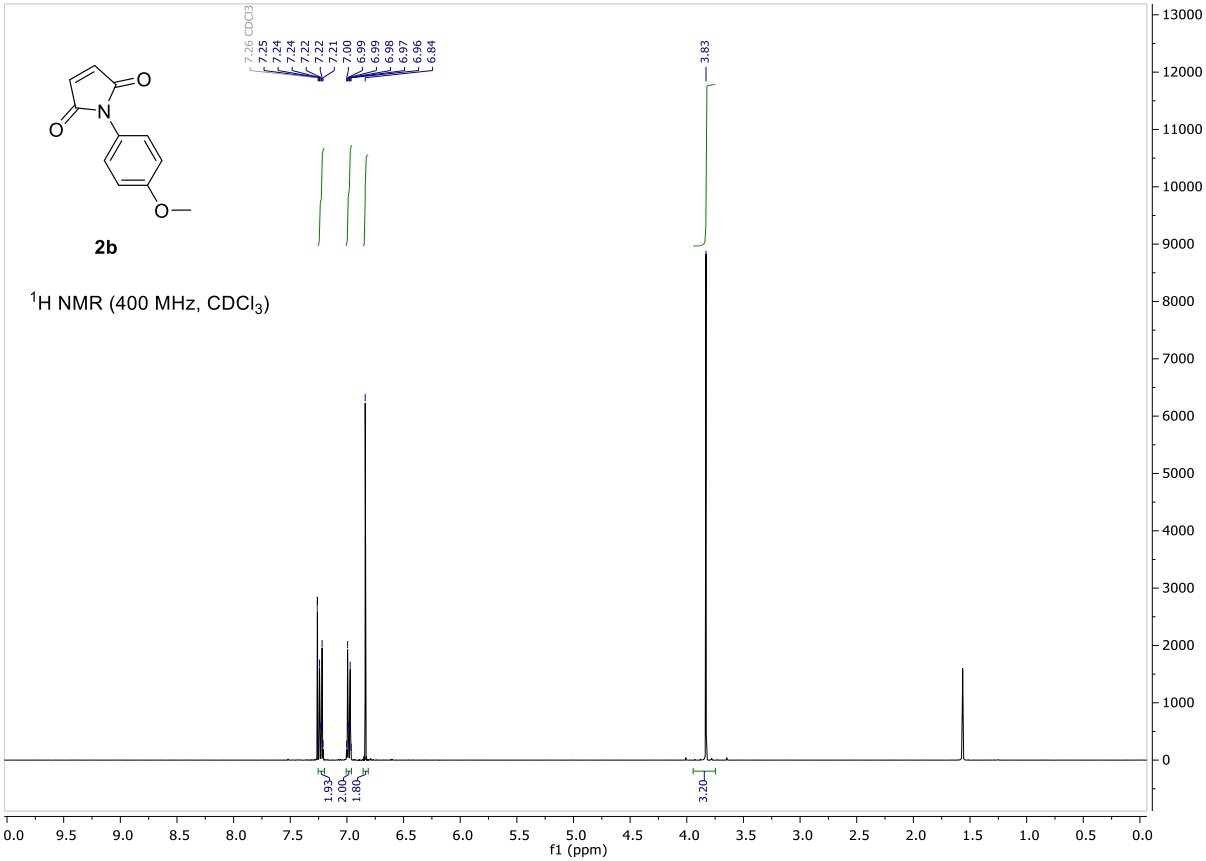

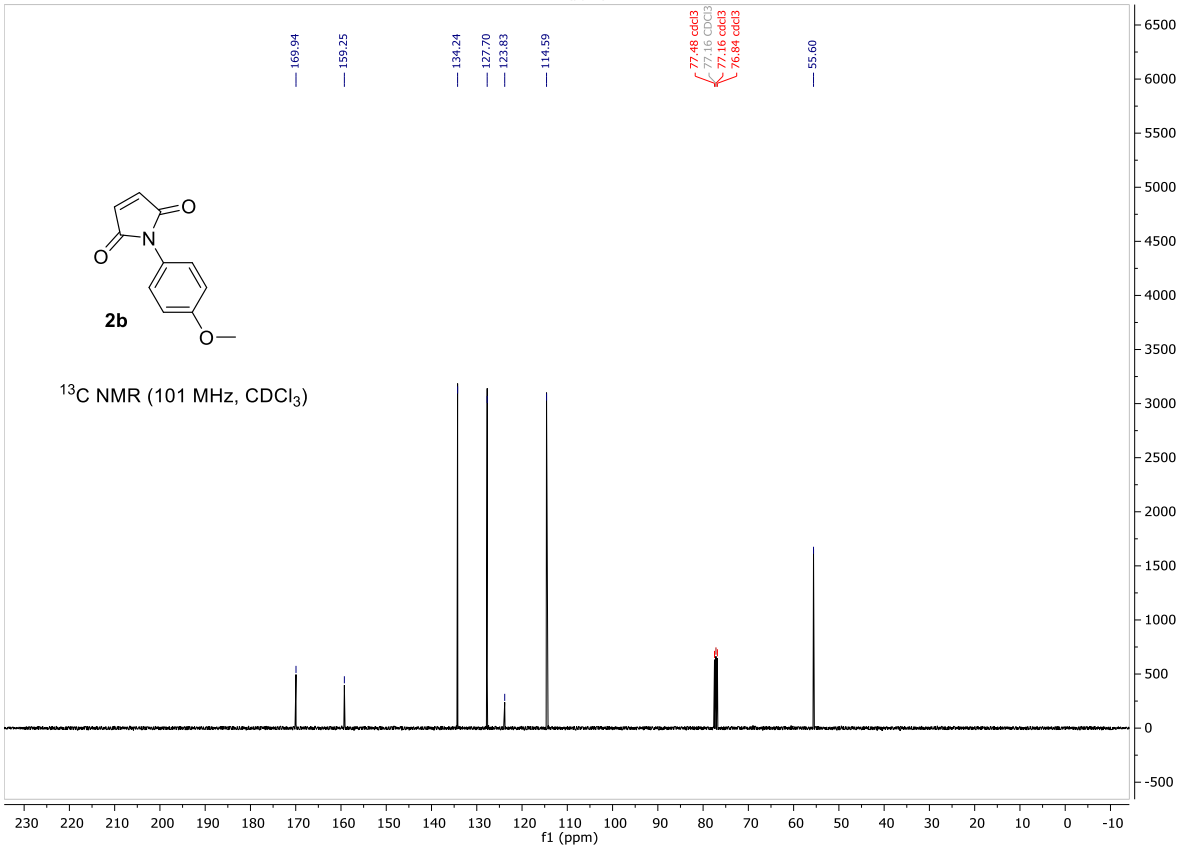

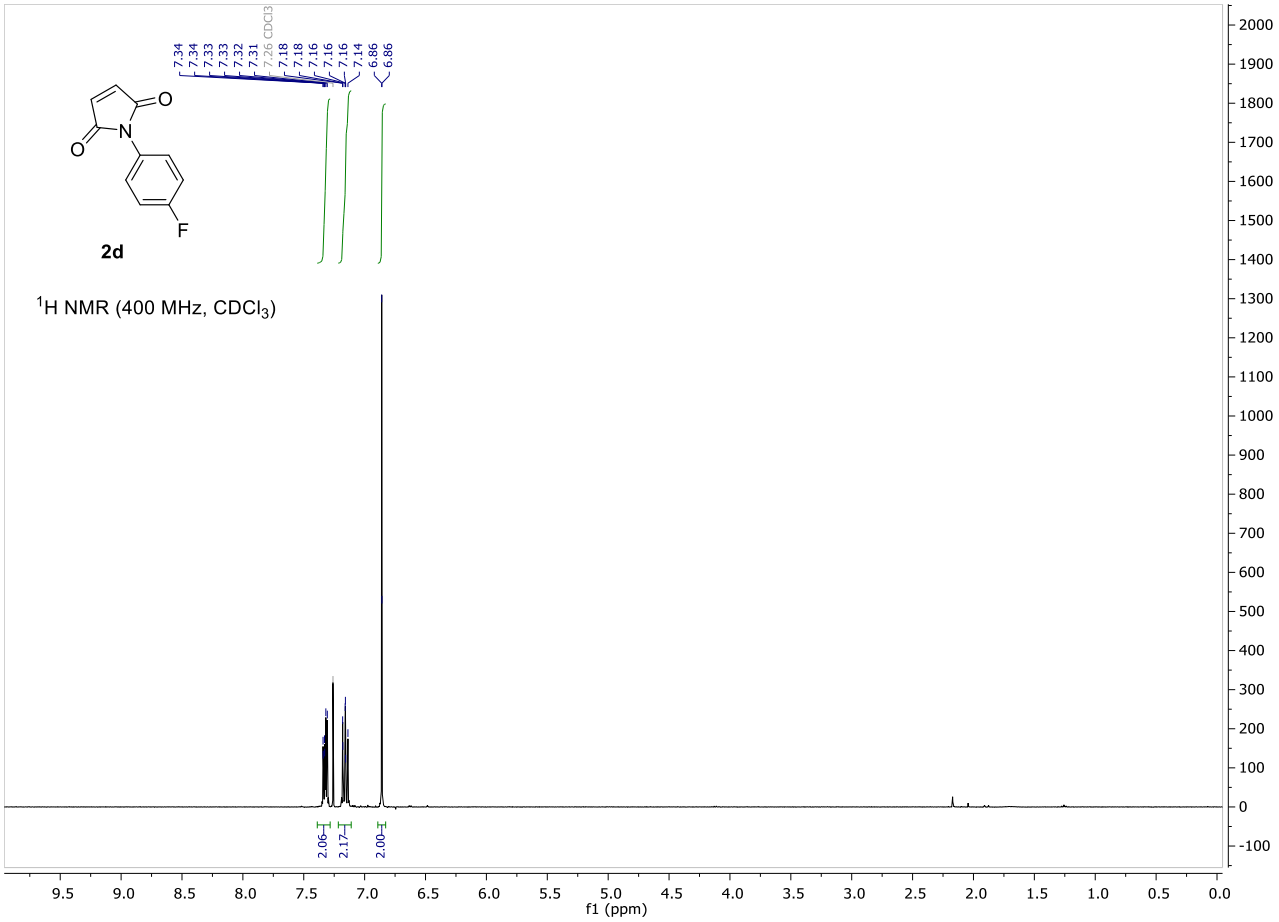
7.34
7.34
7.33
7.33
7.32
7.31
7.26 CDCl3
7.18
7.18
7.16
7.16
7.16
7.14
6.86
6.86
O
O
N
F
2d
1H NMR (400 MHz, CDCl3)
2.06
2.17
2.00
f1 (ppm)

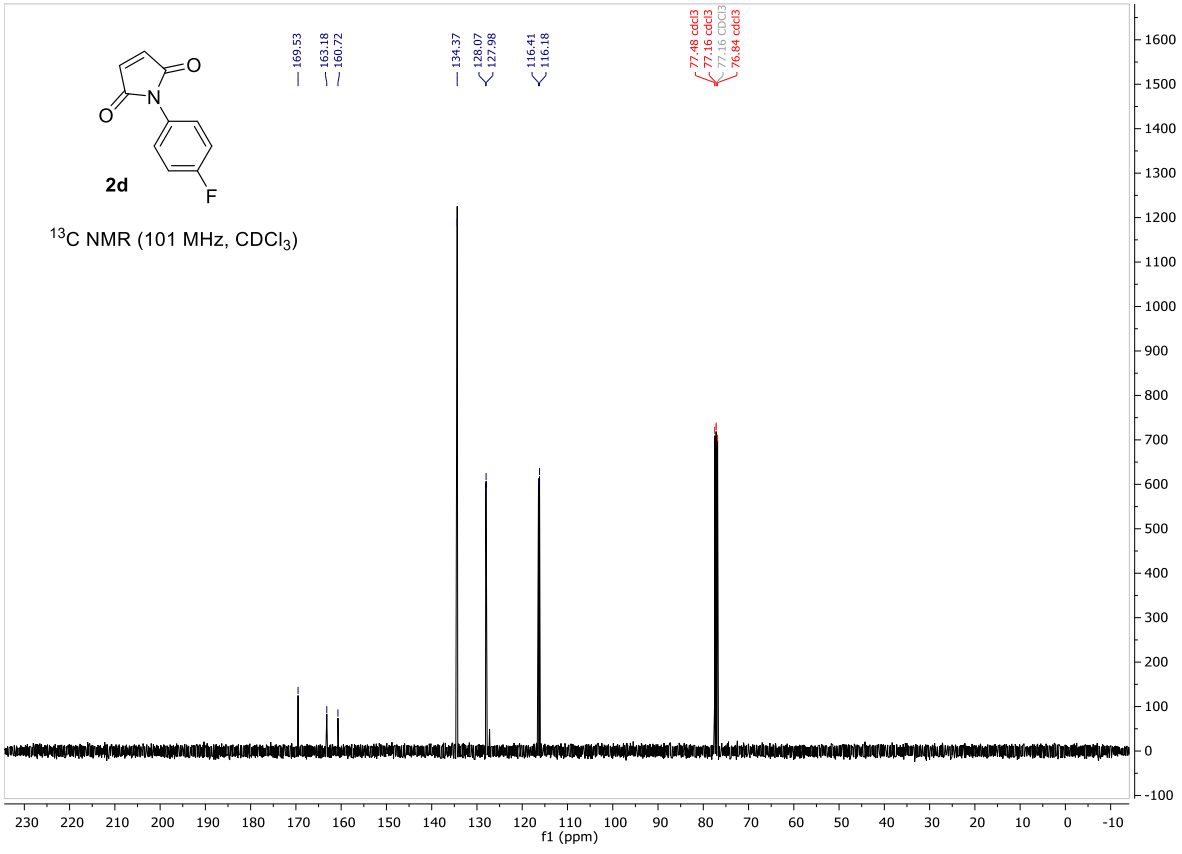
169.53
163.18
160.72
134.37
128.07
127.98
116.41
116.18
77.48 cdcl3
77.16 cdcl3
76.84 cdcl3
O
O
N
F
2d
13C NMR (101 MHz, CDCl3)
f1 (ppm)

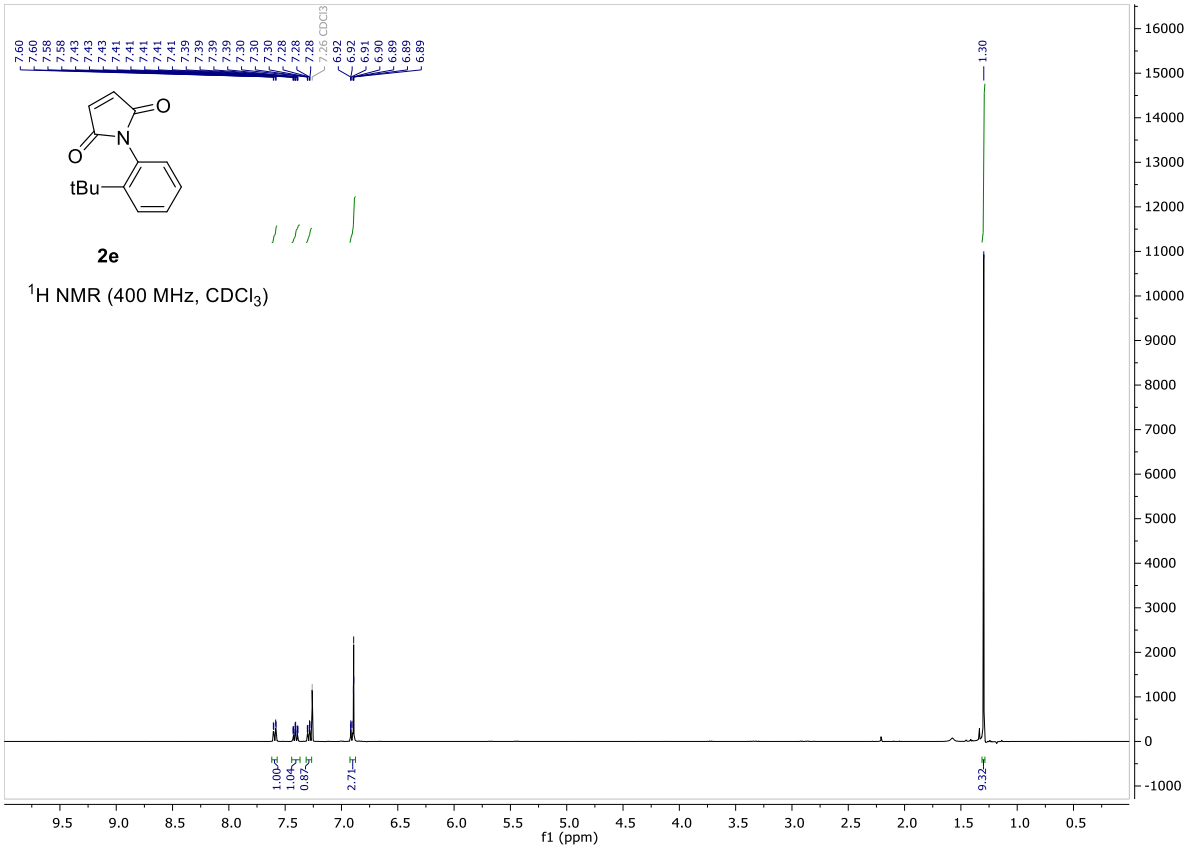

2e

^{1}H NMR (400 MHz, $CDCl_3$)

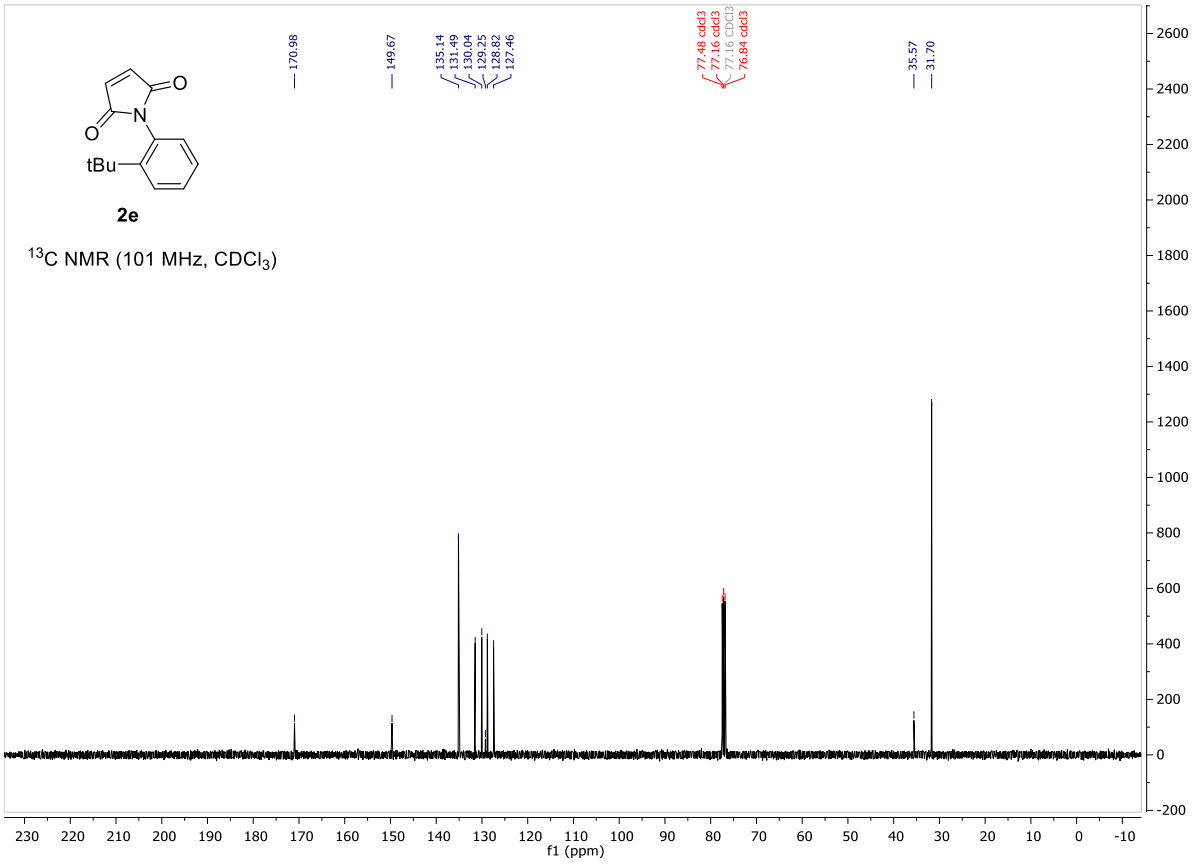

2e

^{13}C NMR (101 MHz, $CDCl_3$)

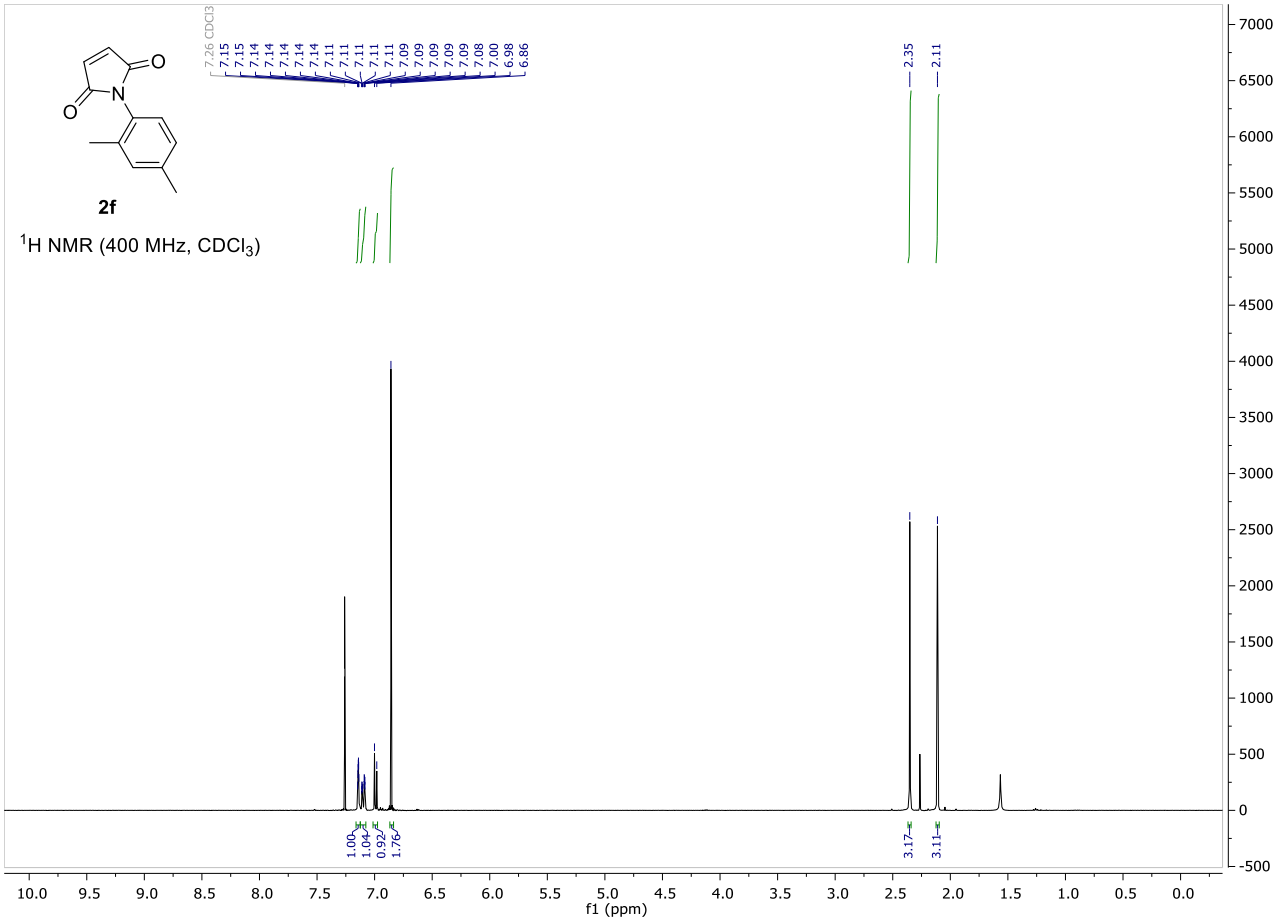
2f
^{1}H NMR (400 MHz, $CDCl_3$)
f1 (ppm)

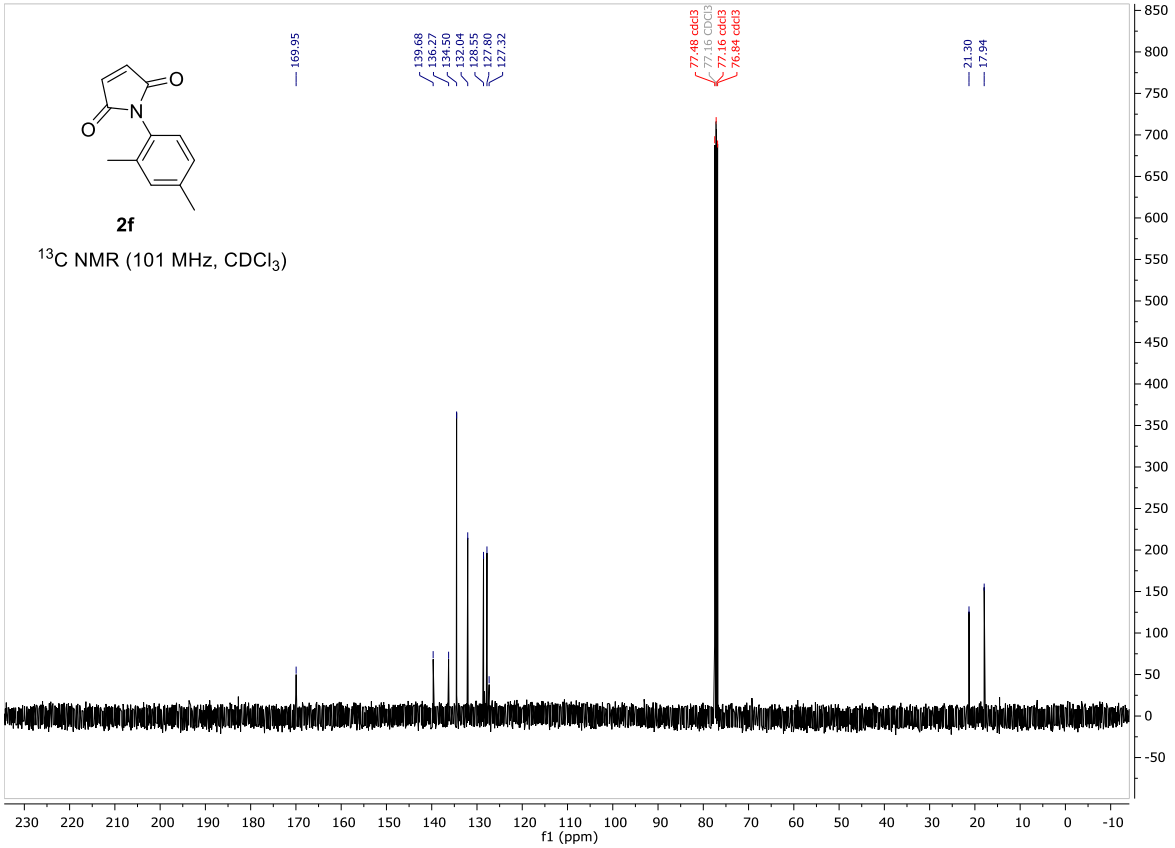
2f
^{13}C NMR (101 MHz, $CDCl_3$)
f1 (ppm)

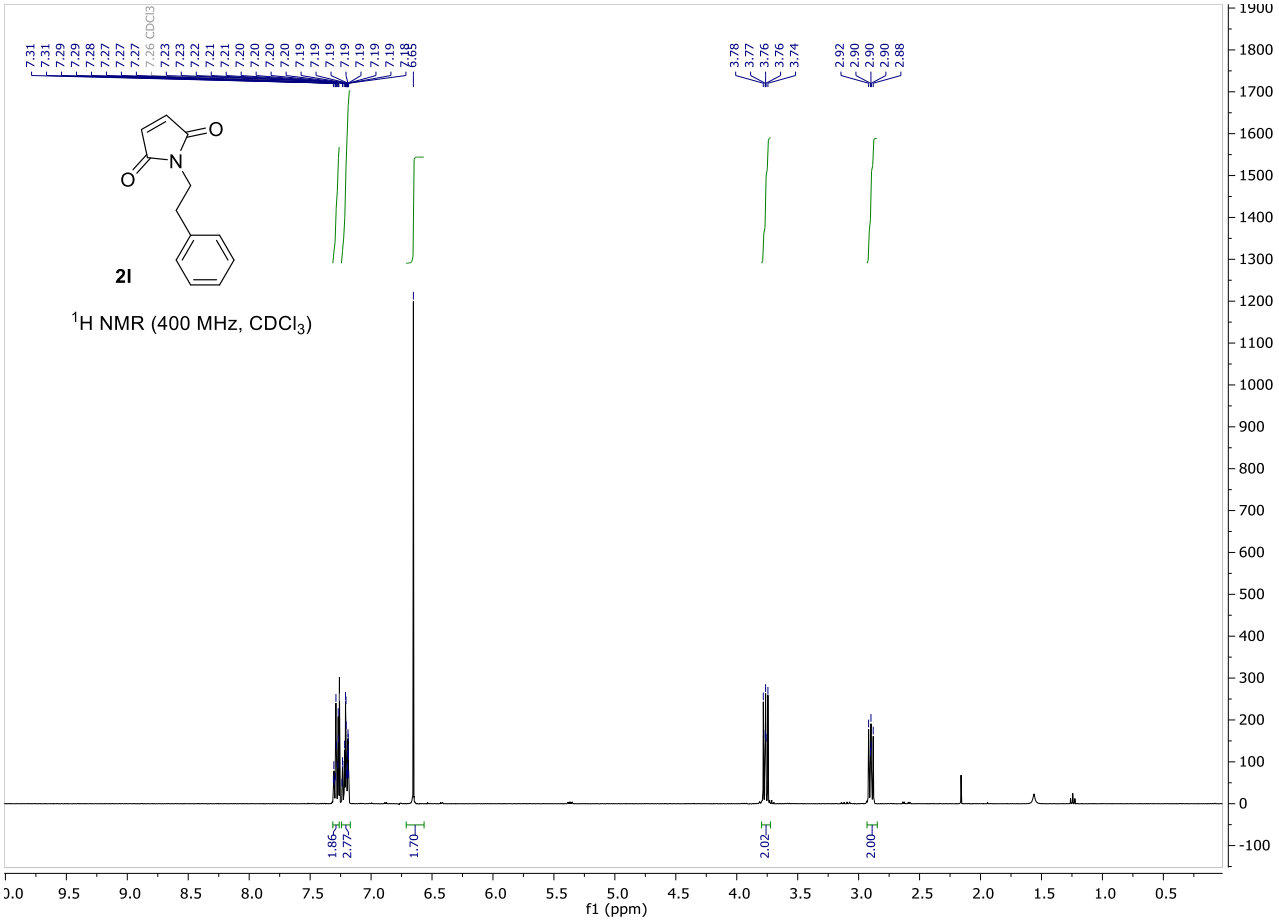
2l
^{1}H NMR (400 MHz, $CDCl_3$)
f1 (ppm)

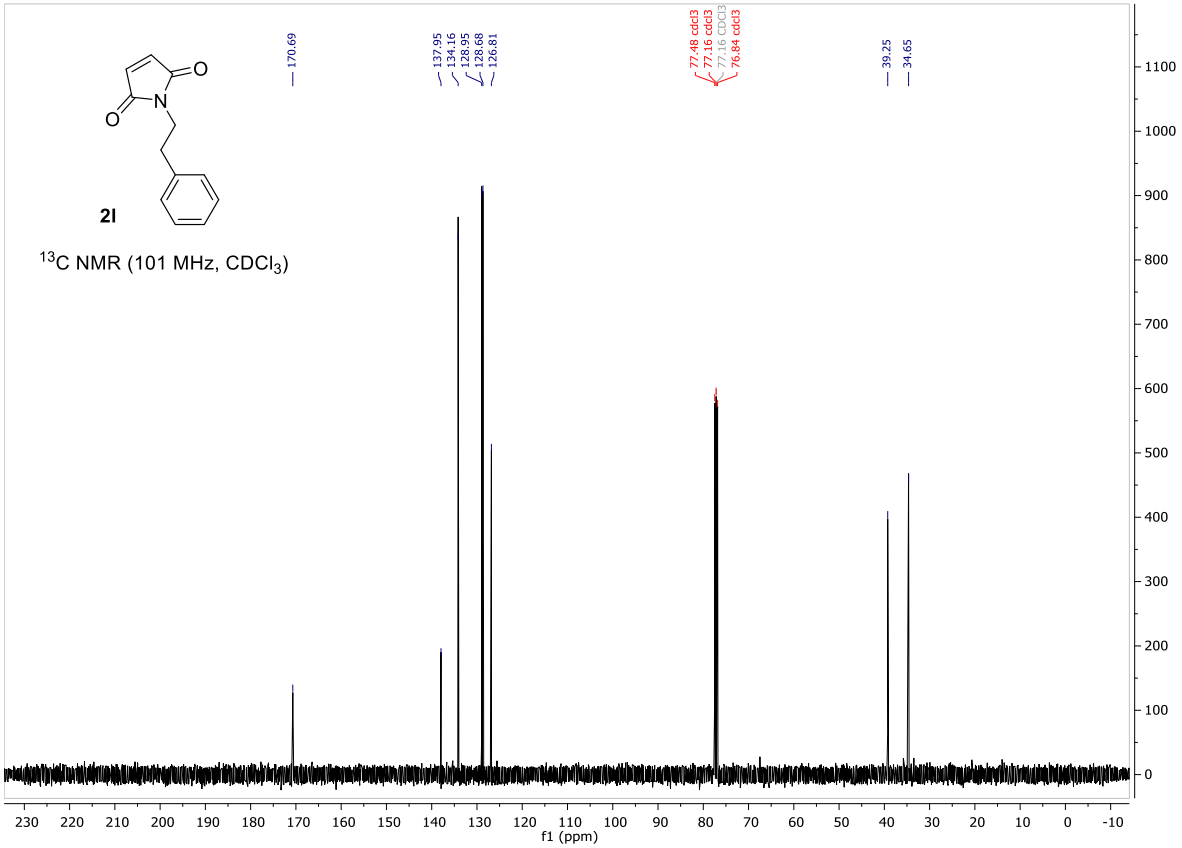
2l
^{13}C NMR (101 MHz, $CDCl_3$)
f1 (ppm)

Tetrahydriquionoline products

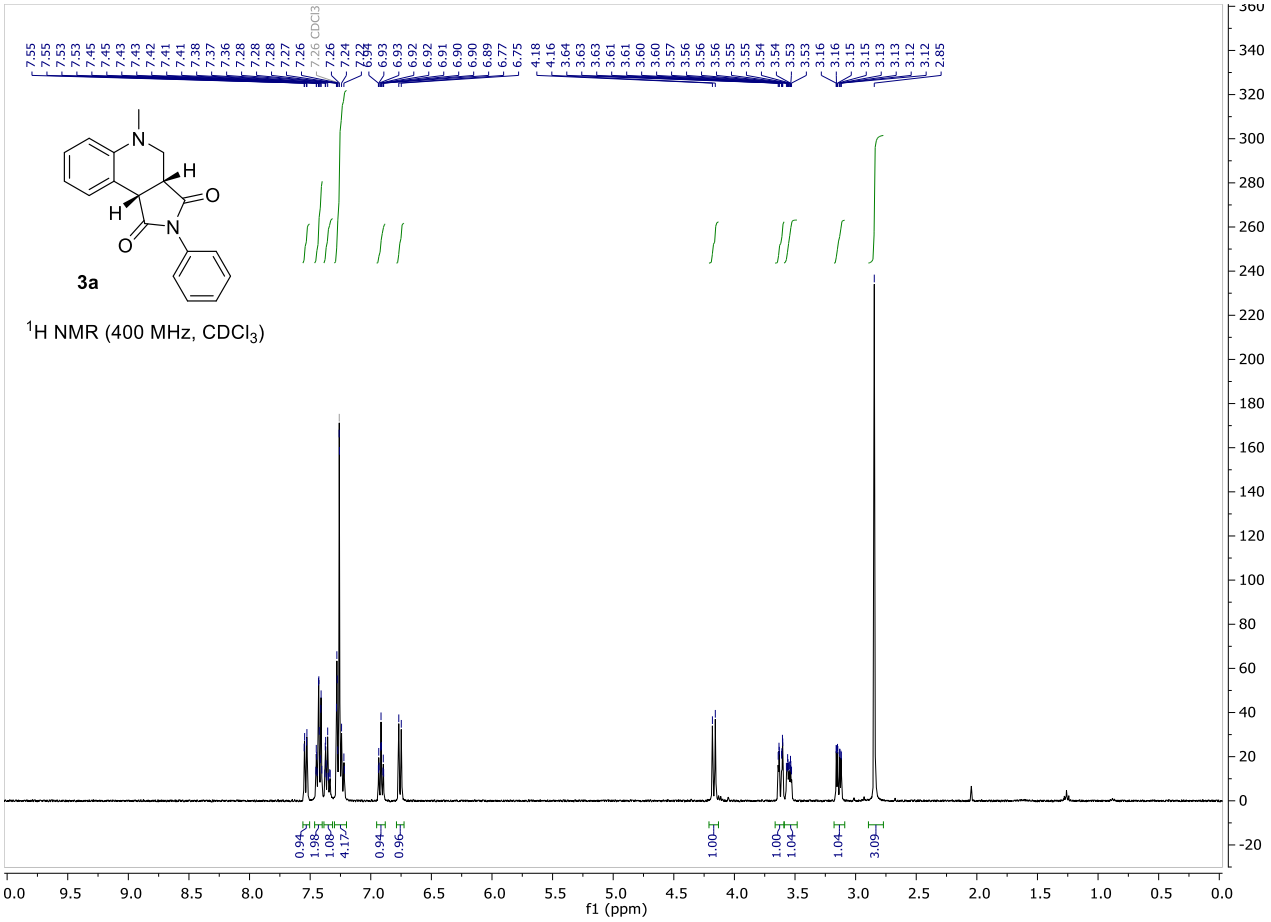

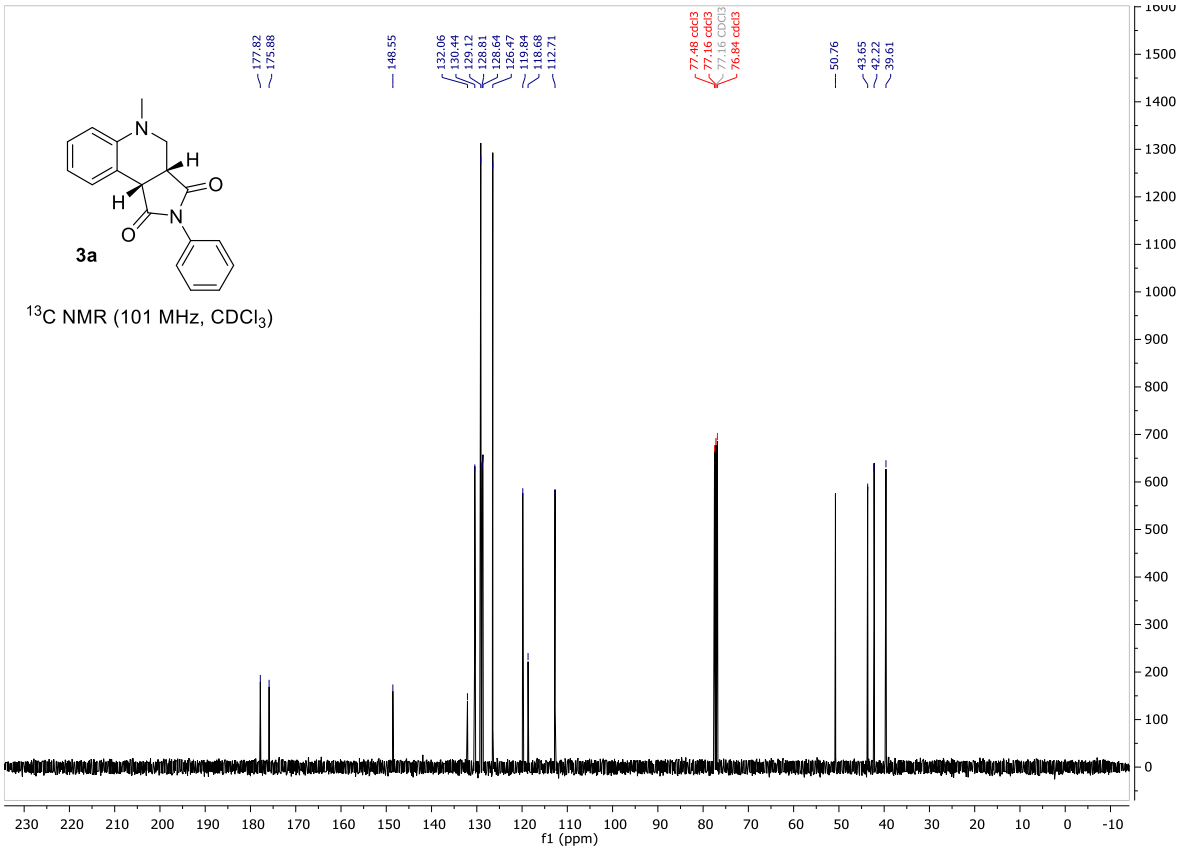

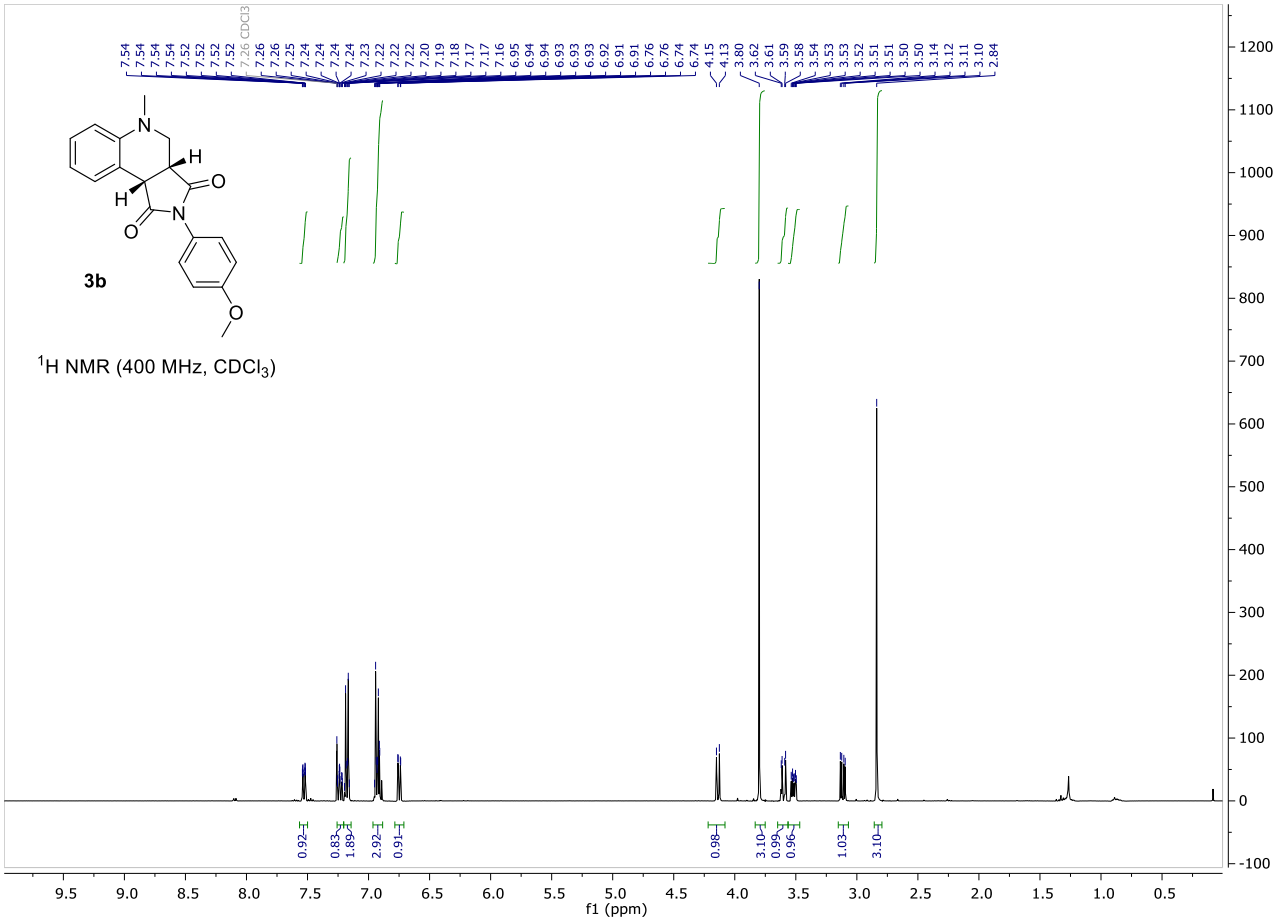
3b
^{1}H NMR (400 MHz, $CDCl_3$)
f1 (ppm)

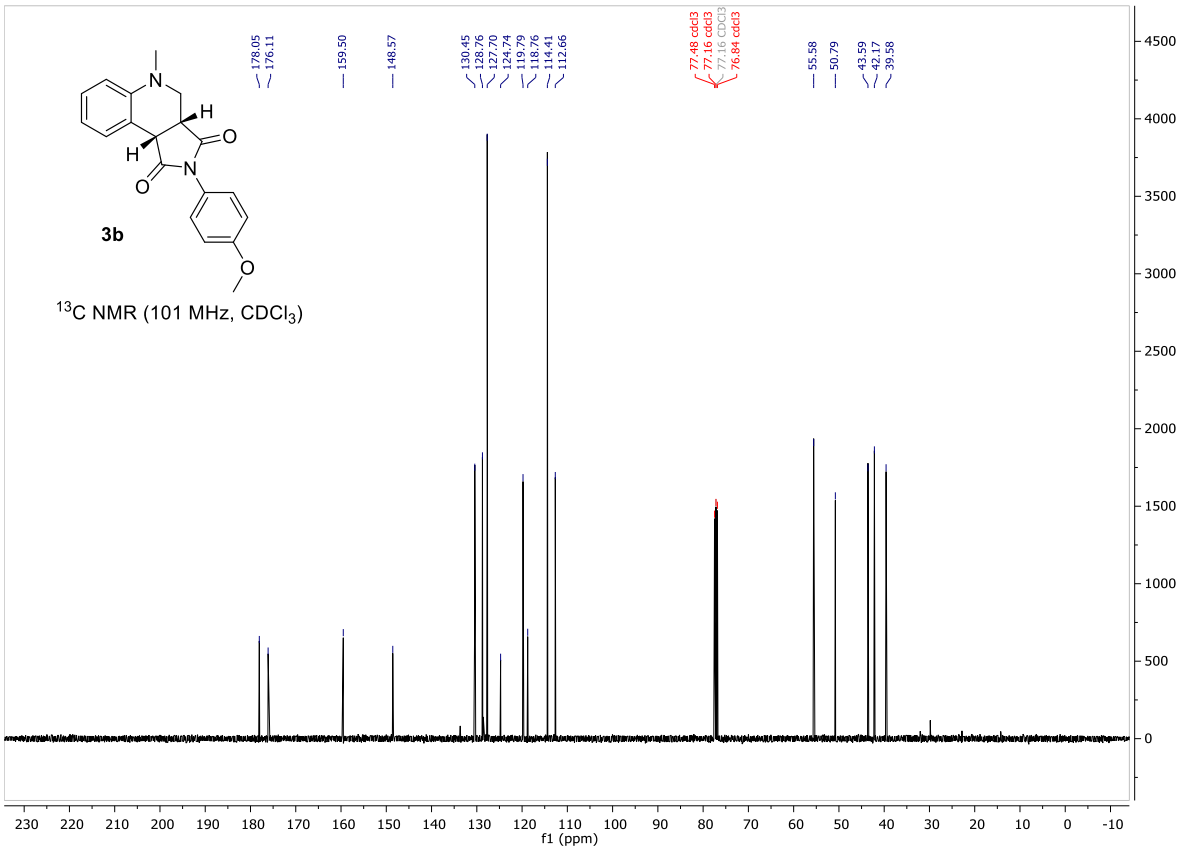
3b
^{13}C NMR (101 MHz, $CDCl_3$)
f1 (ppm)

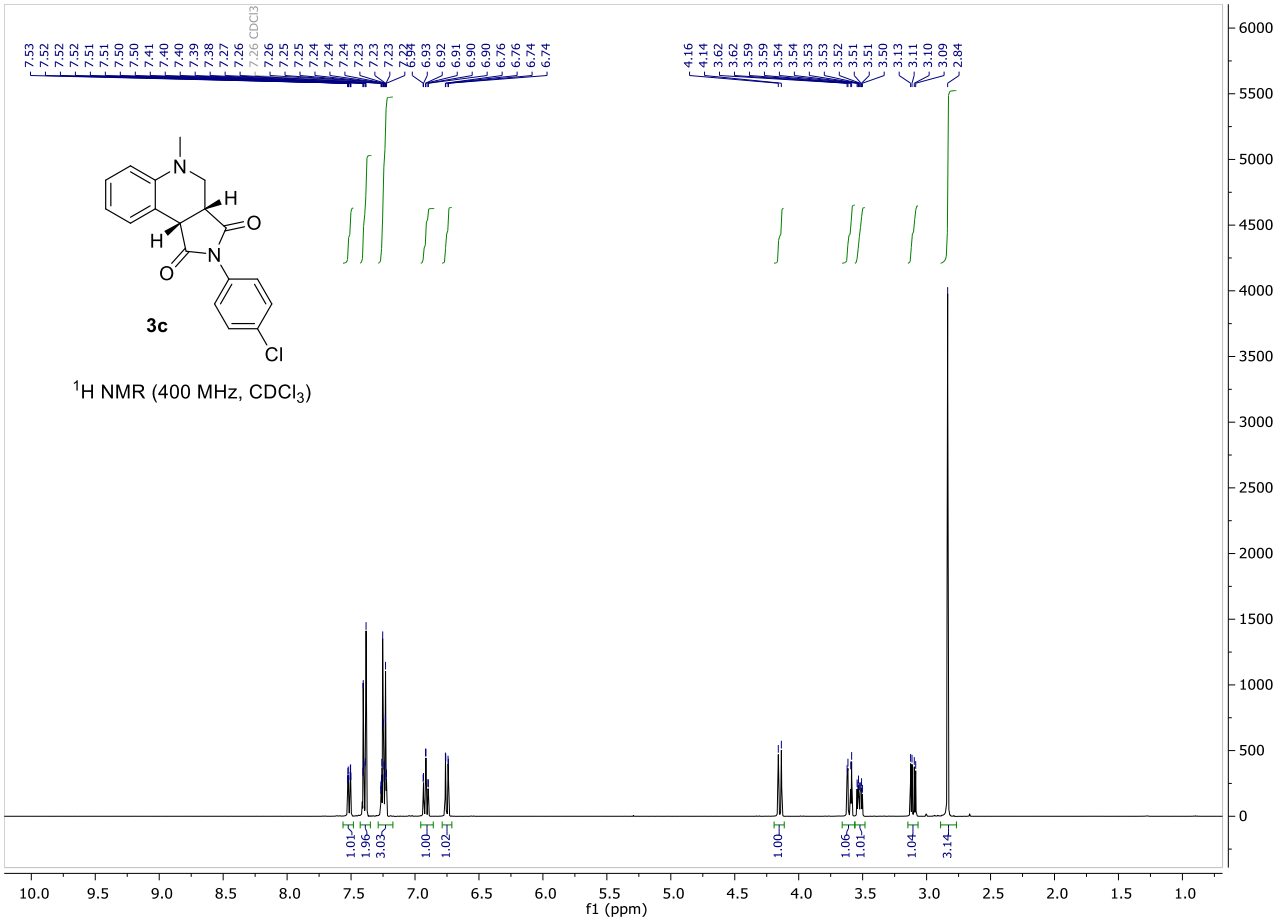
3c
^{1}H NMR (400 MHz, $CDCl_3$)
f1 (ppm)

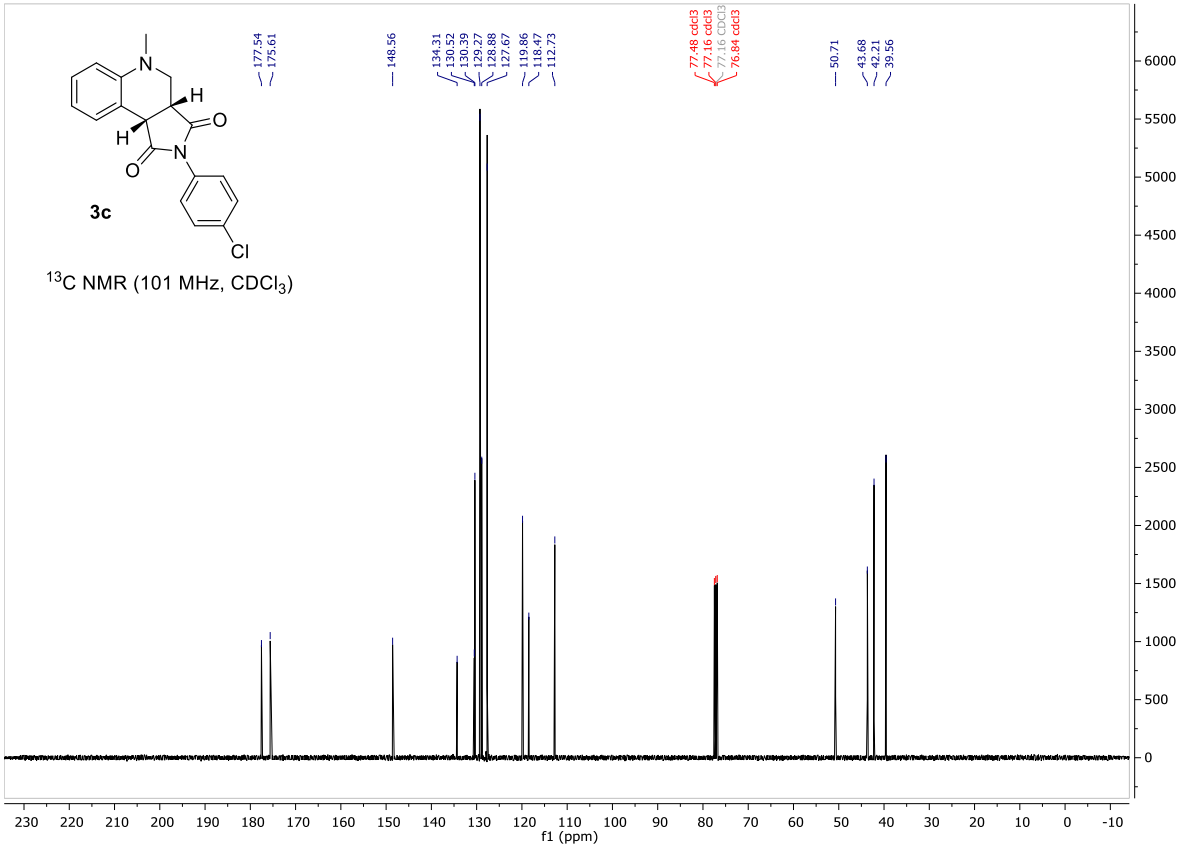
3c
^{13}C NMR (101 MHz, $CDCl_3$)
f1 (ppm)

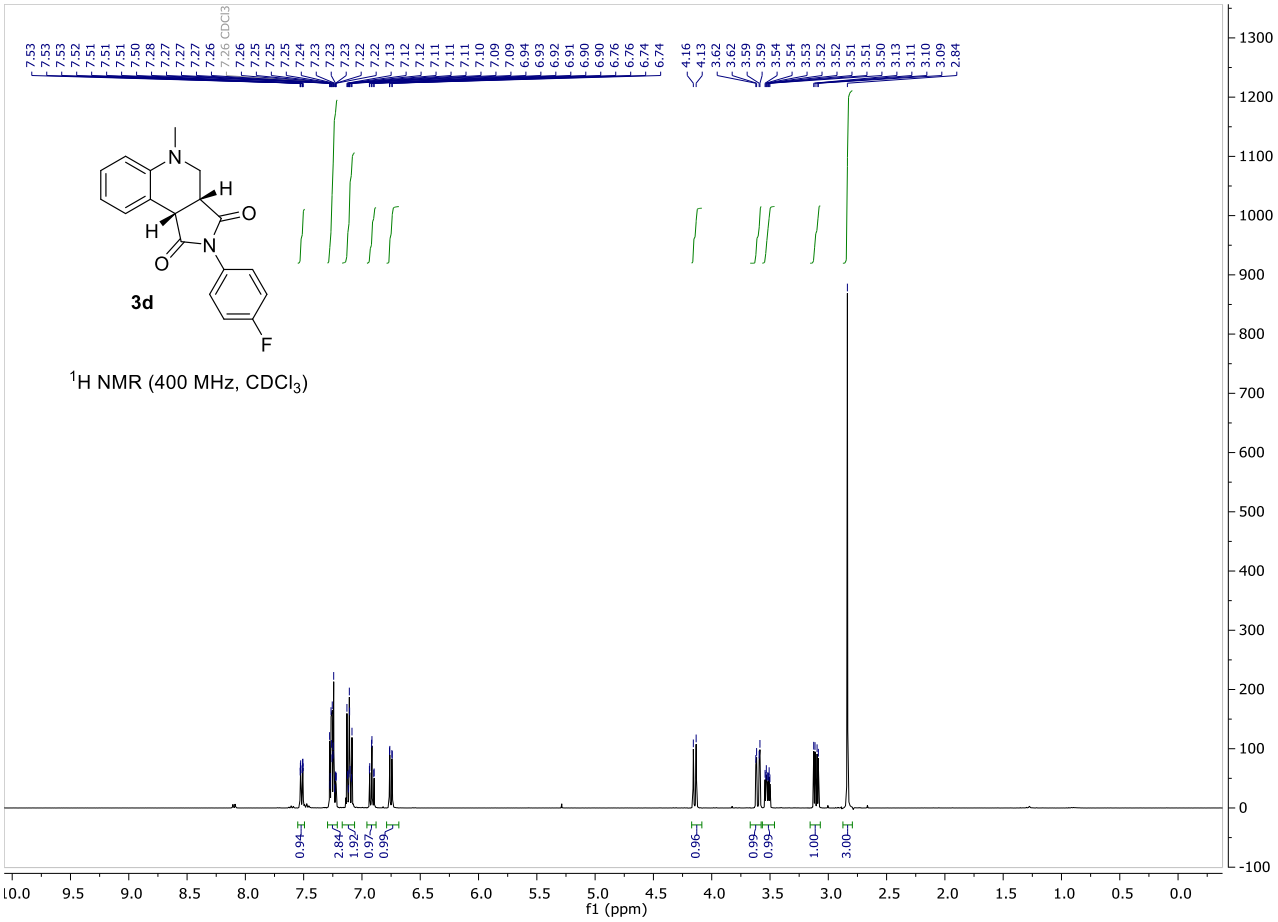
3d
^{1}H NMR (400 MHz, $CDCl_3$)
f1 (ppm)

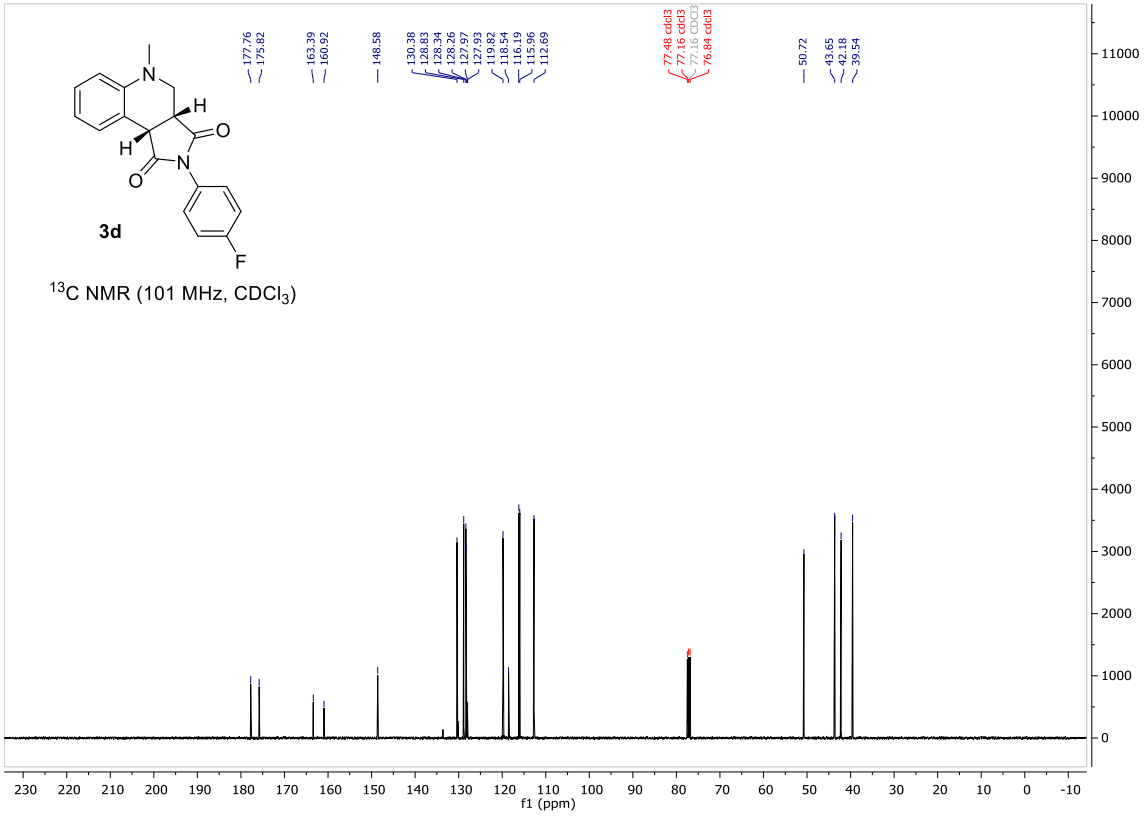
3d
^{13}C NMR (101 MHz, $CDCl_3$)
f1 (ppm)

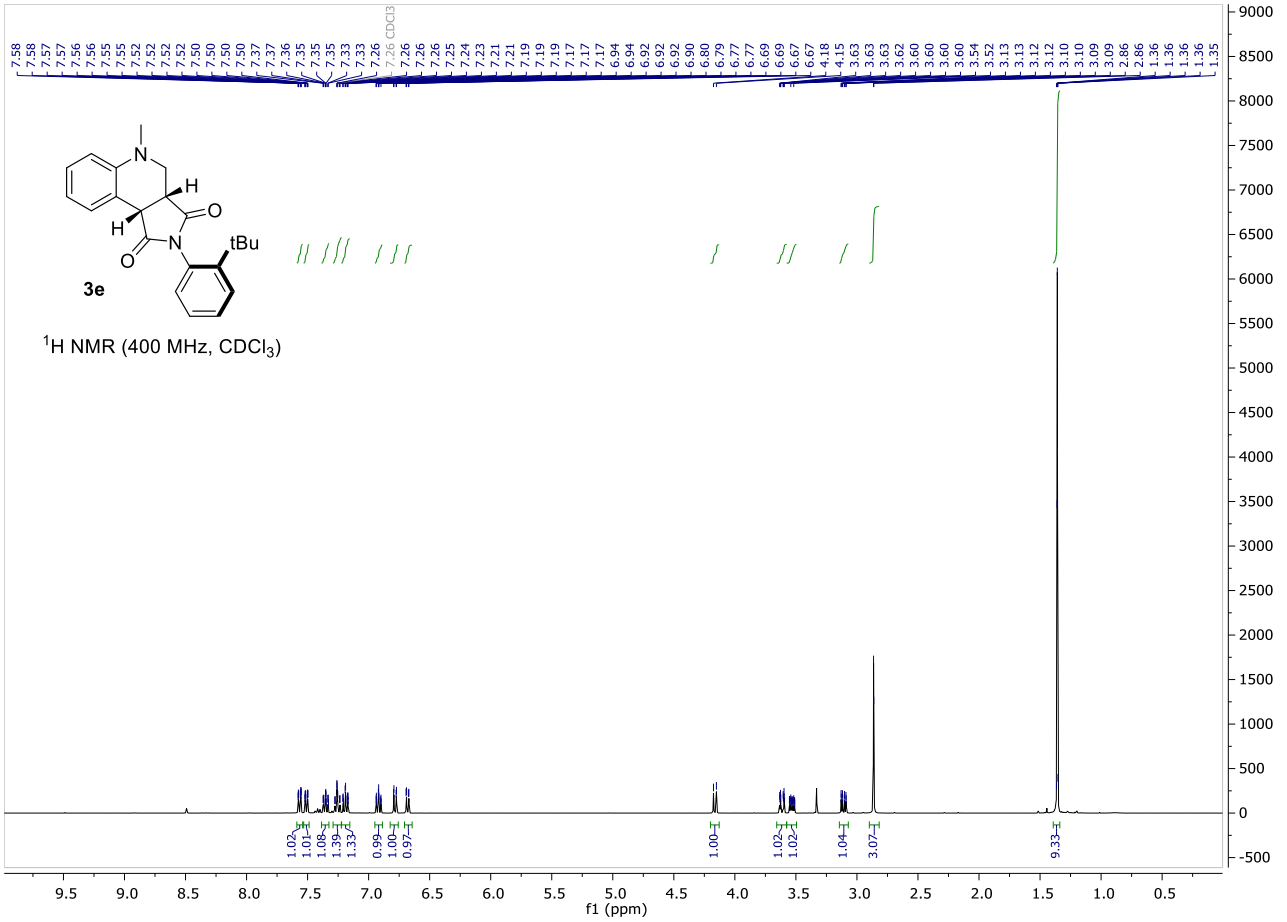
3e
^{1}H NMR (400 MHz, $CDCl_3$)
f1 (ppm)

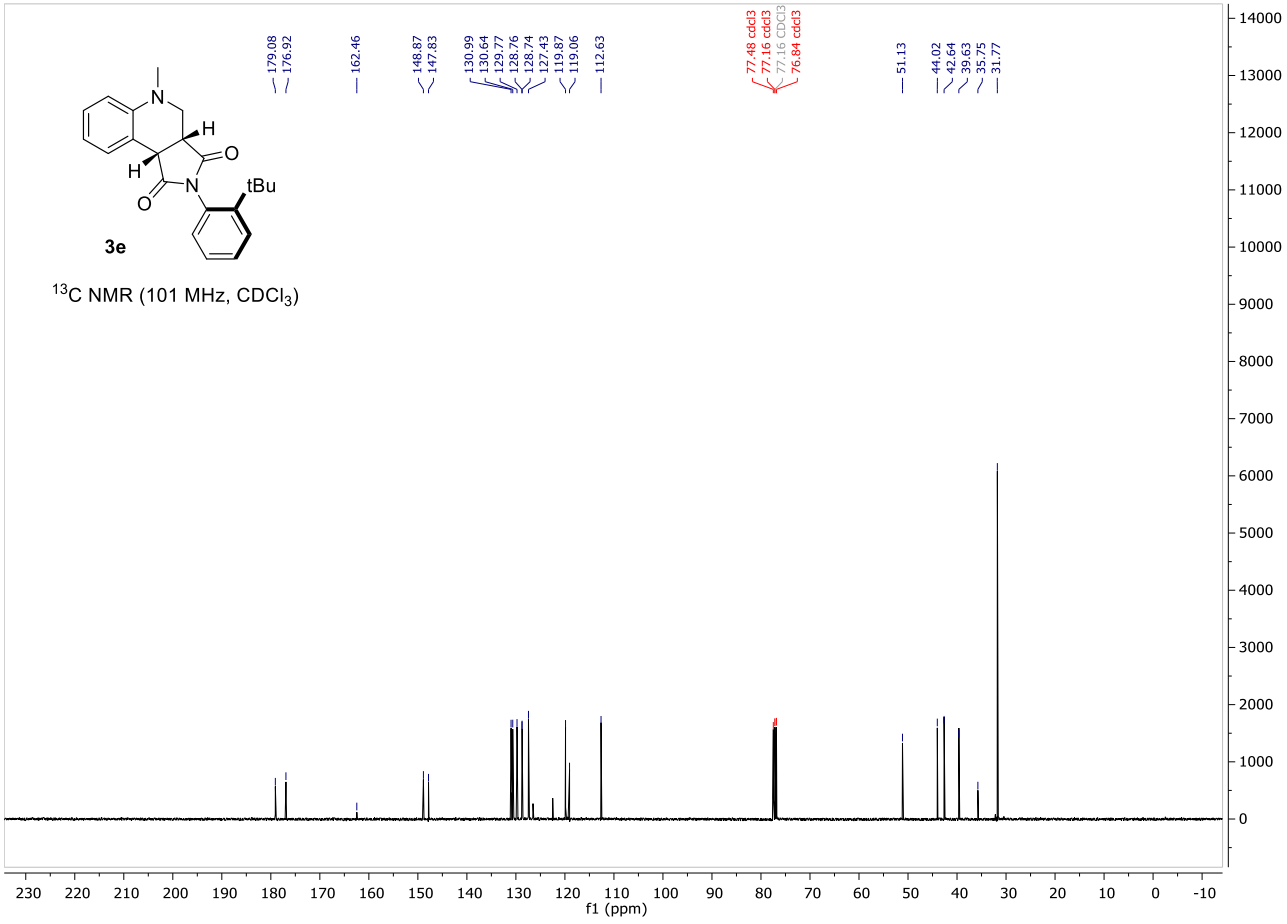
3e
^{13}C NMR (101 MHz, $CDCl_3$)
f1 (ppm)

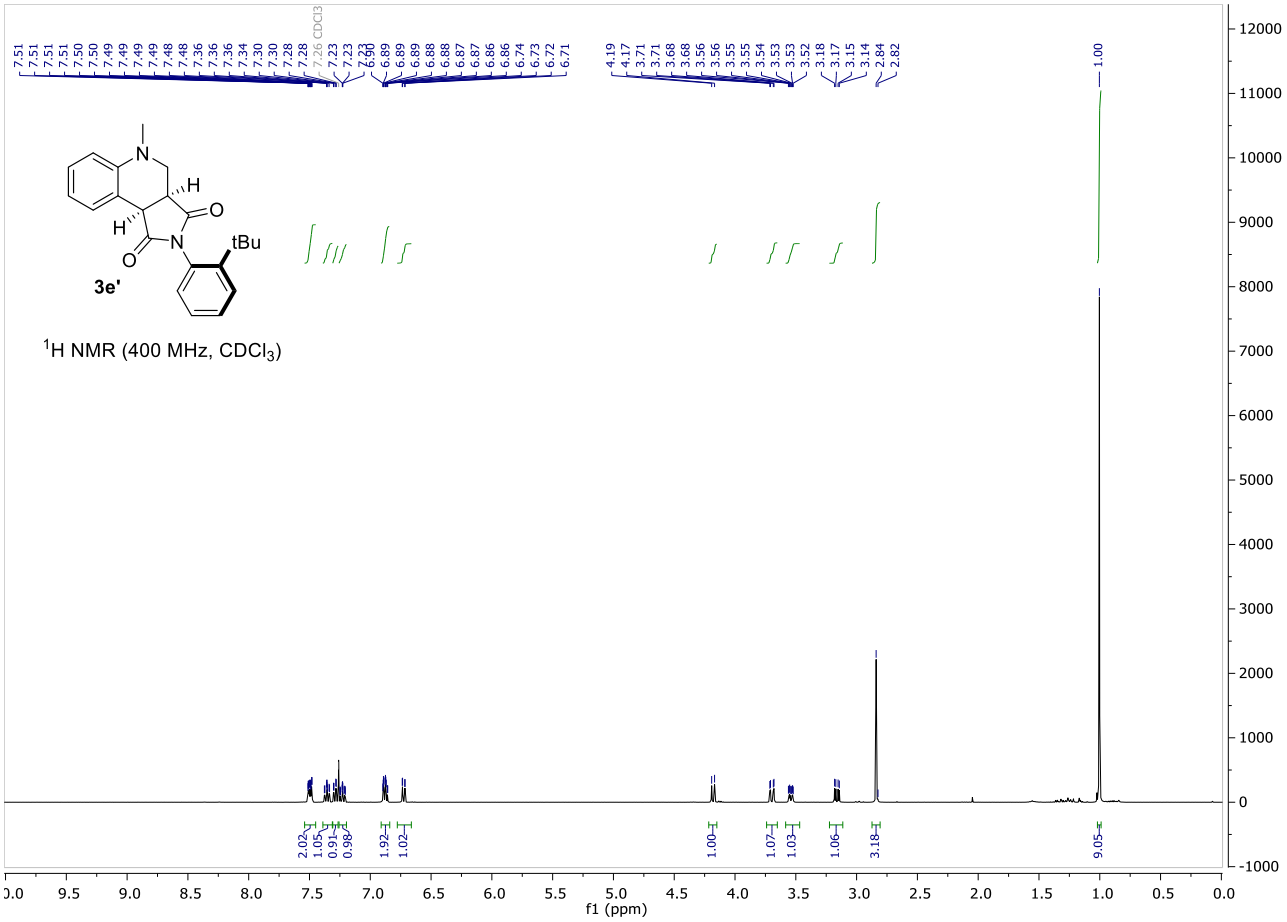

^{1}H NMR (400 MHz, $CDCl_3$)

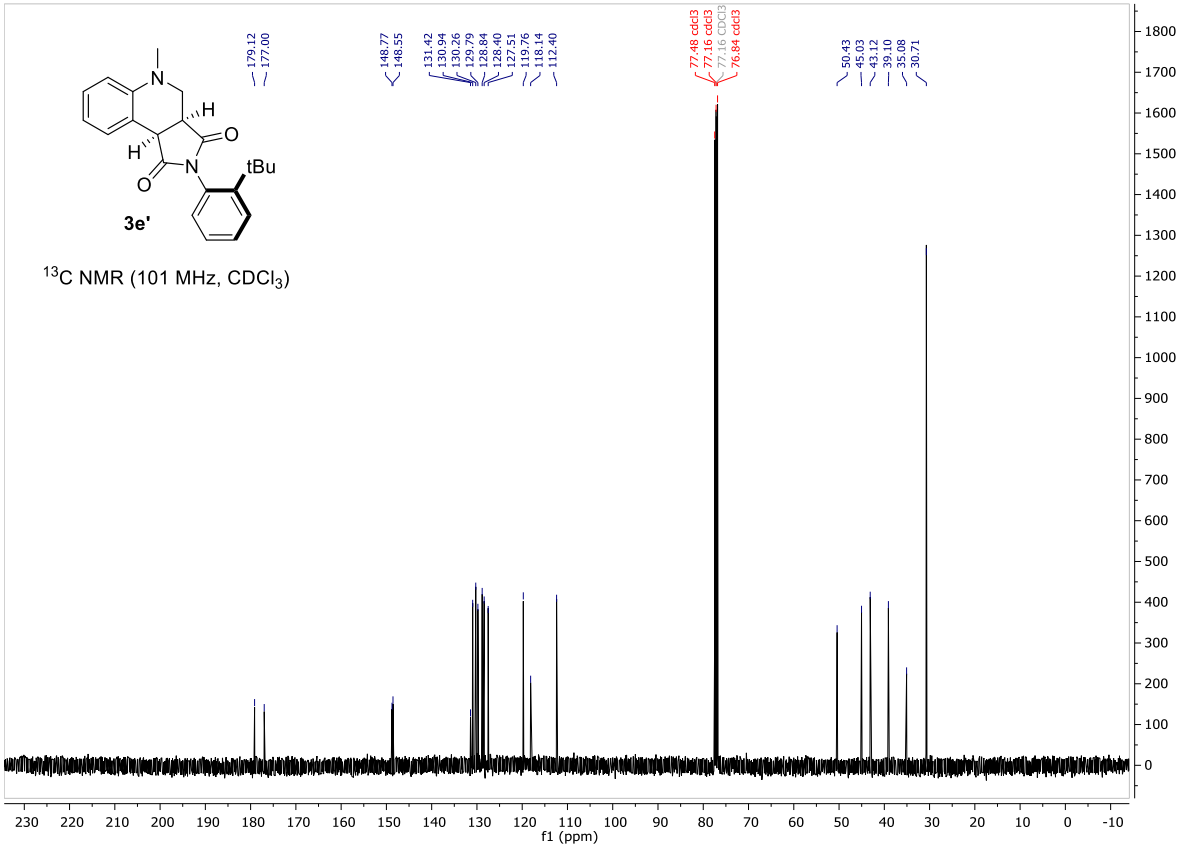

^{13}C NMR (101 MHz, $CDCl_3$)

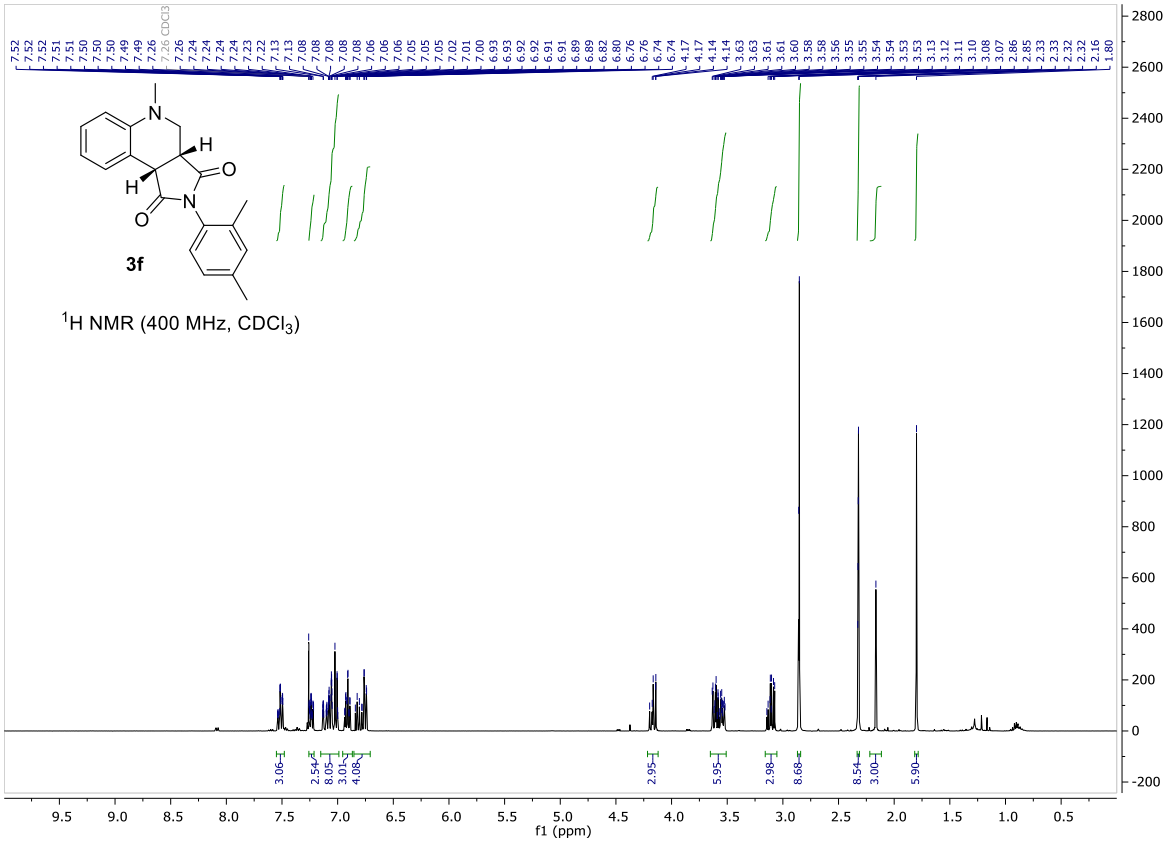
3f
^{1}H NMR (400 MHz, $CDCl_3$)
f1 (ppm)

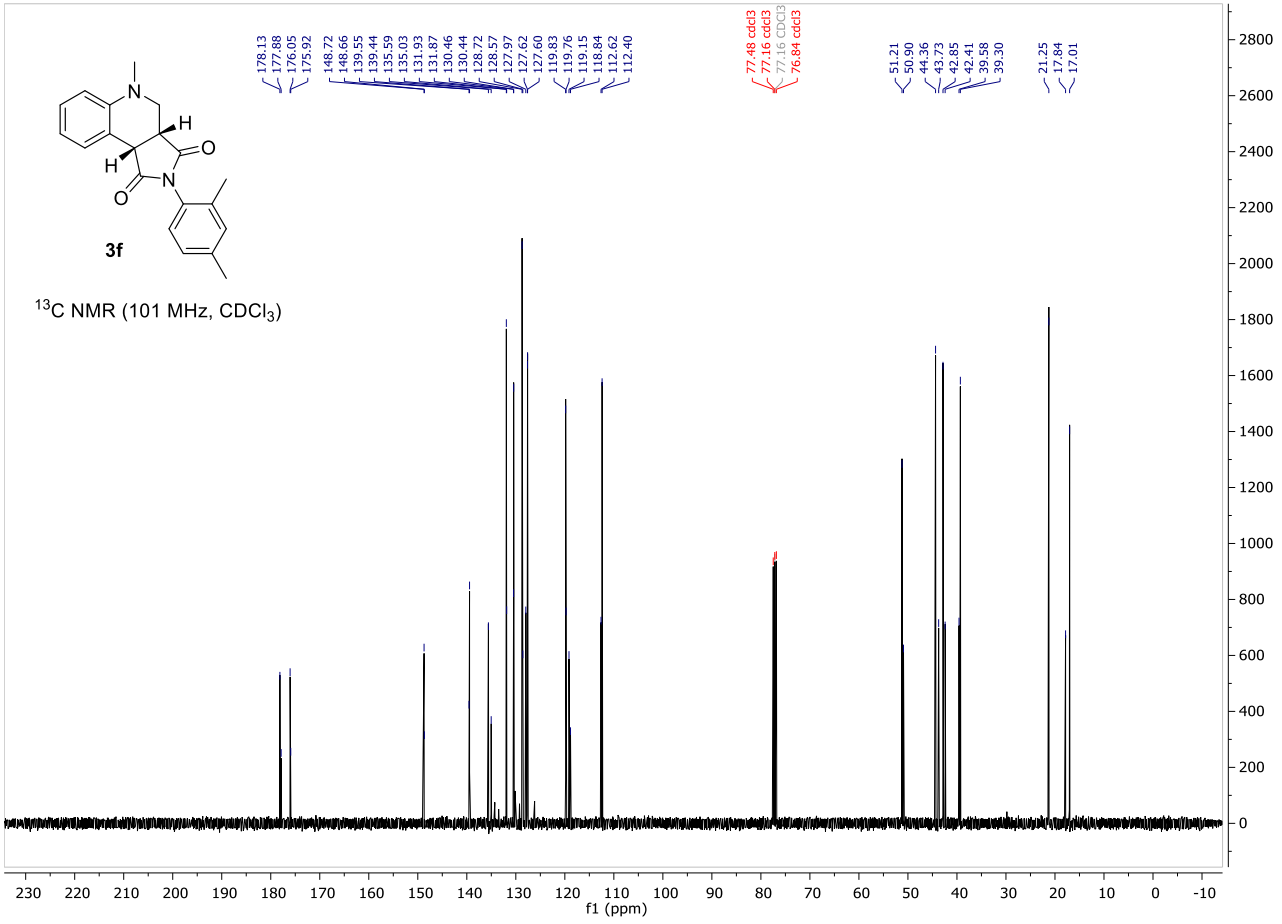
3f
^{13}C NMR (101 MHz, $CDCl_3$)
f1 (ppm)

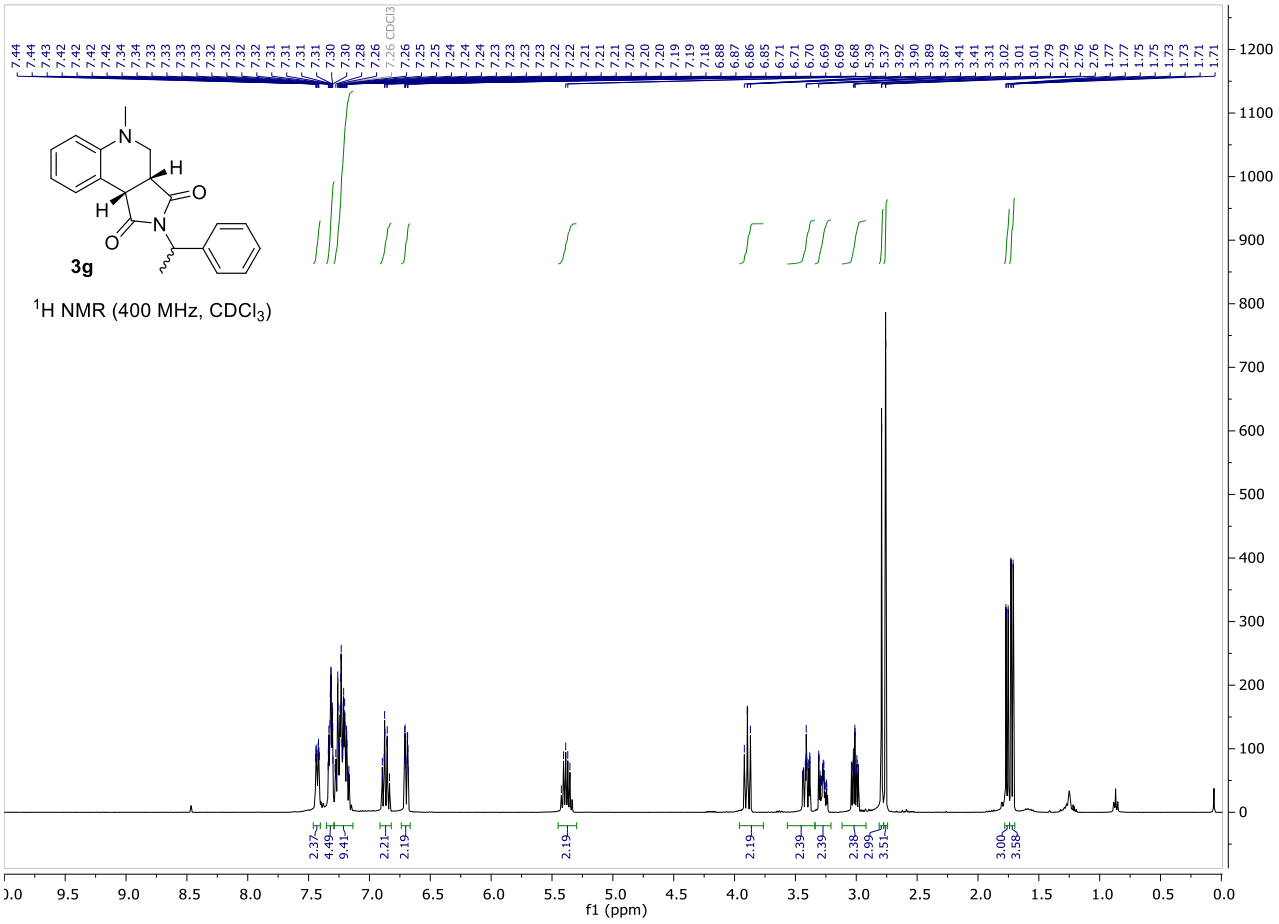
3g
^{1}H NMR (400 MHz, $CDCl_3$)
f1 (ppm)

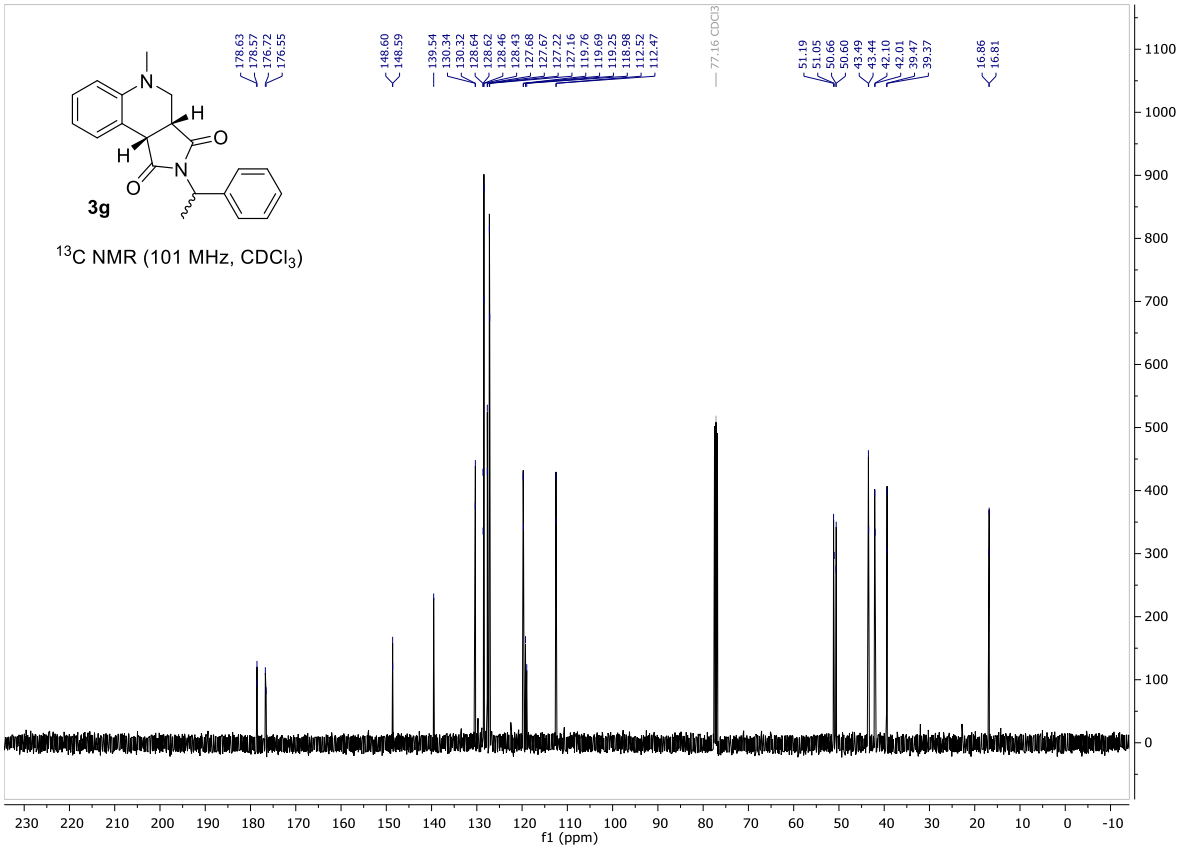
3g
^{13}C NMR (101 MHz, $CDCl_3$)
f1 (ppm)

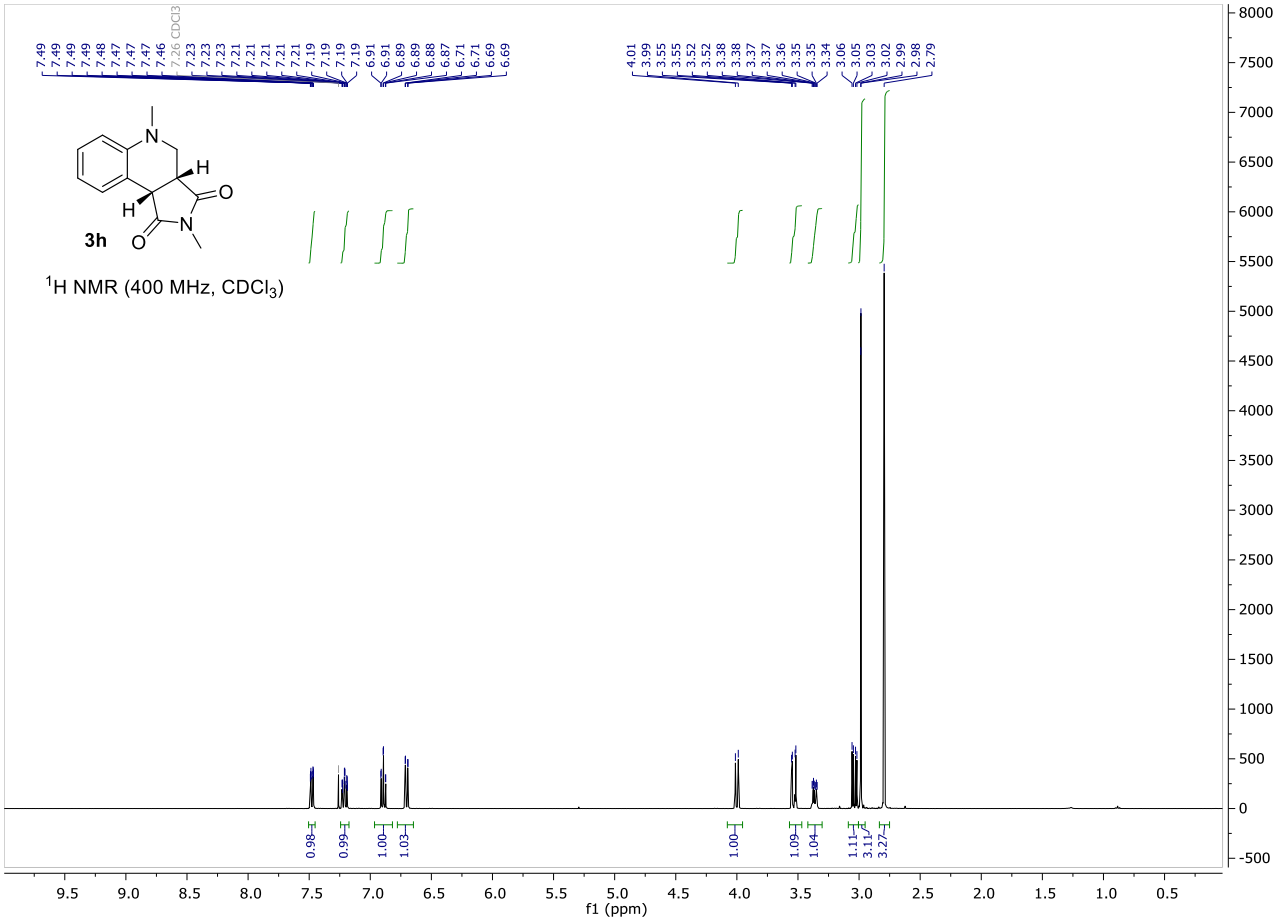
3h
^{1}H NMR (400 MHz, $CDCl_3$)
f1 (ppm)

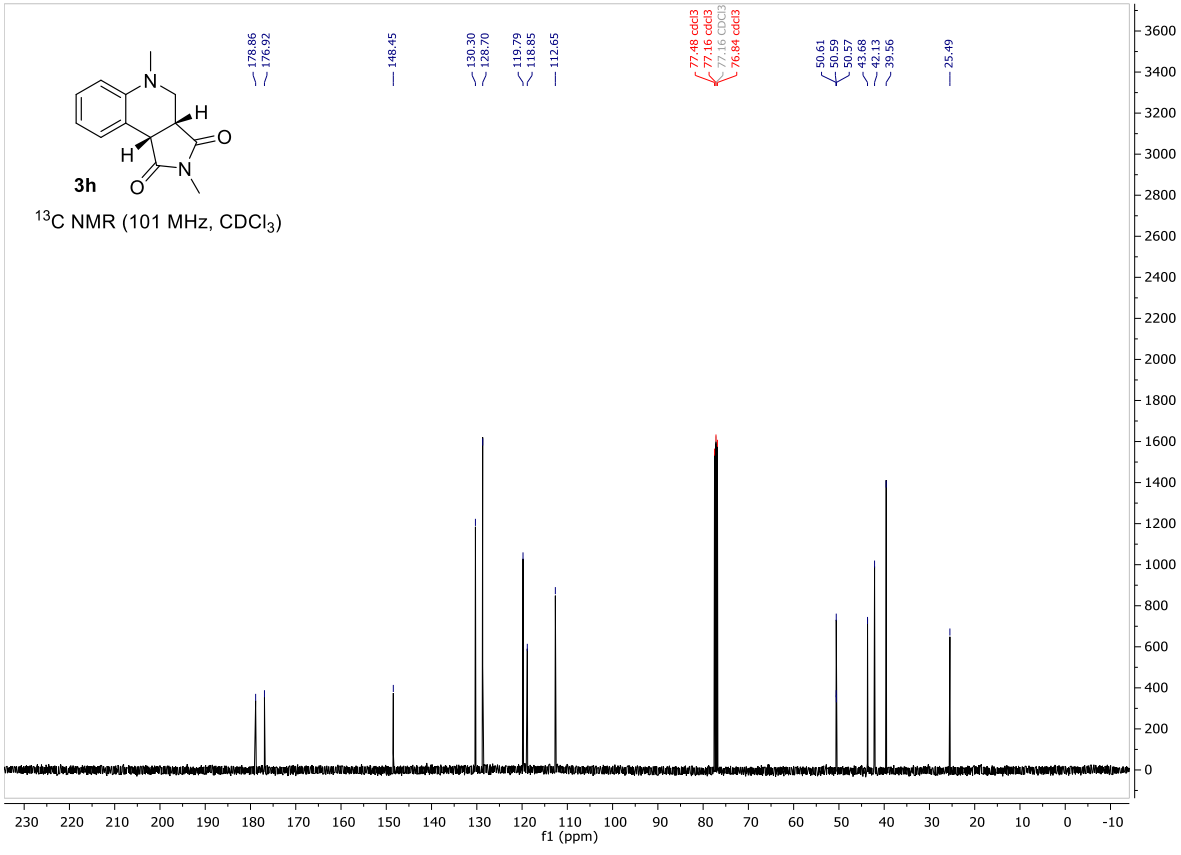
3h
^{13}C NMR (101 MHz, $CDCl_3$)
f1 (ppm)

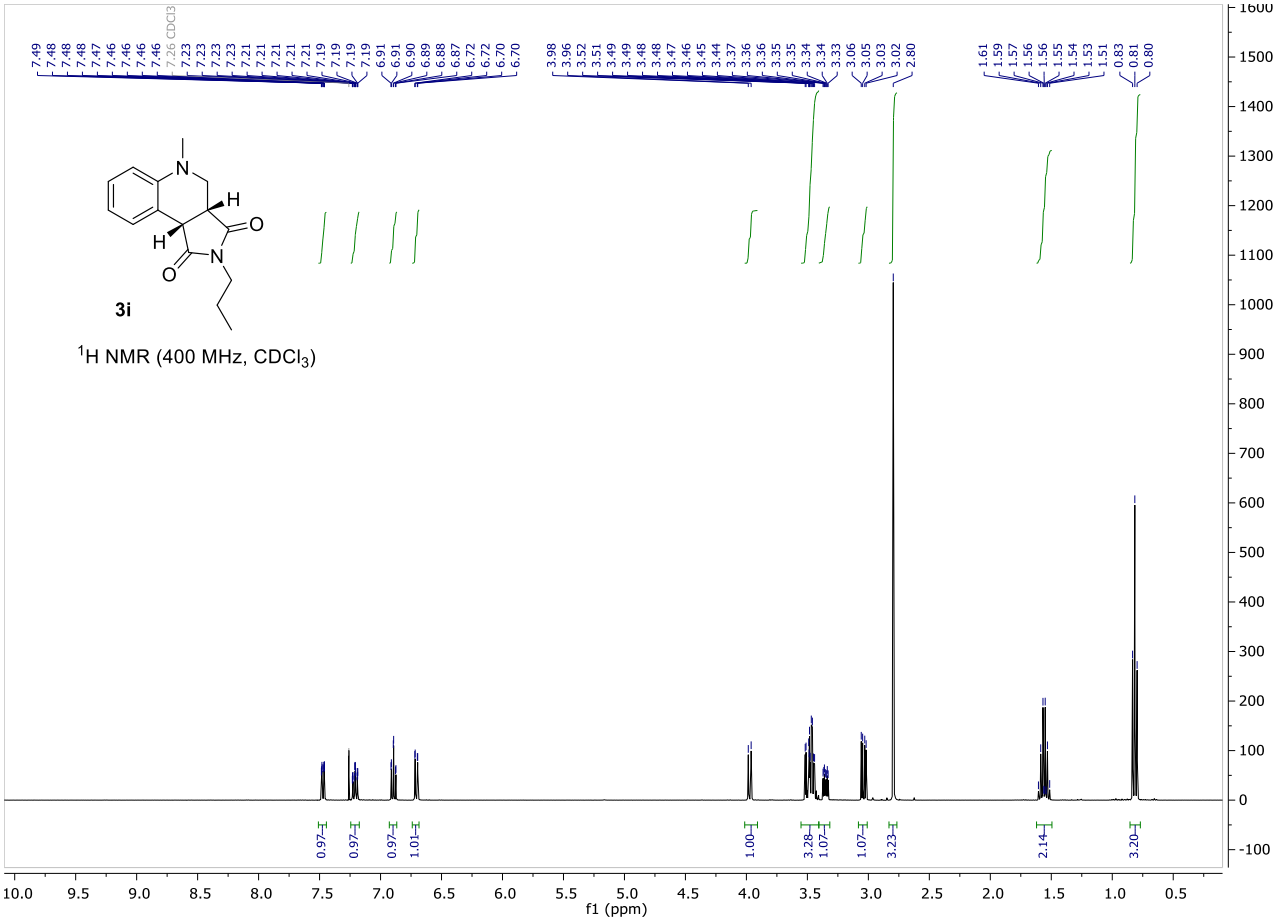
3i
^{1}H NMR (400 MHz, $CDCl_3$)
f1 (ppm)

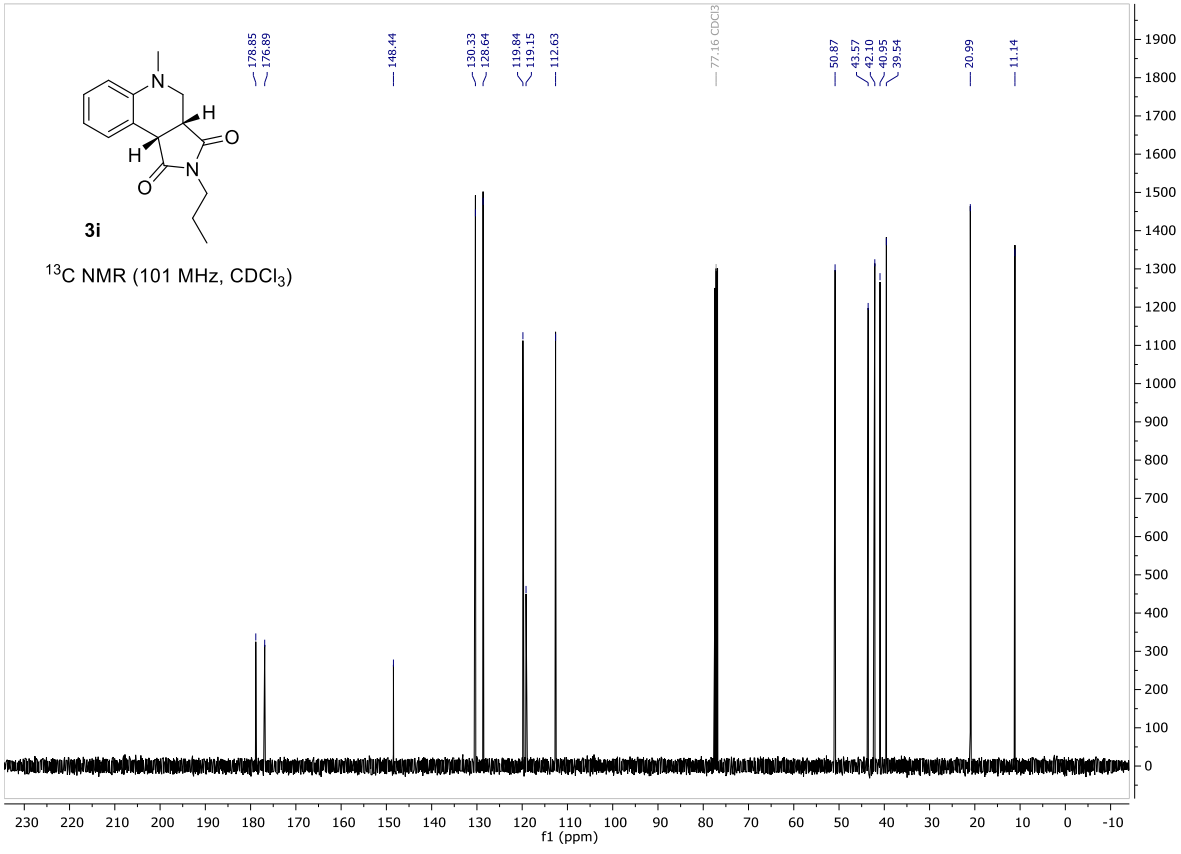
3i
^{13}C NMR (101 MHz, $CDCl_3$)
f1 (ppm)

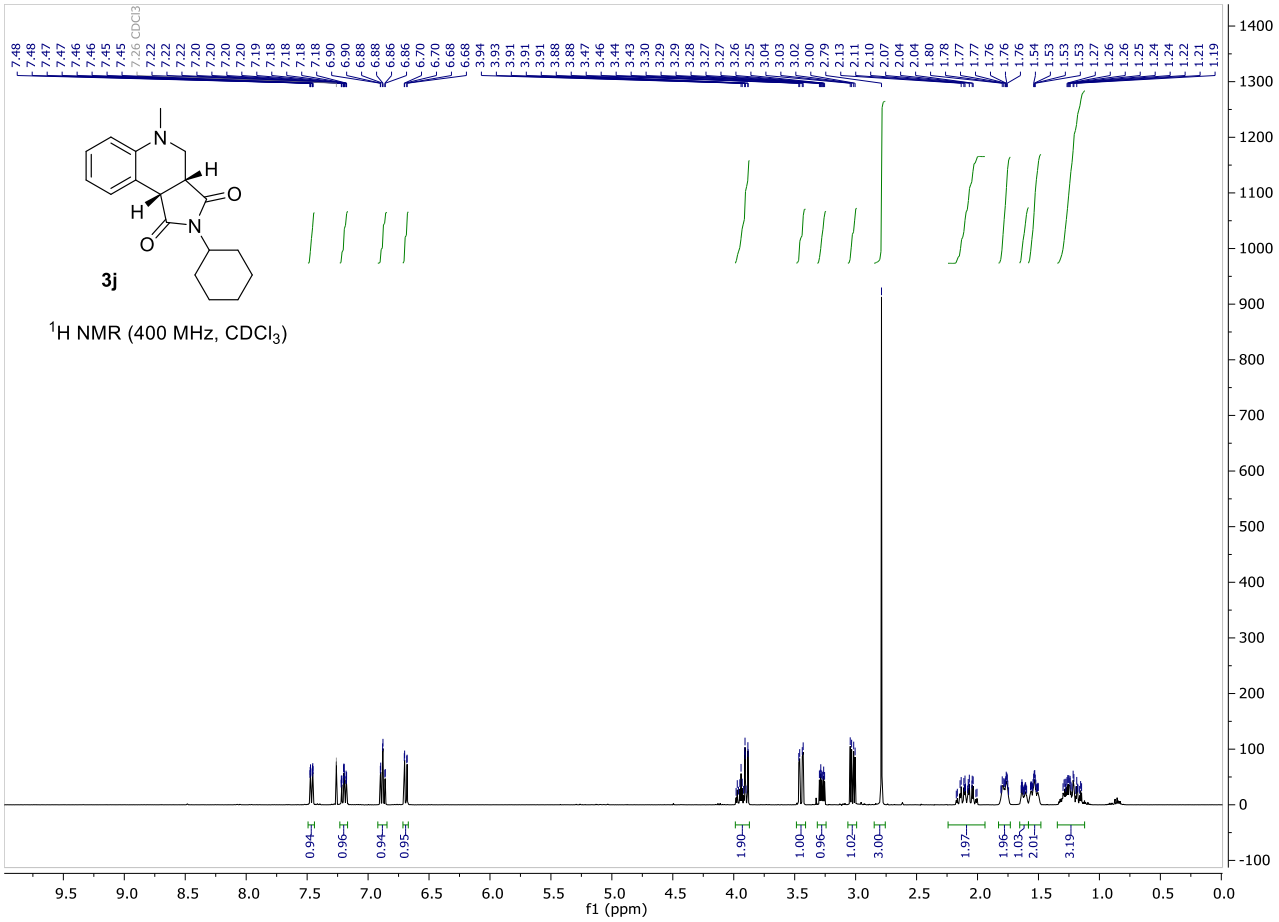
3j
^{1}H NMR (400 MHz, $CDCl_3$)
f1 (ppm)

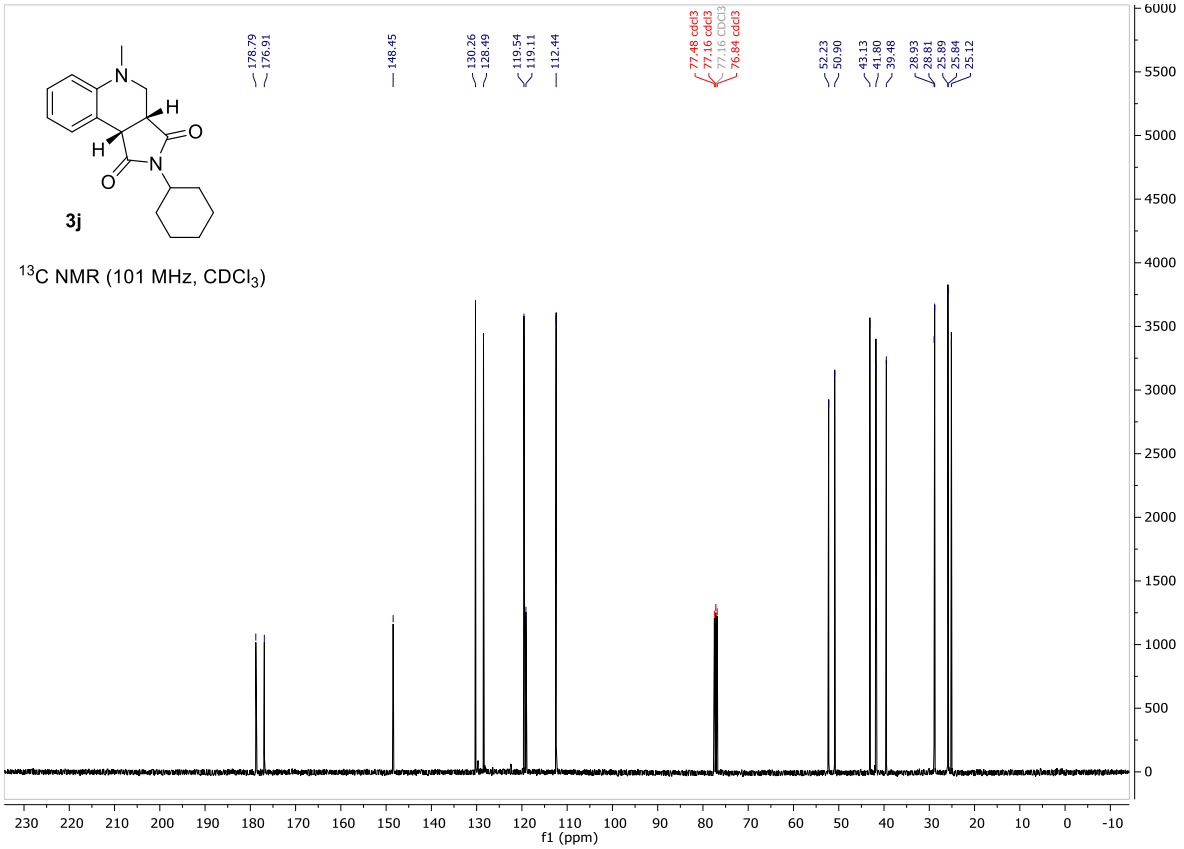
3j
^{13}C NMR (101 MHz, $CDCl_3$)
f1 (ppm)

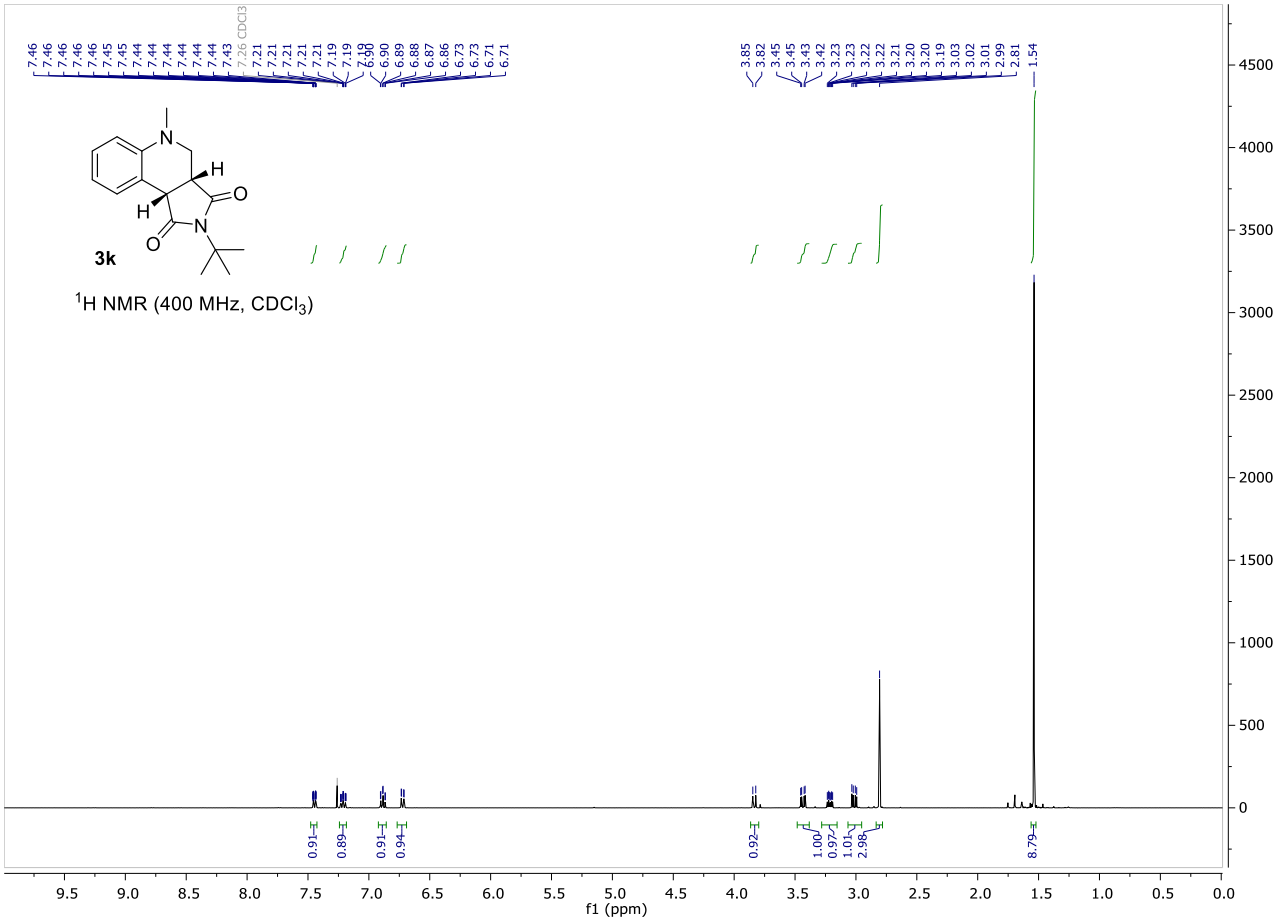
3k
^{1}H NMR (400 MHz, $CDCl_3$)
f1 (ppm)

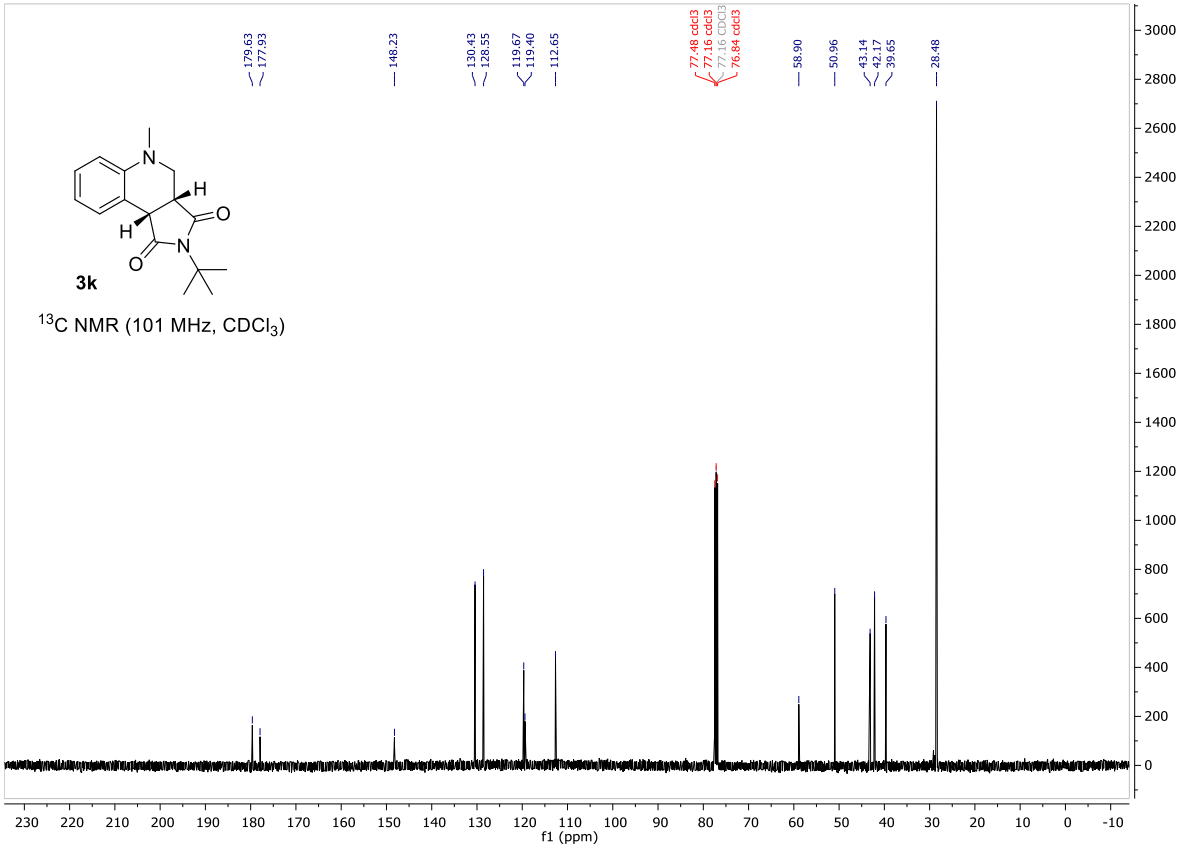
3k
^{13}C NMR (101 MHz, $CDCl_3$)
f1 (ppm)

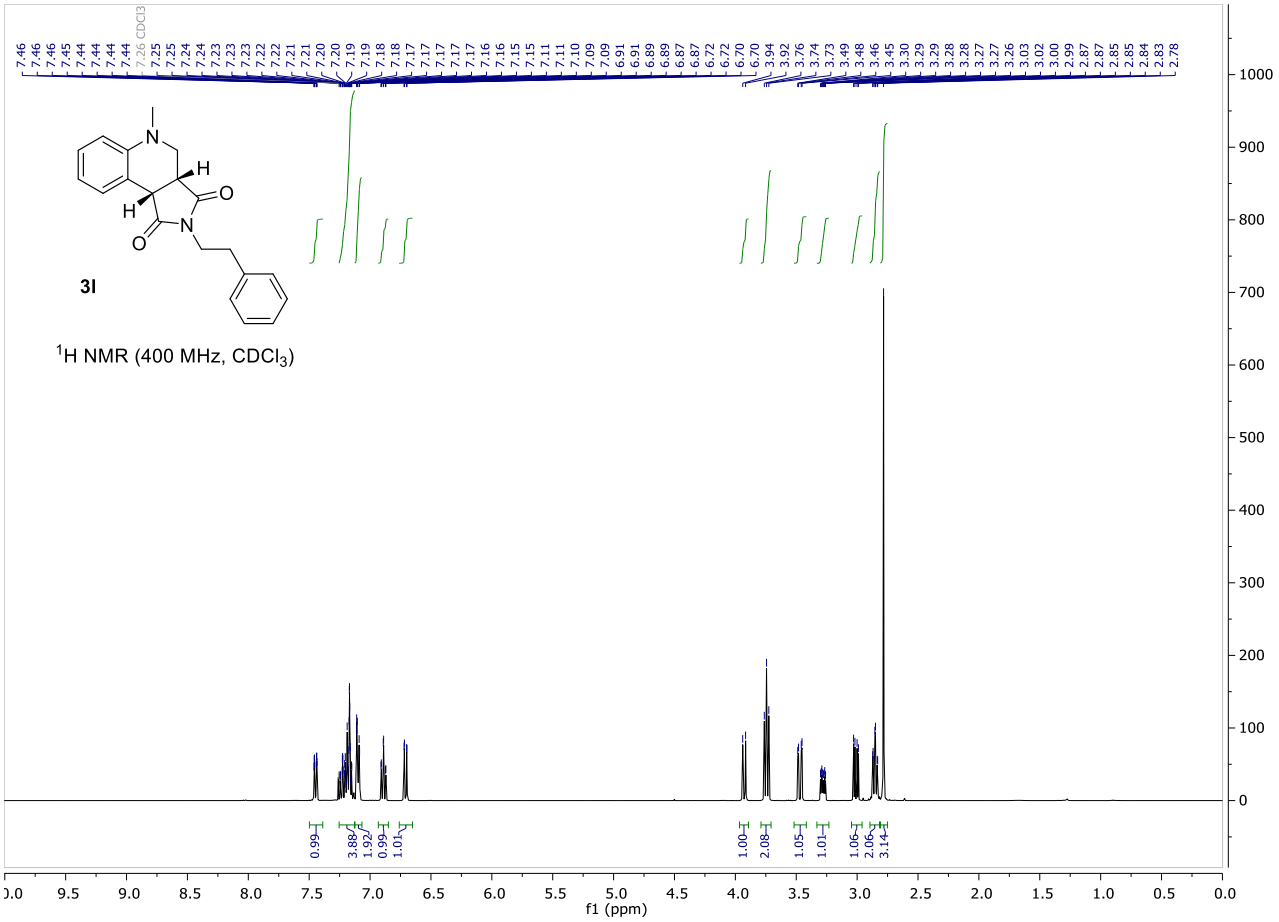
3l
^{1}H NMR (400 MHz, $CDCl_3$)
f1 (ppm)

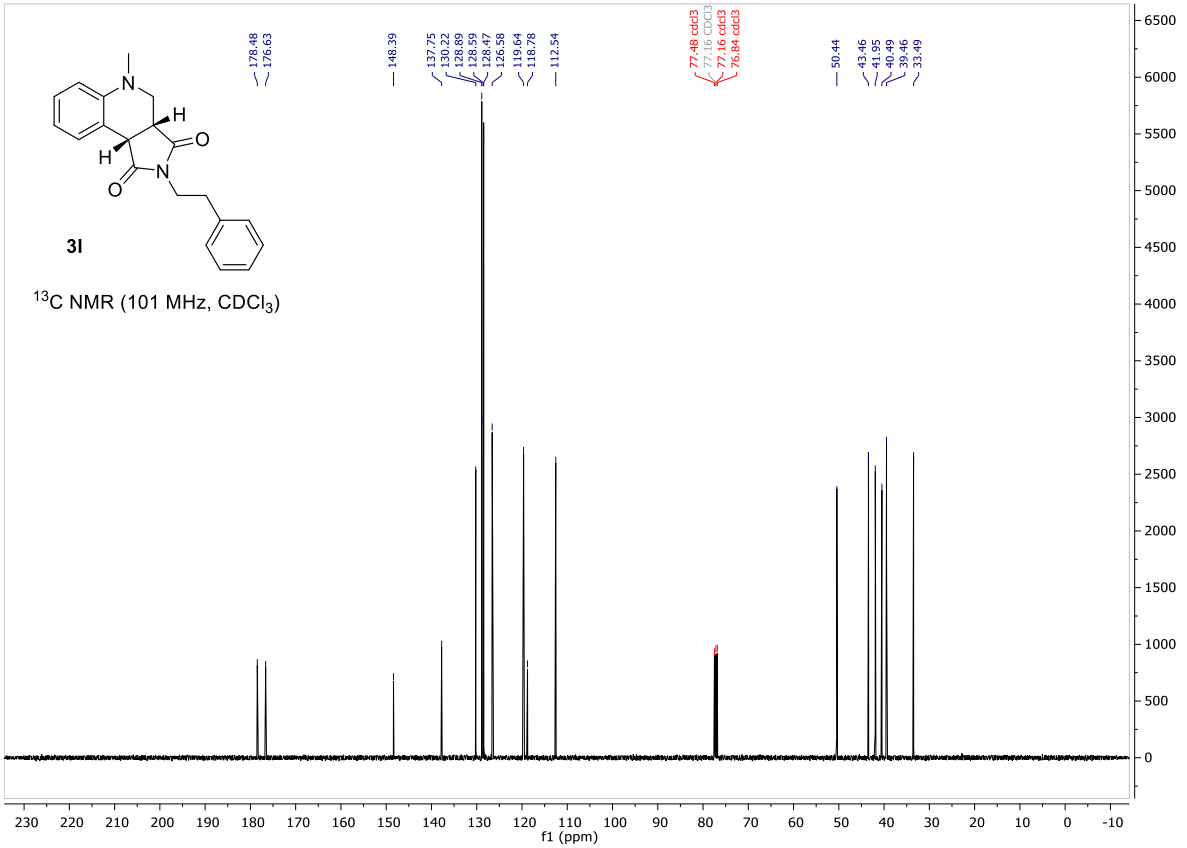
3l
^{13}C NMR (101 MHz, $CDCl_3$)
f1 (ppm)

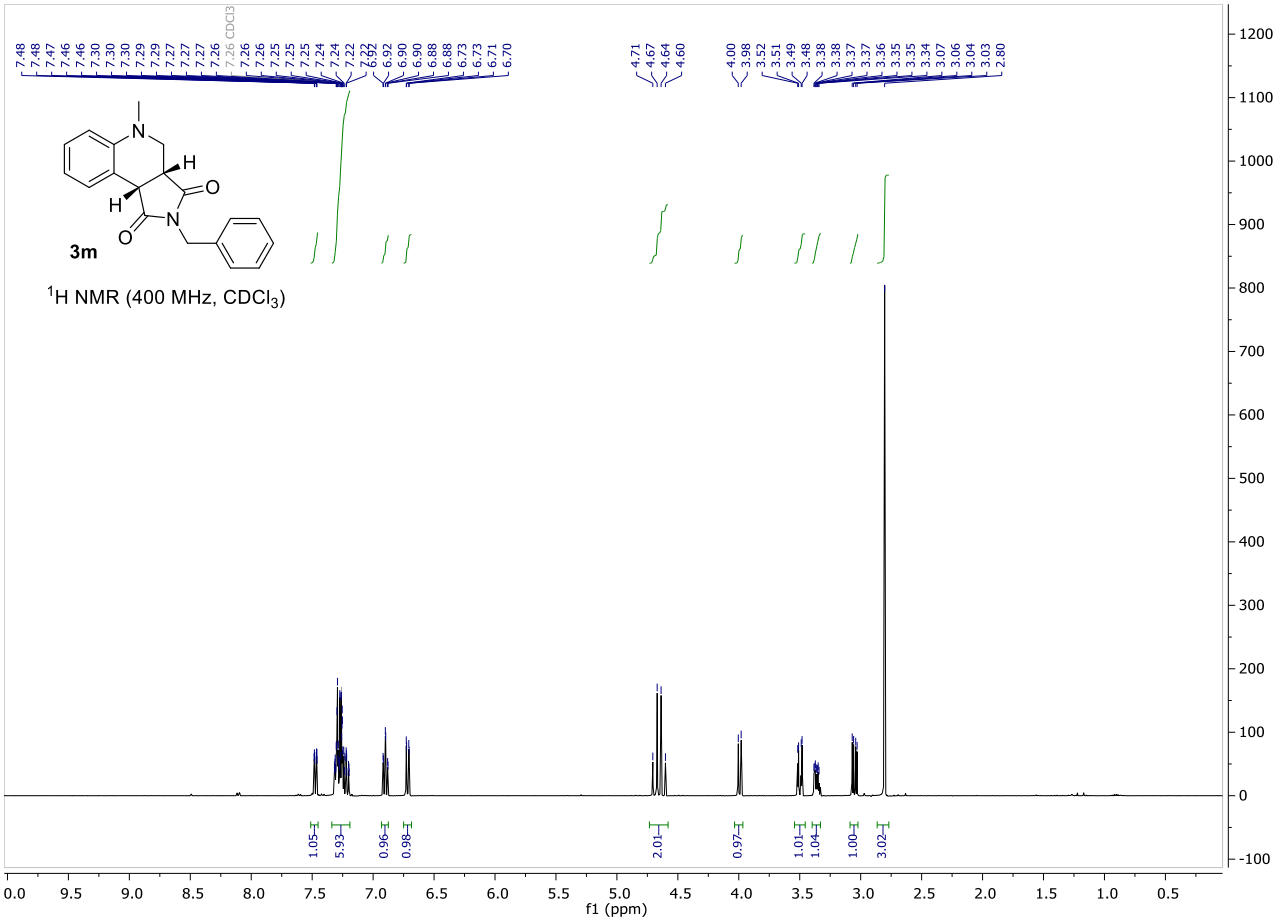
3m
^{1}H NMR (400 MHz, $CDCl_3$)
f1 (ppm)

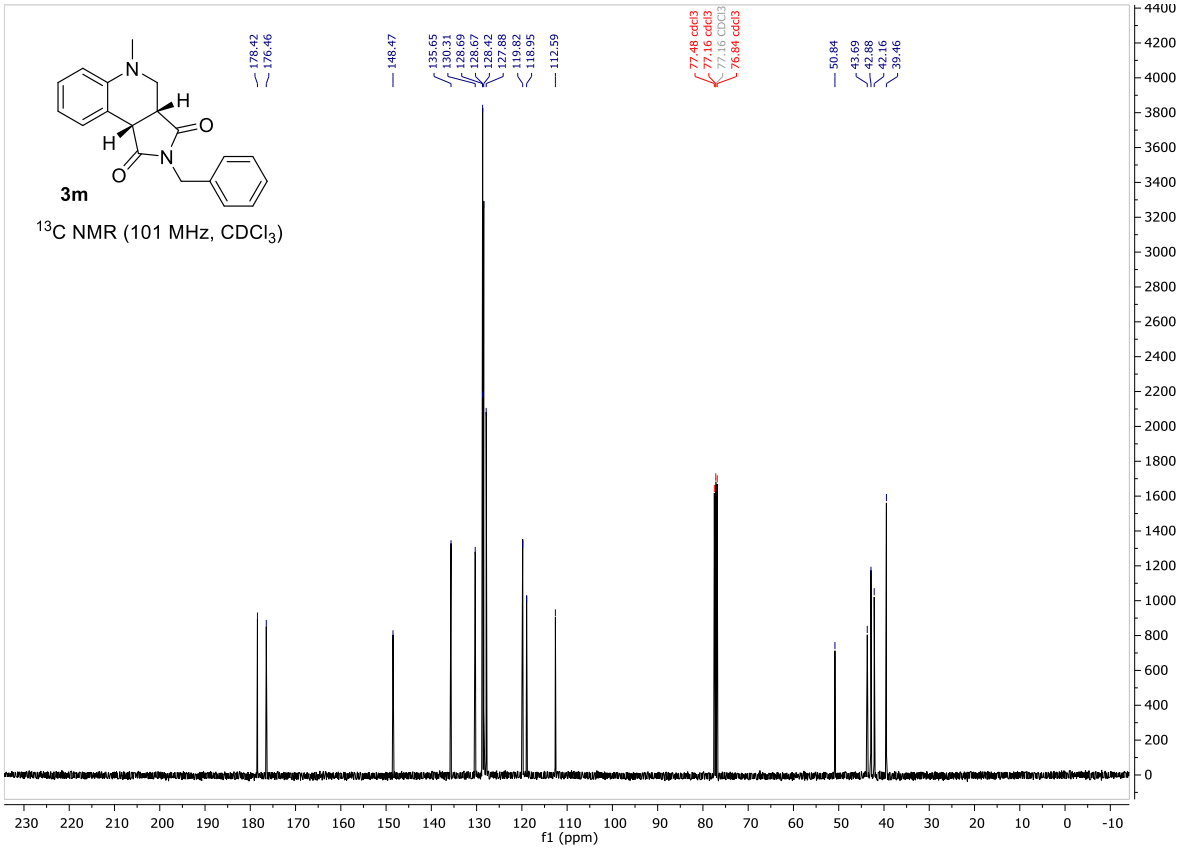
3m
^{13}C NMR (101 MHz, $CDCl_3$)
f1 (ppm)

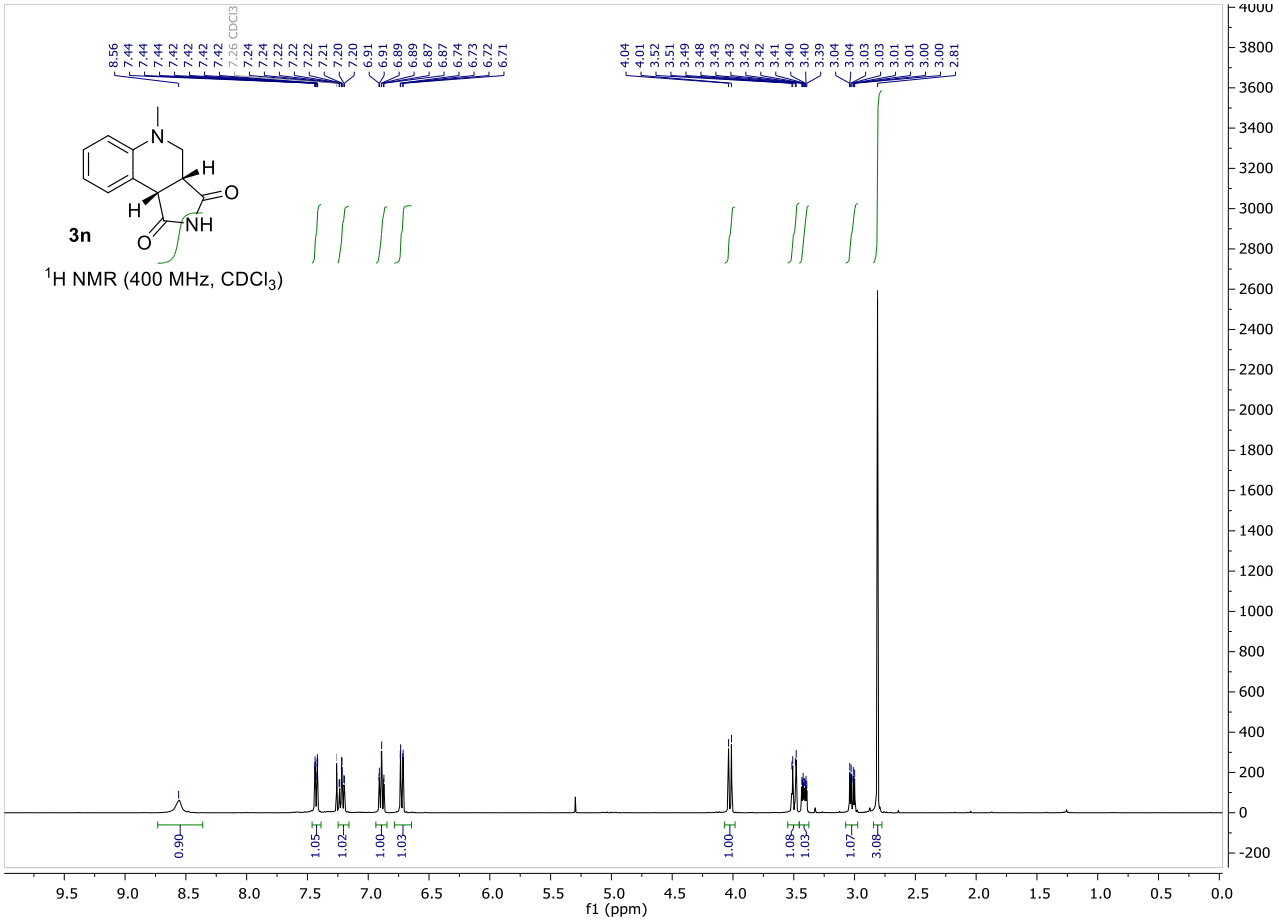
3n
^{1}H NMR (400 MHz, $CDCl_3$)
f1 (ppm)

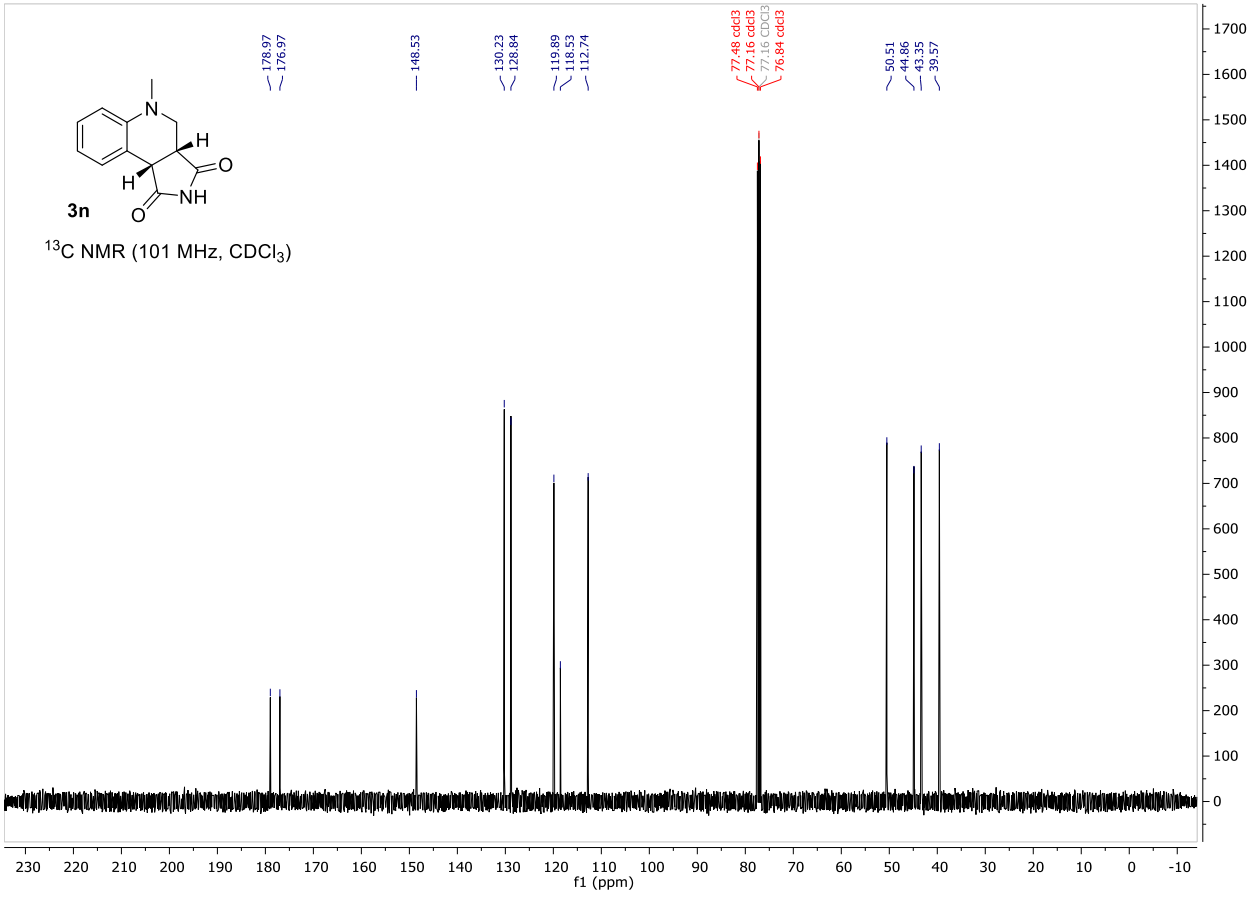
3n
^{13}C NMR (101 MHz, $CDCl_3$)
f1 (ppm)

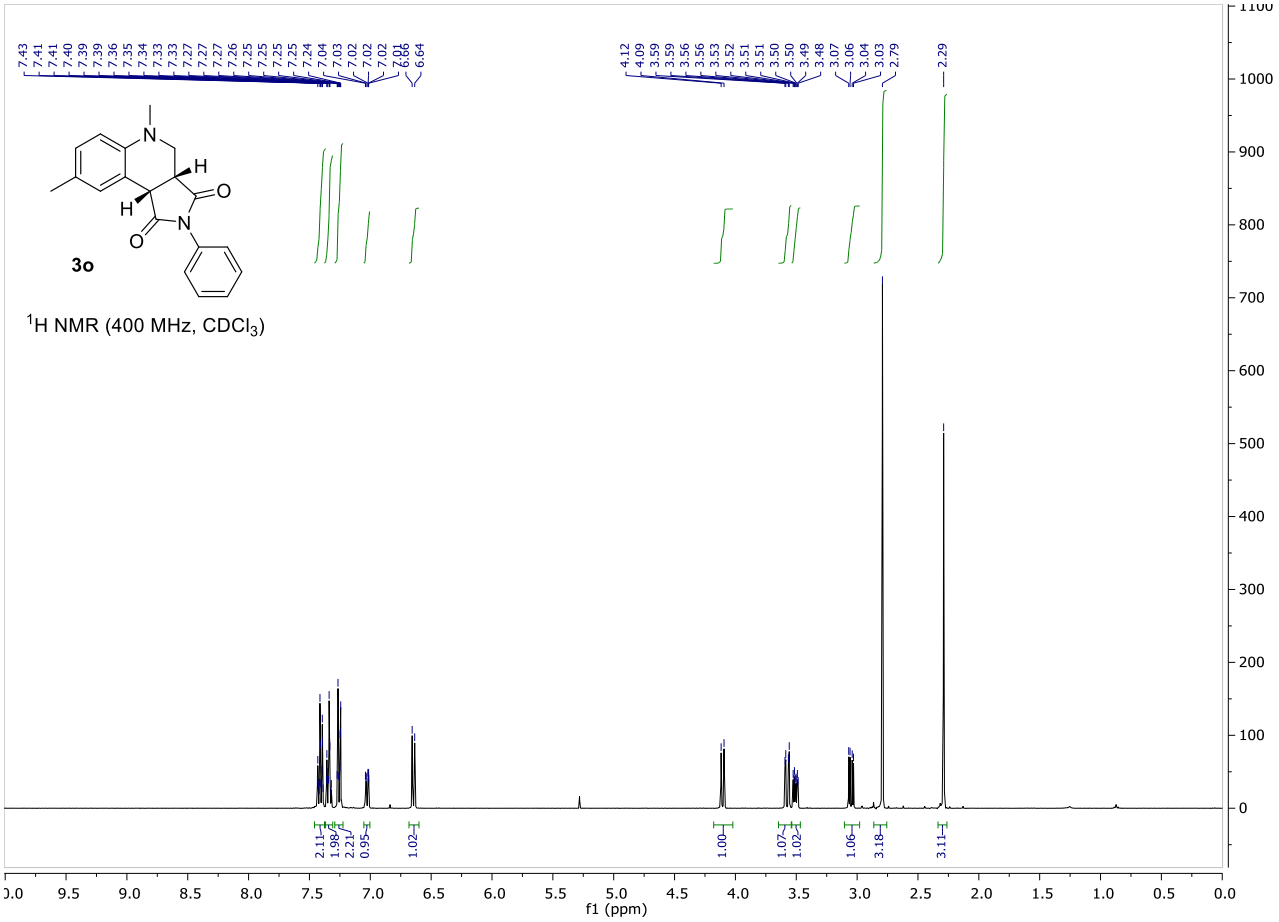
3o
^{1}H NMR (400 MHz, $CDCl_3$)
f1 (ppm)

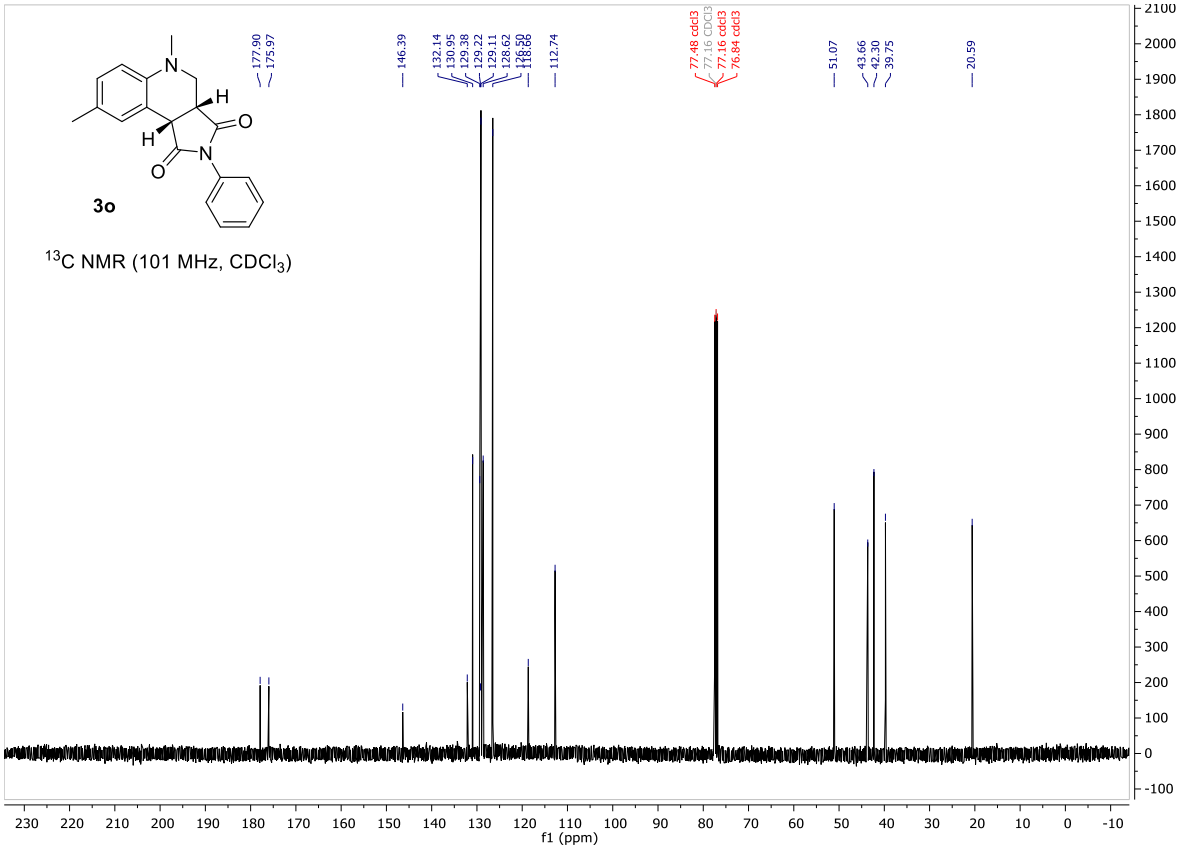
3o
^{13}C NMR (101 MHz, $CDCl_3$)
f1 (ppm)

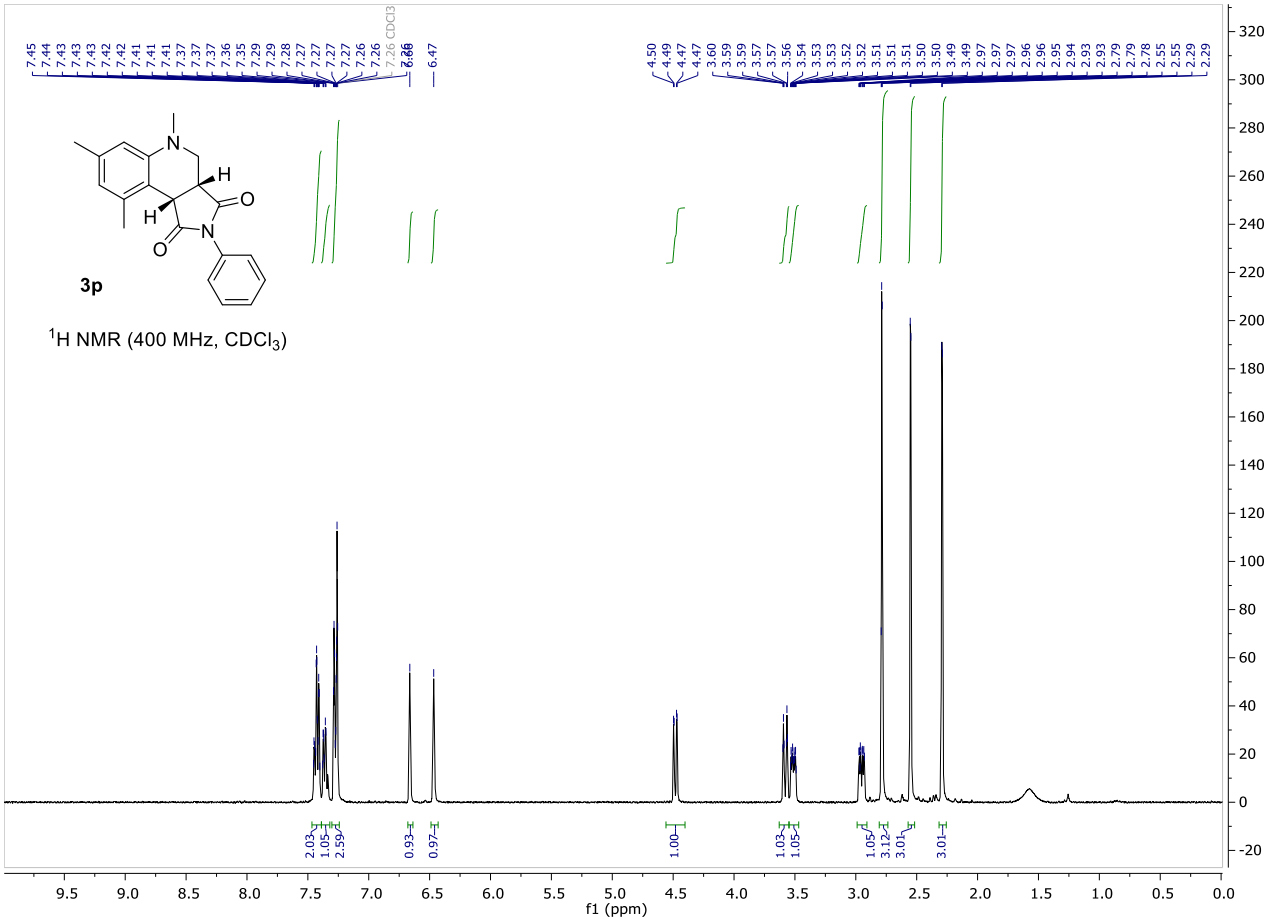
3p
^{1}H NMR (400 MHz, $CDCl_3$)
f1 (ppm)

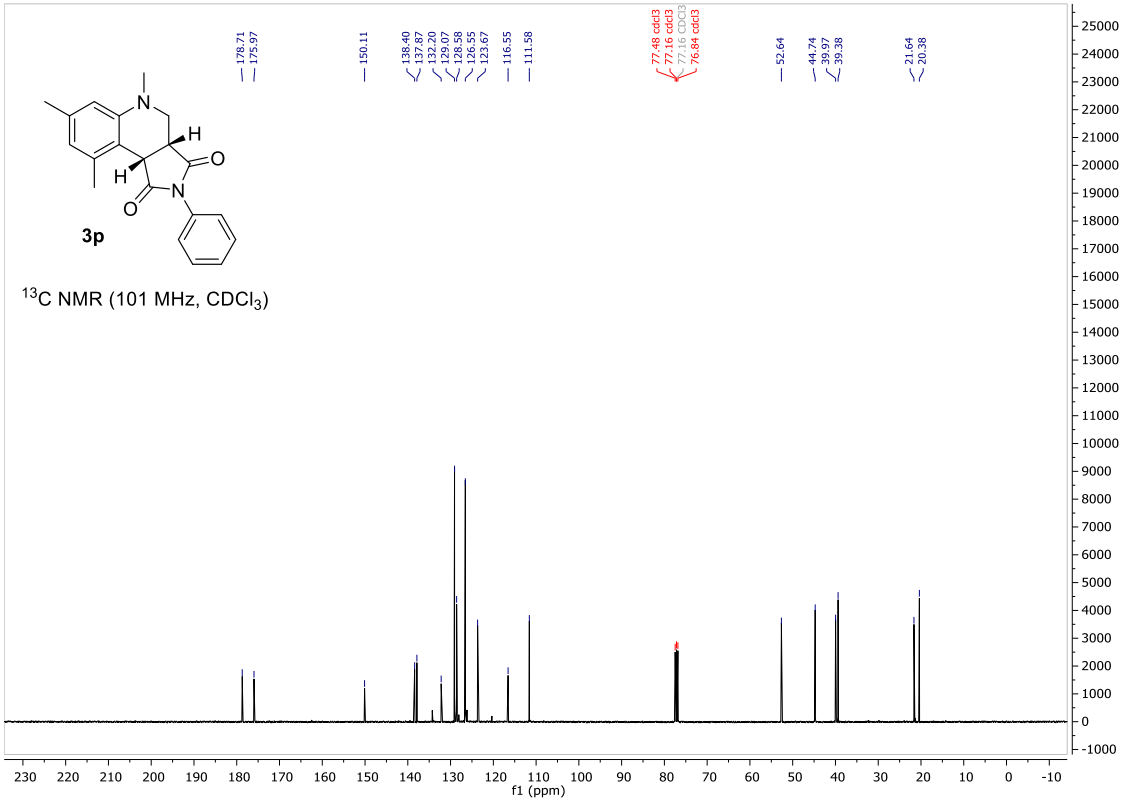
3p
^{13}C NMR (101 MHz, $CDCl_3$)
f1 (ppm)

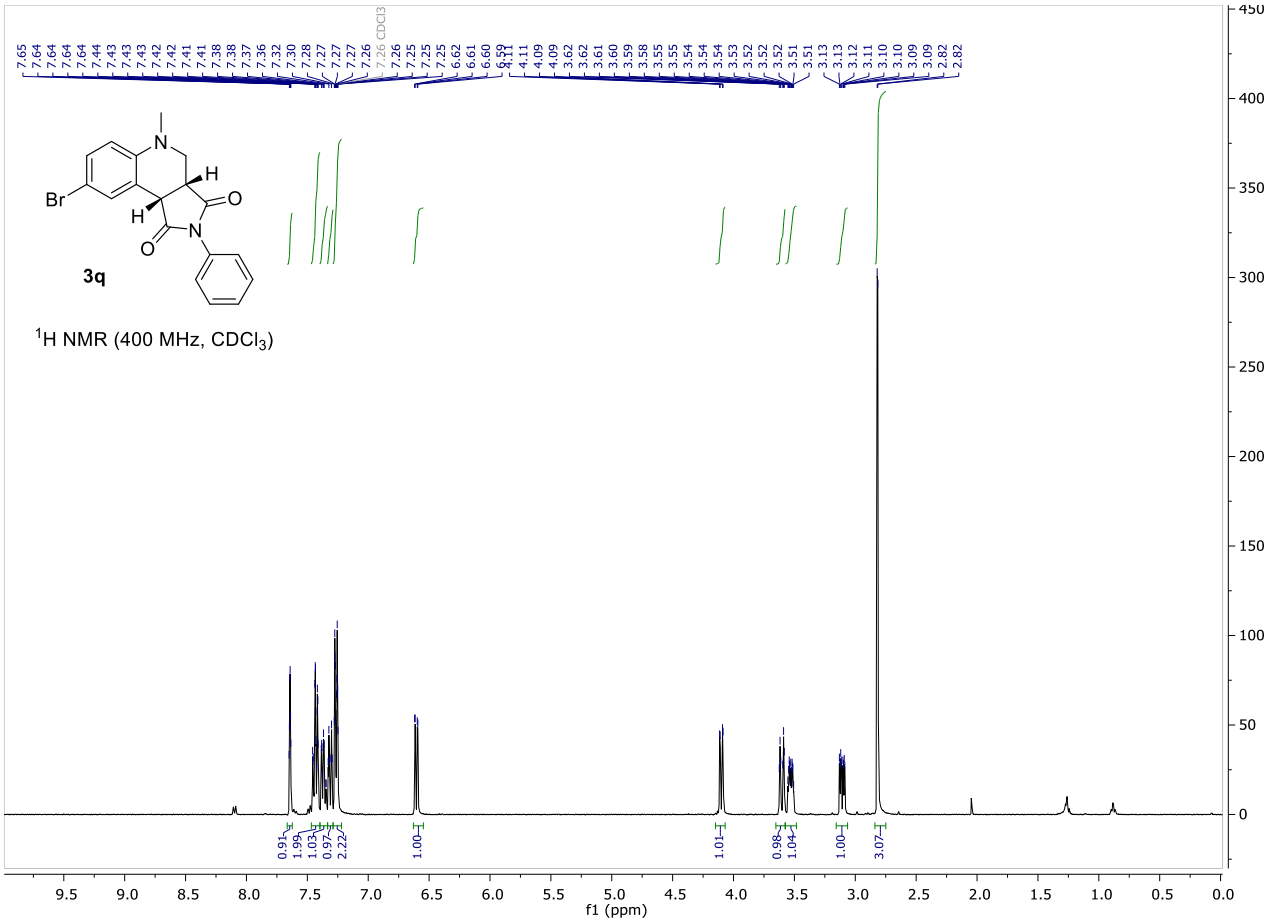
3q
^{1}H NMR (400 MHz, $CDCl_3$)
f1 (ppm)

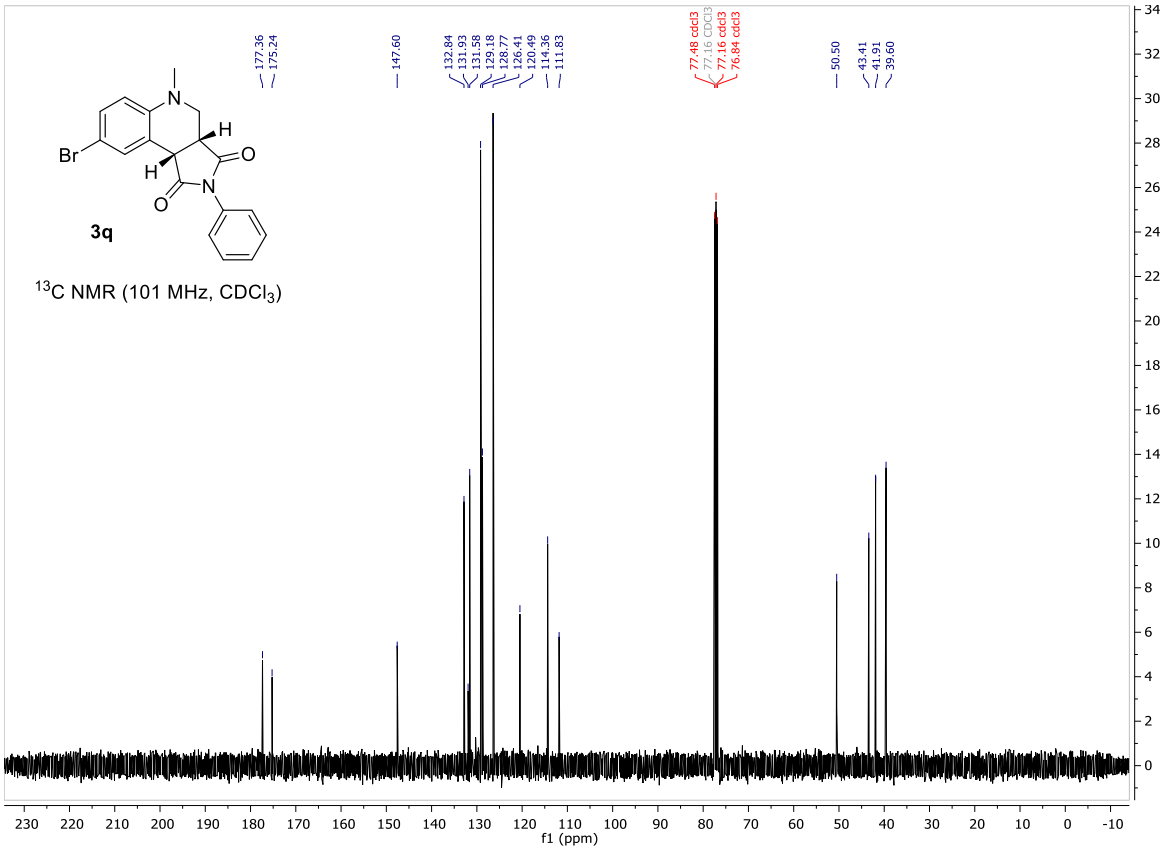
3q
^{13}C NMR (101 MHz, $CDCl_3$)
f1 (ppm)

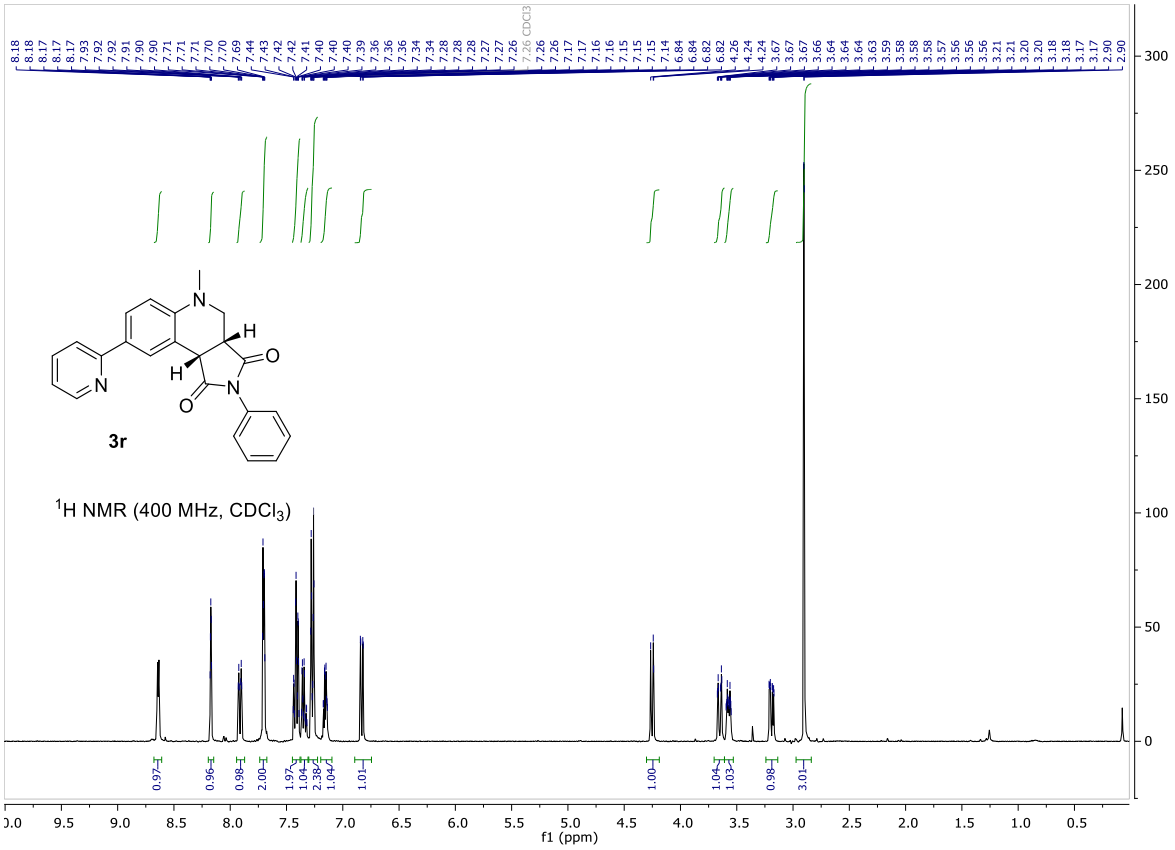
3r
^{1}H NMR (400 MHz, $CDCl_3$)
f1 (ppm)

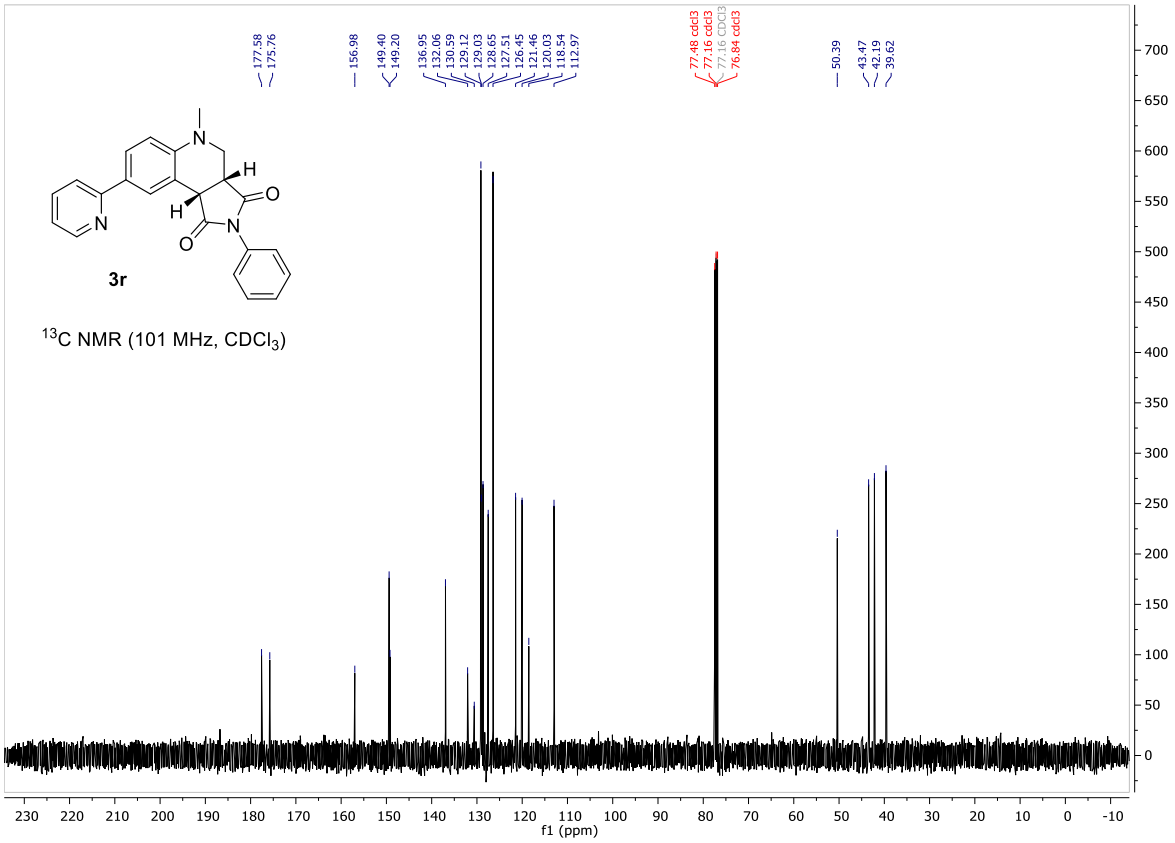
3r
^{13}C NMR (101 MHz, $CDCl_3$)
f1 (ppm)

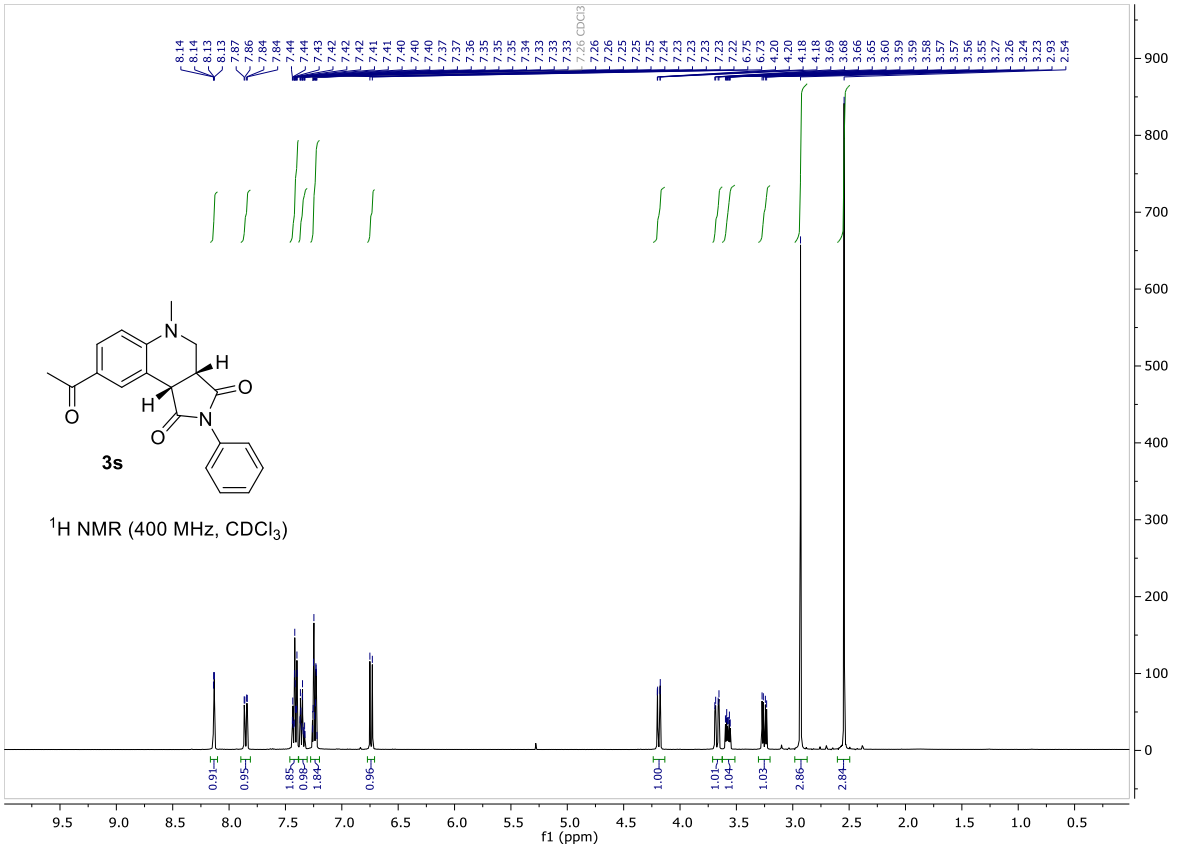
3s
^{1}H NMR (400 MHz, $CDCl_3$)
f1 (ppm)

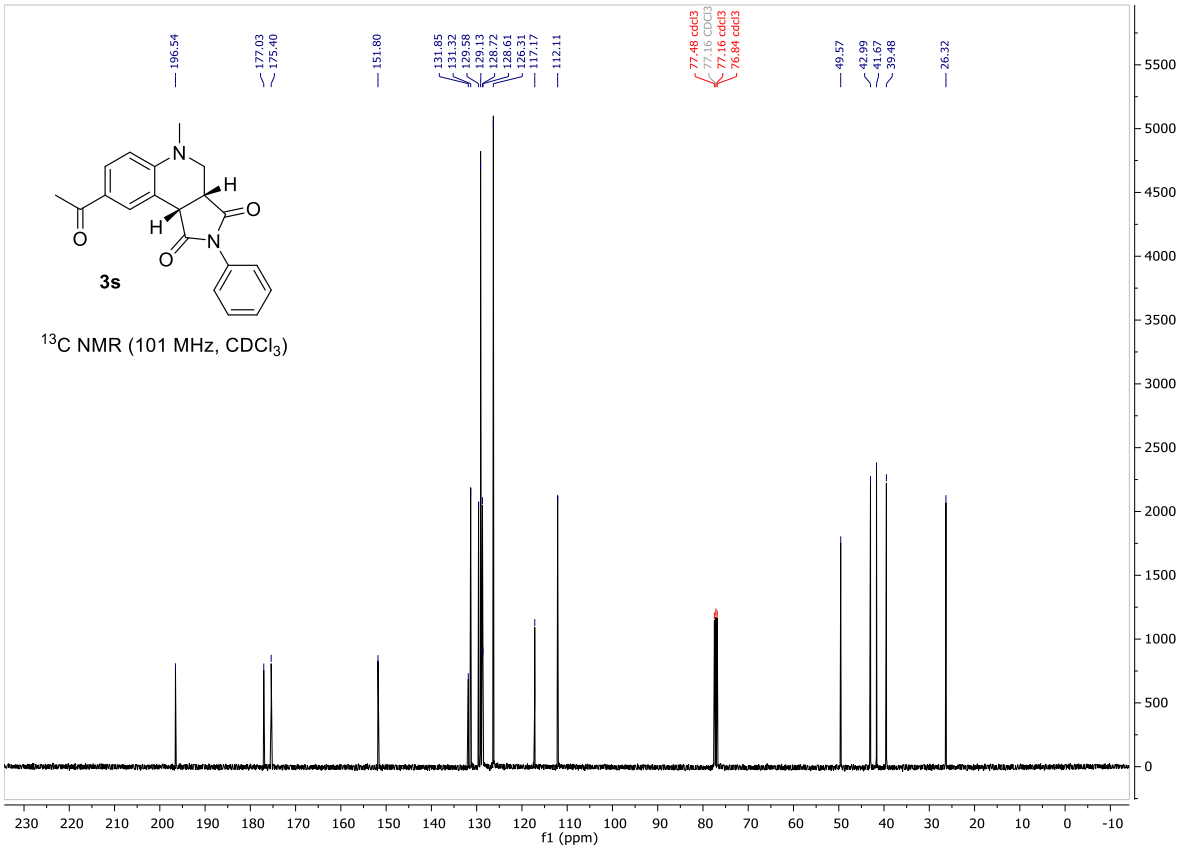
3s
^{13}C NMR (101 MHz, $CDCl_3$)
f1 (ppm)

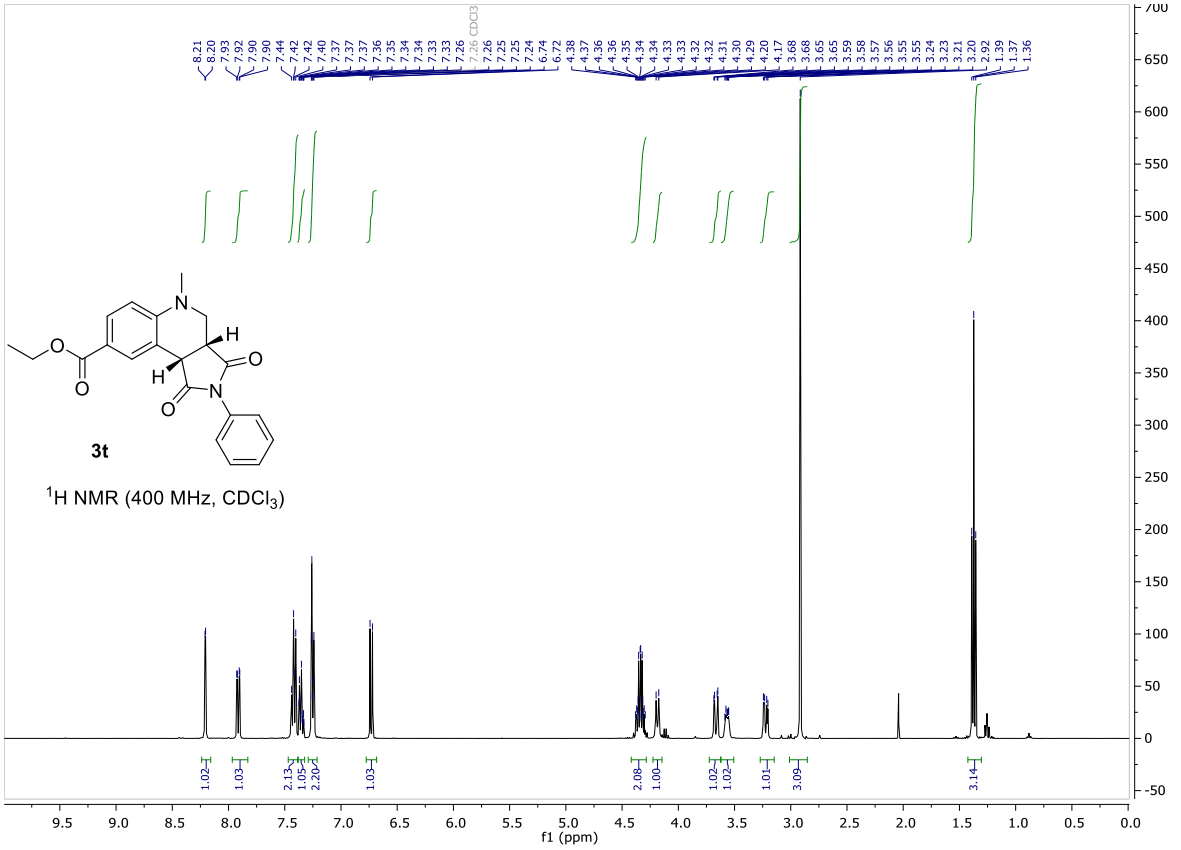
3t
^{1}H NMR (400 MHz, $CDCl_3$)
f1 (ppm)

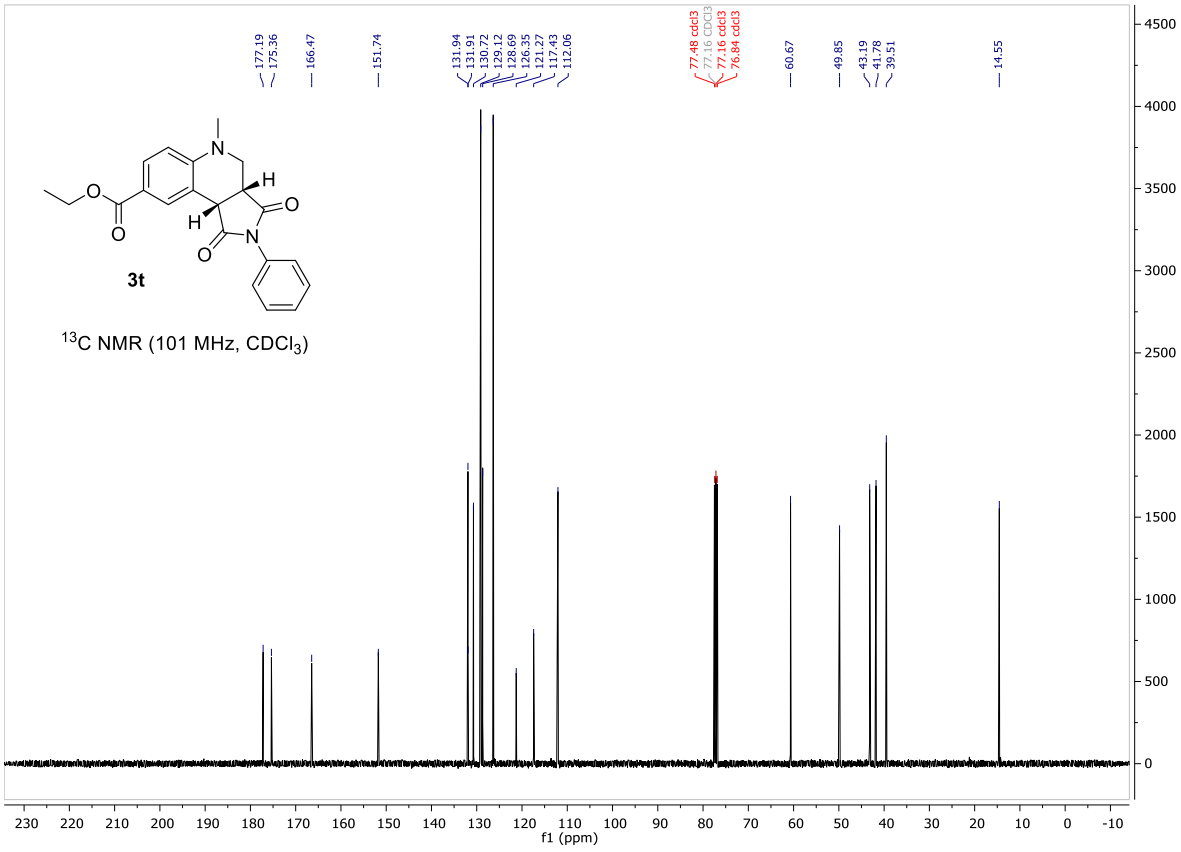
3t
^{13}C NMR (101 MHz, $CDCl_3$)
f1 (ppm)

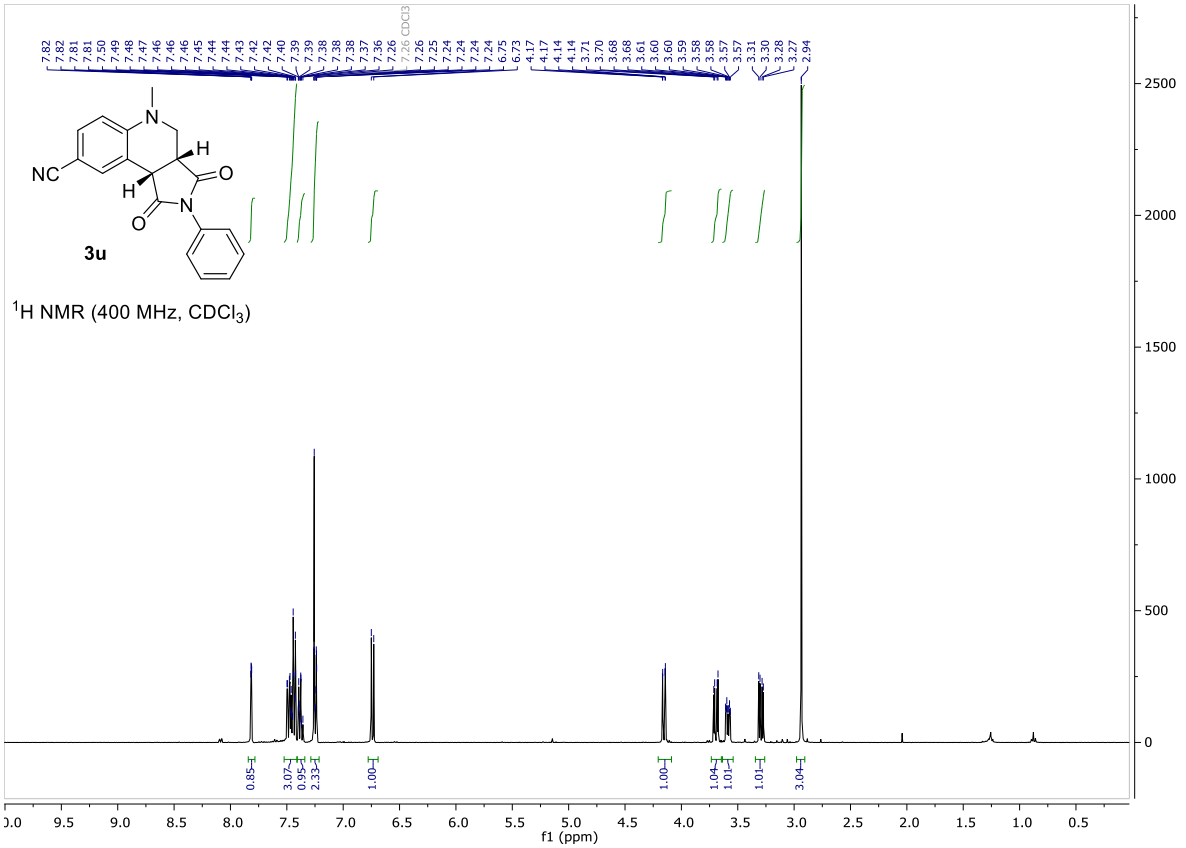
3u
^{1}H NMR (400 MHz, $CDCl_3$)
f1 (ppm)

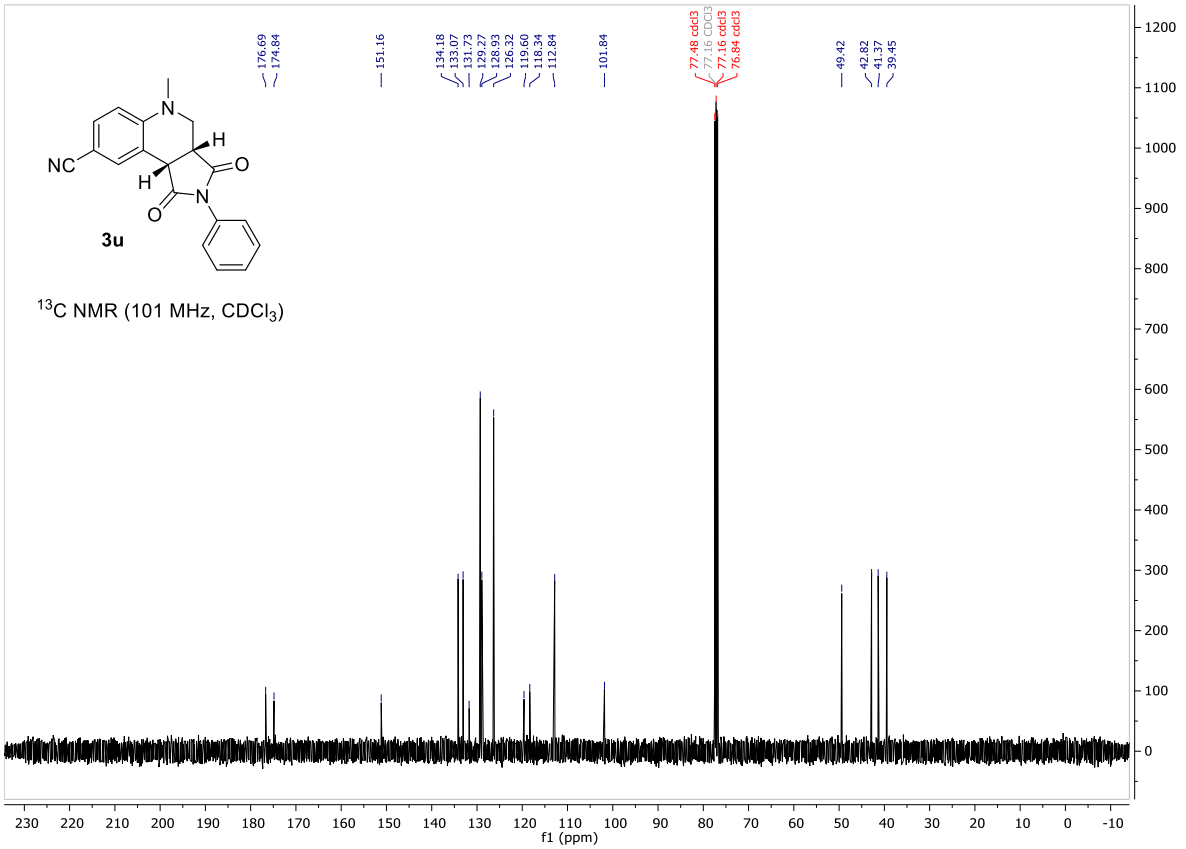
3u
^{13}C NMR (101 MHz, $CDCl_3$)
f1 (ppm)

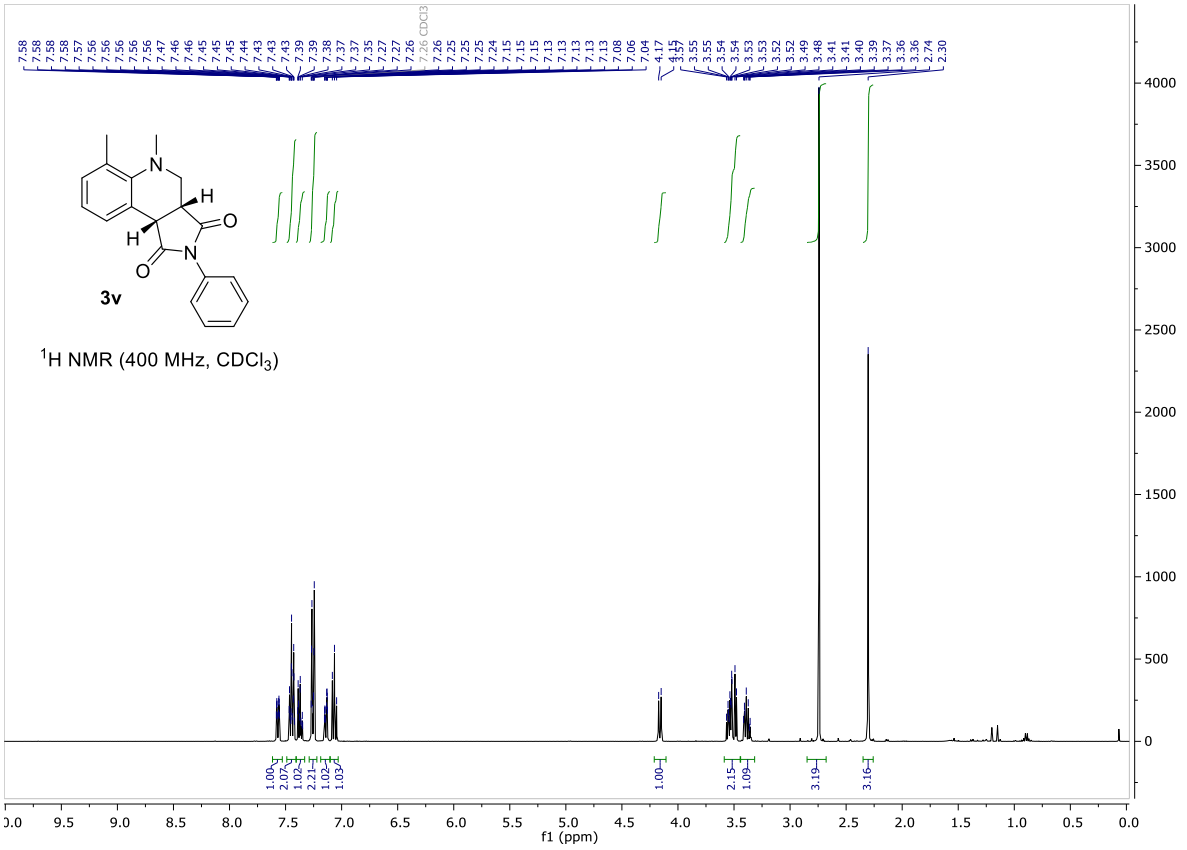
3v
^{1}H NMR (400 MHz, $CDCl_3$)
f1 (ppm)

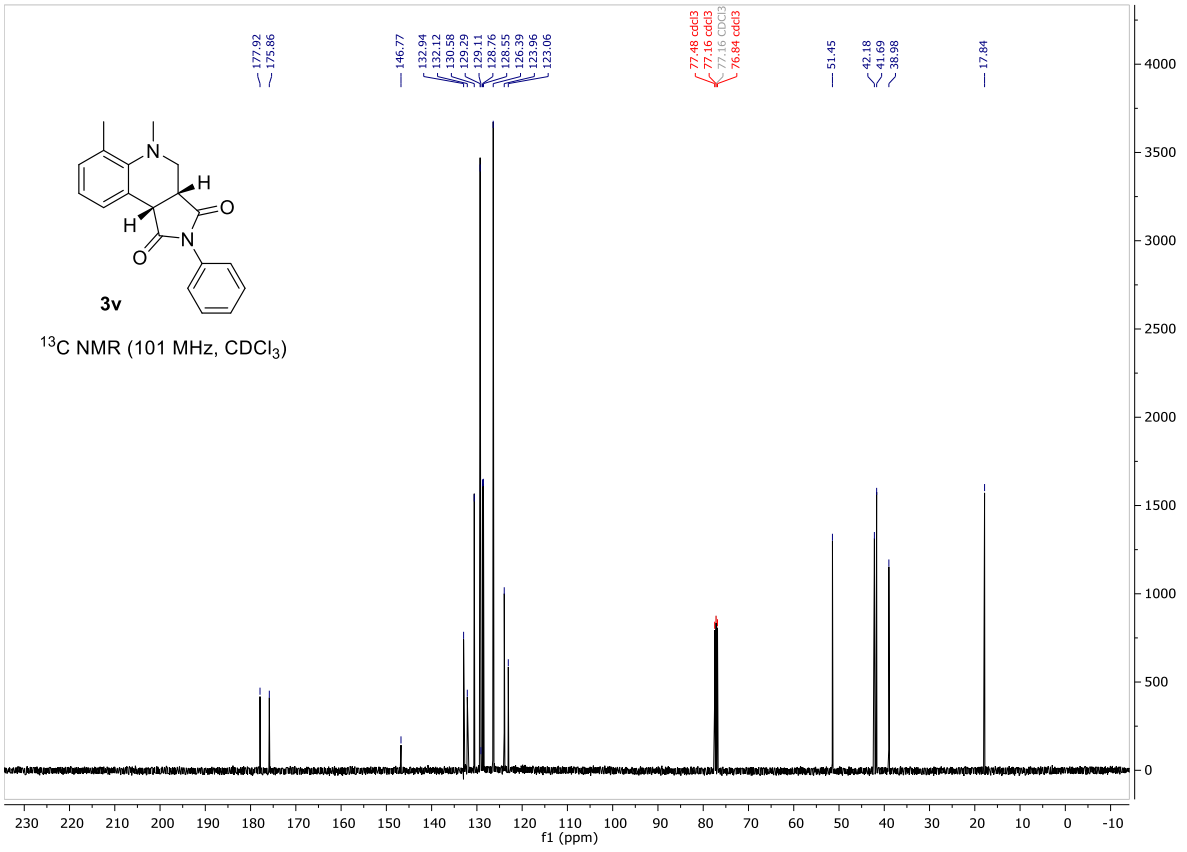
3v
^{13}C NMR (101 MHz, $CDCl_3$)
f1 (ppm)

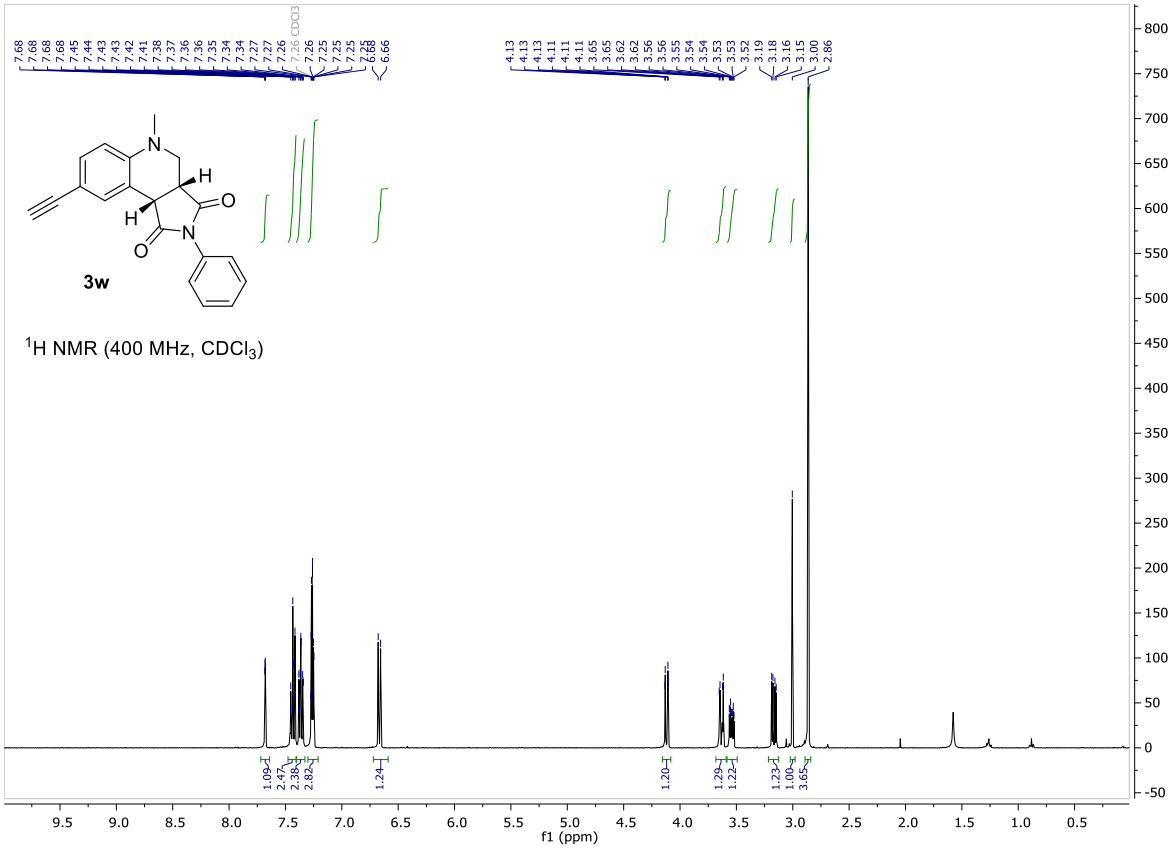
3w
^{1}H NMR (400 MHz, $CDCl_3$)
f1 (ppm)

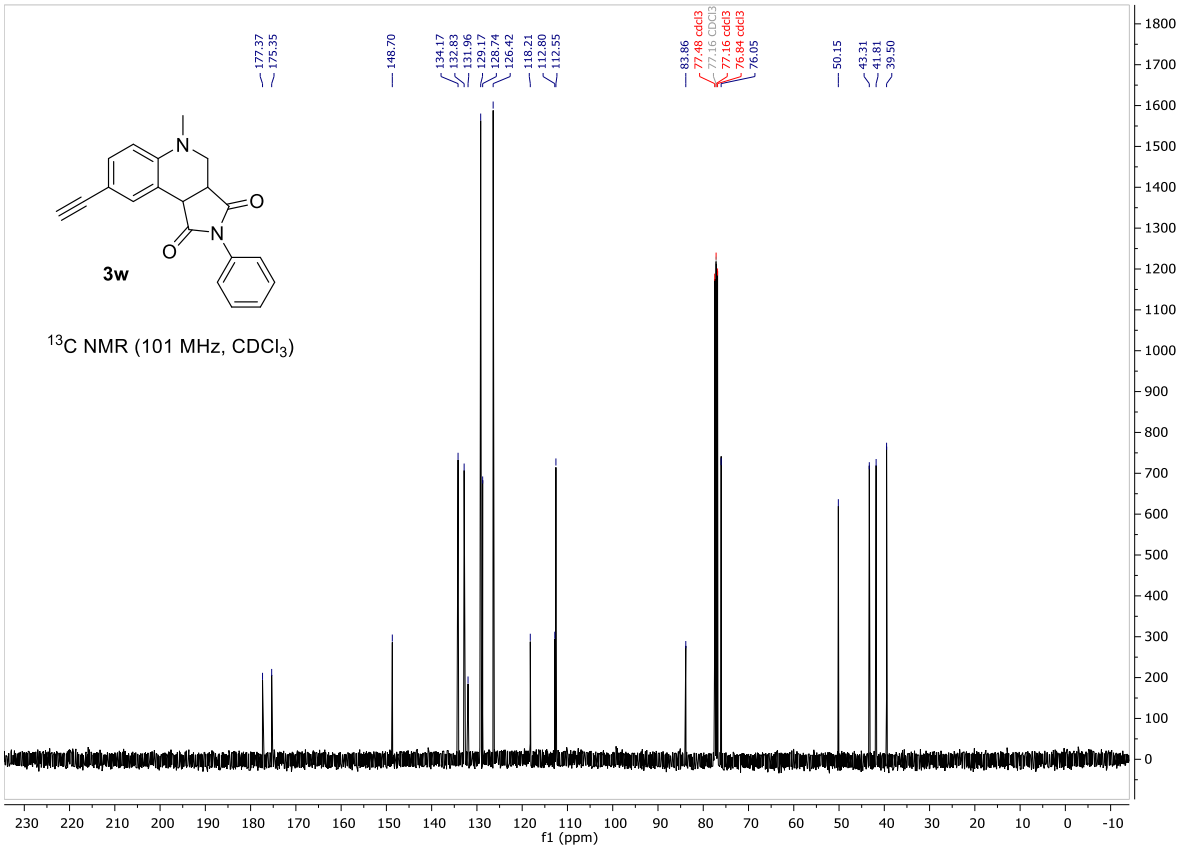
3w
^{13}C NMR (101 MHz, $CDCl_3$)
f1 (ppm)

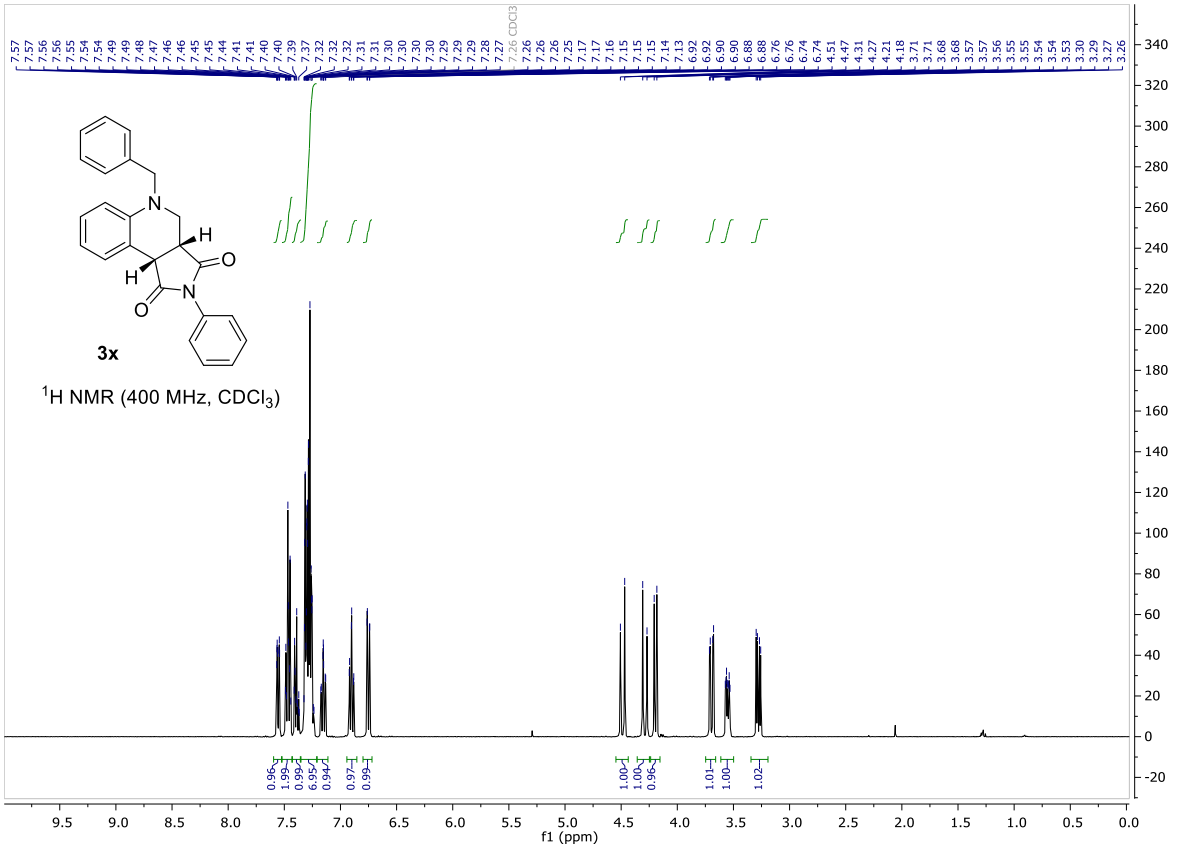
3x
^{1}H NMR (400 MHz, $CDCl_3$)
f1 (ppm)

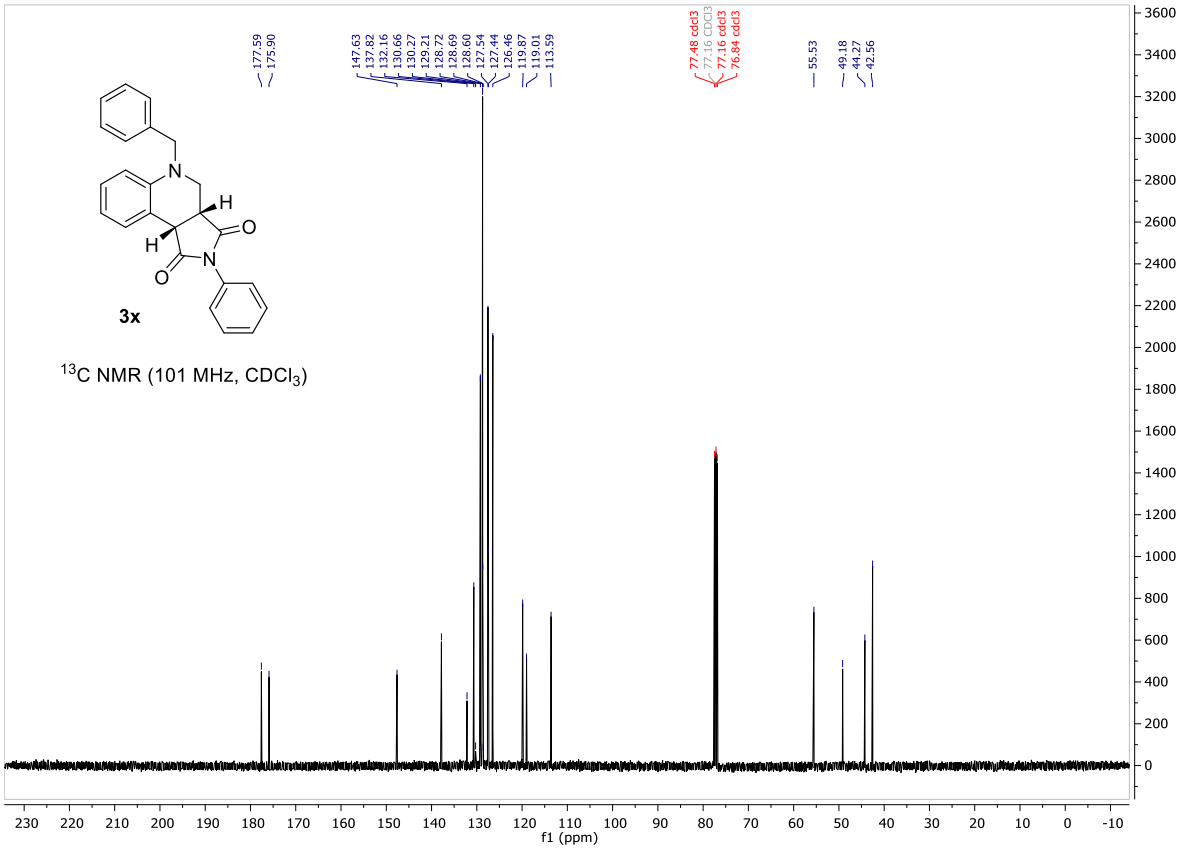
3x
^{13}C NMR (101 MHz, $CDCl_3$)
f1 (ppm)

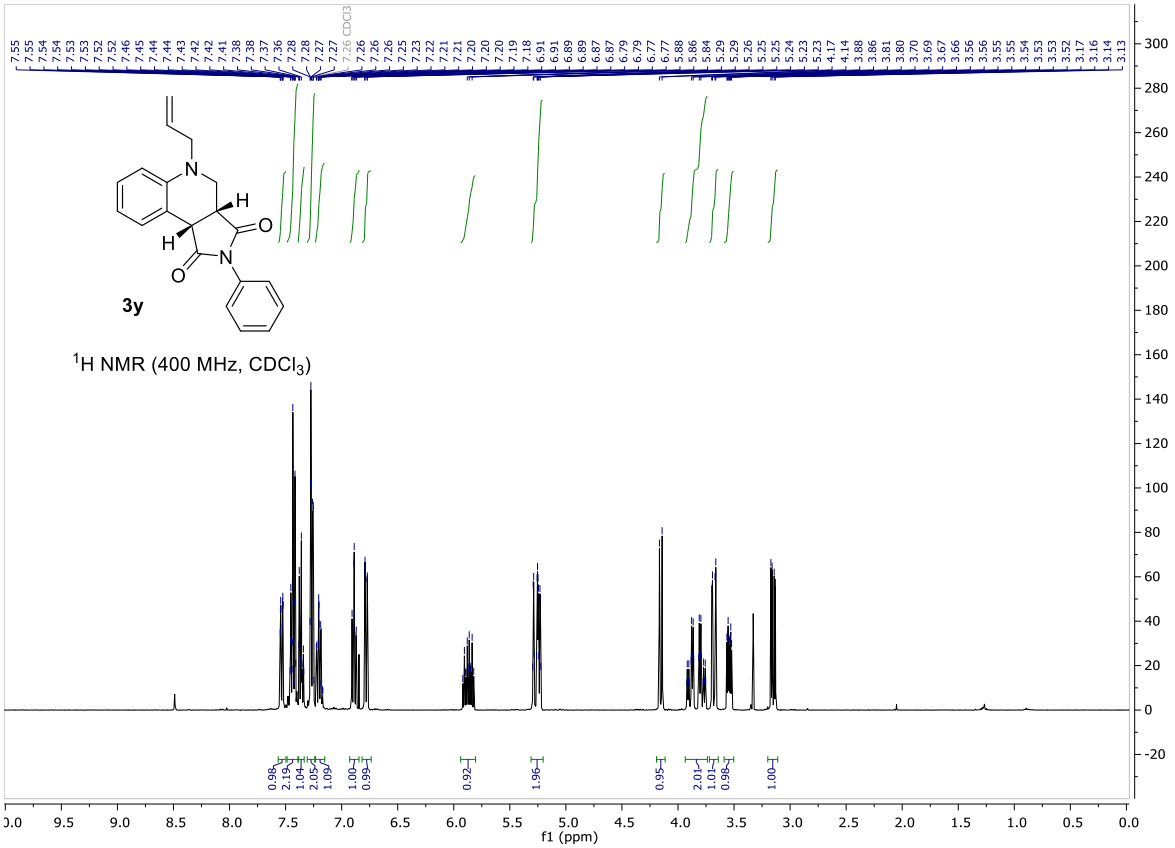
3y
^{1}H NMR (400 MHz, $CDCl_3$)
f1 (ppm)

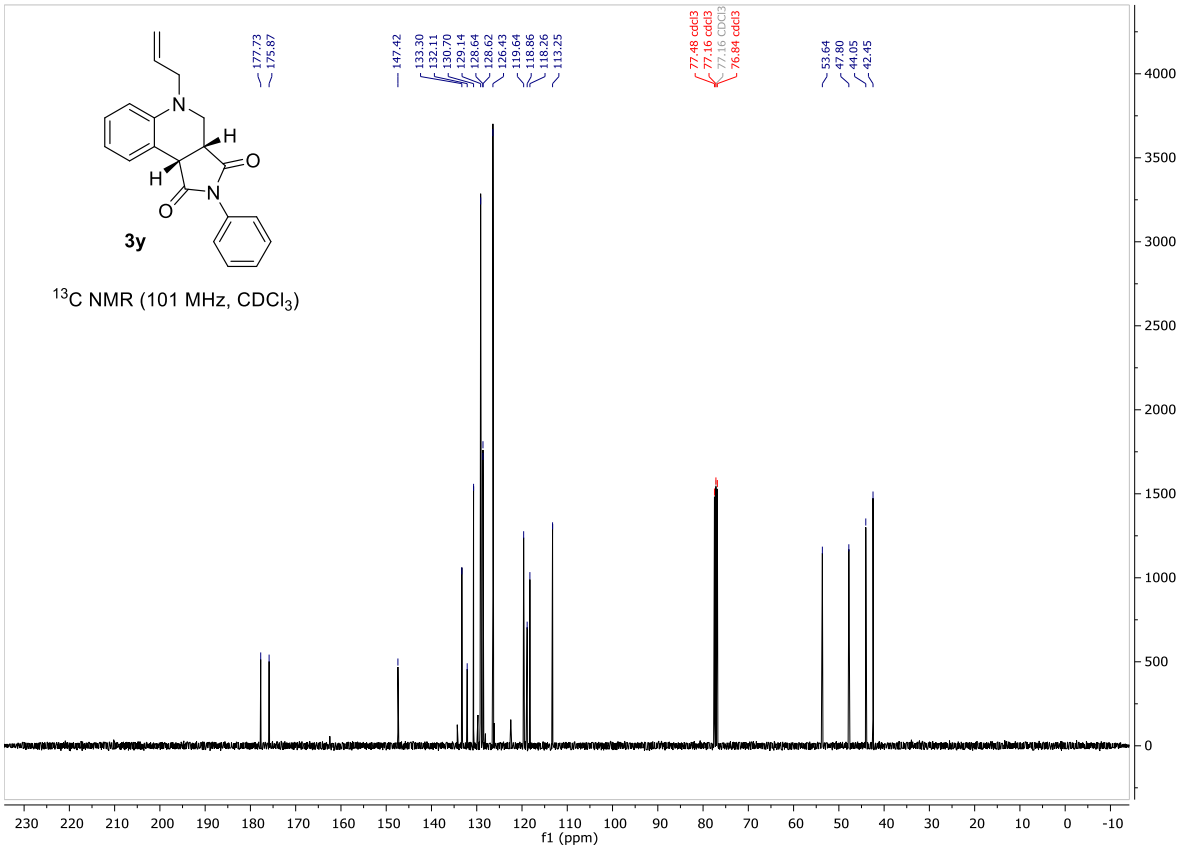
3y
^{13}C NMR (101 MHz, $CDCl_3$)
f1 (ppm)

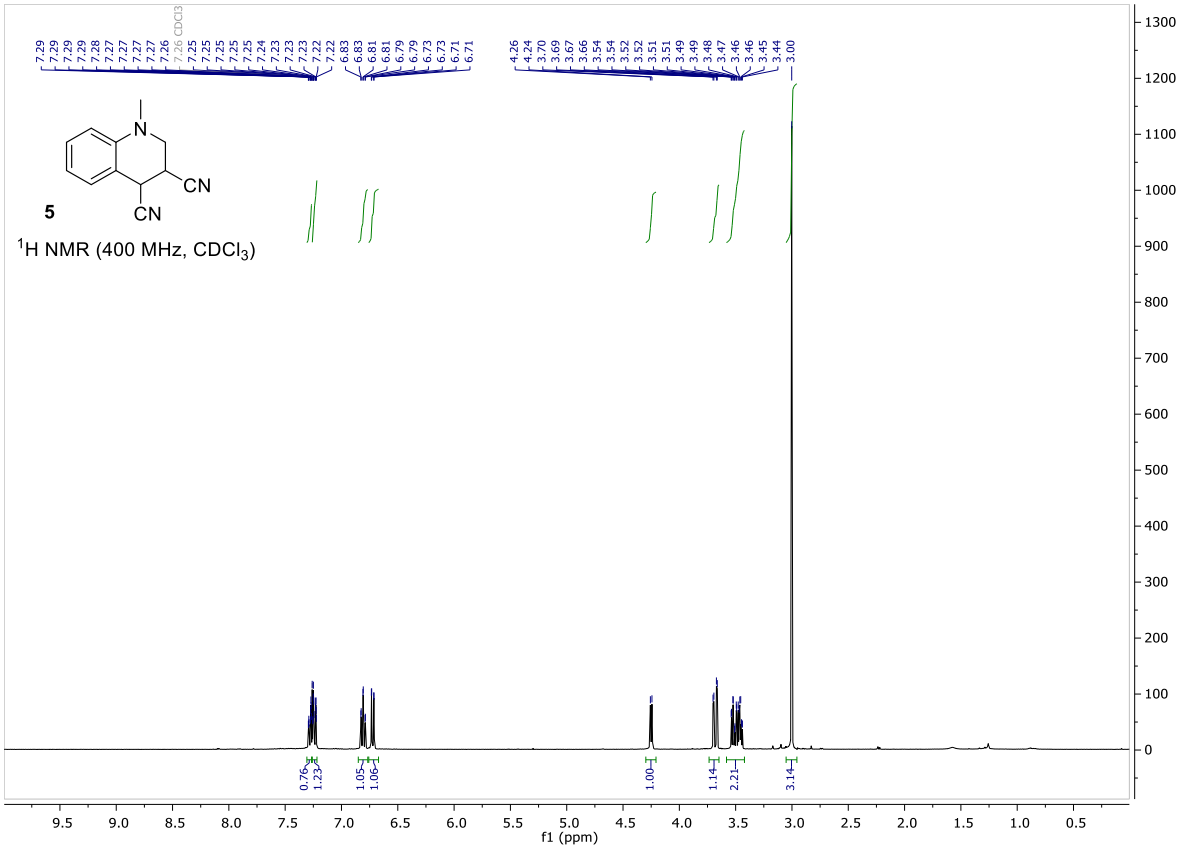
5
CN
CN
^{1}H NMR (400 MHz, $CDCl_3$)
f1 (ppm)

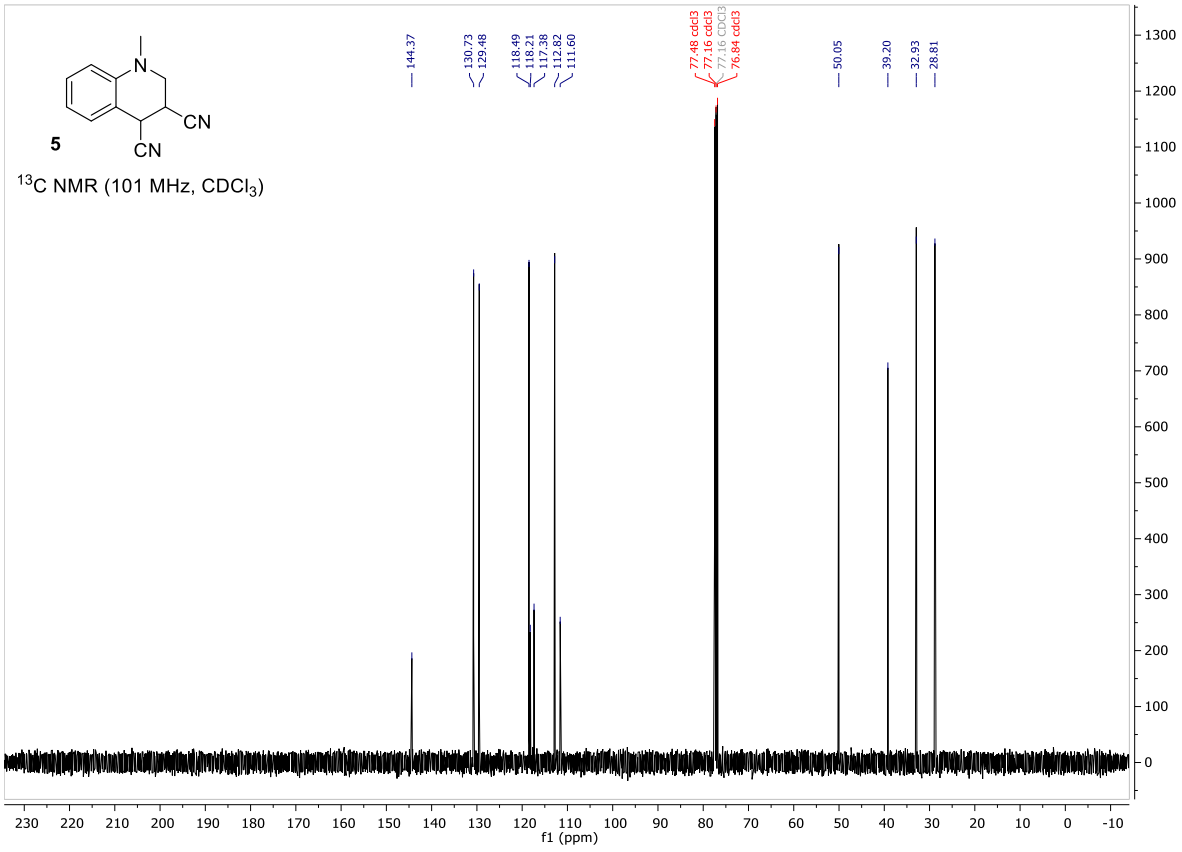
5
CN
CN
^{13}C NMR (101 MHz, $CDCl_3$)
144.37
130.73
129.48
118.49
118.21
117.38
112.82
111.60
77.48 cdcl3
77.16 cdcl3
76.84 cdcl3
50.05
39.20
32.93
28.81
f1 (ppm)

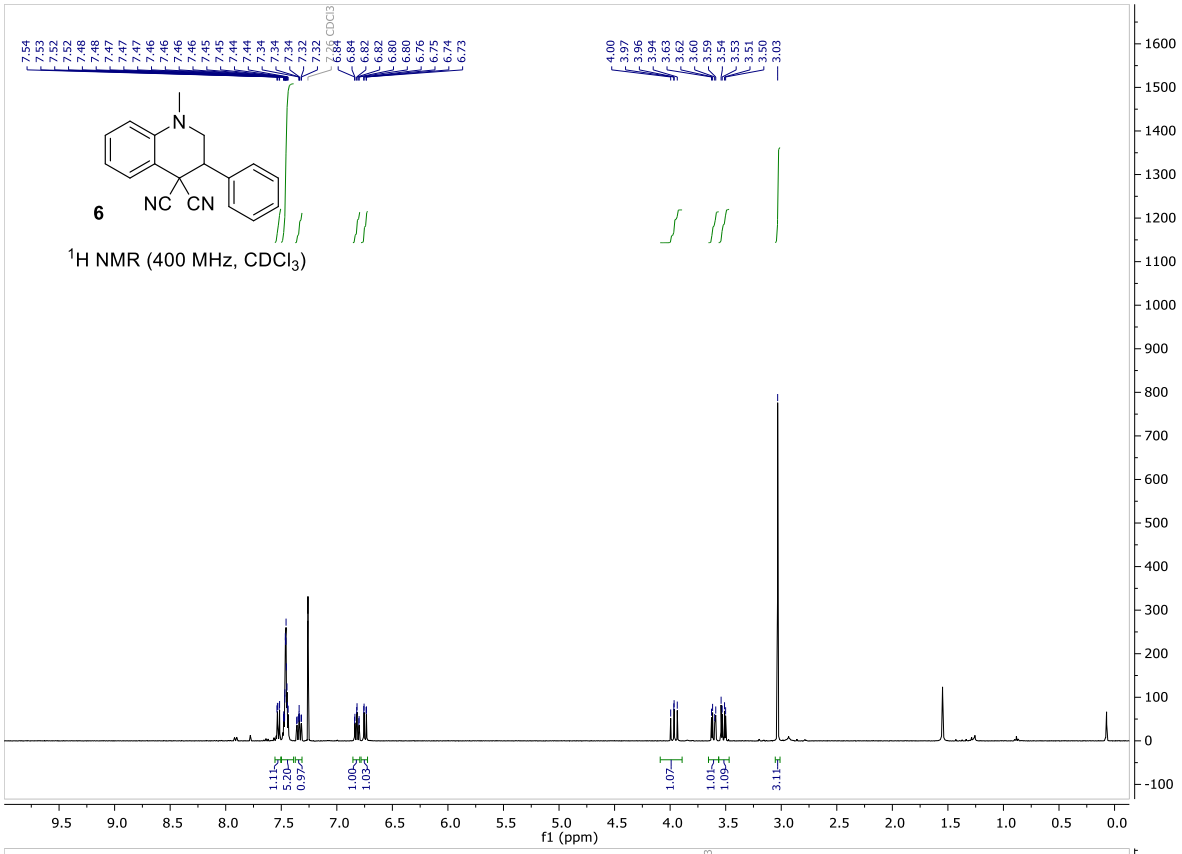
6
NC CN
^{1}H NMR (400 MHz, $CDCl_3$)
f1 (ppm)

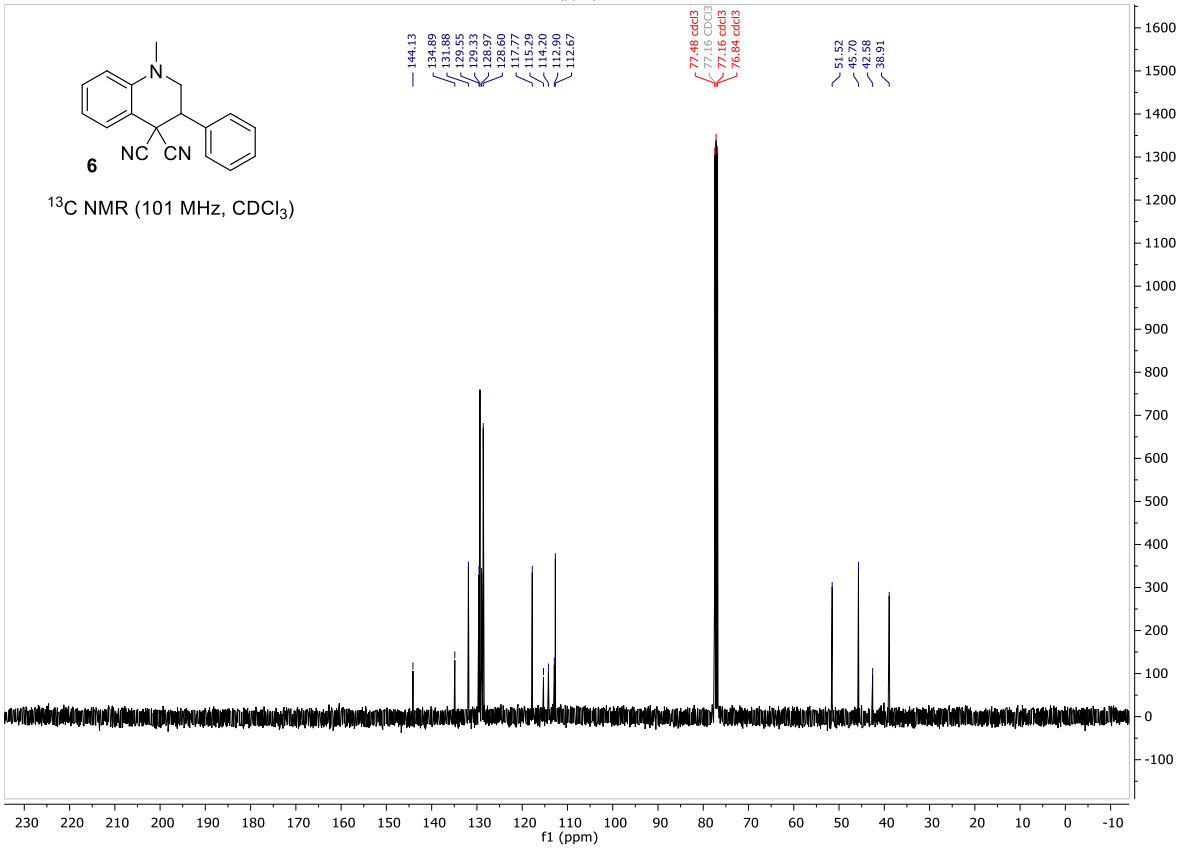
6
NC CN
^{13}C NMR (101 MHz, $CDCl_3$)
f1 (ppm)

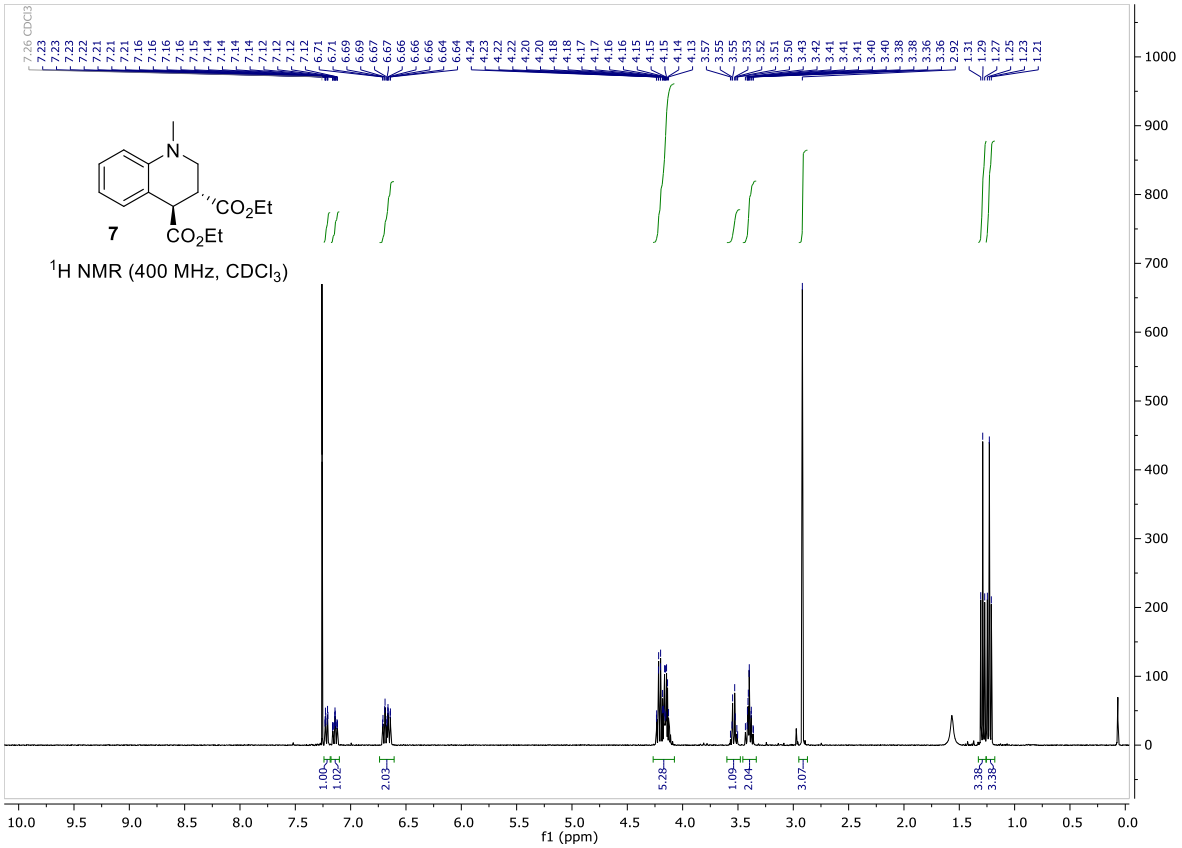
7.26 CDCl3
7.23
7.23
7.23
7.22
7.21
7.21
7.21
7.16
7.16
7.16
7.15
7.14
7.14
7.14
7.14
7.12
7.12
7.12
7.12
6.71
6.71
6.69
6.69
6.67
6.67
6.66
6.66
6.66
6.64
6.64
4.24
4.23
4.22
4.22
4.20
4.20
4.18
4.18
4.17
4.17
4.16
4.16
4.15
4.15
4.15
4.14
4.13
3.57
3.55
3.55
3.53
3.52
3.51
3.50
3.43
3.42
3.41
3.41
3.40
3.40
3.38
3.38
3.36
3.36
2.92
1.31
1.29
1.27
1.25
1.23
1.21
N
CO2Et
CO2Et
7
1H NMR (400 MHz, CDCl3)
1.00
1.02
2.03
5.28
1.09
2.04
3.07
3.38
3.38
f1 (ppm)

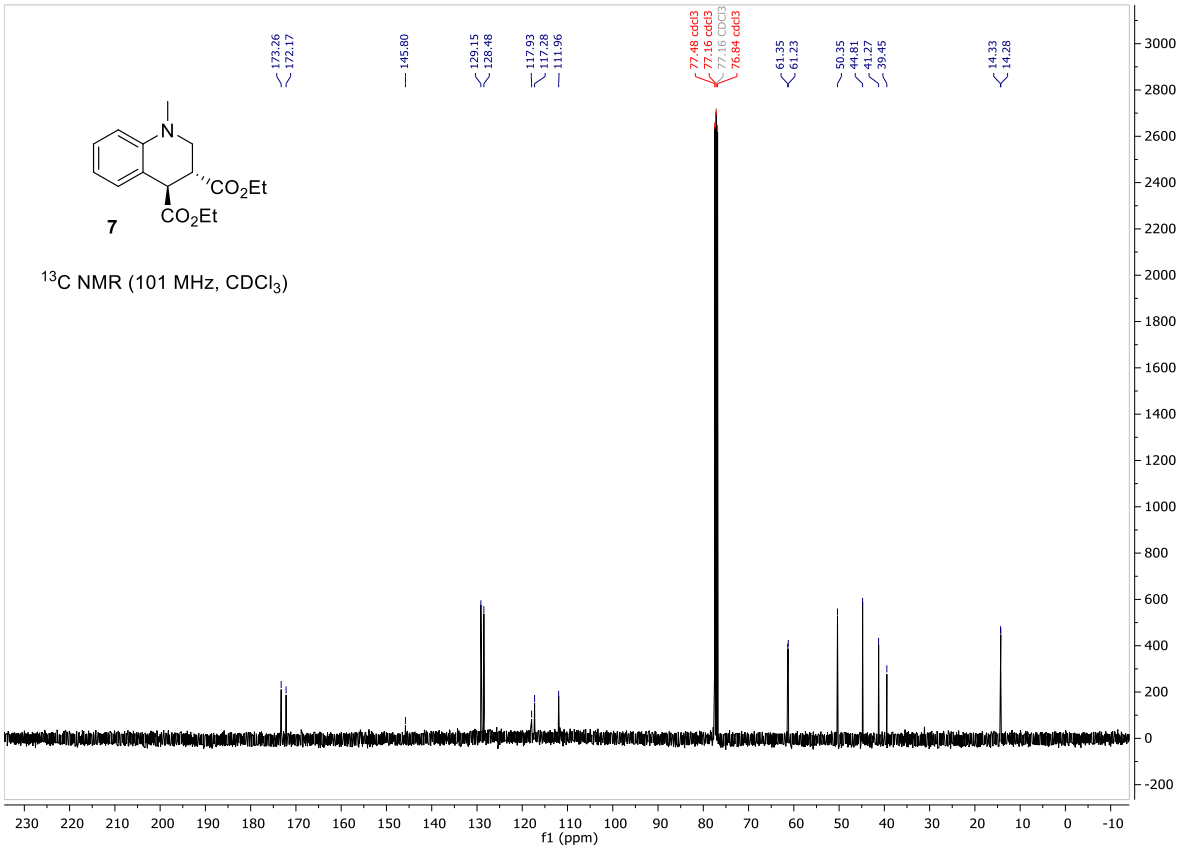
173.26
172.17
145.80
129.15
128.48
117.93
117.28
111.96
77.48 cdcl3
77.16 cdcl3
76.84 cdcl3
61.35
61.23
50.35
44.81
41.27
39.45
14.33
14.28
N
CO2Et
CO2Et
7
13C NMR (101 MHz, CDCl3)
f1 (ppm)